SEDIMENT TRANSPORT IN THE CANADIAN BEAUFORT SEA

by
D.B. Fissel and J.R. Birch

Prepared for
Atlantic Geoscience Centre
Bedford Institute of Oceanography
Dartmouth, N.S.

Arctic Sciences Ltd.
1986 Mills Road
R.R. 2, Sidney, B.C.
V8L 3S1

(604) 656-0177
Telex 049-7476

ASL File 35-060-F
December, 1984

ARCTIC SCIENCES LTD

NOTICE

This report was prepared for the Atlantic Geoscience Centre, Bedford Institute of Oceanography, Dartmouth, N.S. To provide the broadest possible description of physical oceanographic processes important to sediment transport, the use of oceanographic data collected by oil companies was arranged through the Scientific Authority. Certain portions of these data remain proprietary to the oil companies. These are the 1981-1982 current meter data sets collected by Dome Petroleum and Esso Resources, referenced in Sections 2.5.2 and 3.1.1.

To protect the rights of the companies involved, prior permission should be obtained from the Scientific Authority (Dr. Phil Hill or in his absence, Mr. Steve Blasco), before citing results from this report.

TABLE OF CONTENTS

LIST OF FIGURES

LIST OF TABLES

ABSTRACT

In this study, the transport and dispersal of sediments in the Canadian Beaufort Sea, were examined in terms of the underlying physical mechanisms. Results of oceanographic, meteorological, hydrological and sediment studies for the region were reviewed and summarized to provide a description of the physical environment. Analyses on the oceanic bottom boundary layer were carried out using existing data to examine the response of bottom currents to wind forcing and the correlation between suspended sediment concentrations with bottom currents. The descriptive and anlytical results were used to prepare a conceptual model of sediment transport in the Beaufort Sea and its relation to physical forcing mechanisms. From this model, a number of deficiencies in our present understanding were identified and discussed; recommendations for further investigations are presented.

ACKNOWLEDGEMENTS

The authors would like to thank Steve Blasco and Phil Hill of the Atlantic Geoscience Centre (AGC), Bedford Institute of Oceanography. Dr. Hill, as Scientific Authority, provided much helpful advice and insight into sedimentation processes for which we are indebted. Dr. John Harper, formerly of Woodward-Clyde Consultants and presently at Dobrocky Seatech Ltd., contributed to defining the various sediment transport processes both through his earlier report for the AGC and through direct consultation in this project. Dr. H. Melling and Mr. R. Herlinveaux, of the Institute of Ocean Sciences, offered many helpful comments based on a review of a draft version of this report. Dome Petroleum Ltd. and Esso Resources Canada Ltd. kindly provided access to oceanographic data they had collected in the Beaufort Sea.

Our thanks to other Arctic Sciences personnel who contributed to this report: Dr. J. Marko for assistance in the description of sea-ice conditions and satellite-imagery data; S. Oberski and R. Chave for computer programming; N. Goody for processing much of the hydrological, CTD and turbidity data; S. Norton for the word processing; and B. Clarke and N. Andrew who prepared the many figures in this report.

1. INTRODUCTION

1.1 GENERAL BACKGROUND

The continental shelf of the Canadian Beaufort Sea, an area of intense offshore oil and gas exploration, receives a large amount of suspended sediment each year from the Mackenzie River. This study was undertaken to improve understanding of the dispersal of these sediments over the continental shelf. Based on a review and analysis of existing data, the important physical mechanisms involved in sediment transport were examined.

The Mackenzie River is the largest of the North American rivers which empty into the Arctic Ocean. It is 3,700 km long and drains approximately 1.8 million square kilometres of British Columbia, Alberta, Saskatchewan, the Northwest and Yukon territories. The total average yearly discharge amounts to 2.7 x 10^{11} m^3/yr (based on a mean annual flow of 8,500 m^3/s; Davies, 1975). The mean annual sediment discharge from the Mackenzie River has been estimated (C.P. Lewis, 1982, cited in Harper and Penland, 1982) as 85.6 x 10^6 m^3/yr. Of the total river sediments delivered to the Arctic Ocean, the Mackenzie River is the largest single source; while the Ob, Yenisei and Lena Rivers of the Eurasian Arctic each have larger volume discharges, their combined sediment discharge is estimated to be only 60% of that of the Mackenzie River (Milliman and Meade, 1983). Mackenzie River sediment accounts for over 95% of the total sediment input to the Canadian Beaufort Sea (Harper et al., 1984).

The Canadian Beaufort Sea (Figure 1) consists of a broad continental shelf extending from the coastline to distances of up to 150 km offshore. Depths of 70 to 100 m characterize the boundary between the continental shelf and slope. The continental shelf is divided into two parts by the deep water of the Mackenzie trough which penetrates at water depths of 100 m or greater to within 30 km of the coastline. To the east of the Mackenzie trough, a series of shallow, gentle-sided valleys traverse the shelf.

1.2 PREVIOUS SEDIMENT DISPERSAL STUDIES

Pelletier (1975) developed a sediment dispersal model for the Beaufort Sea based, in large part, on the measured distribution of surficial sediments obtained during the Beaufort Sea Project of 1974 - 1975 (Figure 2). Sediments of river origin have been identified in the form of fine particle size (silts and clay), extending from the coastline between Herschel Island and

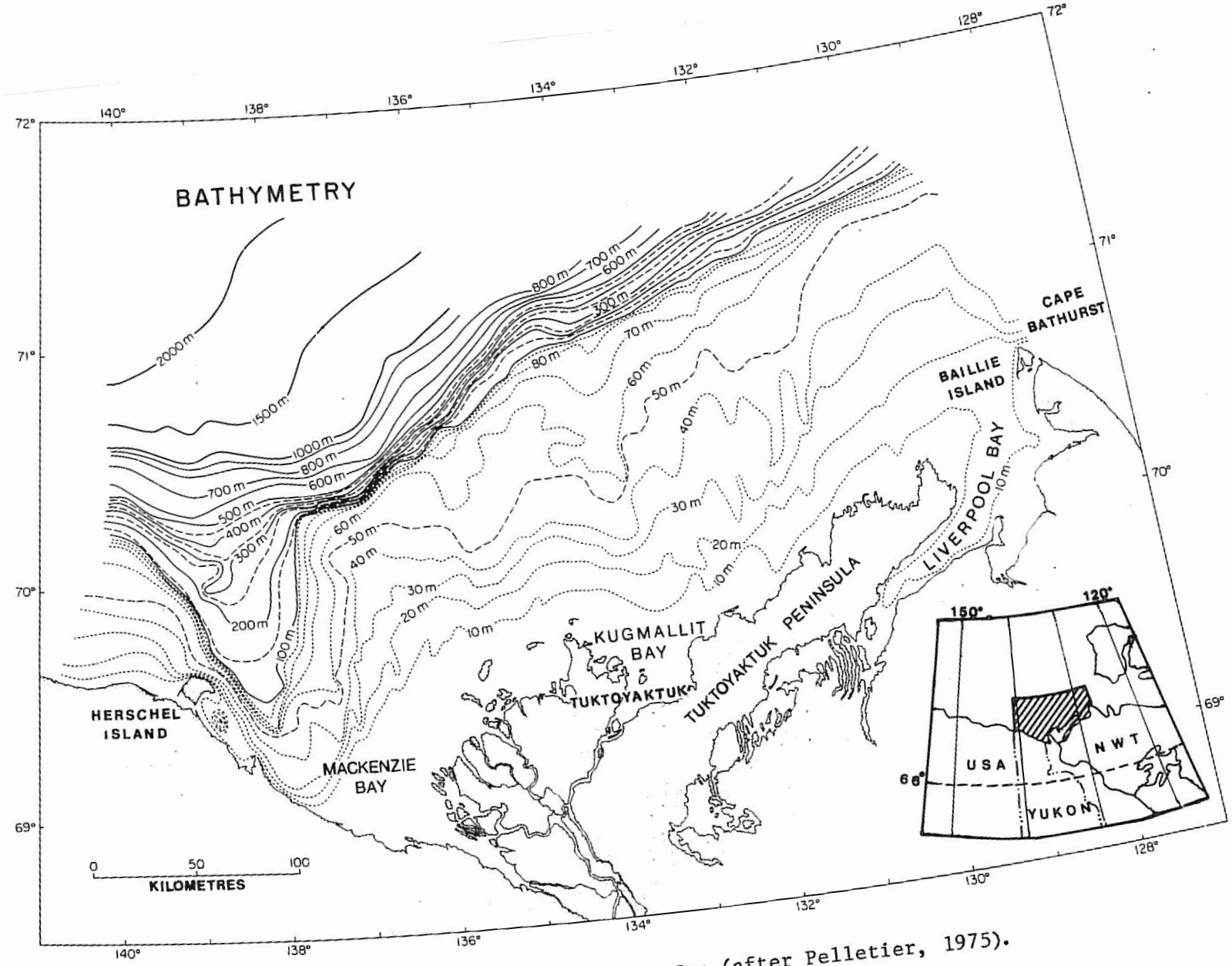

Figure 1: The bathymetry of the Canadian Beaufort Sea (after Pelletier, 1975).

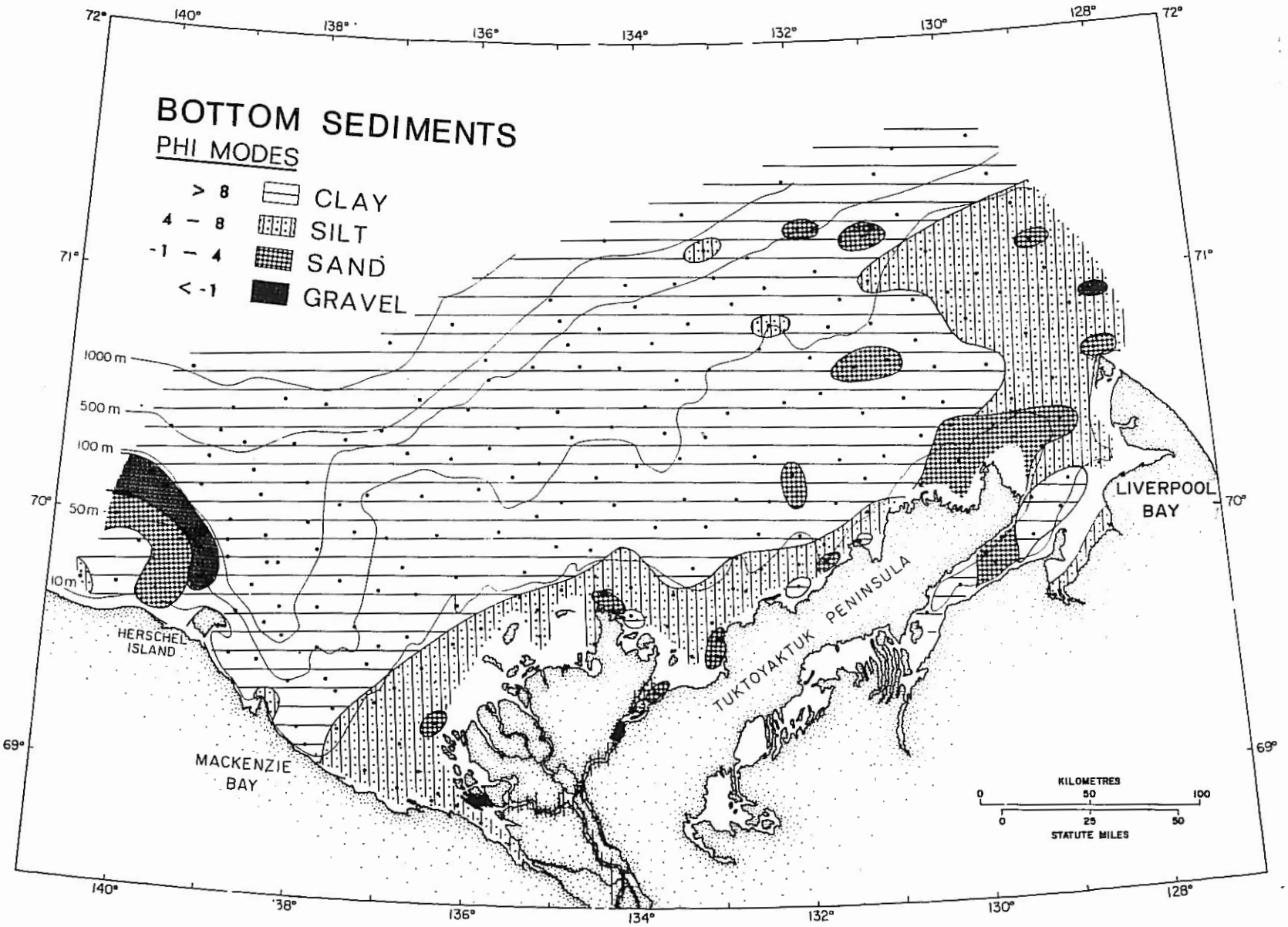

Figure 2: The distribution of bottom sediments in the Canadian Beaufort Sea (after Pelletier, 1975).

the eastern tip of the Tuktoyaktuk Peninsula to the deep waters of the continental slope. To the west of Herschel Island on the Yukon Shelf, sand and gravel are abundant, while offshore of Liverpool Bay and further to the east, sand and silt sizes predominate. The larger particle size of the surficial sediments suggests a reduced influence of the River in these areas.

Recently, a new sediment dispersal model has been developed for the Canadian Beaufort Sea (Harper and Penland, 1982; Harper et al., 1984). This model, while incorporating some of the results of the earlier study of Pelletier (1975), also makes use of more recent information, as described below.

The rate of sediment accumulation on the continental shelf has been estimated by Harper et al. (1984) on the basis of the post-glacial mud thickness data of Meagher (1978) and O'Connor (1982). Based on these data, in conjunction with a post-glacial sea-level curve (Forbes, 1980), the average sedimentation rates over the past 8,000 years were computed as shown in Figure 3. The largest sedimentation rates of 2 mm/yr or greater occur a) within the 30 m isobath from Mackenzie Bay to immediately offshore of Kugmallit Bay and b) over the deeper water of the inner portion of the Mackenzie trough. Further offshore and eastwards, the sedimentation rate is markedly reduced, generally to levels of 0.5 mm/yr or less. Seaward of the continental shelf, there is contradictory information on the amount of sediment reaching the sea floor. Estimates of deposition rates range from very low levels (O'Connor, 1982) to relatively high values of approximately 1 mm/yr on the continental slope (Hill et al., 1984).

Based on the sedimentation rates of Figure 3, the sediment sinks were computed as to 50 to 80% of the total volume of sediment contributed from the Mackenzie River (Harper and Penland, 1982). The discrepency between the estimates for the major source (River) and sink (shelf accumulation) terms in the sediment budget for the Canadian Beaufort Sea are attributed by Harper et al. (1984) to:

- a significant portion of the sediment escaping across the shelf to the north or to the east and/or;
- errors in the estimates of shelf accumulation due primarily to inaccurate mud thickness measurements for the Mackenzie trough region.

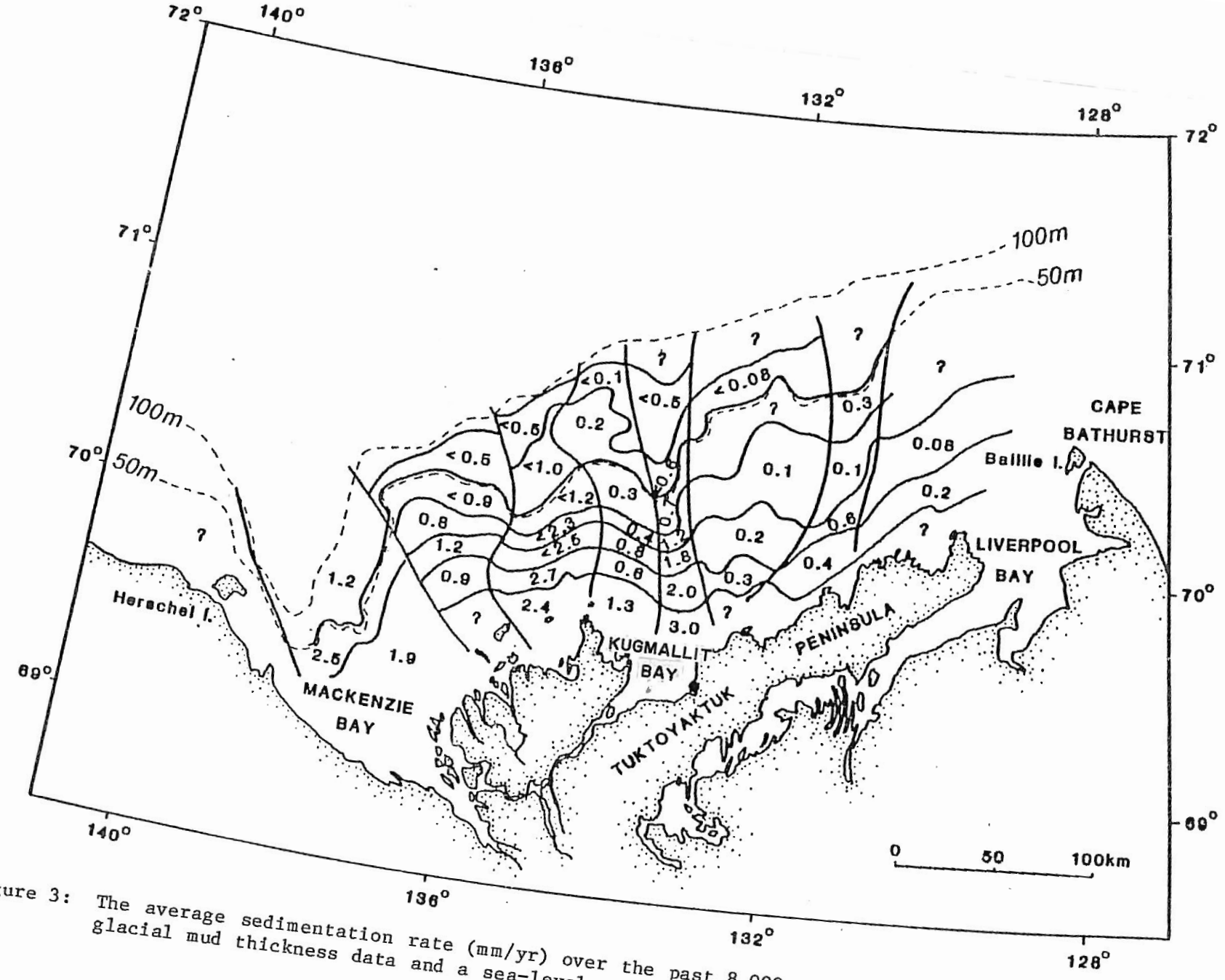

Figure 3: The average sedimentation rate (mm/yr) over the past 8,000 years computed on the basis of post-glacial mud thickness data and a sea-level curve (after Harper et al., 1984).

Harper et al. (1984) considered four distinct processes which could potentially transport sediments along the coast or across the shelf. These are:

a) **Surface Plume Dispersal:** On entering the Beaufort Sea, the less dense River water occurs as a surface plume. An analysis using LANDSAT satellite data (Harper and Penland, 1982) indicated that the surface plume consists of a concentrated inner portion adjacent to the Mackenzie River delta isobath and a highly variable and much larger diffuse outer portion. The boundary between the inner and outer sediment plumes is generally marked by a very pronounced spatial gradient (in the surface sediment concentrations) within the 10 m depth contour. The plume responds strongly to the surface wind; under easterly winds, the inner plume is deflected to the west into Mackenzie Bay while the outer diluted plume extends offshore to the north and east. Under westerly winds, cloud cover usually obscures the satellite images; from the one image available (July 7, 1975), the plume was deflected in a narrow band along the Tuktoyaktuk Peninsula coast.

b) **Wave Generated Transport:** Based on the wave hindcast model of Baird and Hall (1980) applied to the ten year period, 1970 to 1979, the dominant wave approach direction is from the northwest and west. Using an assumed threshold velocity for sediment resuspension of 40 cm/s, bottom sediments, having the following frequency of disturbance levels according to water depth, were computed:

Water Depth (m)	Frequency of Disturbance
<5	50%
5-10	10-50%
10-20	1-10%
20-35	<1%

At depths greater than 35 m (47 m off the eastern end of Tuktoyaktuk Shelf), bottom disturbance is negligible.

c) **Bottom Current Transport:** Using bottom current meter data collected during the Beaufort Sea Project of 1974-1975 (Huggett et al., 1977) and by Dome Petroleum Ltd. from 1976 to 1977 (Fissel, 1981), the average transport is northeasterly to easterly on the Tuktoyaktuk Shelf.

Note that all data were collected at locations seaward of the 30 m isobath. The maximum observed speeds were less than 40 cm/s at all measurement locations except one site to the west of Herschel Island.

d) **Ice-Related Transport:** Ice scouring in the winter months was judged to have the potential to disturb and mix sediments but not to result in any significant transport. Thus, the importance of sea-ice is relegated to an indirect role in limiting significant levels of wave and current activity to the few months of open water (July through September).

Based on the results summarized above, Harper et al. (1984) summarized transport paths and mechanisms as follows:

> "The Mackenzie River surface plume is generally deflected to the east (Figure 4) even during the frequently occurring easterly wind events...
>
> Wave energy provides the dominant energy source for bottom sediment transport and also maintaining high sediment concentrations in the surface plume. Three across-shelf zones (Figure 4) illustrate differing shelf sediment transport regimes, based on the frequency of sediment disturbance due to oscillatory wave motion on the seabed. The zone of occasional storm reworking extends into deeper water in the east. The turbulent nearshore zone probably acts as an important conduit for moving sediment from the proximal delta area eastwards along the coast; much of this transport may occur in a bottom boundary layer under the combined effects of oscillatory waves and wind-driven currents. It is of significance to note that most of the wave energy (hence transport potential) is concentrated in westerly storms that also drive eastward wind-driven currents and deflect the surface plume of the Mackenzie River to the east."

A number of major uncertainties remain in the present understanding of sediment dispersal in the Canadian Beaufort Sea. In particular, understanding of the sediment fate is poor: shelf accumulation is estimated to account for 50 to 80% of sediment sources, and the volume and distribution of sediment lost beyond the shelf is not known. The presence of sand lenses in cores obtained at mid-shelf locations indicate that sediment transport may be more active than presently thought; however, it is not known whether these sand deposits reflect an ongoing process or relict processes which occurred during lower sea level stands.

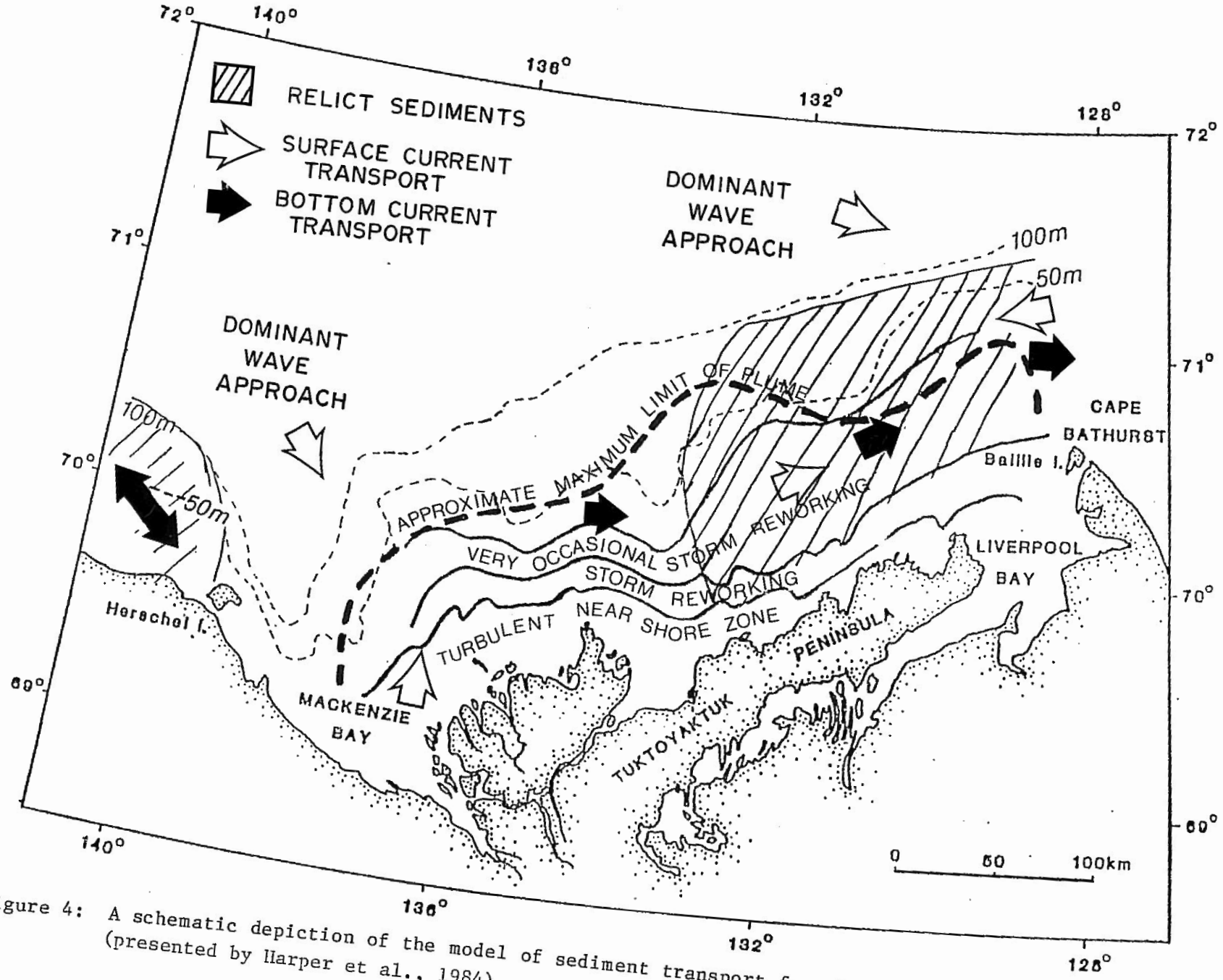

Figure 4: A schematic depiction of the model of sediment transport for the Canadian Beaufort Sea Shelf (presented by Harper et al., 1984).

Finally, near-bottom maxima in vertical profiles of turbidity have been widely measured (Bornhold, 1975; Giovando and Herlinveaux, 1981) at locations extending out to the continental slope; this feature would not be anticipated in view of the low wave and current energies presented in the results of Harper et al. (1984).

1.3 STUDY OBJECTIVES AND ORGANIZATION

The objective of this study was to provide an improved quantitative evaluation of suspended sediment transport in the Canadian Beaufort Sea, building upon the results of the recent studies of Harper and Penland (1982) and Harper et al. (1984). Particular emphasis was placed on transport in the near-bottom boundary layer over the middle and outer portions of the continental shelf (depths >10 m). As noted above, empirical evidence (bottom sediment distributions and turbidity profiles) suggests that significant sediment transports are occurring over most of the continental shelf; the physical mechanisms responsible are not well understood.

Analyses were carried out on existing data to provide more insight into some of the important physical processes involved in sediment transport:

a) An analysis of bottom current meter data to delineate the importance of various physical processes (inertial oscillations, tidal, wind and longer period motions).

b) An analysis of synchronous CTD and transmissivity profile data to determine the spatial scales of suspended transport and to identify, where possible, relationships to thermohaline circulation, fluvial-sediment discharge, and wind forcing.

c) Examination of other relevant aspects of the physical environment: surface winds, waves, fetch (extent of open water between coastline and pack ice edge), and the Mackenzie River sediment and volume discharges.

A description of important aspects of the physical environment (Mackenzie River input, surface winds, sea-ice cover and the physical oceanography), with emphasis on the temporal and spatial variability, is presented in Section 2. The results of the analyses using existing data are detailed in Section 3. In order to define all significant portions of sediment transport in the Canadian Beaufort Sea, from discharge input through the Mackenzie River to final deposition (or advection outside of the

study area), a conceptual model is presented in Section 4. This approach is intended to highlight the extent of our present understanding, and equally important, to identify the most significant deficiencies. Based on this approach, summary and conclusions are given in Section 5 and recommendations for future research are provided in Section 6.

2. DESCRIPTION OF THE PHYSICAL ENVIRONMENT

In this section, aspects of the physical environment, important in relation to sediment dispersal, are identified. These processes are described according to known temporal and spatial scales of variability.

2.1 MACKENZIE RIVER DISCHARGE

The longest continuous record of Mackenzie River daily volume transport has been obtained at a site just upstream from the junction with Arctic Red River (plots for 1973 to 1982 inclusive are presented in Appendix A). Freshet on the river commences in early May, following a period of reduced but nearly constant flow over the winter and early spring. Peak discharge levels occur in late May or June, with maximum values ranging from 26,000 m^3/s (1980) to 32,000 m^3/s (1976). Following the rapid increase in flows of the freshet, significant variations in discharge occurring over synoptic periods (a few to several days) are superimposed on the general trend to reduced levels throughout summer and autumn. In addition, interannual variability is largest for the summer; compare, for example, the generally high levels of July and August 1974 with the reduced levels of 1978.

For the purposes of the present study, the quantity of primary interest is river sediment transport rather than volume transport. Unfortunately, the amount of available sediment data is limited. Data at Arctic Red River only were available for portions of three years (1974, 1980 and 1981), while data were also available at a location further downstream, East Channel at Inuvik in 1975. Sediment discharges (plotted in Appendix A by individual years, where available) appear to fall off very rapidly following freshet. However, on some occasions very large increases in sediment discharge levels were evident over synoptic periods accompanied by comparatively minor peaks in the volume discharge. This non-linear relationship is most evident over a five-day period, August 9-14, 1974, when sediment levels attained values (26,000 tonnes/day) that far surpassed the monthly mean levels for August of 1974 (900 tonnes/day, excluding this one event) or the maximum levels recorded in other years at this same site (1200 tonnes/day in 1980, 175 tonnes/day in 1981). While the causes of the large synoptic and interannual variations in sediment discharge are not well documented, it seems probable that they are associated with events (e.g. collapse of banks) in comparatively small portions of the drainage basin. The absence of a simple relationship between sediment and volume transport (Figures 5 and 6) and the large degree of interannual

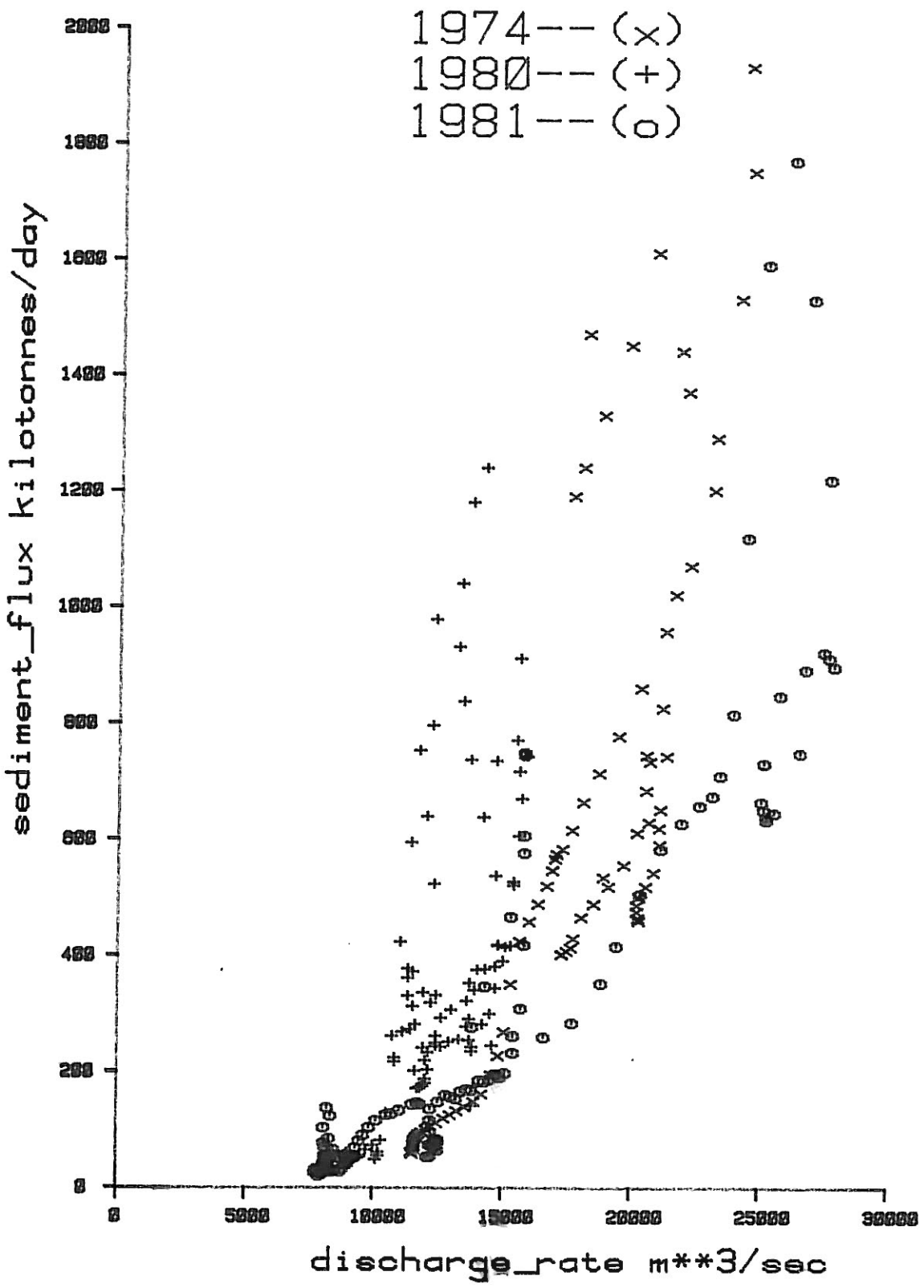

Figure 5: A scatter plot of sediment transport rate versus volume discharge rate on the Mackenzie River, at Arctic Red River for the summer of 1974, 1980 and 1981. Note that in the summer of 1974, the peak values occurring above 2,000 kilotonnes/day are not shown.

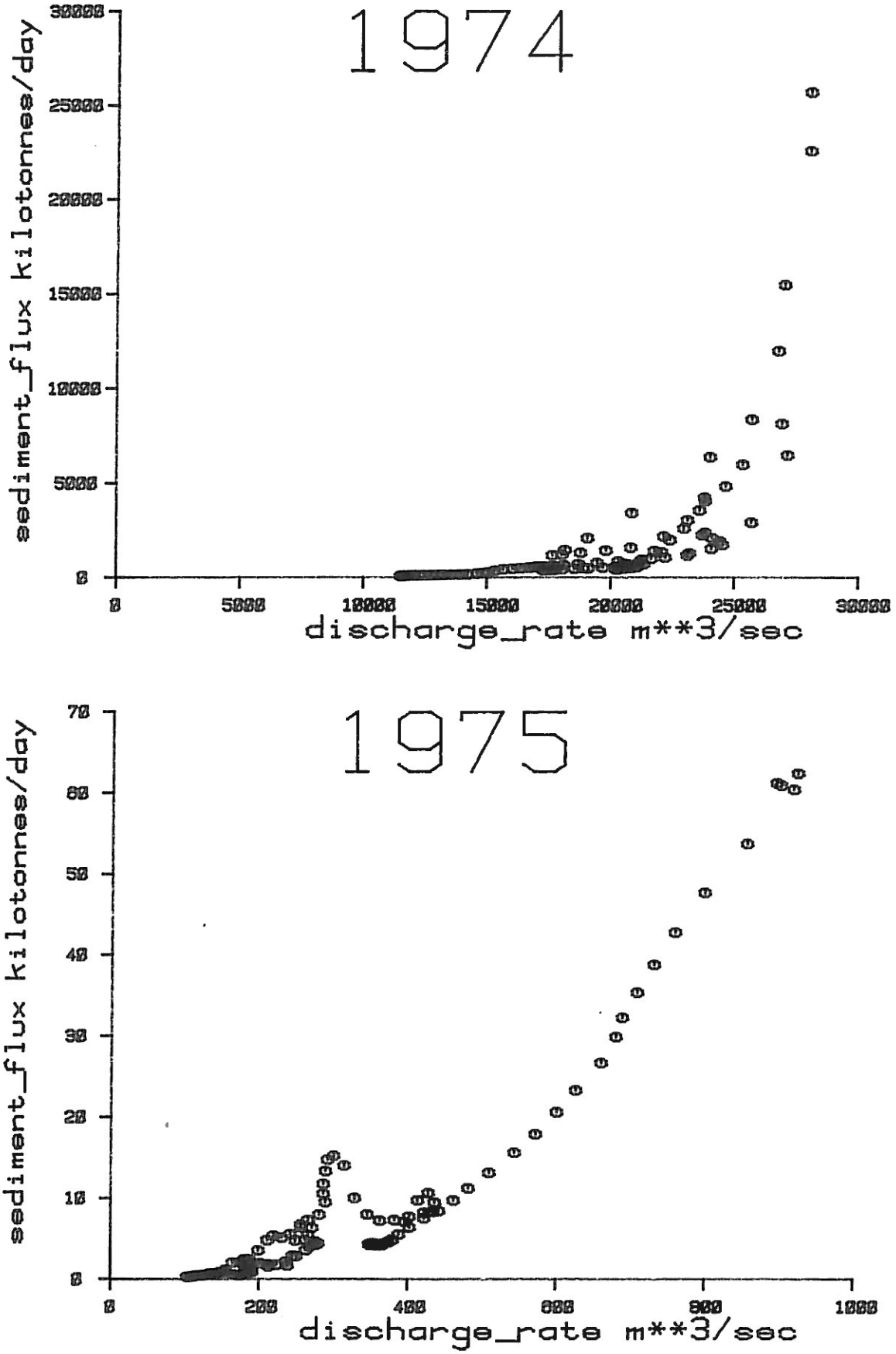

Figure 6: A scatter plot of sediment transport rate versus volume discharge rate in the Mackenzie River: a) at Arctic Red River, June 20-September 30, 1974 and b) at Inuvik on East Channel, June 1-September 30, 1975.

ariability, precludes any possibility of using the longer data base available for volume discharge as an index of sediment discharge.

2.2 SURFACE WINDS

Once sediments have entered the Beaufort Sea proper, surface winds, through the generation of waves and currents, are the dominant driving force in producing sediment transport.

Winds over the Beaufort Sea follow a marked bimodal character with the most frequent winds blowing from the northerly to westerly sector and from the southeasterly to northeasterly sector.

Directional distributions (Figure 7) based on wind measurements from coastal stations (Harper and Penland, 1982) reveal that virtually all strong winds with speeds in excess of 40 km/h (11.1 m/s) are from the northwest (i.e. northwesterly). However, a survey of easily accessible summer wind data (Figure 8) from offshore locations indicates that considerable interannual variability is present in the summer wind roses for high wind speeds. In some years (e.g. 1979 and 1982) occurrences of strong easterly winds are more common than westerly winds while in other years, strong easterly winds are virtually non-existent.

Danard and Gray (1984) have computed extreme summer winds for the Beaufort Sea based on a statistical analysis of Tuktoyaktuk hourly winds measured in the months June to October, 1979 to 1982 inclusive. During this period, the highest measured wind speed was 18.9 m/s. By fitting the wind speed data to a Gumbel distribution, Danard and Gray (1984) derived extreme winds for Tuktoyaktuk as: 15.7 m/s (2 year return period), 18.1 m/s (5 years), 19.7 m/s (10 years), 21.8 m/s (25 years), 23.3 m/s (50 years) and 24.1 m/s (70 years).

Hodgins et al. (1981) have noted the existence of two classes of extreme storms in the Beaufort Sea. The first of these are a result of large scale (approx. 1,000 km) low pressure systems travelling from west to east, often centred over the ice pack edge. These storms can be determined as geostrophic winds from large-scale pressure charts, although an absence of offshore data points presents limitations to this method. A second storm type occurs as deep low pressure systems of much smaller spatial scale, with peak wind speeds of up to 20 m/s. Such storms are not resolvable on standard pressure charts, having distance scales of 75 to 200 km. Hodgins et al. (1981) suggest that these

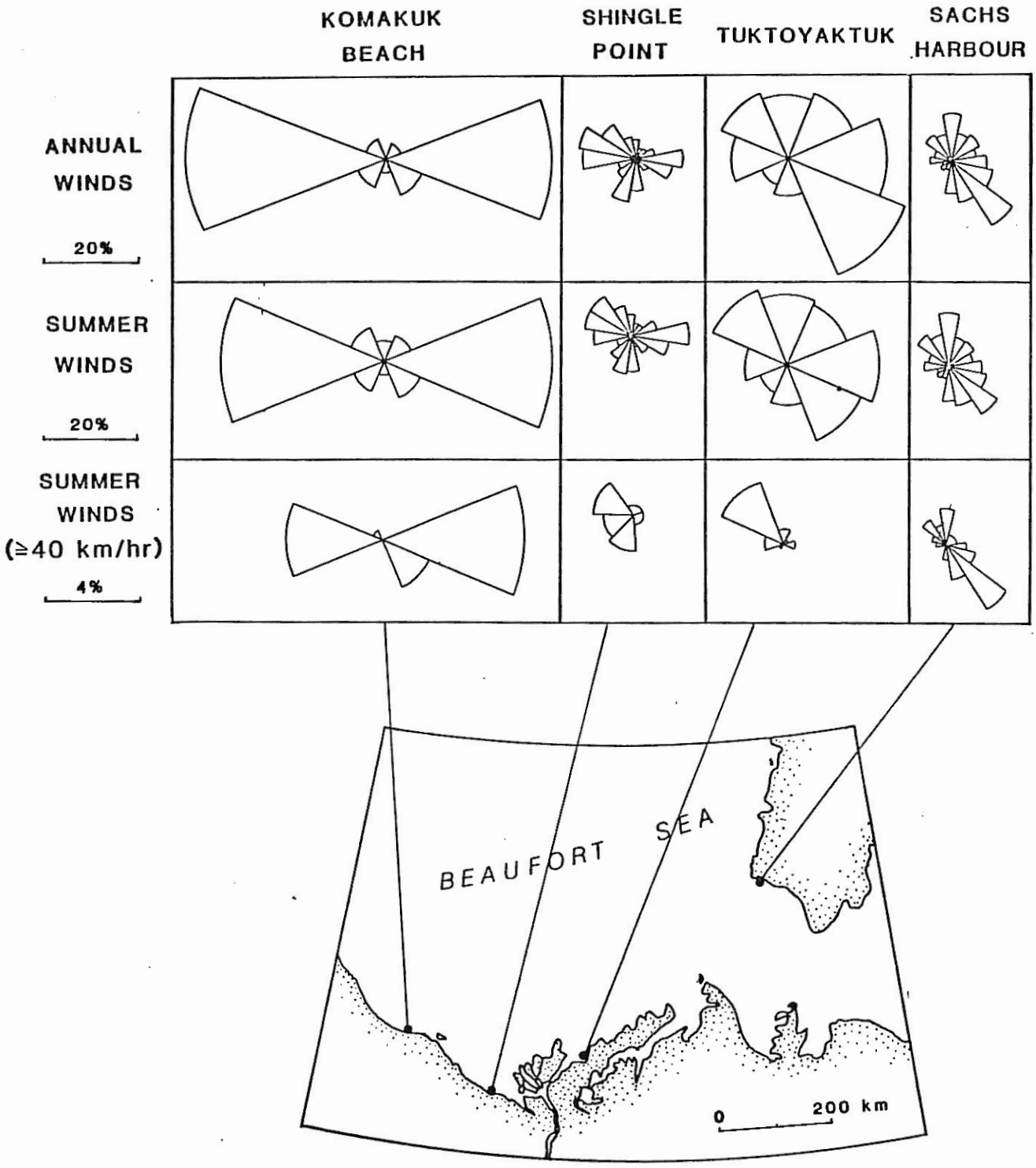

Figure 7: The directional distribution of winds at stations along the Beaufort Sea coast (from Harper and Penland, 1982). The number of years of data used in constructing these distributions is not stated.

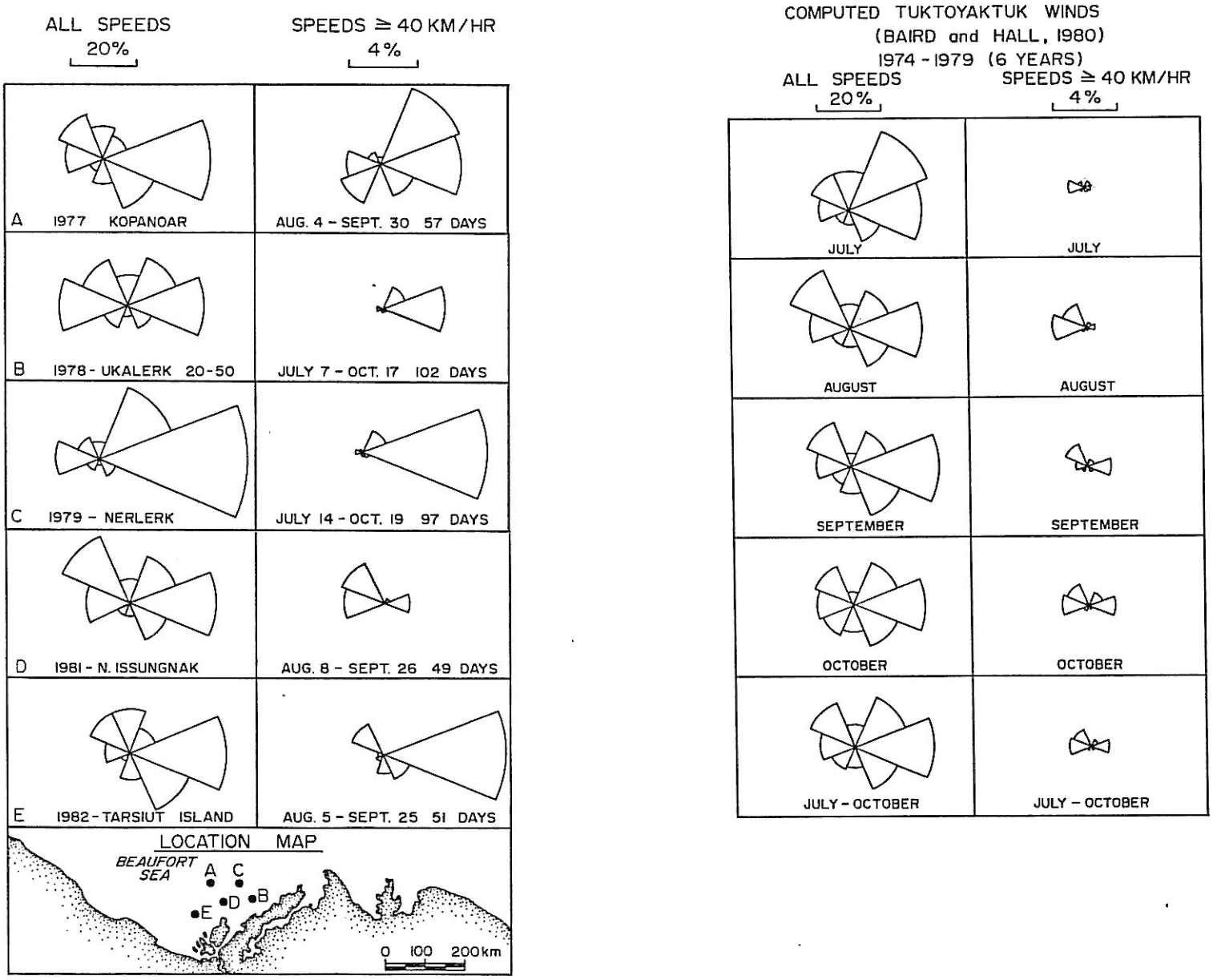

Figure 8: The directional distribution of summer winds for offshore locations in the Canadian Beaufort Sea.

intense, small-scale cyclonic disturbances result from an onshore flow of cold air originating over the pack ice. A large uptake of heat from the relatively warm open water generates instabilities resulting in an intense cyclonic disturbance.

Wind Auto-Spectra

Winds within the study area are dominated by variations over the broad synoptic time scale, from periods of 2.5 to approximately 30 days (see Figure 9). At shorter periods comparatively little variability occurs; the only significant peak occurs in summer at one cycle per day due to a weak land-sea breeze at Tuktoyaktuk. Within the broad synoptic band, individual peaks are apparent at 12-18 days, 5-8 days, and 2.5-3 days over the open-water period of summer and early autumn and peaks at 14-18 days, 5-9 days and 3.5-4 days in the ice- covered period of winter and spring.

The degree of variability in the winds at even longer periods remains unclear. The auto-spectral results (Figure 9) suggests a levelling off or possibly a decrease in activity at these very long periods. An examination of averaged monthly wind statistics over many years of observations published by AES (Canadian Climate Normals, Volume 5 - Wind) at Tuktoyaktuk and Cape Parry (Figure 10) suggests that the amplitude of the annual cycle in the surface winds is small. Monthly wind speeds remain virtually constant throughout the year although there is evidence that the frequency of occurrence and mean strength of westerly and northwesterly winds increases in the autumn and winter months while the easterly winds may exhibit the opposite tendency. On the basis of the auto-spectral results (Figure 9), synoptic activity in the wind field is generally somewhat larger in the period of ice cover (November-May) than at times of open water (July-October), particularly at periods greater than 5 days.

2.2.1 COMPARISON OF WINDS AT TUKTOYAKTUK WITH WINDS OFFSHORE

Background

Wind measurements are obtained routinely at Tuktoyaktuk every 6 hours by the Atmospheric Environment Service (AES). The availability of these data year-round over the past several years makes them attractive for use in studies involving wind forcing over the continental shelf of the Beaufort Sea. Comparisons between the winds at Tuktoyaktuk and those offshore were carried out to determine the applicability of the former to the offshore in the Canadian Beaufort Sea.

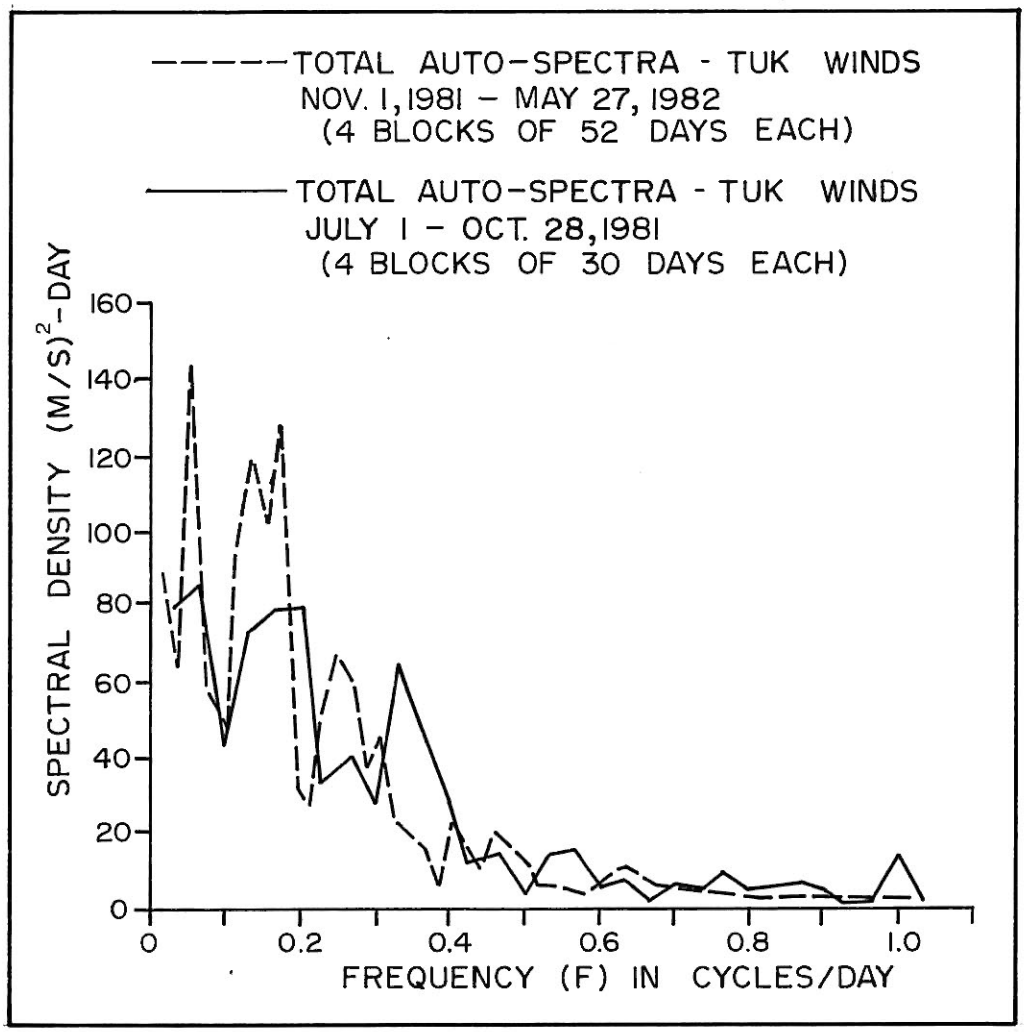

Figure 9: Auto-spectra of Tuktoyaktuk winds for summer (July 1-October 28, 1981) and winter (November 1, 1981-May 27, 1982) conditions.

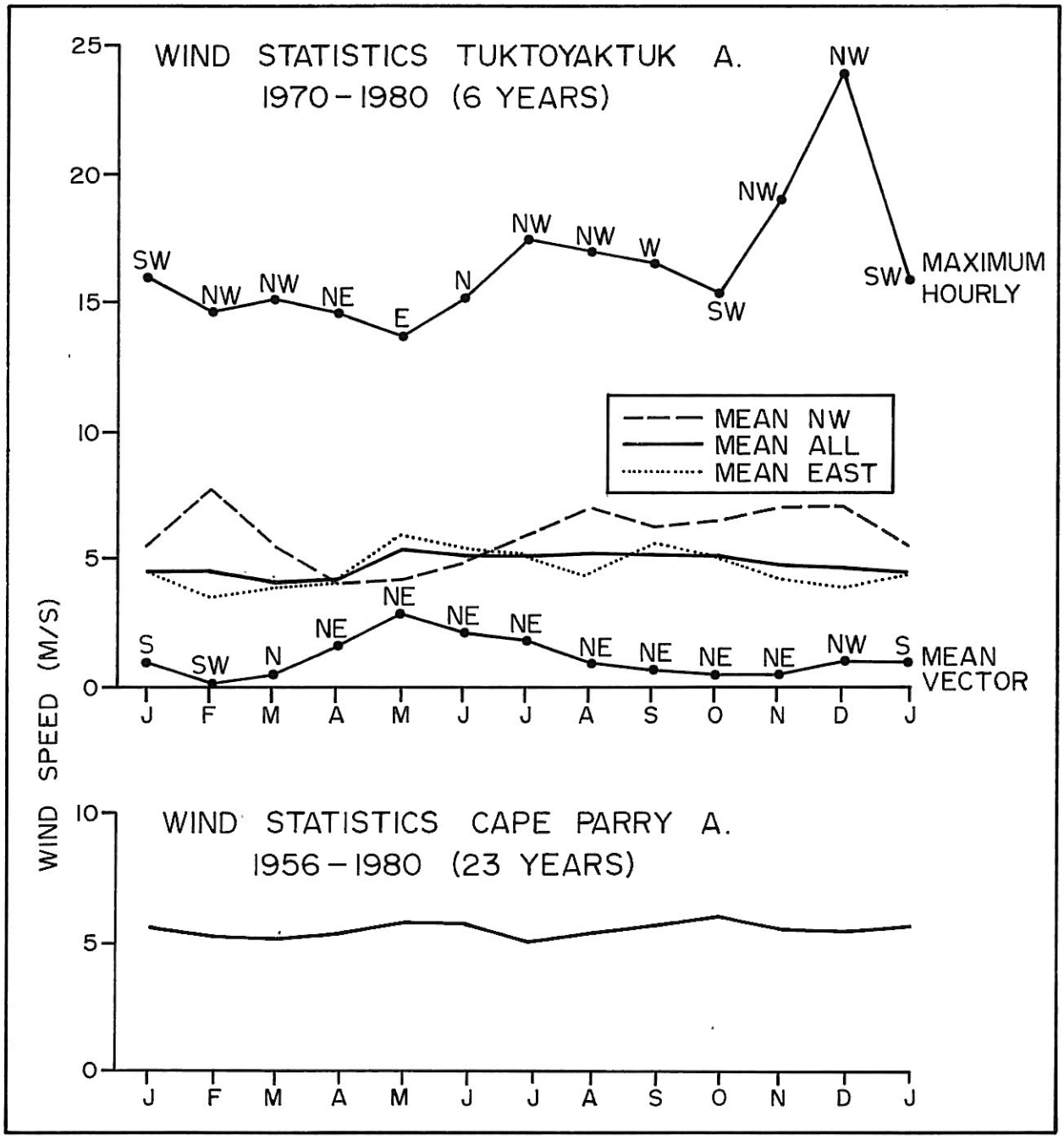

Figure 10: Seasonal variations in wind speed statistics for Tuktoyaktuk and Cape Parry.

Winds measured at shore stations are generally weaker than those over the adjacent waters. Richards et al. (1966) showed that the ratio of overwater to overland wind speeds varied with the wind speed itself, atmospheric stability (air temperature minus water temperature), and fetch. The ratios determined by Richards et al. (1966) ranged from 0.75 and 3.0. For moderate winds (5.5-8.5 m/s) and stable atmospheric conditions, the ratios were between 0.9 and 1.75. At a constant atmospheric stability, the wind ratio became smaller as the wind speed increased (Figure 11). The profile of the wind ratio appeared to increase exponentially as the wind speed approached zero. Baird and Hall (1980) criticized these results, claiming an overestimation of wind speed over water at low speeds. Based on comparisons of speed histograms for on- and offshore their calculated water/land speed ratios had a much narrower range, from 1.0 to 1.15, with the higher values centred near 7 m/s (Figure 11).

Using a more theoretical approach, McKay (1966) developed the relation $R=(Z/10)^N$; where Z is the height at which surface topography becomes insignificant, and N depends on the difference in roughness of the land and water surfaces. This equation does not apply for light wind conditions. Berry et al. (1975), as part of the Beaufort Sea Project, used McKay's equation and predicted a value of R = 1.22 for Tuktoyaktuk; i.e. the offshore winds should be 1.22 times those measured at Tuktoyaktuk.

In this study, regression analyses have been applied to simultaneous wind measurements obtained at Tuktoyaktuk and at offshore drilling platforms in order to determine water/land wind ratios and direction shift. The offshore data sets used were: Kopanoar, August 4-September 30, 1977; Nektoralik, July 31-October 13, 1977; Nerlerk, July 14-October 19, 1979; Issungnak, August 8-September 27, 1981; and Tarsiut, August 5-September 25, 1982. Figure 12 shows the locations of these sites. All offshore wind data were converted to 10 m equivalent height using the relationship of Bussinger (1973), assuming neutral atmospheric stability. The required adjustments to 10 m height will vary according to atmospheric conditions and may also be influenced by flow interference of the drillship's superstructure. However, these effects are expected to be negligible over the many samples used in this study.

Kopanoar/Tuktoyaktuk Regression

The regression analysis for the 1977 Kopanoar wind data were carried out in more detail than for other offshore data sets. Hourly drillship wind data were subsampled at 6-hourly intervals

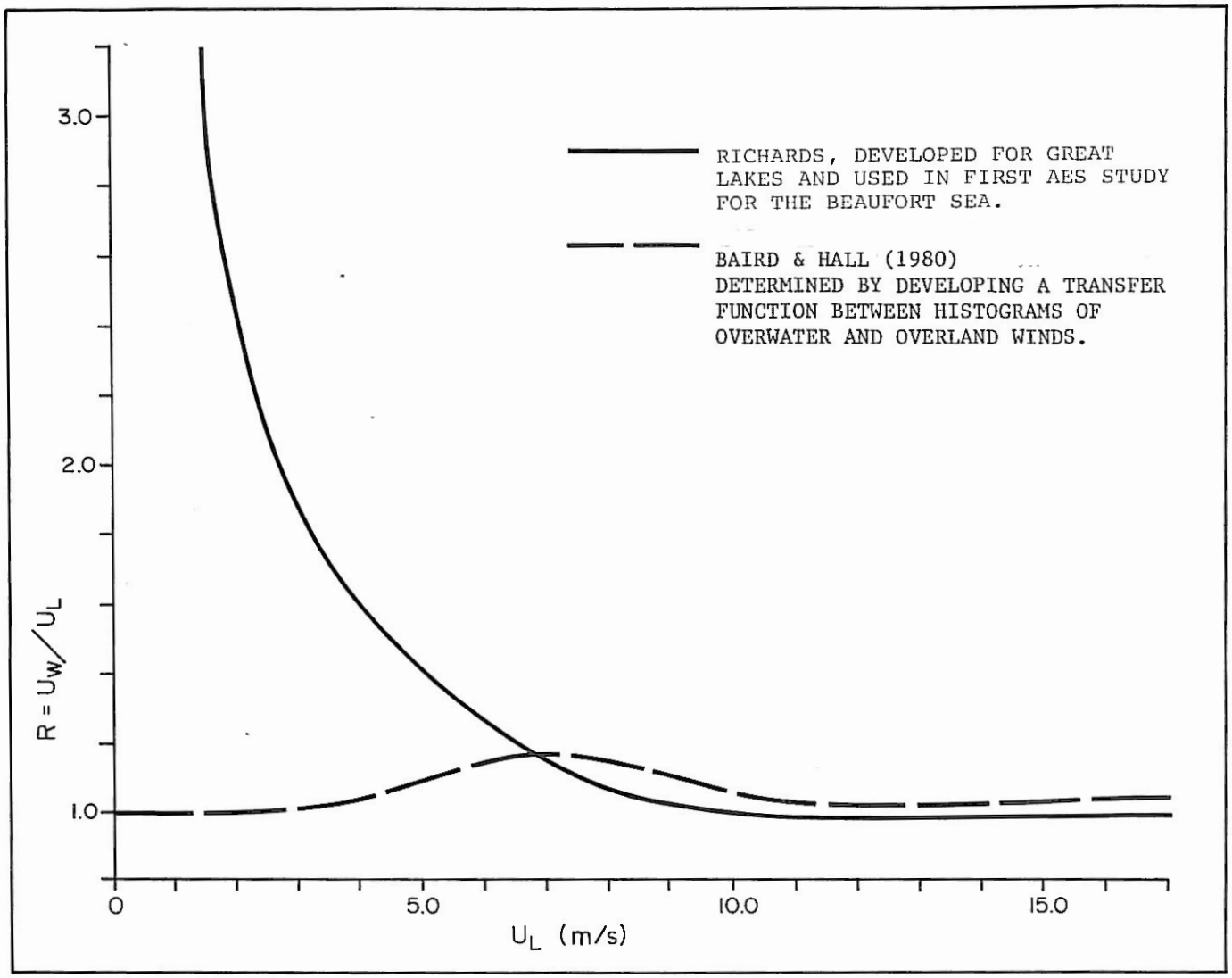

Figure 11: The ratio of overwater (U_W) to overland (U_L) wind speed as a function of overland wind speed (U_L), as derived by Richards et al. (1966) and Baird and Hall (1980).

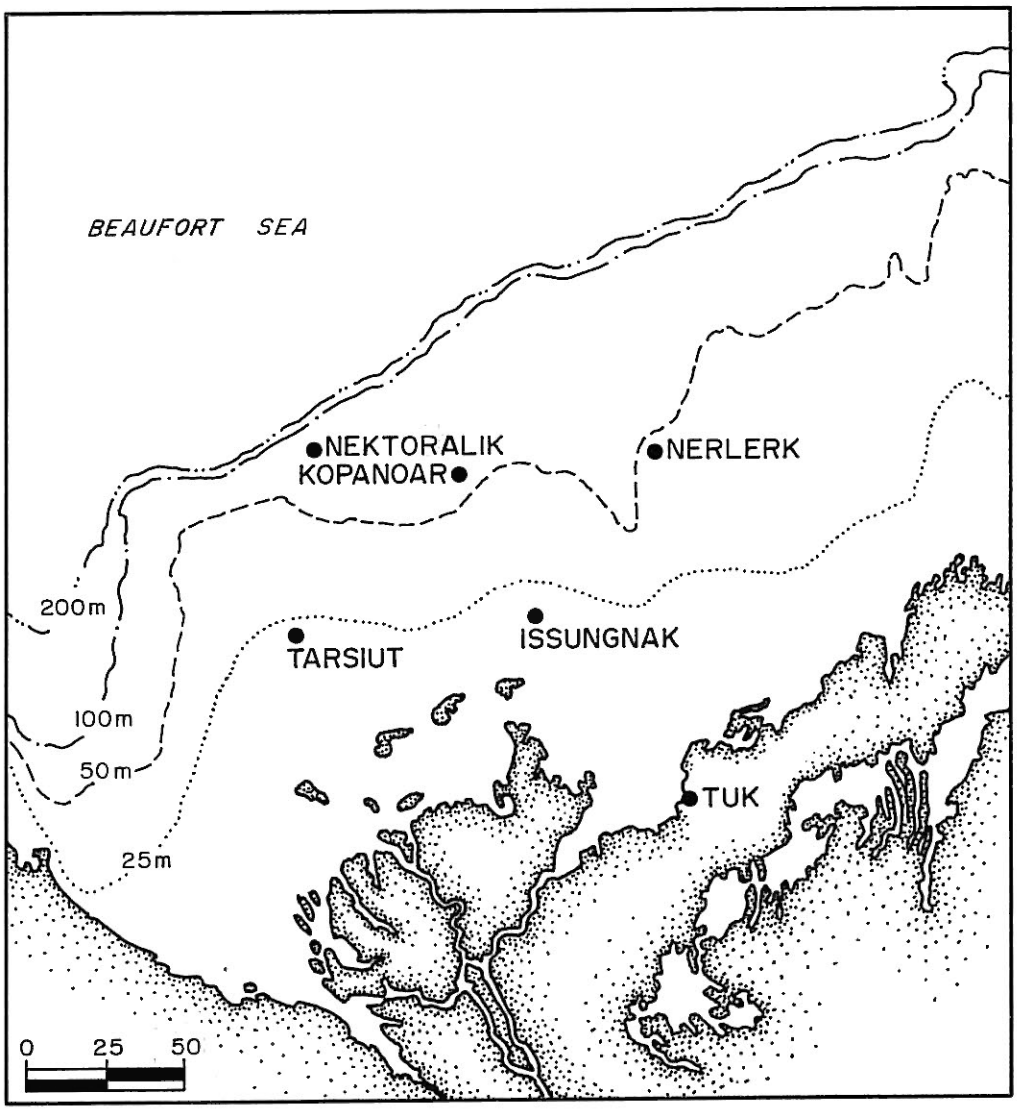

Figure 12: The locations of offshore wind data used in regression analyses with wind data at Tuktoyaktuk.

to be consistent with the available Tuktoyaktuk data. Correlation analyses revealed the Tuktoyaktuk signal to be consistently leading the offshore winds by about 6 hours. All Kopanoar/Tuktoyaktuk regressions were subsequently done with the Tuktoyaktuk record lagged by one record (6 hours). The results are shown in Figure 13. All data have been used, with no distinction by speed class, atmospheric stability, or fetch.

The dominant winds were oriented east-west. The regression analysis results indicate that the E-W wind component measured offshore is 19% larger than at Tuktoyaktuk. The ratio for total wind speed, water to land, is 1.29. The two directional records are generally in good agreement; the least square fit suggests a slope of 0.98 with a zero intercept. Given the Tuktoyaktuk wind direction, the direction offshore can be predicted to better than $\pm 40°$.

Because winds with lesser speeds (below 4 m/s) do not contribute significantly to the forcing of the shelf dynamics, regression analyses were also carried out separately using only those data where the marine wind speed was $\geq$ 4 m/s (Figure 14), and $\geq$ 8 m/s (Figure 15). As expected, the correlation coefficients for wind components and directions improve markedly. The direction records continued to agree well given the Tuktoyaktuk wind direction for wind speed $\geq$8 m/s, the wind direction offshore could generally be predicted to within $\pm 25°$. The offshore to Tuktoyaktuk ratio of wind speed increases however, as the range of speeds increases:

Table 1: The regression coefficient for winds measured at offshore locations with Tuktoyaktuk winds given for all wind speeds and wind speed classes exceeding 4 m/s and 8 m/s.

	Marine Wind Speed Class		
Water/Land Ratio	**All**	**$\geq$ 4 m/s**	**$\geq$ 8 m/s**
Speed	1.29	1.34	1.47
EW Component	1.19	1.20	1.32

Other Regression Analyses

Regression analyses were then performed using the four other marine wind data sets. The Tuktoyaktuk records were lagged by 6 or 12 hours in order to best fit the marine records using wind speeds. The results are presented in Table 2. (Note that the

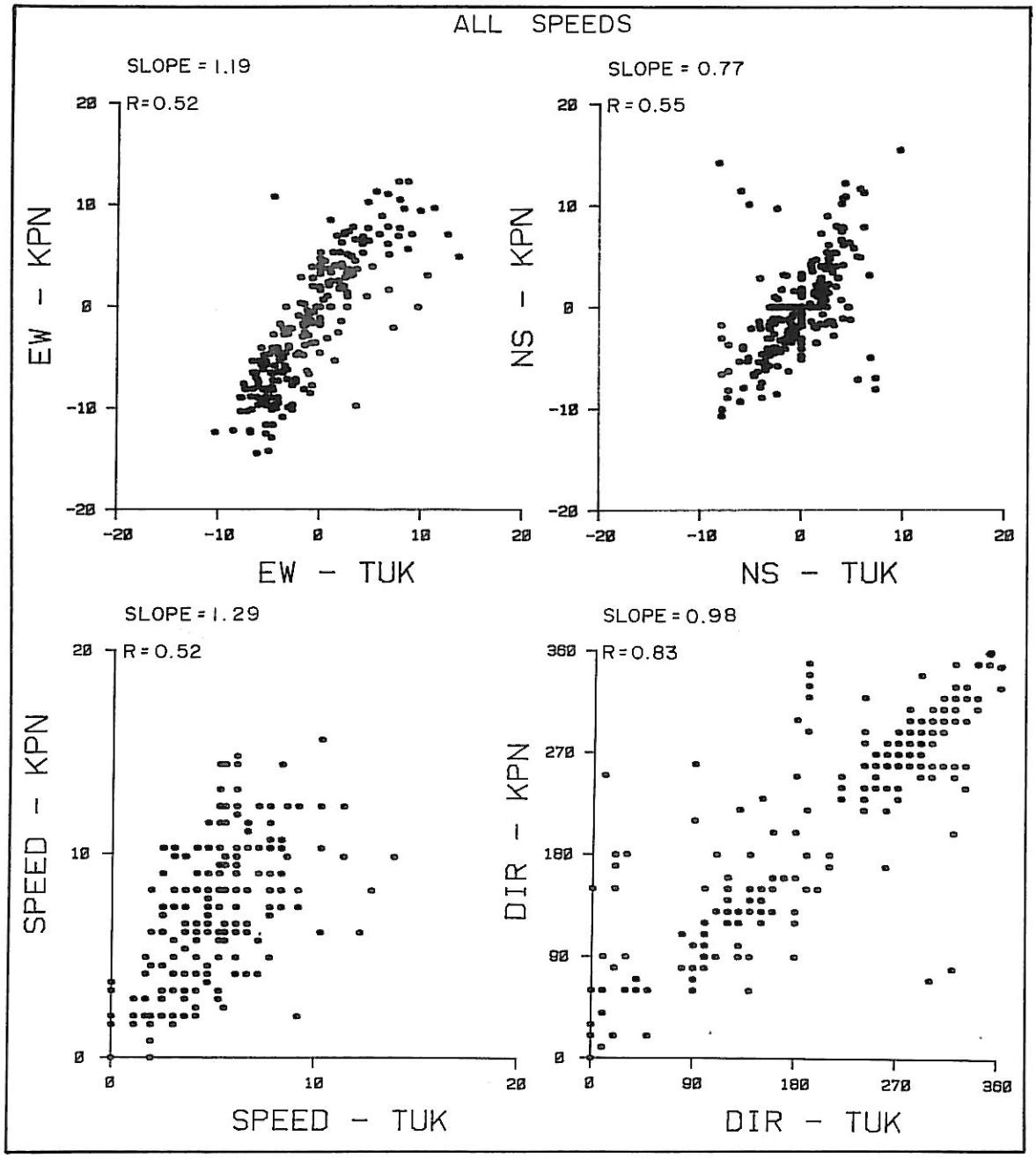

Figure 13: Scatter plots for all offshore winds as measured at Kopanoar (KPN) and at Tuktoyaktuk, August 4-September 30, 1977. The regression fits have been contained through zero.

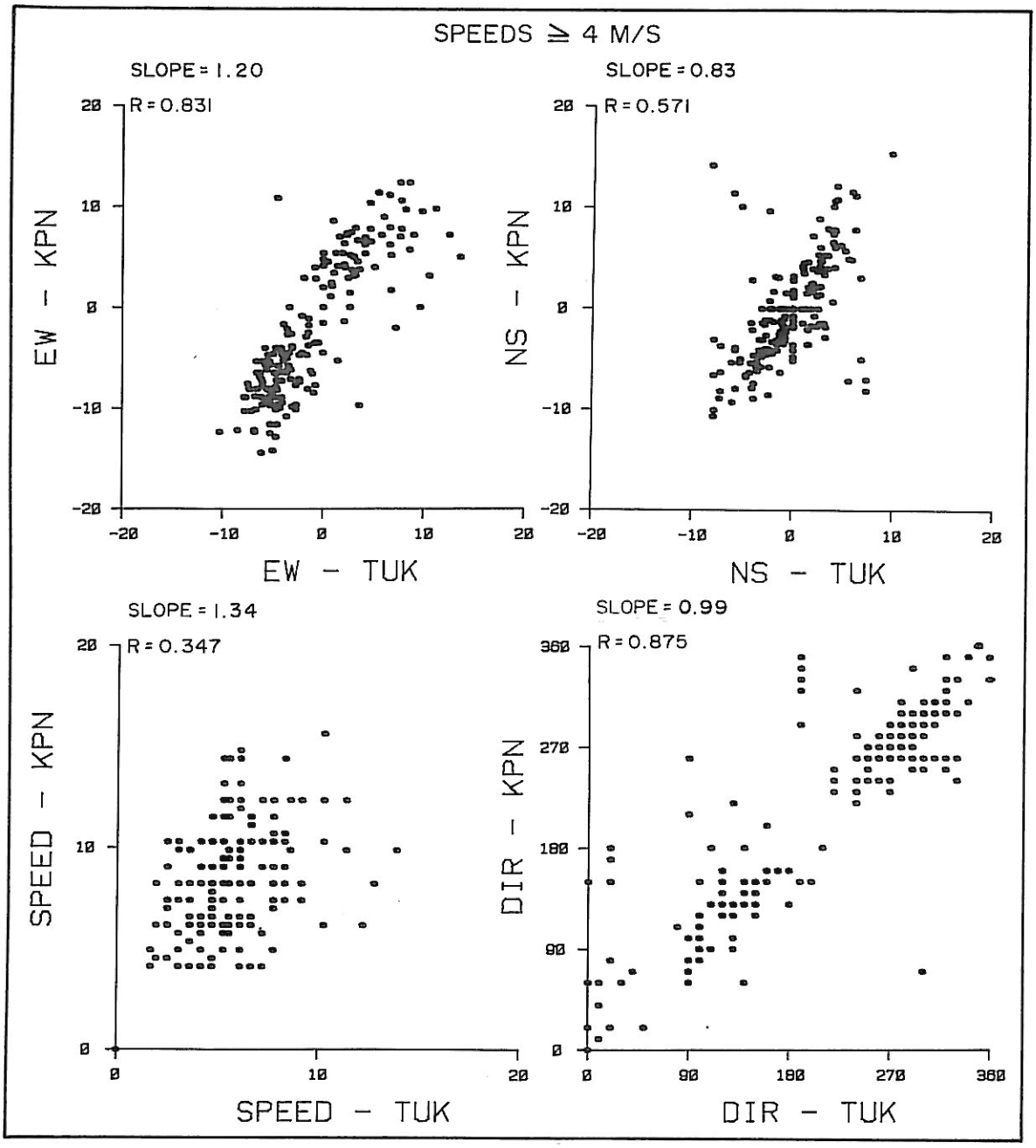

Figure 14: Scatter plots for offshore winds as measured at Kopanoar (KPN) and at Tuktoyaktuk, August 4-September 30, 1977, excluding winds <4 m/s at Tuktoyaktuk. The regression fits have been contained through zero.

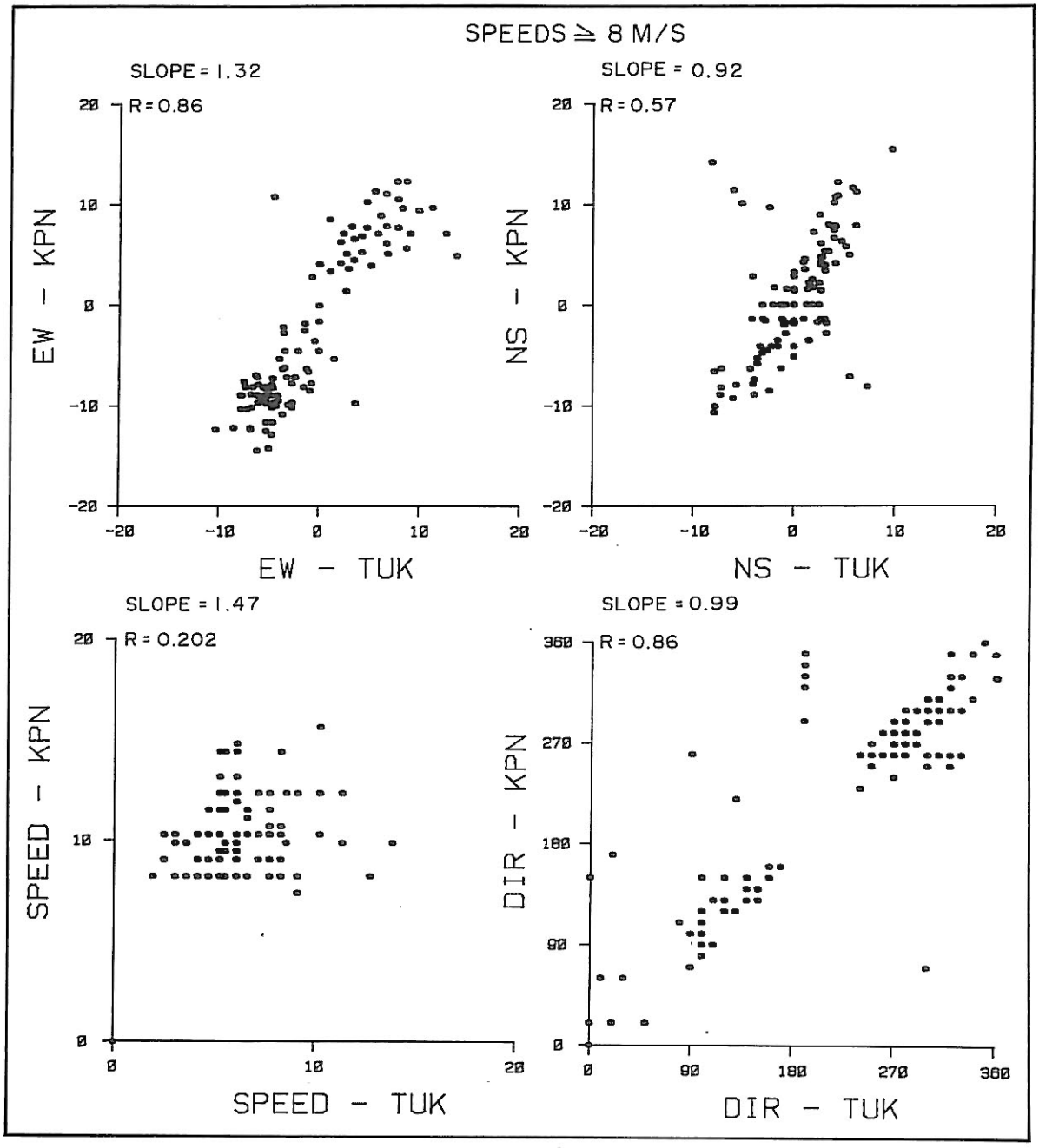

Figure 15: Scatter plots for offshore winds as measured at Kopanoar (KPN) and at Tuktoyaktuk, August 4-September 30, 1977, excluding winds <8 m/s at Tuktoyaktuk. The regression fits have been contained through zero.

results derived from the Issungnak data are anomalous although no explanation could be found for this.)

Using the results from these other four sites, offshore winds are generally 20 to 30% larger than those measured at Tuktoyaktuk. For winds over 8 m/s the water/land wind speed ratio is often larger, in the 1.33 to 1.55 range. In cases where no offshore wind data are available, the best approximation can be obtained by increasing the Tuktoyaktuk wind speeds by 20%. The wind direction offshore is typically within 10° of that at Tuktoyaktuk, particularly for wind events with speeds exceeding 8 m/s. However, in the Nerlerk 1979 and the Issungnak 1981 cases, the wind direction offshore was 20-30° and 10-20° respectively to the left of the direction at Tuktoyaktuk for roughly 75% of the wind events with speeds exceeding 8 m/s. Baird and Hall (1980) note that wind directions measured at Tuktoyaktuk were unreliable in 1978 and 1979. Therefore the 20-30° difference of 1979 may not be significant. The computed 6 to 12 hour lag of the offshore winds behind those of Tuktoyaktuk are puzzling; in the absence of any obvious physical explanation, there may be a systematic difference in the wind data such as inconsistent time zones.

Table 2: Summary of the wind ratio regression results for all wind speed classes, based on comparisons of data from 5 offshore sites with the Tuktoyaktuk winds.

Offshore Sites	Period	Water/Land Ratio		Hours Tuk Leading for Best Fit
A. Kopanoar	Aug.4- Sept.30,1977	Speed	1.29	6
		E-W	1.19	
B. Nektoralik	July 31-Oct.13,1977	Speed	1.26	6
		E-W	1.19	
C. Nerlerk	July 14-Oct.19,1979	Speed	1.23	12
		E-W	1.20	
D. Issungnak	Aug.8-Sept.27,1981	Speed	1.04	6
		EW-W	1.03	
E. Tarsiut	Aug.5-Sept.25,1982	Speed	1.27	6
		EW	1.20	

Since the regression computations of the present study were completed, we have become aware of a similar analysis carried out by Danard and Gray (1984). In this latter study, wind speed measurements obtained at eight offshore drilling rigs in the summer of 1982 were compared with simultaneous Tuktoyaktuk wind data. The comparisons were limited to those wind speed observations at Tuktoyaktuk having directions from 253° through north to 073°, and speeds exceeding 5.5 m/s (20 km/h). The average wind speed ratio of offshore to Tuktoyaktuk measurements was determined to be 1.18 with "little directional difference" (Danard and Gray, 1984). This result is in good agreement with our computational results described above.

2.3 SEA-ICE

General Characteristics

The sea-ice regime of the Beaufort Sea has been described by numerous authors (Marko, 1975; Giovando and Herlinveaux, 1981; Marko et al., 1983) and most recently in the oil industry's Environmental Impact Statement (Dome Petroleum et al., 1982) in relation to regional development plans. Briefly, this aspect of the environment can be understood in terms of three more or less distinct ice regimes as represented in Figure 16:

1) The landfast ice: which begins forming around the regional shorelines in October, and by mid-winter has extended outward to cover the sea surface with essentially immobile sea-ice out to roughly the 20 m depth contour. Virtually all of this ice is less than one year old and is usually characterized by numerous ridges and their underwater keel counterparts. The latter projections often make direct contact with the sea bottom producing most of the regional seabed scouring and providing the main mechanism for the stability of the landfast ice zone over its seasonal lifetime (November to July) (see Table 3).

2) The Beaufort Sea "gyral" pack ice: which consists of preponderantly thicker, older (second- and multi-year) ice together with smaller concentrations of younger ice forms. This ice body covers the major fraction of the deep water Canadian Basin, moving on the average according to a clockwise gyre centred at approximately 76°N, 145°W (Newton, 1973).

3) The transition zone: which separates the above two extreme regions. Ice motion in this area differs

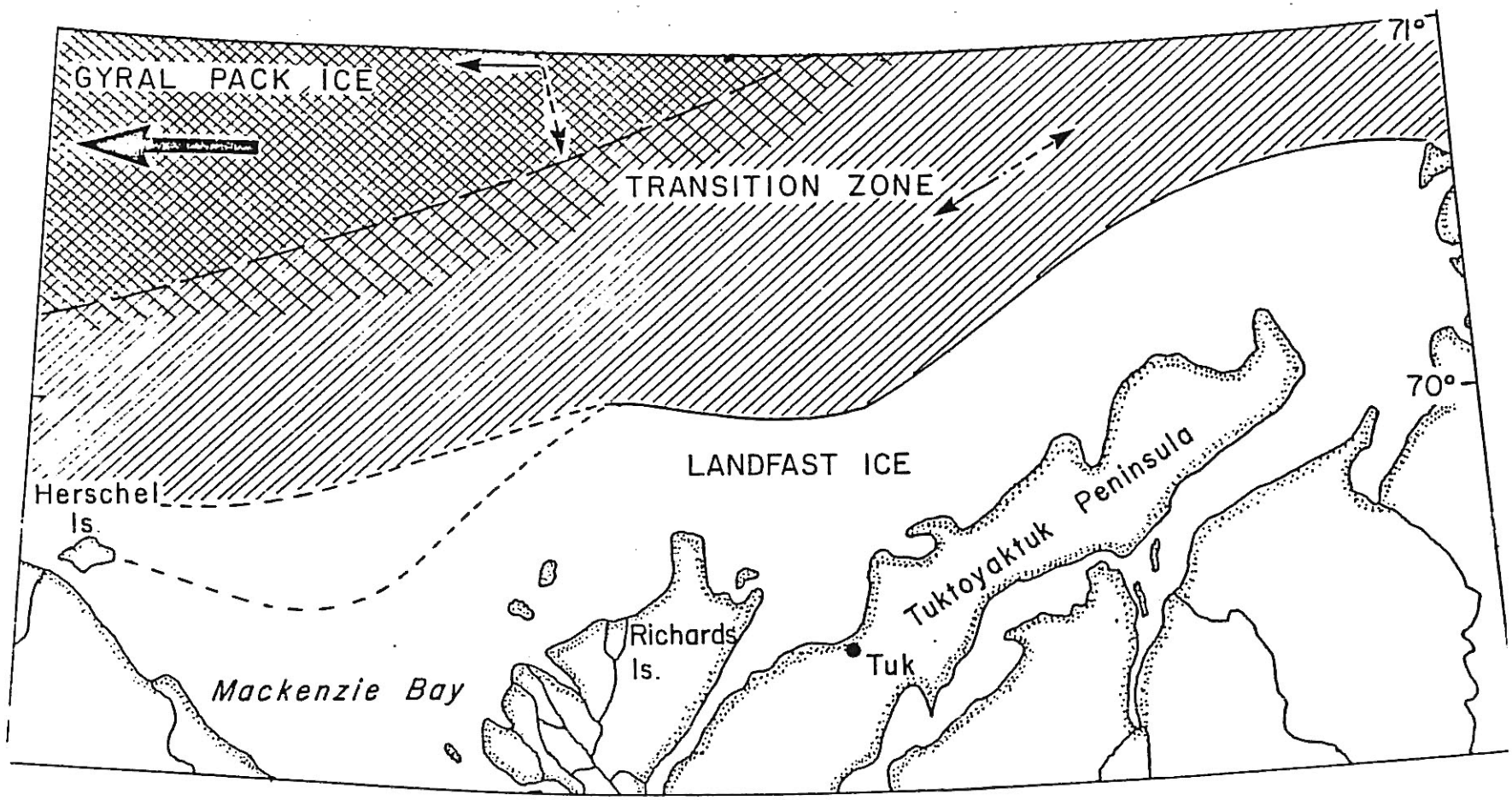

Figure 16: A schematic representation of the different ice zones of the southeastern Beaufort Sea. The large solid arrows indicate the direction of the prevailing average gyral motion while the lesser solid and broken-line arrows, respectively, represent the direction of the dominant motion in the winter-spring and summer-fall periods. The variable positioning of the landfast is indicated by broken boundaries merging at Herschel Island (from Marko et al., 1983).

slightly from that found further offshore in the pack-ice zone due to circulation effects associated with the presence of the outer continental shelf and through "frictional" interactions with the landfast ice boundary. This extremely dynamic region almost always contains considerable areas of open water or thin ice.

Table 3: Dates of important steps in the break-up and dispersal of the landfast ice (from Dome Petroleum Ltd., 1983).

Year	Fast Ice Barrier Breaches Across Mackenzie Bay	Fast Ice Barrier Breaches Across Kugmallit Bay	Landfast Ice Completely Removed
1973	June 27	June 28	July 20
1974	July 7	July 18	August 5
1975	June 24	July 1	July 15
1976	July 5	July 2	July 23
1977	June 12	June 19	July 6
1978	July 5	July 6	August 3
1979	June 19	June 30	July 22
1980	June 28	July 2	July 10
1981	June 15	June 27	July 4
1982	June 23	July 10	July 18

The growth of large areas of open water in the southeastern Beaufort Sea usually begins in the early spring (April and May) with an expansion of the transition zone open water areas by ice melting and wind-induced offshore ice movements. The rise of river discharges in late May produces open-water in the landfast ice through flooding and discoloration of the ice surface in the vicinity of the river mouths (Reimnitz et al., 1974; Marko et al., 1983). The thermal input of the River Water and the increased absorption of radiant and sensible heat in these initial melt areas eventually leads to the removal of most of the ice from the shoreward portion of the landfast ice zone. The remaining offshore portion of the landfast ice initially remains intact, effectively confining much of the warm, turbid river water in a vast nearshore lagoon. The breaching of the outer landfast ice sometime during the late-June to mid-July period releases these waters and allows their wider dispersal over the shelf.

In most years, the edge of the offshore pack and transition zone ice moves offshore during the June and July period increasing the size of the open water area which exists outside

of the rapidly clearing landfast ice zone. However, the motion of this ice edge is highly variable being closely keyed to wind speeds and directions.

To evaluate the possibility that variations in the Mackenzie River thermal input may affect the position of the offshore ice in the period after the break-up of the landfast ice (late June and July) it is relevant to examine the annual accumulated July 15 river and net atmospheric heat inputs for the 1973-1979 period.

Table 4: Annual data for the accumulated river and net atmospheric heat inputs from the start of freshet to July 15.

	Accumulated River Input Relevant to -1.5°C (Marko et al., 1983)	Accumulated Net Atmospheric Energy Input to July 15 (Includes Radiative and Turbulent Heat Exchange Terms) (from Tummers, 1980)
1973	$148 \cdot 10^{16}$cal	
1974	$142 \cdot 10^{16}$cal	$750 \cdot 10^{16}$cal
1975	$155 \cdot 10^{16}$cal	$1350 \cdot 10^{16}$cal
1976	$140 \cdot 10^{16}$cal	
1977	$145 \cdot 10^{16}$cal	
1978	$125 \cdot 10^{16}$cal	
1979	$150 \cdot 10^{16}$cal	

It is seen that the extreme range of variation in the river heat input, approximately $30 \cdot 10^{16}$, is at most a few percent of the atmospheric energy contribution which varies itself by amounts on the order of 100%. The variations in the latter dominant input are quite closely keyed to the wind fields which either remove or retain ice in the transition zone area.

The situation is somewhat different in the landfast ice zone where early in the season, because of water containment due to the presence of the ice cover and the stability of water column, the river heat input can dominate the atmospheric input. In this case, year-to-year variations in the river heat may affect the rate of melting and clearance of this ice.

The extent and location of the resulting areas of open water in the region may be deduced from the positions of the offshore ice edge as deduced from the contours of 8/10 ice concentration as extracted from the AES Canada charts of ice conditions for the 1971-1976 summer periods (Figures 17 to 19).

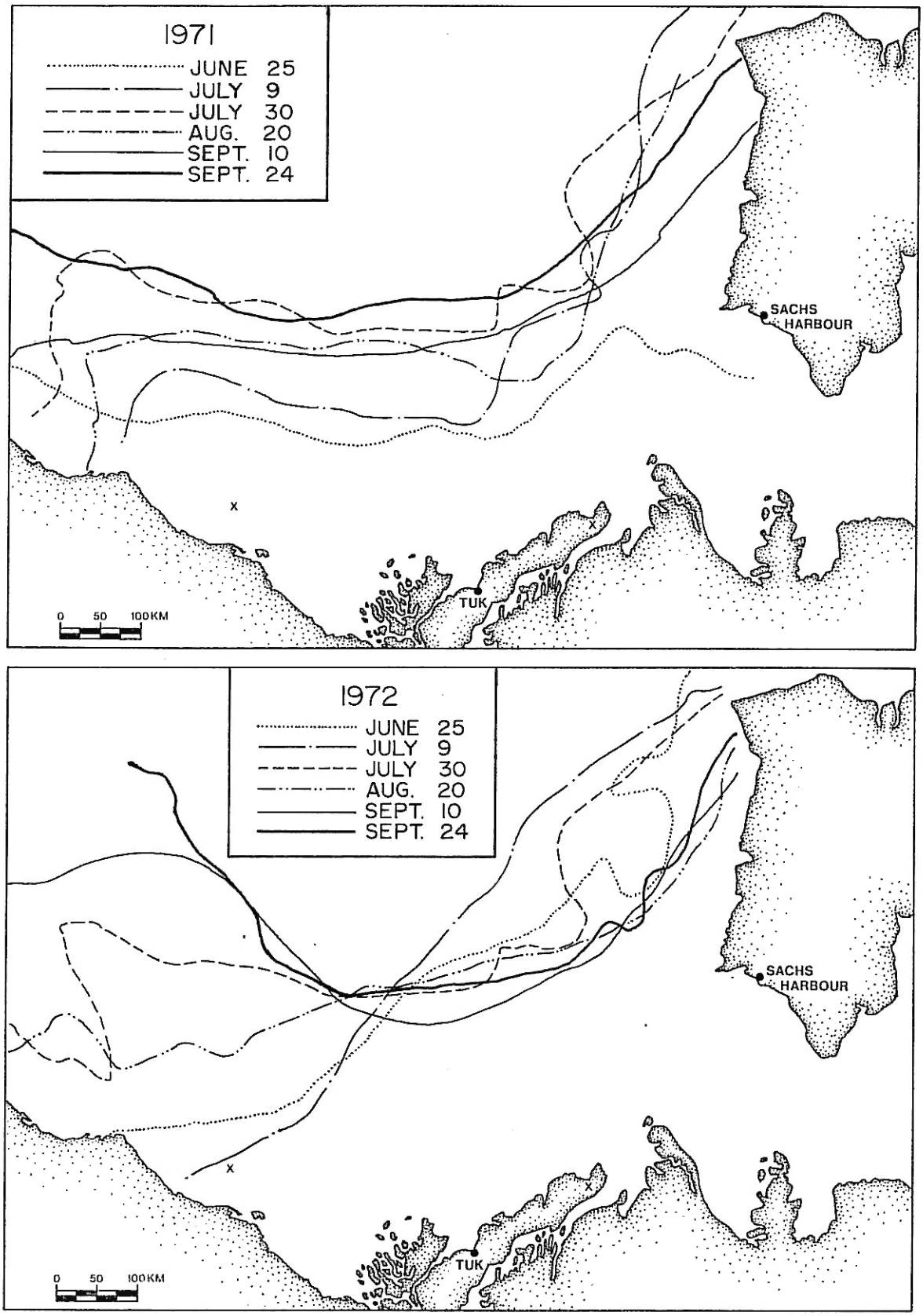

Figure 17: The position of the offshore ice edge from June 25 to September 24 for the years: a) 1971 and b) 1972.

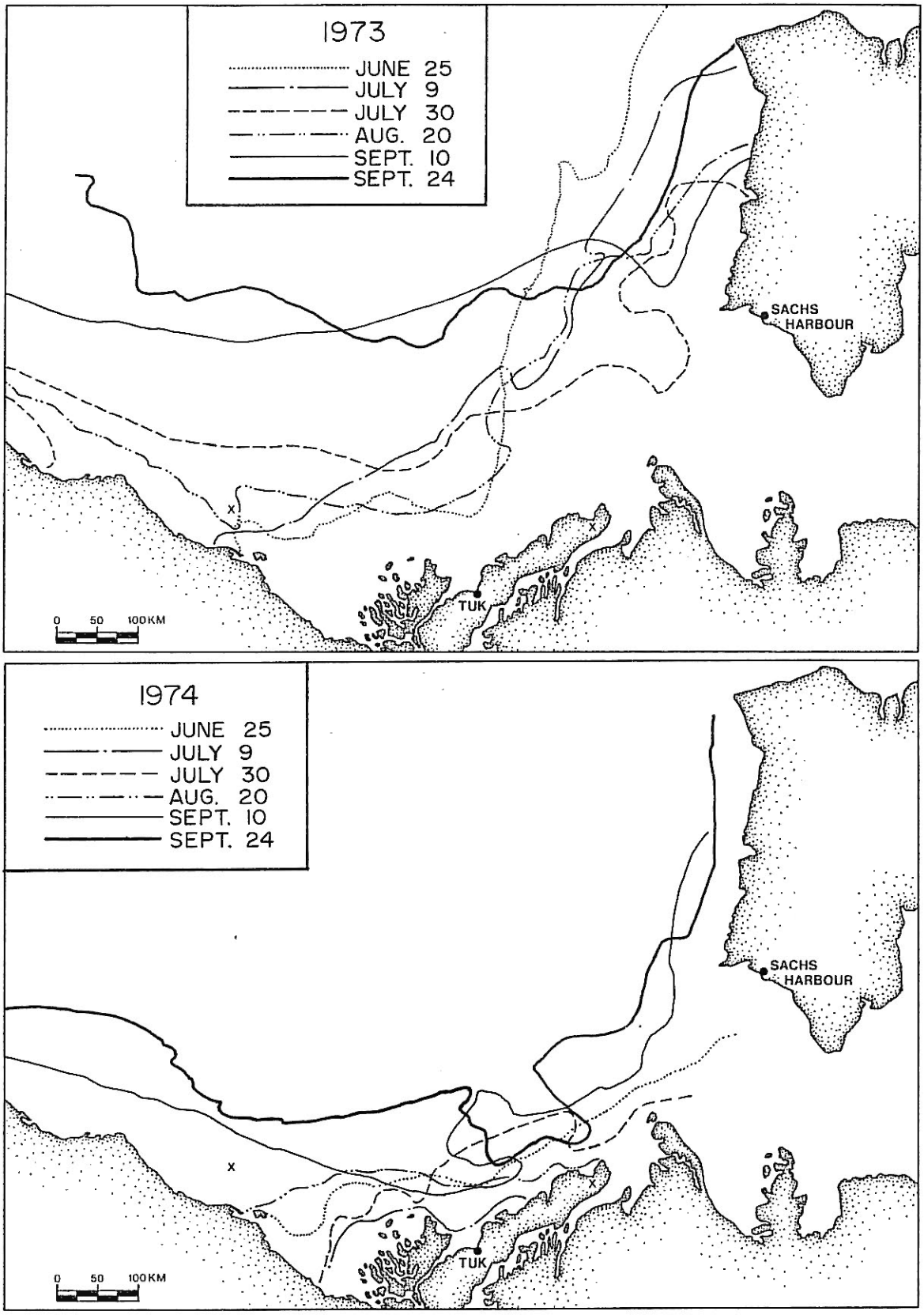

Figure 18: The position of the offshore ice edge from June 25 to September 24 for the years: a) 1973 and b) 1974.

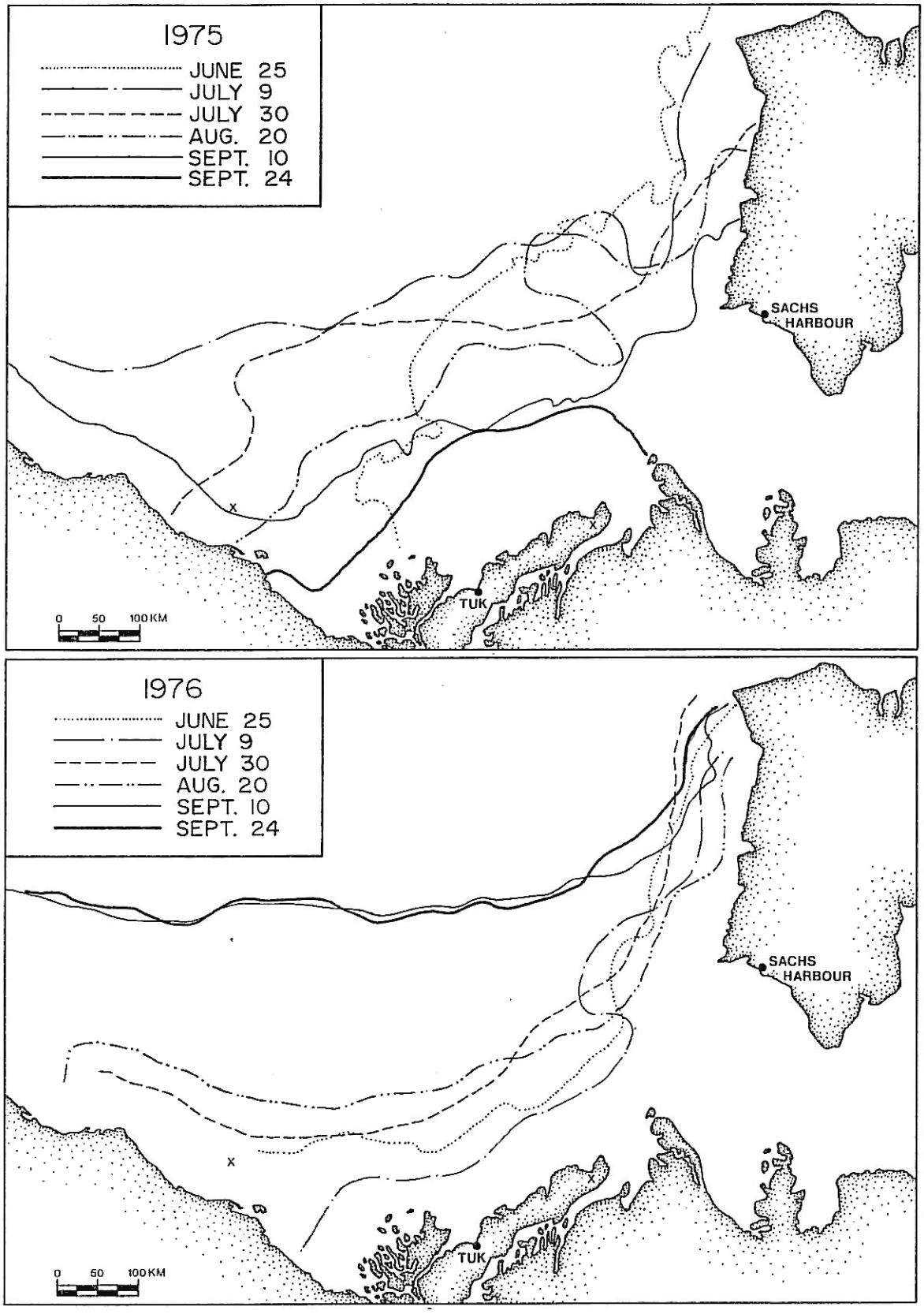

Figure 19: The position of the offshore ice edge from June 25 to September 24 for the years: a) 1975 and b) 1976.

If, for the moment, one ignores the 1974 results (Figure 18) which corresponded to minimal ice clearing due to unusually persistent onshore winds, the boundary data broadly reflect an offshore movement trend over the included late June to September period. Small reversals of the offshore trend appeared to have occurred in each August, but the retreat of the ice edge generally resumed and strengthened in the month of September. The extent of the latter late summer movements was greatest in the western portion of the region, roughly north of Mackenzie Bay. In the eastern portion of the regions adjacent to Banks Island, there is also considerable evidence of shoreward (eastward) movement of the ice edge where a convergence tends to occur involving the southerly gyral flow and westerly and northwesterly flow of ice out of Amundsen Gulf.

Movements of ice edges over the 2 to 3 week period between observations are typically on the order of 50 to 100 km with perhaps the largest shift noted between August 20 and September 10, 1976 when an edge retreat of roughly 250 km was observed. The variability between the late season ice edge positions in alternatively good (1973, 1976) and bad (1974, 1975) years can be at least as large as 300 km.

The sea-ice environment has a direct effect on sediment transport through three basic mechanisms which:

a) resuspend and transport sediments by ice keel scouring and by the advection of ice containing sediments acquired by River Water overflow and/or direct contact with the sea bottom;

b) limit the fetch and hence the effectiveness of northerly and westerly winds in generating ocean waves of sufficient amplitude and persistence to re-suspend sediments;

c) determine the position and directions of dispersal of turbid, warm River Water by physical confinement. A springtime example of this process was noted above in connection with the nearshore lagoon which annually forms in the inner portion of the landfast ice zone. In this instance, the confinement occurs because of the restriction of movement in the upper water column produced by the still intact portion of the landfast ice. A more unusual but perhaps equally significant confinement occurs in those years, such as 1974, when the offshore pack ice is held close to the boundary of

the landfast zone by onshore winds. In this case, the break-up and dispersal of the landfast ice is inhibited and the confinement of the turbid waters can extend well into September. Documentation of the 1974 events (Herlinveaux and de Lange Boom, 1975) indicated that the eventual "breakout" of the confined waters occurred in the vicinity of the entrance to Amundsen Gulf leading to unusual concentrations of turbid River Water off the southwestern corner of Banks Island.

Ice data are presently sufficient to quantitatively describe the range of variability in only the second of these mechanisms. Examination of the ice edge positions in Figures 17 to 19 indicates that over a given July to September period, wind fetches can range upward from a few kilometres prior to landfast ice breakup to more than 800 km and 400 km in the westerly and northerly directions respectively. The year-to-year differences in the available fetches at a particular point in the summer season can be as large as 300 km and the rapid response of ice edge positions to wind fields means changes of a few tens of kilometres per week are commonplace. While historical data clearly favour increasing fetches through most of the summer season, reversals of such trends have been observed in individual years at virtually all points in the seasonal progressions.

2.4 WAVES

Surface waves, generated during the open water season, are important to sediment transport in three ways:

1) The wave orbital velocities flowing over the ocean bottom, if sufficiently large, can result in resuspension of bottom sediments;

2) Wave orbital velocities within the water column will result in mixing of suspended sediments; in particular, the high levels occurring at the surface within the highly concentrated Mackenzie River plume will be redistributed downwards;

3) Breaking waves along the shoreline result in a transport of sediment along the coastline (longshore currents), along with erosion of the coastal sediments themselves.

The wave climate of the Beaufort Sea is highly variable, often being limited by the short fetch of the wind blowing over open water. In the summer months, the wind fetch can shift markedly, according to changes in the location of the offshore pack-ice edge (Section 2.3). In some years, when the pack-ice remains within 100 km of shore throughout the summer (e.g. 1974), the wave climate is very mild, with the largest waves limited to significant heights of less than 1.5 m. The other extreme occurs in those years when the pack ice retreats far offshore by mid-September to late October. Based on 11 years of summer ice cover data, Brower et al. (1977) identified one occasion when the ice pack retreated to distances in excess of 300 km over the entire length of the Beaufort Sea from Banks Island to west of Point Barrow; under these conditions, westerly winds would have maximum fetches of over 850 km.

A wave hindcast study for the Canadian Beaufort Sea derived for the years 1970 to 1979 inclusive, has been presented by Baird and Hall (1980). In this study, a wave-climate model was developed using standard wind-wave generation hindcast algorithms (Bretschneider, 1977). The winds were assumed to be uniform over the study area, and were computed from Tuktoyaktuk wind data scaled upwards by a variable factor (maximum of 1.15 at 6.5 m/s - see Figure 11). Wind fetches were estimated using straight line estimates from the hindcast location to the topographic or sea-ice boundaries, with the latter being deduced from the location of the one-tenth edge of the ice cover, as represented on mean monthly ice charts. The tabulated results of the Baird and Hall (1980) study provide a convenient data base for deriving useful indices related to sediment transport.

Harper and Penland (1982) used the Baird and Hall (1980) results to compute wave power roses (Figure 20). Wave power (P) was computed as:

$$P = \rho g H^2 \cdot C/16 \qquad (1)$$

where ρ is the water density (kg/m^3), g is the gravitational constant (m/s^2), H is the deepwater wave height (in metres - taken as the significant wave height) and C is the deepwater phase velocity (m/s). The largest waves originate from the west and northwest sectors, with westerly waves more common in the eastern portion of the study area and northwesterly waves more common to the west and north of Mackenzie trough. Considering only intense storm waves, taken as those having amplitudes of 2 m or more, the dominance of waves originating from the west and northwest is very pronounced.

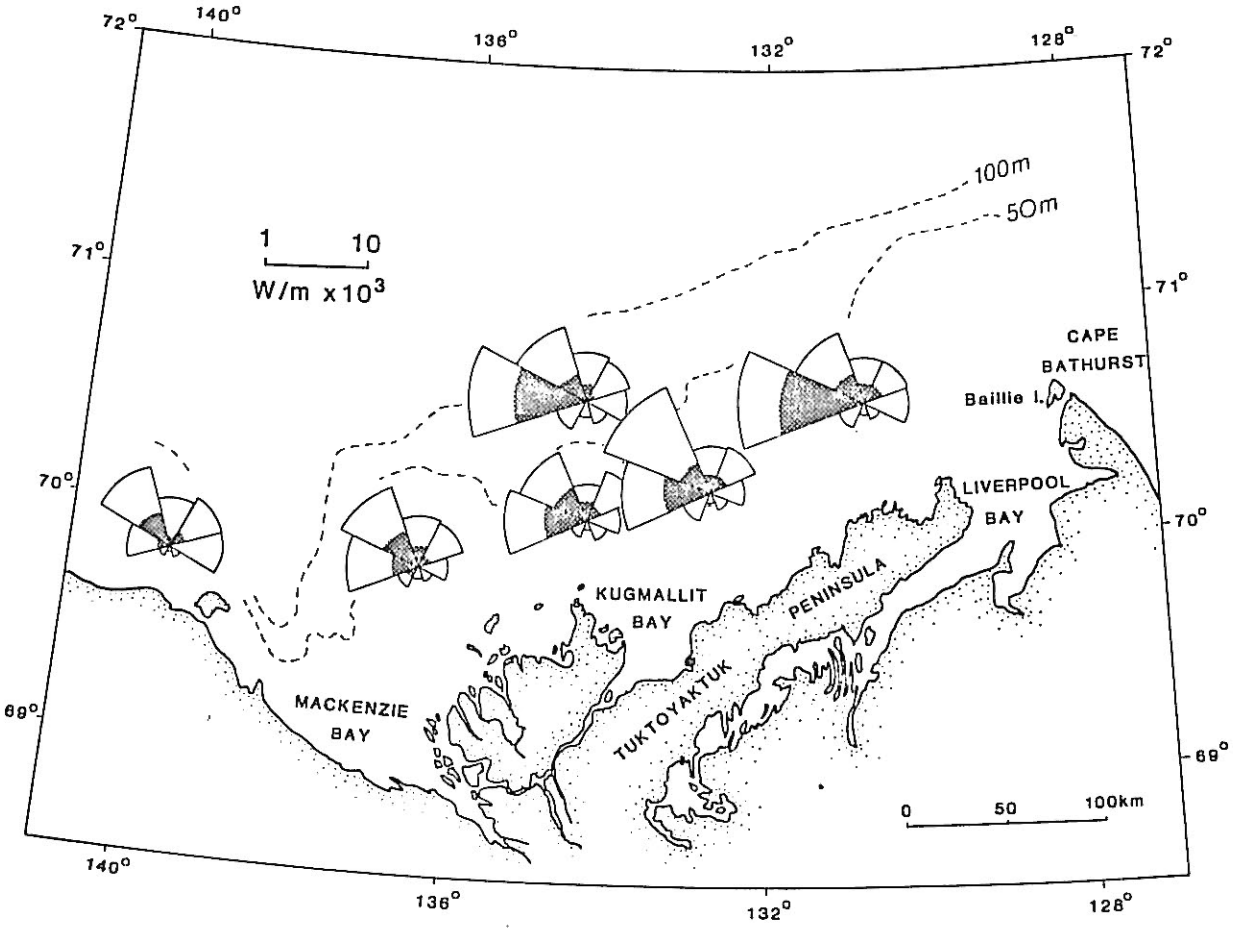

Figure 20: Diagrams of the directional distribution of wave power computed from the ten-year wave hindcast results of Baird and Hall (1980). The shaded areas represent the contribution from wave heights exceeding 2 m (after Harper and Penland, 1982). Direction is from which waves propagate.

Based on the directional distribution of wave power, Harper and Penland (1982) concluded that coastal longshore transport would be southeastward along the Yukon coastline, onshore on the Mackenzie delta coast and northeastward along the coastline of the Tuktoyaktuk Peninsula. Surveys of the erosion of abandoned artificial islands (Harper and Penland, 1982) also exhibit a rapid deterioration to depths of 5 m below sea level, with the island material usually being moved to the south and east.

Near-bottom wave orbital velocities were computed from the ten-year hindcast results of Baird and Hall. The near-bottom wave orbital velocities (V) were computed as:

$$V = C \cdot k \cdot \tfrac{1}{2} \cdot H/\sinh(k \cdot d) \qquad (2)$$

where C and k are the phase speed and wavenumber of the waves, H is the significant wave height and d is the depth (Phillips, 1966). The dispersion equation for ocean gravity waves is:

$$C = \frac{\omega}{k} = \left[(g/k \cdot \tanh(kd)\right]^{\frac{1}{2}} \qquad (3)$$

where ω is the rotational frequency ($\omega = 2\pi/T$; T is the wave period). In deep water where $k \cdot d > \pi/2$, $0.92 < \tanh(kd) < 1$, and equation (2) reduces to:

$$V = \pi H/\left[T \cdot \sinh(4\pi^2 d/T^2 g)\right] \qquad (4)$$

The wave orbital velocities were computed at six locations at various depths for percent exceedance levels of 50, 20, 10, 5, 2 and 1 (see Table 5 and Figure 21).

For mean conditions (50% exceedance levels), the wave orbital velocities derived from the Baird and Hall results are small, being less than 1 cm/s in water depths of 18 m or more. At depths shallower than 12 and 8 m, wave orbital velocities exceed 5 to 15 cm/s, respectively. Bottom speeds of 40 cm/s are reached only in depths less than 5 m. Occasionally, much larger wave orbital velocities can be realized. Ten percent of the time, wave orbital bottom currents exceed 1 cm/s at depths of 40-42 m, 5 cm/s at depths of 27 m, 15 cm/s at depths of 20 m, and 40 cm/s at depths of 12 m. For the uppermost 1% of the computed wave heights, at maximum depths of 66 to 74 m, wave orbital speeds exceed 1 cm/s; at 46 to 53 m wave orbital speeds exceed 5 cm/s; at 32 to 36 m wave orbital speeds exceed 15 cm/s; and at 21 to 23 m wave orbital speeds exceed 40 cm/s.

Table 5: Wave orbital speeds computed at various depths for the locations of Baird and Hall (1980). The speeds are computed for the 1, 2, 5, 10, 20 and 50% exceedence levels by wave height based on ten years (1970-1979) of hindcast results. The orbital velocities (V) computed for significant wave heights (H) with period (T). For entries labelled 'n', orbital velocities could not be computed using deep water wave theory.

		50%			20%			10%			5%			2%			1%		
Site	Depth	H	T	V	H	T	V	H	T	V	H	T	V	H	T	V	H	T	V
	m	m	s	cm/s	m	s	cm/s	m	s	cm/s	m	s	cm/s	m	s	cm/s	m	s	cm/s
A	20	0.8	3.6	0.3	1.2	4.8	4.8	1.5	5.5	12.0	1.7	6.0	19.2	2.1	6.7	33.7	2.4	7.0	43.2
	25			0.0			2.0			6.1			10.9			21.1			28.0
	30			0.0			0.8			3.2			6.2			13.4			18.4
B	10	0.8	3.8	8.2	1.2	4.9	29.8	1.5	5.6	50.4	1.8	6.0	68.9	2.1	6.7	96.3	2.4	7.0	n
	15			2.0			12.5			25.0			36.5			55.0			n
	20			0.5			5.4			13.0			20.3			33.7			43.2
	25			0.1			2.3			6.8			11.5			21.1			28.0
	30			0.0			1.0			3.6			6.6			13.4			18.4
C	30	0.8	3.8	0.0	1.2	4.9	1.0	1.5	5.5	3.2	1.8	6.0	6.6	2.1	6.7	13.4	2.4	6.9	17.3
	35			0.0			0.4			1.6			3.8			8.5			11.3
	40			0.0			0.2			0.8			2.1			5.4			7.4
	45			0.0			0.1			0.4			1.2			3.5			4.9
D	40	0.8	3.9	0.0	1.3	5.0	0.3	1.6	5.7	1.2	1.8	6.3	3.1	2.1	6.9	6.5	2.4	7.5	11.5
	50			0.0			0.1			0.4			1.1			2.8			5.6
	55			0.0			0.0			0.2			0.7			1.8			3.9
	60			0.0			0.0			0.1			0.4			1.2			2.7
	70			0.0			0.0			0.0			0.1			0.5			1.3
	80			0.0			0.0			0.0			0.1			0.2			0.7
	100			0.0			0.0			0.0			0.0			0.0			0.2
E	20	0.8	3.8	0.5	1.3	4.9	5.8	1.6	5.7	14.9	1.8	6.2	22.8	2.1	6.8	35.1	2.4	7.2	46.3
	25			0.1			2.5			8.0			13.4			22.2			30.6
	30			0.0			1.1			4.3			7.9			14.3			20.5
	35			0.0			0.5			2.3			4.7			9.2			13.9
F	30	0.7	3.9	0.0	1.3	5.1	1.5	1.5	5.7	4.0	1.8	6.0	6.6	2.1	6.7	13.4	2.4	7.0	18.4
	35			0.0			0.7			2.2			3.8			8.5			12.2
	40			0.0			0.3			1.1			2.1			5.4			8.0
	50			0.0			0.0			0.3			0.7			2.2			3.5
	60			0.0			0.0			0.0			0.2			0.9			1.6
	70			0.0			0.0			0.0			0.0			0.4			0.7
	80			0.0			0.0			0.0			0.0			0.2			0.3

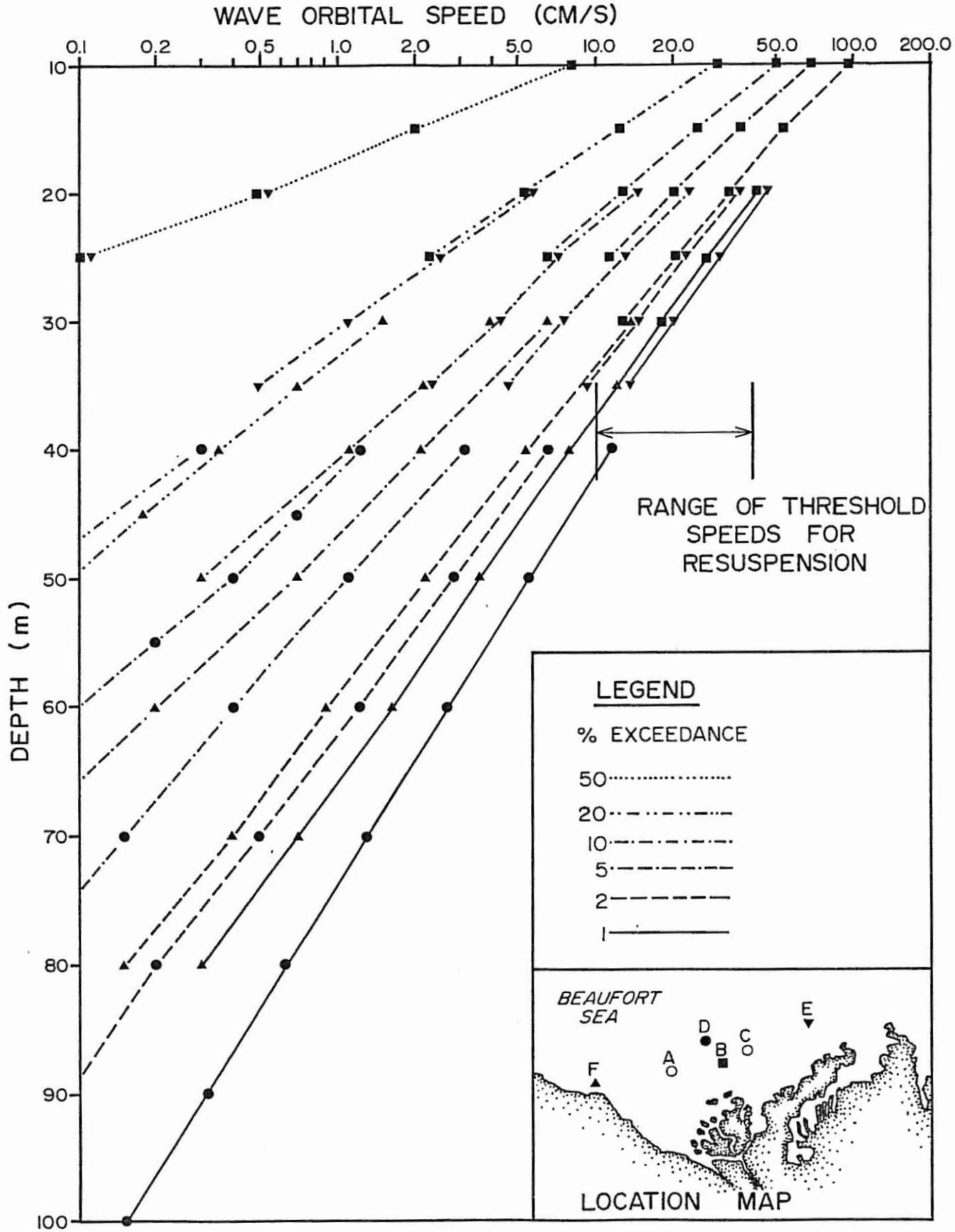

Figure 21: Wave orbital speeds computed for various depths and locations for the 1, 2, 5, 10, 20 and 50% exceedance levels of wave heights as computed by Baird and Hall (1980).

Based on these results, Harper and Penland (1982) classified the Beaufort Sea shelf into various depth ranges, according to likelihood of attaining sufficient wave orbital velocities to resuspend sediments.

The frequency of resuspension of bottom sediments requires knowledge of the minimum critical shear stress (often characterized by a threshold velocity) required to lift sediment off the bottom. These values depend on the particle size distribution of the sediments, along with their cohesive properties. For fine sand, the assumed value of the threshold velocity is 15 cm/s, while coarse sand has a corresponding value of 40 cm/s. Although the sediments are fine grained, Harper and Penland (1982) considered the higher value (40 cm/s) as being more realistic for the Beaufort Sea, since the cohesion of the fine silty particles would make the material more difficult to resuspend. Based on the 40 cm/s threshold velocity, Harper and Penland (1982) categorized the Beaufort Sea shelf as follows:

1) A wave dominated zone (depths of 10 m or less) where bottom sediments are disturbed more than 10% of the time;

2) A transitional zone (depths of 10 to 20 m) where bottom sediments are occasionally (1 to 10% of the time) disturbed by wave action;

3) A dormant zone (depths of 20 to 35 m) where bottom sediments are rarely (less than 1% of the time) disturbed by wave action;

4) An offshore zone (depths in excess of 35 to 47 m) in which sediments are not disturbed by wave action even during infrequent high energy events.

The depths (and areas) of each of these zones defined by Harper and Penland (1982) depend on the threshold velocity chosen (40 cm/s) and the representativeness of the ten year hindcast results of Baird and Hall (1980). For the threshold velocities, there are no data available for the Beaufort Sea bottom sediments on which to choose the correct value. Grant and Madsen (1979) note that the combined interaction of steady currents and wave orbital velocities results in greater shear stresses on the bottom due to non-linear current interaction; this effect reduces the threshold velocities needed to resuspend sediments. Near-bottom currents over the middle and outer portions of the Beaufort shelf are generally low (mean speeds of 5 to 10 cm/s; maximum speeds of 16 to 41 cm/s; see Section 2.5.2). The bottom

current speeds are related to the wind speed with the result that relatively large currents will tend to coincide with large waves (Section 3.1.1).

Based on a recent survey of measured critical shear stresses for the erosion of cohesive substrates (Amos and Greenberg, 1980) in laboratory and non-Beaufort Sea field studies, the likely range of threshold velocities is 10 to 40 cm/s (see Appendix B). The median level of threshold velocity is approximately 20 cm/s.

If the assumed threshold velocity were reduced by a factor of two from the values of Harper and Penland (1982) to 20 cm/s (Appendix B), the depth ranges of the zones of wave influence would increase by approximately 70%. Indeed, simultaneous measurements of near-bottom transmissivity data with current or wind speeds, indicate that the bottom boundary layer turbidity may increase with currents having speeds as low as 5-10 cm/s (Section 3.2). For a threshold velocity of 20 cm/s, the wave dominated zone would extend to depths of 17 m (from 10 m), the transitional zone would apply to depths of up to 32-34 m (from 20 m), and the dormant zone would extend over most of the remainder of the continental shelf, to depths of approximately 70-80 m (from 35-47 m).

A recent wave hindcast study for the Beaufort Sea by Hodgins et al. (1981) indicates that the occurrence of large and extreme waves may be more common than the results of Baird and Hall (1980) would indicate.

This study used a two-dimensional storm-based wind field derived from a review of a ten year climatology. The storm of August 26-28, 1975 was selected as the prototype for an extreme storm, having an estimated return period of one year. Extreme storms having return periods of 10, 50 and 100 years were derived as intensifications of this storm, having peak wind speeds matching the extrapolated speeds deduced from an assumed Gumbel extrapolation. The wind fields were then used as input to a two-dimensional surface wind model. Ice conditions were defined as the further observed ice-edge (Brower et al., 1977) having an estimated return period of 5 to 8 years. Because the return periods are based solely on wind fields, and the open-water conditions have their own probability of occurrence, the return period designations are "slightly conservative" (Hodgins et al., 1981). The results of the Hodgins et al. (1981) study reveal that the near-bottom wave orbital velocities could be considerably larger than expected on the basis of the Baird and Hall (1980) results (see Table 6 and Figure 22). For a one year return period at nearby deepwater locations (stations 7 and D;

Table 6: Comparison of wave orbital speeds for one year and ten year return periods, computed from the results of (I) Baird and Hall (1980) and (II) Hodgins et al. (1981). The station locations are designed by letters (I) and numbers (II) for locations shown in Figure 22. Note that the compared stations are separated by considerable distances and, in some cases, lie in much different water depths. The most directly comparable stations are the deep water locations of sites D and 7. The orbital velocities (V) were computed for the significant wave heights (H) having periods (T) for return periods of one and ten years. Note that for entries labelled 'n', deep water wave theory was not appropriate for use in computing orbital velocities.

			One Year						Ten Year					
			I			II			I			II		
Site	Station Depth m	Depth m	H m	T s	V cm/s	H m	T s	V cm/s	H m	T s	V cm/s	H m	T s	V cm/s
A	23	20	2.6	6.8	43.4	-	-	-	4.1	6.9	71.1	-	-	-
		25			27.6			-			45.7			-
		30			17.7			-			29.7			-
B	26	10	2.7	6.8	n	4.9	9.9	n	4.2	7.3	n	5.5	10.4	n
(3)	10	15			n			n			n			n
		20			45.1			n			83.8			n
		25			28.6			n			55.9			n
		30			18.4			n			37.8			n
C	28	30	2.7	6.9	19.5	-	-	n	4.3	7.3	38.7	-	-	-
		35			12.8			n			26.4			-
		40			8.3			n			18.0			-
		45			5.5			n			12.3			-
D	58	40	2.5	6.6	5.9	6.5	11.4	n	4.4	9.8	54.6	9.2	13.6	n
(7)	56	50			2.3			79.6			35.2			n
		55			1.5			67.4			28.4			n
		60			0.9			57.2			22.9			n
		70			0.4			41.5			15.0			97.1
		80			0.1			30.2			9.9			76.8
		90			0.1			22.1			6.5			61.1
		100			0.0			16.2			4.3			48.8
E	27	20	2.7	6.8	45.1	4.1	9.1	n	5.1	10.3	n	5.6	10.6	n
(5)	21	25			28.6			n			n			n
		30			18.4			69.5			n			n
		35			11.9			53.4			88.6			103.0
F	35	30	2.4	6.5	13.3	5.1	10.1	n	3.6	6.5	20.0	7.0	11.8	n
(1)	70	35			8.3			85.0			12.4			n
		40			5.1			68.3			7.7			n
		50			2.0			44.9			3.0			92.8
		60			0.8			29.9			1.1			67.8
		70			0.3			20.0			0.4			50.0
		80			0.1			13.5			0.2			37.2

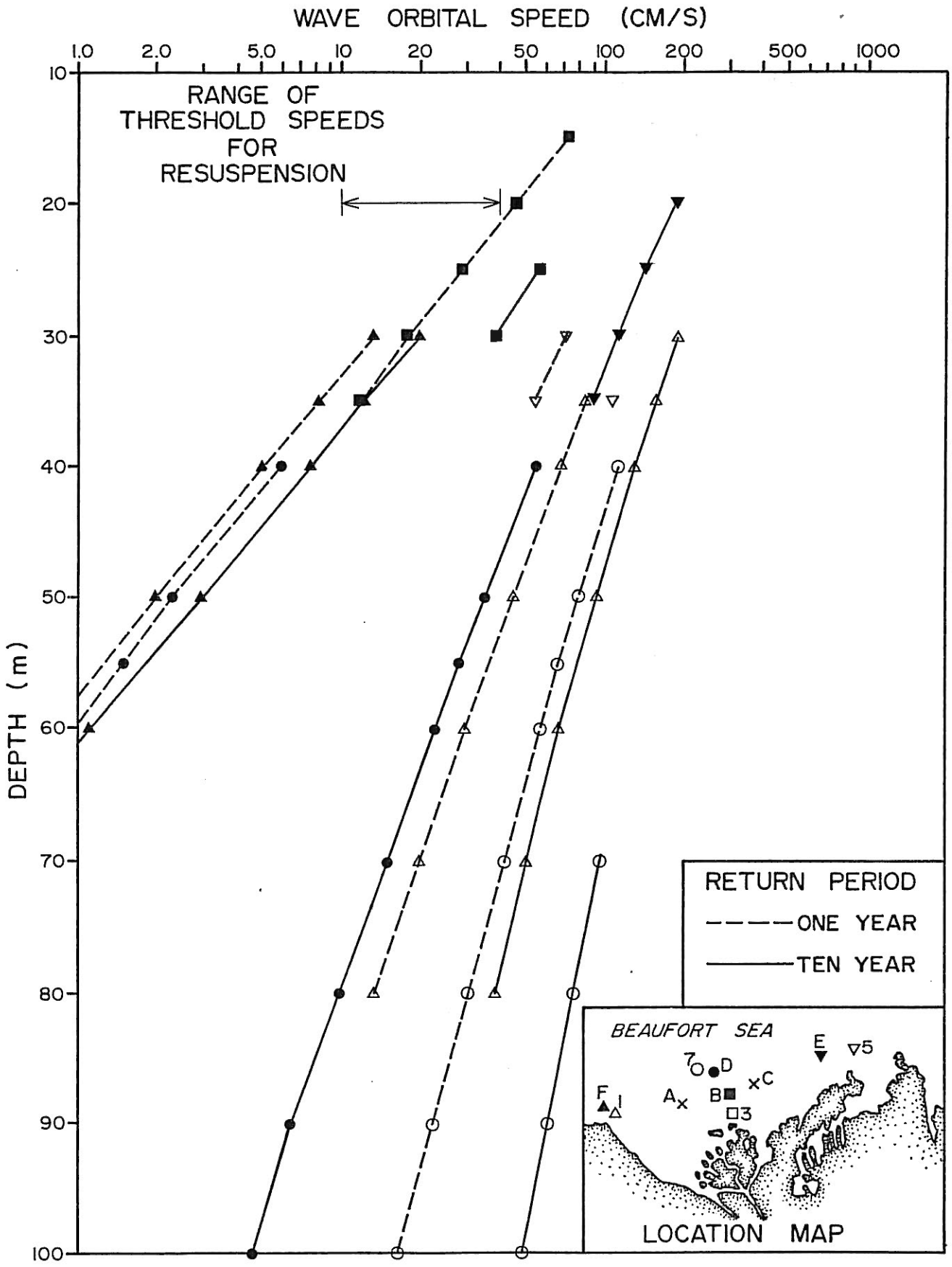

Figure 22: Wave orbital speeds computed for various depths and locations for the one year and ten year return periods of wave heights as computed by Baird and Hall, 1980 (closed symbols) and Hodgins et al., 1981 (open symbols).

Figure 22) speeds of 40 cm/s or more occur to depths of 71 m as compared to less than 30 m. The comparative figures for the ten year return period are 110 m and 47 m.

The marked discrepancy between the results of the two wave hindcast studies appears to be a consequence of three systematic differences:

1) The wind speeds used by Baird and Hall (1980) appear to be too low. The two year return period value of 17 m/s is less than the one year value of 20 m/s of Hodgins et al. (1981). Comparative values for ten year return periods are 22.5 m/s and 35 m/s. The results of regressions between offshore and Tuktoyaktuk winds (used by Baird and Hall, 1980) presented in Section 2.2.1, indicate that the latter winds should be scaled upwards by a factor of at least 1.2, considerably greater than the scaling factor function applied by Baird and Hall (1980). Further evidence of the underestimation of strong winds by Baird and Hall (1980) can be found in comparisons of their 10 m winds with the measured offshore winds at the 10 m level (Figure 8).

2) The fetch distances used in both studies are unrealistic. In Baird and Hall (1980), the fetches are determined by monthly mean conditions; this will lead to underestimates of large fetch distances associated with offshore pack-ice movements occurring over time scales of less than one month (see Section 2.3). On the other hand, Hodgins et al. (1981) used the maximum observed fetch length for all hindcasts; the reduced fetch lengths which occur are ignored.

3) The Baird and Hall (1980) wave hindcast results assumes spatially uniform wind fields. Intense cyclonic disturbances of small spatial scale (Hodgins et al., 1981 - see Section 2.2) will not be resolved in their results.

The actual wave conditions expected for the Beaufort Sea likely fall between those of the two hindcast studies. Further improved hindcasting analysis applied to many (>10) years of available wind and ice cover data, along with review and analyses of the now fairly extensive sets of direct wave measurements (MEDS waverider data, 1975-1983) are required to better resolve the wave climate of the Beaufort Sea.

2.5 OCEANOGRAPHY

2.5.1 GENERAL OCEANOGRAPHIC CHARACTERISTICS

The spatial distribution of temperature and salinity over the continental shelf of the Canadian Beaufort Sea is primarily determined from the influence of two major water sources: marine waters originating in the Arctic Ocean proper and the fresh water discharge of the Mackenzie River. At locations on the outer portions of the shelf, the water column exhibits the relatively narrow range of temperature and salinity values typical of the Arctic Water Mass of the Arctic Ocean. Beneath the surface layer, typically confined to depths of 50 m or less, temperatures are within 1°C of the freezing point and salinities range between 31.0 and 33.5 (see Figure 23). The T-S (temperature-salinity) properties at the surface vary over a wider range of values, due primarily to the seasonal changes in surface heat exchange. In summer the large levels of solar insolation combined with the extensive areas of open water results in temperatures of up to 6°C and salinities as low as 25. In the winter, the loss of heat to the atmosphere and resulting ice formation reduces surface temperatures to within a few tenths of a degree of freezing point and increases surface salinities to levels exceeding 31.

The influence of the Mackenzie River discharge can extend considerable distances (hundreds of kilometres) from the source, in the form of reduced salinities at and near the surface. The inner or nearshore portion of the river layer is characterized by very low salinities of $5^{o}/oo$ or less, and has a typical thickness of 3 to 5 m in Mackenzie and Kugmallit Bays and adjoining regions (Fraker et al., 1979). Temperatures are generally high in early summer, with the typical values of 5 to 16°C resulting from the warm temperatures of the Mackenzie River discharge at this time of year and the large amount of solar insolation. The river layer temperatures steadily decrease as summer progresses, and approach near-freezing levels in September.

In summer, the horizontal extent of the River Water itself (characterized by surface salinities of $5^{o}/oo$ or less and high sediment concentrations) is usually confined to within 50 km of the coastlines off Mackenzie Bay, Richards Island and Kugmallit Bay. A much larger river-influenced area lies beyond the River Water per se, and is characterized by reduced (but not zero) suspended sediment concentrations and a pronounced halocline extending to the surface, at salinities of $20^{o}/oo$ or less. This zone covers much of the surface water area off the coastlines between Herschel Island and Cape Bathurst, can extend more than 100 km offshore, and has been observed as far east as

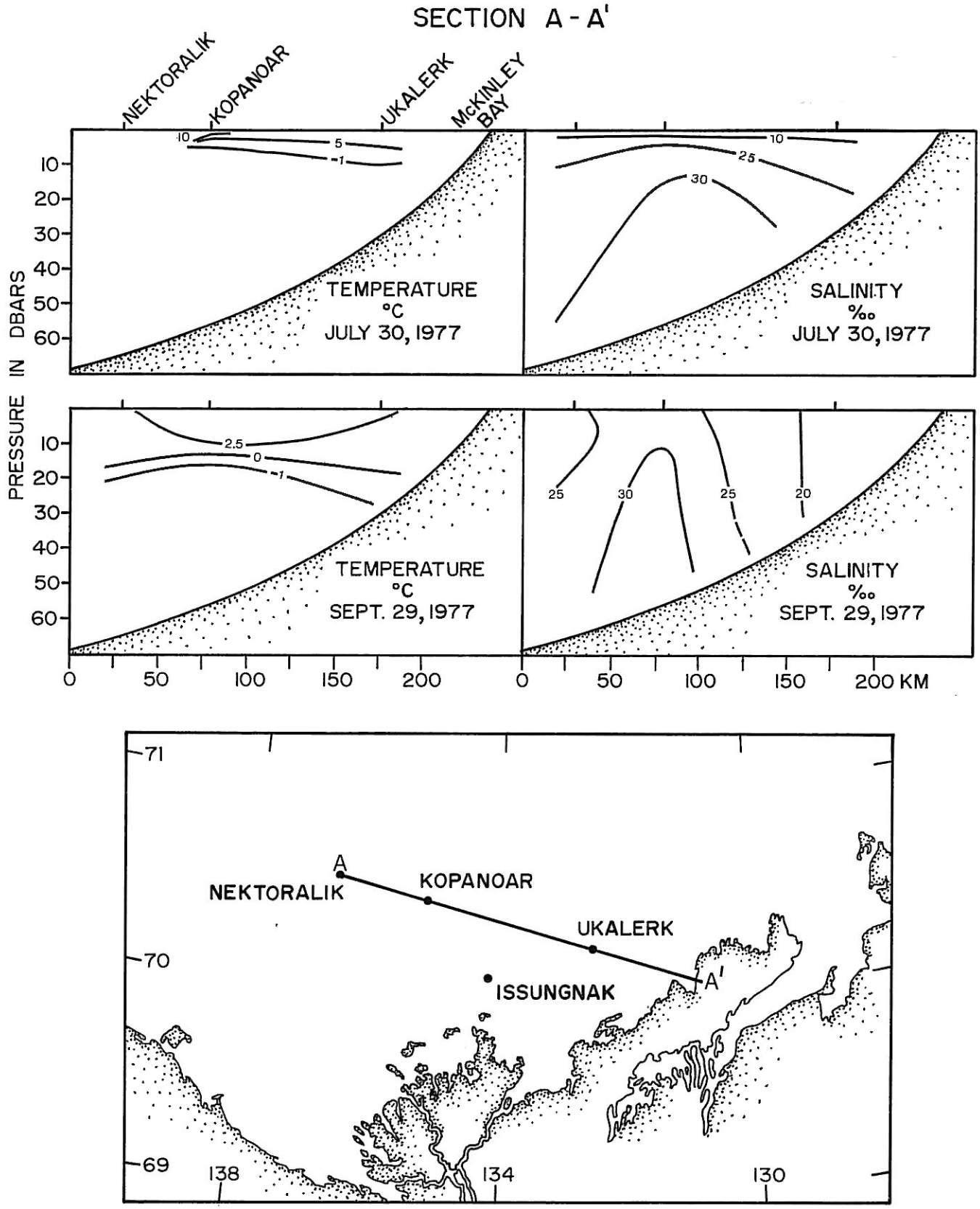

Figure 23: Vertical sections of temperature and salinity along a northwesterly-southwesterly transect on July 30 and September 19, 1977. Data were collected from Canmar drillships as reported in Lemon and Kowalski (1982).

southwestern Banks Island. Occasional extension of this water into the eastern Alaskan coastal zone is also suspected on the basis of satellite observations of turbid water. River-influenced zones would appear to be strongly controlled by the wind, although they are also affected by levels of river flow, sea state and the sea-ice distribution.

An important factor in determining the temporal variability in the spatial distribution of temperature and salinity is the prevailing wind conditions. Under westerly or northwesterly winds, the pack ice is turned to the right of the wind due to the Coriolis force, and therefore has an onshore component of motion which reduces the area of open water. The river plume is also affected by the Coriolis force and causes it to turn eastwards; this tendency complements the wind-induced surface water motions (MacNeill and Garrett, 1975). For westerly to northwesterly winds, the net result is a concentration of the River Water along the entire coastline eastward of Mackenzie Bay. Under easterly winds, the ice pack drift generally has an offshore component which expands the area of open water. The easterly wind also counteracts the tendency of the river plume to turn to the right, causing the plume to extend much further offshore and to remain in the western portion of the area rather than spreading eastward along the coast.

The importance of the wind in explaining changes in the T-S properties of the upper portion of the water column is evident in the thermistor chain data obtained near the Issungnak site in late July and August of 1981 (Figure 24). The surface layer exhibits large changes in temperature and salinity in response to the major wind events. Increasing salinities and decreasing temperatures in the upper layer are associated with westerly wind events, while during and following easterly wind events, salinities decrease and temperatures increase. The responses are opposite to those expected from wind-driven coastal upwelling and downwelling. Because the measurement site is located midway between the two major Mackenzie River discharge channels, westerly winds apparently concentrate the warm, less saline River Water inshore of this location and the surface layer is cold, saline Arctic Ocean Water. Alternatively, easterly winds drive the Kugmallit Bay River discharge offshore to the measurement site and beyond.

During the winter and early spring, the character of the river-influenced area differs dramatically from that described above for the summer period. These changes are due, in large part, to the much reduced river discharge and the almost complete coverage of the sea surface by ice which virtually eliminates

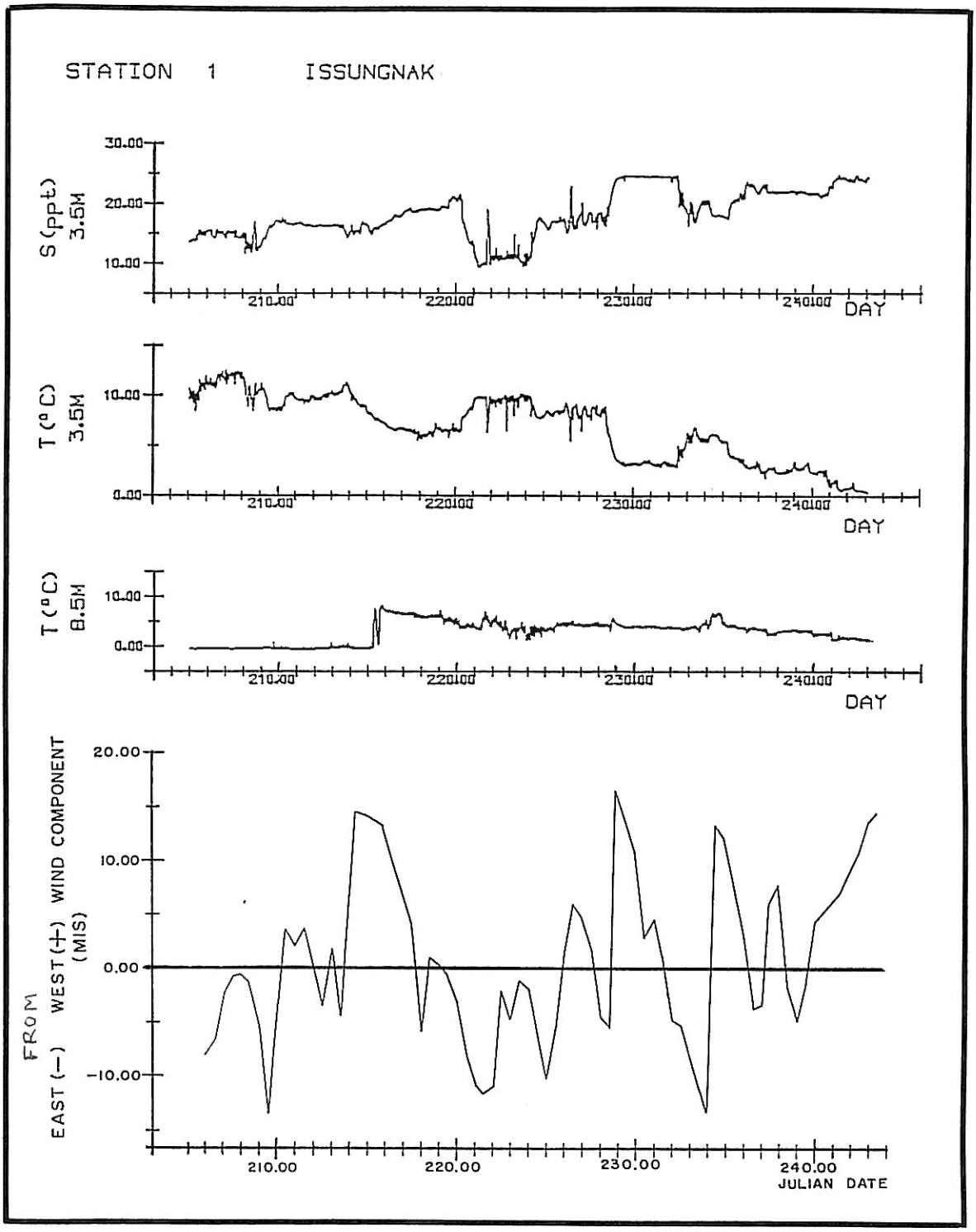

Figure 24: Moored CTD and thermistor chain data obtained near the Issungnak site, July 24 to August 30, 1981 (Erickson et al., 1983). Also shown are twice daily values of the east-west wind component as measured at Issungnak.

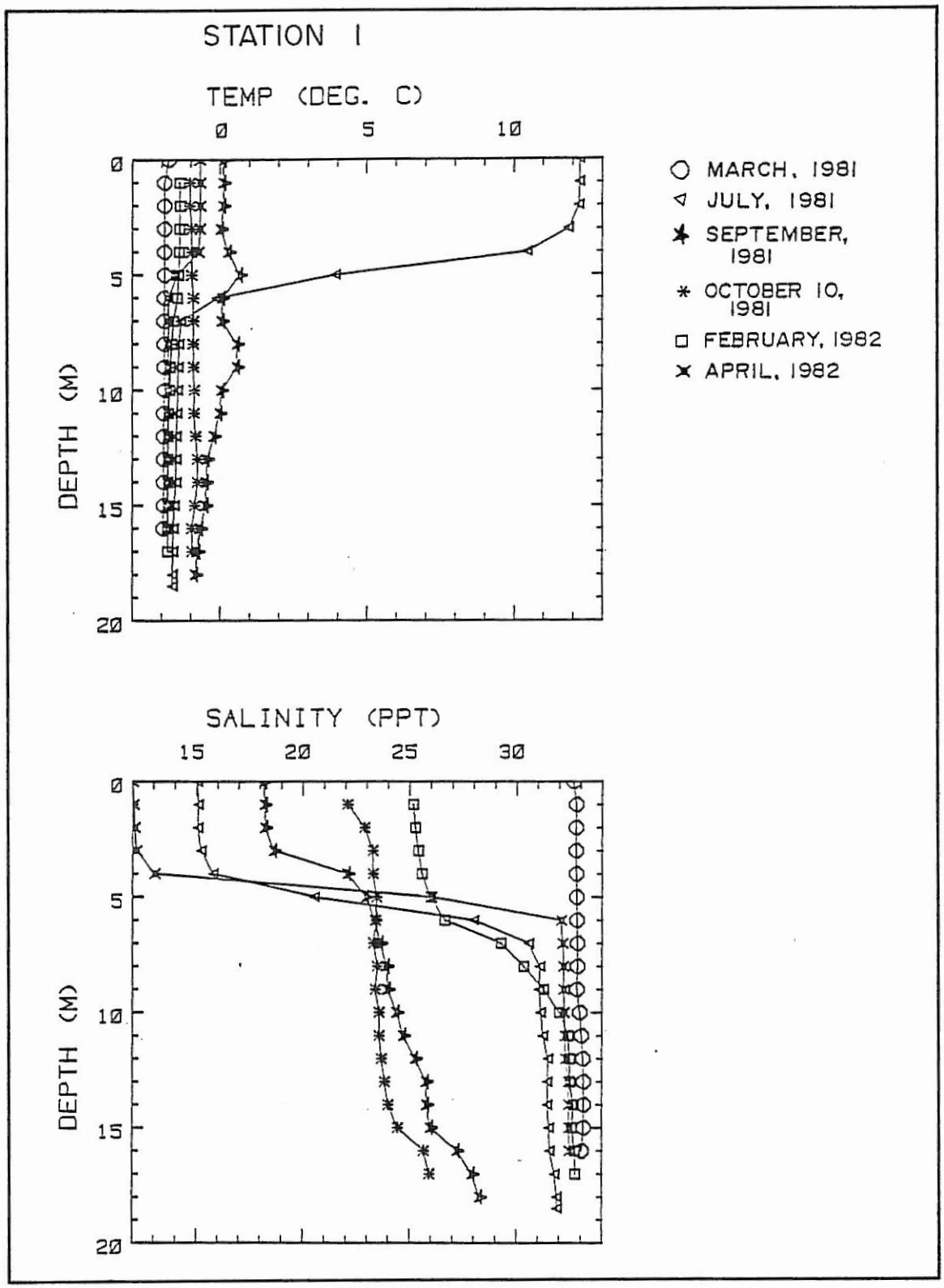

Figure 25: Vertical profiles of temperature and salinity near Issungnak obtained on 6 occasions between March, 1981 and April, 1982 (Erickson et al., 1983).

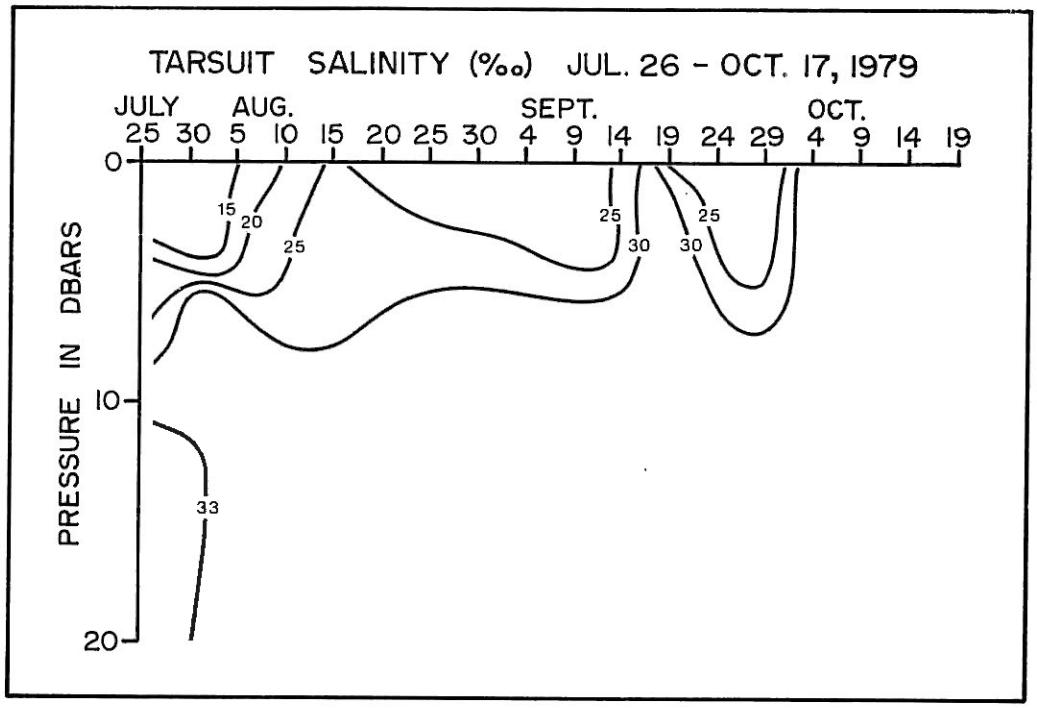

Figure 26: Salinity at the Tarsiut site from July 25 to October 19, 1979. Data were collected from the Canmar drillship as reported in Lemon and Kowalski (1982).

direct wind-driven surface water movements. Following the onset of landfast ice formation in November to December, fresh water gradually accumulates beneath the ice from the relatively small, but nearly constant Mackenzie River discharge. Based on the very few data sets available for the winter and spring seasons, the River Water forms a shallow (3 to 5m) surface layer beneath the landfast ice, separated from the underlying Arctic Water by an intense halocline located at depths of 5 to 10 m. The horizontal extent of the River Water appears to have a large interannual variability. In the spring of 1975, the layer was observed near the offshore edge of the landfast ice, 20 to 30 km offshore, and extended at least 100 km alongshore from Kugmallit Bay (Herlinveaux et al., 1976). In 1981, the areal extent appears to be reduced as no indication of low salinities were observed at four widely separated stations on the outer reaches of the landfast ice, including one site located approximately 15 km offshore of the eastern end of Kugmallit Bay (Melling, pers. comm.).

The seasonal cycle of the temperature and salinity profiles is illustrated in Figure 25, derived from March 1981 to April 1982 CTD profiles obtained near the Issungnak site, located immediately north of Richards Island at a depth of approximately 20 m (Erickson et al., 1983). A well developed surface layer is evident in July, with high temperatures (>12°C) and low salinities (approx. 15). In March 1981, the water column was nearly uniform with depth, having temperatures just above the freezing point and high salinities (approx. 33). However, in February and April of the following year, the influence of the river discharge was apparent, as indicated by the development of a surface layer of reduced salinity (25 in February, 13 in April) to a depth of 4-6 m.

The transition from summer to winter oceanographic conditions is characterized by a marked increase in surface salinity and a corresponding reduction of vertical stratification (Figures 23 and 26). In late summer and early autumn, the lower half of the water column over the shelf can increase in temperature and decrease in salinity due to downward mixing of heat and the less saline waters from the surface (Figure 24). At first, the higher surface salinities and decreased stratification are associated with the reduced river discharges, the greater degree of dispersal associated with increased open water conditions and, possibly, increased storm activity, experienced as the summer progresses. Prolonged periods of strong easterly winds can result in the upwelling of deeper, more saline water to the surface, reducing stratification and leading to cool, saline surface waters.

By mid-autumn, a marked increase in salinity occurs throughout the water column over most of the continental shelf. On the basis of vertical profile data collected over the outer half of the continental shelf and over the continental slope in November 1979, Melling and Lewis (1982) found that the average salinity over the uppermost 50 m of water was 33°/oo near the 50 m depth contour on the continental shelf. This value exceeded that recorded (<32) on the seaward continental slope. The trend toward increasing salinity in the direction of the shoreline is opposite to that encountered during the summer, on the basis of previous (1952 and 1975) oceanographic data. The mechanisms producing the autumnal increase in salinity have not been definitively identified but have been suggested by Melling and Lewis (1982) to include:

1) upwelling of the more saline water offshore onto the shelf in response to strong easterly winds;

2) an increase of the strength of the Beaufort Sea Gyre in autumn, as was observed in 1979, with an associated upward tilting of isopycnal surface around the periphery of the gyre. This would result in a transport of (fresh) surface water offshore and to the west;

3) the breakup and removal of young landfast ice by early autumn storms, which results in the rapid disappearance of the brackish coastal waters of summer.

2.5.2 NEAR-BOTTOM CURRENTS

For this study, all available near-bottom current meter data sets were obtained. These data (Table 7) were subdivided according to the seasonal coverage, where winter was taken to be January 1 to March 31, spring as April 1-June 30, summer as July 1-September 30 and autumn as October 1-December 31. Due to the dominant low frequency variations in the near-bottom currents, as discussed below, only data sets having a total record length exceeding 30 days, were considered in this study.

Available Data

Extended time series measurements of near-bottom currents were first obtained in 1974-1975 as part of the Beaufort Sea Project (Huggett et al., 1977). In 1976 and 1977, near-bottom current measurements were collected near two of the drilling sites occupied by the Canmar drillships (Fissel, 1981). Near-bottom current data were obtained near the Tarsiut and Uviluk

Table 7: A summary of all available measurements of near-bottom currents, by seasons, with record lengths exceeding 30 days.

Station Des.	Name	Measurement Period	No.of Days	Latitude	Longitude	Current Meter	Depth Meter (m)	Depth Bottom (m)	Speed Mean (cm/s)	Speed Max. (cm/s)	Vector Average Magnitude (cm/s)	Vector Average Direction (°)	B %	Reference
A	BSP-3	8 Aug -30 Sept/75	54	69°55.3	139°23.3	AA-30	50	52	13.1	75.7	2.8	63	21	(1)
		1 Oct -31 Dec /75	92						12.0	69.9	3.7	340	31	(1)
B	BSP-4	9 May -30 June/74	53	69°41.9'	137°9.2'	AA-30	40	43	2.3	23.1	0.4	43	17	(1)
C	BSP-5	30 Apr -30 June/75	62	70°23.1'	136°45.7'	AA-30	64	67	4.5	16.4	*	*	*	(1)
		1 July-11 Sept/75	73						10.8	40.9	8.3(a)	51(a)	77	
D	Tarsiut	1 Jan -30 Mar /82	49	69°53.8'	136°11.6'	AA-60	19	25	3.8	24.0	0.8	354	21	(4)
		18 Jan -30 Mar /81	72	69°57.3'	136°11.8'	AA-30	23	26	5.0	31.7	0.5	54	10	(3)
		1 Apr -30 June/82	91	69°53.8'	136°11.6'	AA-60	19	25	3.8	17.6	0.3	111	8	(4)
		1 Apr - 5 May /81	35	69°57.3'	136°11.8'	AA-30	23	26	3.8	19.5	1.0	93	26	(3)
		1 July-24 Sept/82	86	69°53.8'	136°11.6'	AA-60	19	25	8.2	25.2	2.2	86	27	(4)
		11 Aug -30 Sept/81	50						8.3	26.9	4.4	79	53	(4)
		1 Oct -31 Dec /81	32						12.9	38.4	3.6	281	28	(4)
E	Nektoralik	31 July-30 Sept/77	61	70°28.6'	136°16.9'	HP-60	62 m	64	7.4	22.6	5.9	75	80	(2)
F	Kadluk	6 Aug -25 Sept/82	51	69°46'	136°3.0'	EN-60	11	13	9.5	40.0	2.8	19	29	(6)
G	Kopanoar	4 Aug -30 Sept/77	58	70°22.9'	135°5.6'	HP-60	50	57	8.3	28.8	2.3	90	28	(2)
H	BSP-13	27 Apr -30 June/75	65	70°7.9'	134°19.9'	AA-30	30	33	3.2	20.2	0.6	202	19	(1)
		1 July-30 July/75	30						5.3	15.8	1.1	98	21	(1)
I	Isserk Shoal	5 Aug -14 Sept/82	40	69°56.4'	134°23.2'	NB-60	6	7	8.2	49.3	1.1	94	13	(6)
J	Issungnak	6 Aug -20 Sept/81	43	69°59.0'	134°21.0'	AA-5	15	16	8.8	47.4	1.8	31	20	(5)
K	BSP-15	29 Apr -30 June/75	63	70°17.3'	133°35.3'	AA-30	51	54	5.8	21.6	2.9	150	50	(1)
		1 July- 6 Aug /75	37						6.8	18.5	1.9	87	28	(1)
L	Tingmiark	22 Aug -30 Sept/76	38	70°10.6'	132°58.9'	HP-60	26	28	5.9	19.6	1.8	7	31	(2)
M	Uviluk	18 Jan -30 Mar /81	72	70°15.6'	132°18.7'	AA-30	19	25	5.7	24.0	1.4	78	25	(3)
		1 Apr -30 June/81	91						4.6	25.8	2.3	113	41	(3)
		1 July- 5 Aug /81	35						6.3	20.7	2.3	84	37	(3)
N	W.Atkinson	8 Aug -26 Sept/81	50	69°48.6'	131°59.8'	EN-30	7	8	16.3	56.3	2.1	14	13	(5)
O	BSP-8	26 Apr -30 June/75	65	71°12.9'	131°19.9'	AA-30	74	77	4.8	16.3	*	*	*	(1)
		1 July- 4 Aug /75	35	71°12.9'	131°19.9'	AA-30	74	77	5.7	15.6	*	*	*	(1)
P	BSP-9	26 Apr -30 June/75	65	70°43.7'	131°14.7'	AA-30	42	45	3.9	20.2	*	*	*	(1)
		1 July- 6 Aug /75	36						5.3	21.0	*	*	*	(1)

Table 7 (Cont'd)

Station Des.	Name	Measurement Period	No.of Days	Latitude	Longitude	Current Meter	Depth Meter (m)	Depth Bottom (m)	Speed Mean (cm/s)	Speed Max. (cm/s)	Vector Average Magnitude (cm/s)	Vector Average Direction (°)	B %	Reference
Q	BSP-10	26 Apr -30 June/75	66	71°18.6'	128°54.5'	AA-30	53	56	5.1	16.4	*	*	*	(1)
		1 July- 5 Aug/75	35						4.9	13.5	*	*	*	(1)
R	BSP-11	9 May -30 June/74	52	71°2.5'	128°31.5'	AA-30	25	28	10.0	25.6	5.0	55	50	(1)
		1 July-13 Aug /74	43						12.8	30.7	7.6	65	59	(1)
		26 Apr -30 June/75	66	71°0.2'	128°43.4'		39	41	8.6	38.1	*	*	*	(1)
		1 July- 5 Aug /75	36						8.3	24.7	*	*	*	(1)
S	CM-2	1 Apr -30 June/81	91	70°56.2'	133°31.1'	AA-30	72	77	7.3	25.3	4.9	58	67	(7)
		1 July-16 Aug /81	48						7.1	21.5	43	40	60	(7)
T	CM-1	1 Apr -30 June/81	91	71°11.5'	132°6.9'	AA-30	94	99	7.8	27.1	6.0	39	77	(7)
		1 July-16 Aug /81	48						9.1	22.5	7.4	43	81	(7)
U	CM-3	1 Apr -30 June/81	91	71°23.2'	130°21.3'	AA-30	57	62	10.8	29.0	5.2	70	48	(7)
		1 July-16 Aug /81	48						11.7	32.1	10.0	54	85	(7)

(a) Vector averaged data calculated on reduced number of records (39 days).
* Suspect directional data (BSP-5,8,9,10,11) in spring-summer 1975.

AA - Aanderaa RCM-4
HP - Hydroproducts
EN - Endeco 105
NB - Neil Brown Acoustics

Data Sources:

(1) Huggett et al. (1977)
(2) Fissel (1981)
(3) Fissel et al. (1982)
(4) Birch et al. (1982)
(5) Birch and Fissel (1982)
(6) Birch et al. (1982)
(7) H. Melling (1984, personal communication)

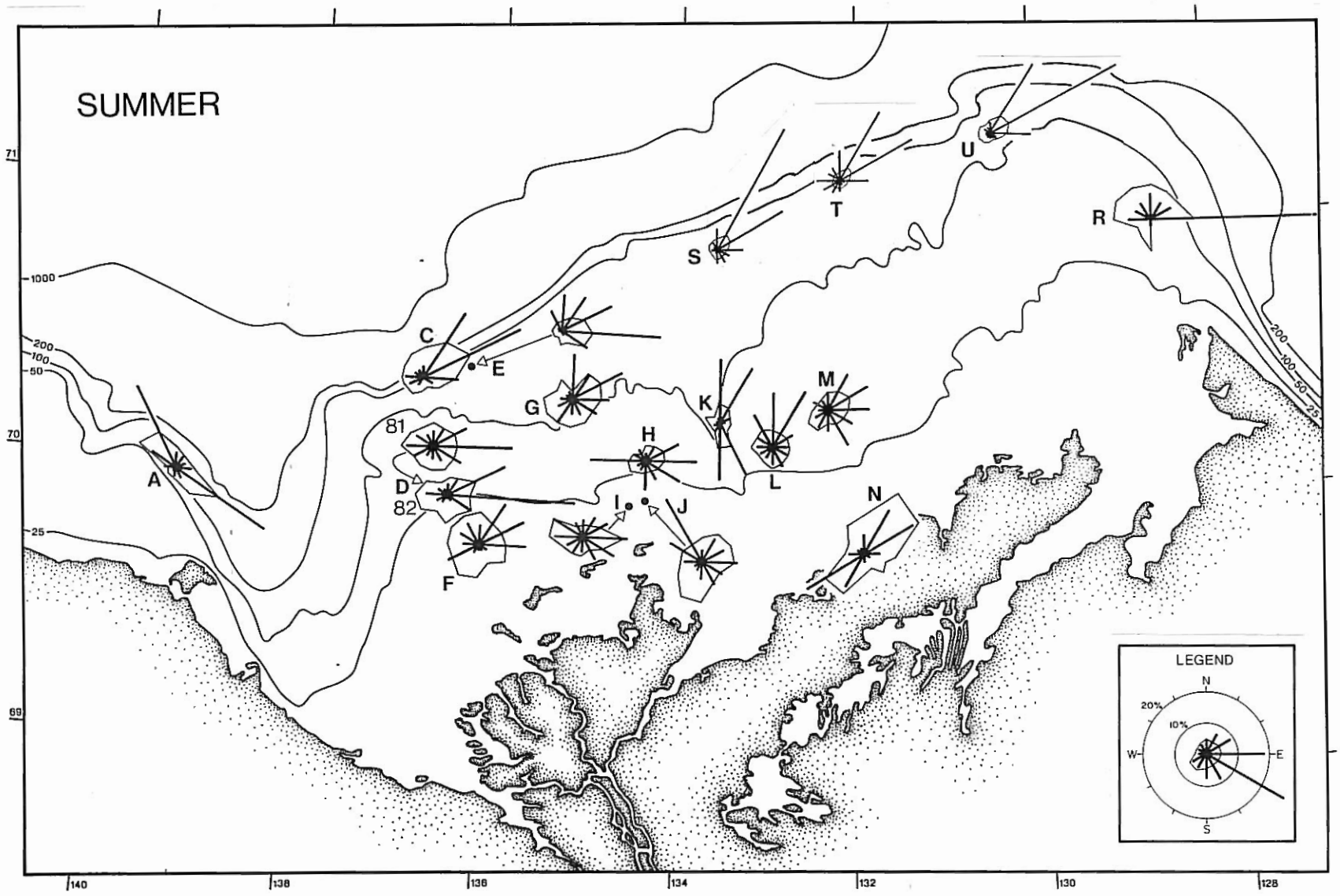

Figure 27: The directional distribution of near-bottom current measurements obtained in the months of July, August and September. Current meter data sets having less than 30 days duration are not included. The radial sticks represent the percentage of observed directions within a given 30° class, scaled as indicated by the values on the rings. The mean speeds for each directional class are also shown, where the scaling is 20 cm/s per ring.

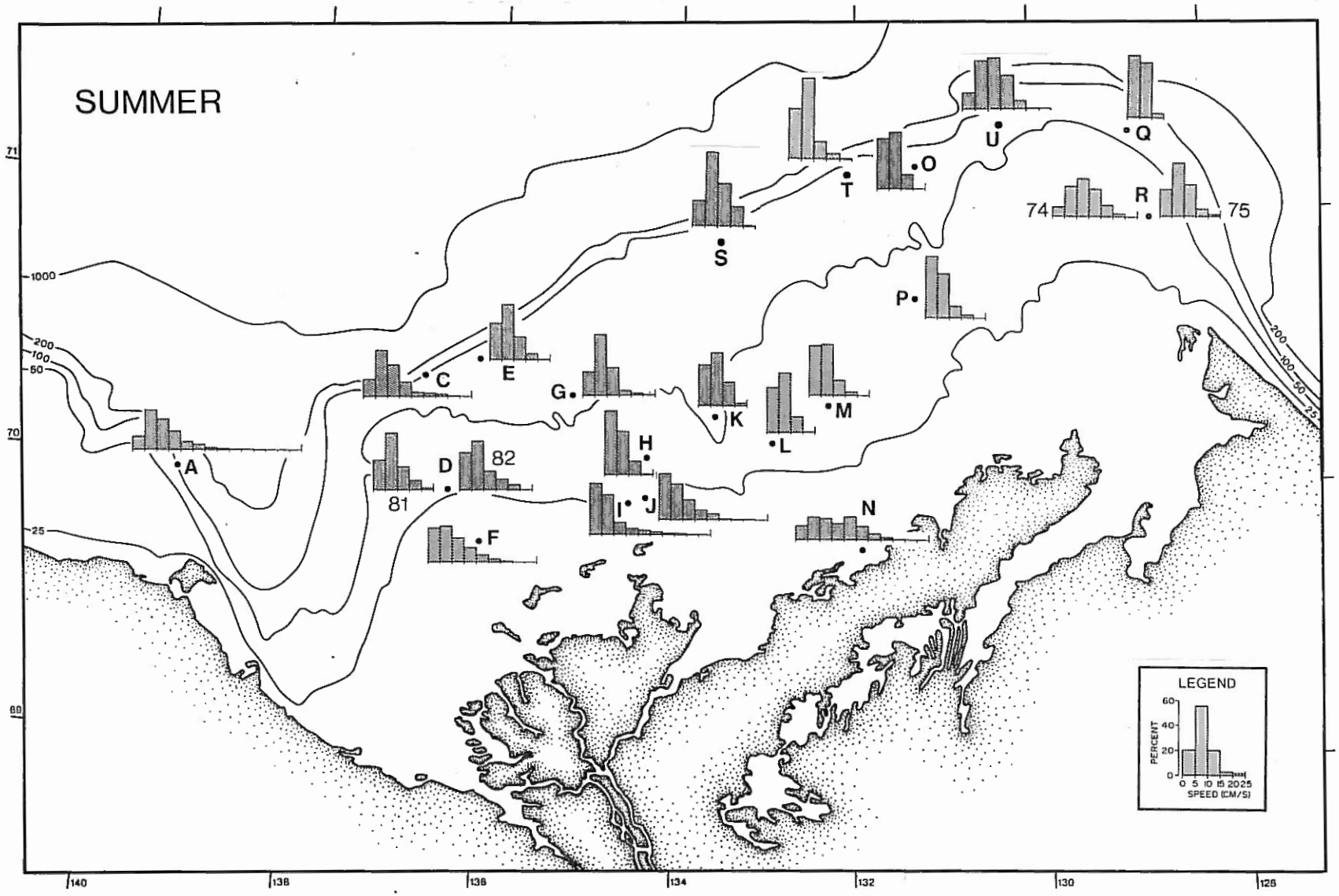

Figure 28: The speed distribution of near-bottom current measurements obtained in the months of July, August and September. Current meter data sets having less than 30 days duration are not included.

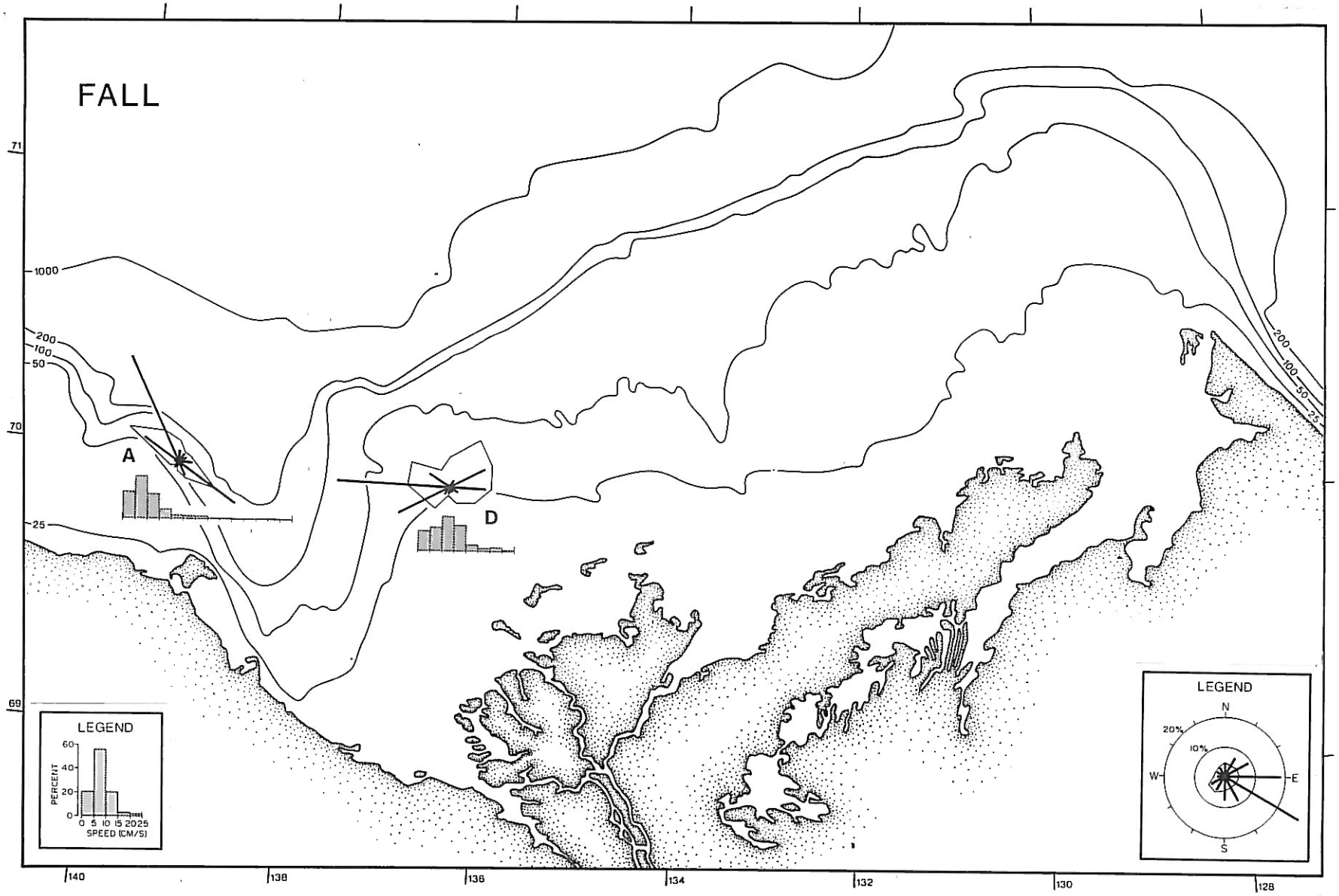

Figure 29: The speed and directional distribution of near-bottom current measurements obtained in the months of October, November and December. Current meter data sets having less than 30 days duration are not included. The radial sticks represent the percentage of observed directions within a given 30° class, scaled as indicated by the values on the rings. The mean speeds for each directional class are also shown, where the scaling is 20 cm/s per ring.

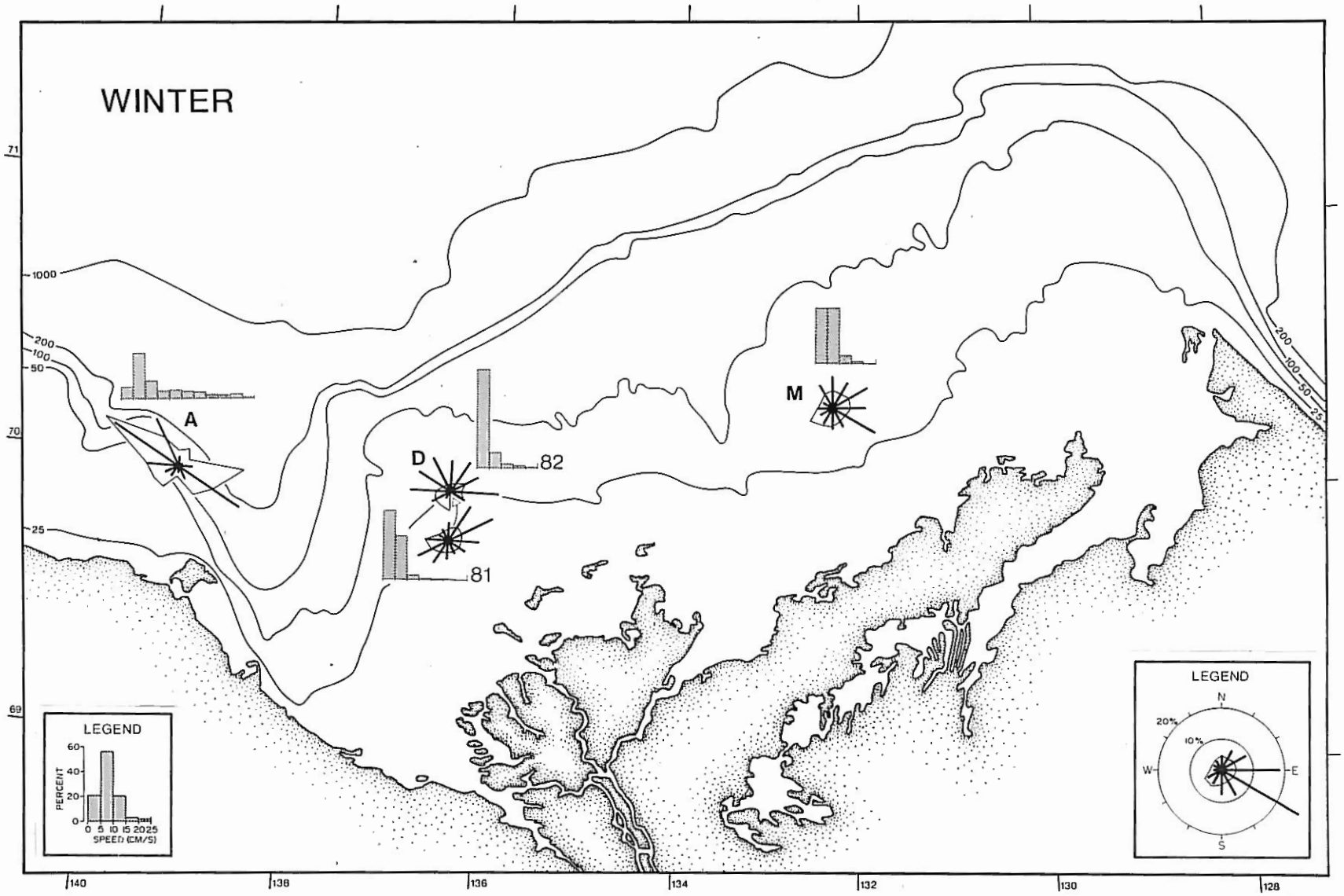

Figure 30: The speed and directional distribution of near-bottom current measurements obtained in the months of January, February and March. Current meter data sets having less than 30 days duration are not included. The radial sticks represent the percentage of observed directions within a given 30° class, scaled as indicated by the values on the rings. The mean speeds for each directional class are also shown, where the scaling is 20 cm/s per ring.

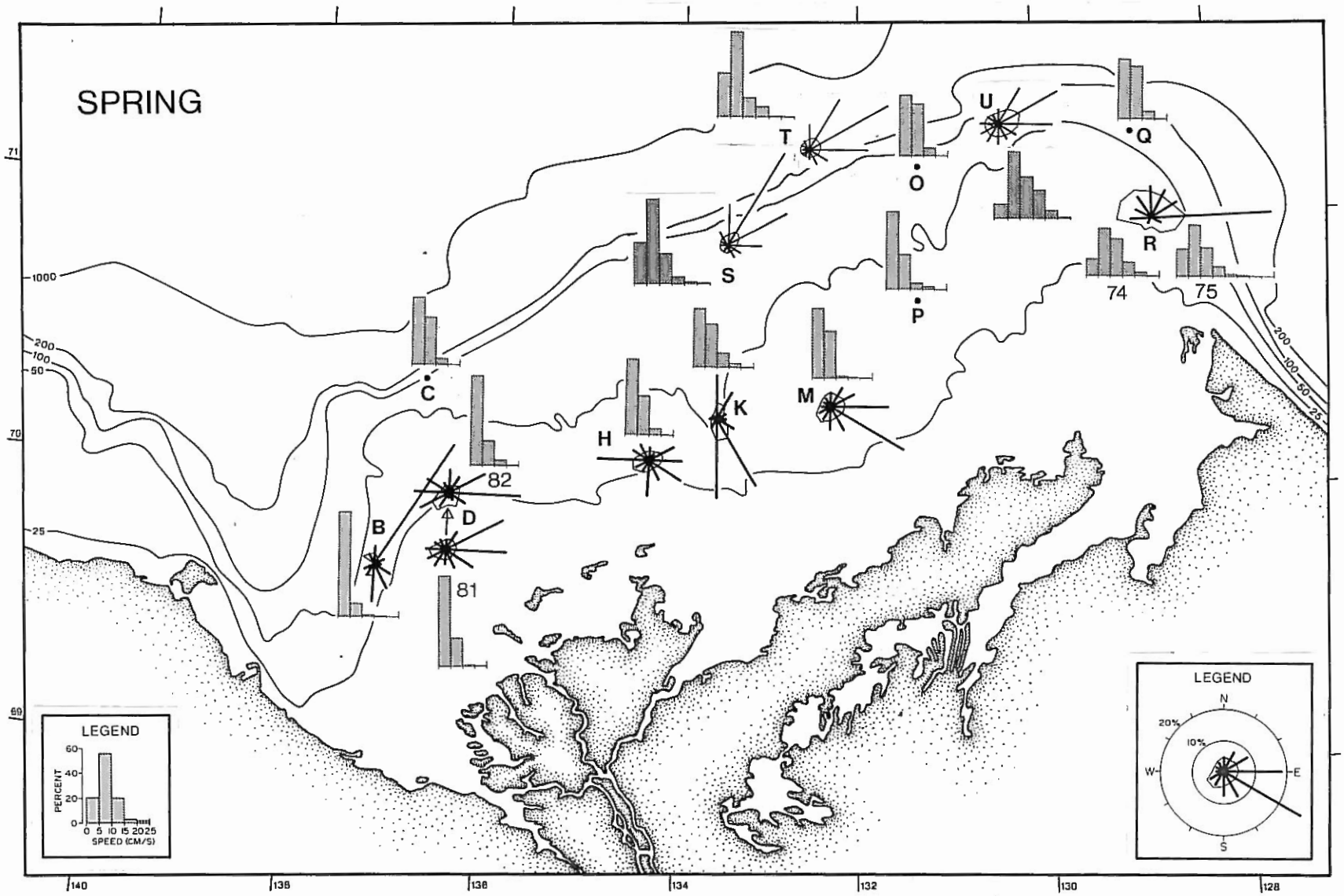

Figure 31: The speed and directional distribution of near-bottom current measurements obtained in the months of April, May and June. Current meter data sets having less than 30 days duration are not included. The radial sticks represent the percentage of observed directions within a given 30° class, scaled as indicated by the values on the rings. The mean speeds for each directional class are also shown, where the scaling is 20 cm/s per ring.

artificial island sites from January to August, 1981 for Dome Petroleum Ltd. (Fissel et al., 1981). A redeployment of the near-bottom mooring in August, 1981 near the Tarsiut site, with recovery in September 1982, resulted in the first year-round current record for the Canadian Beaufort Sea (Birch et al., 1982a). Additional near-bottom current meter data were collected at three locations near the shelf break from late March to mid-August 1981 (Melling, pers. comm.). In 1981 and 1982, current meter data were obtained at shallower locations near artificial island sites on behalf of Esso Resources Canada Ltd. (Birch and Fissel, 1982; Birch et al., 1982b).

The availability of current meter data exhibits a pronounced seasonal bias, with the bulk of the data sets being obtained in summer (19), and spring (12), and very few data sets available for the winter (3) and autumn (2) seasons. In addition to the seasonal bias, the existing data are heavily concentrated at locations over the middle and outer portions (bottom depths ranging from 25 to 80 m) of the Tuktoyaktuk portion of the continental shelf (see Figures 27 to 31).

Data available for water depths less than 25 m are limited to only four locations obtained in the summer of 1981 and 1982. There exists only one set of near-bottom current measurements over the Natsek plain portion of the continental shelf, to the west of Herschel Island. No near-bottom current meter data are available for the continental slope region, including the Mackenzie trough or over the deeper continental rise.

Tuktoyaktuk Shelf

Based on the directional distributions (Figures 27, 29 to 31) and summary statistics (Table 7), the near-bottom currents over the Tuktoyaktuk continental shelf are characterized by a high degree of directional variability. At most locations, the directional distribution indicates a weak preference for flows in two, approximately opposing, directions. The dominant directions usually parallel the local bathymetric contours occurring in the easterly and westerly quadrants, at most locations. The importance of local bathymetry is most apparent at site K, situated in the gently sloping Kugmallit trough; here, the near-bottom currents are oriented along the north-south axis of the trough.

With the exception of the site K data, the degree of bi-modal polarization in the directional distribution appears to be enhanced at the more inshore sites (D, F, I and J) located north of Richards Island and at the single nearshore location (site N),

located approximately 3 km from the nearest coastline. At this latter site, the currents are highly polarized, aligned parallel to the overall trend of the coastline.

On the outer edges of the Tuktoyaktuk continental shelf, the near-bottom currents are different, having a single peak in the directional distribution, occurring in the easterly to northerly quadrant (sites C, E, R, S, T and U).

On the basis of the summer near-bottom current speed distributions (Figures 28 to 31, Table 7) the continental shelf can be subdivided into a relatively energetic inshore zone (depths < 20 m), a middle portion of noticeably lower energies and the outer portion of the shelf with intermediate energy levels. In the inshore zone (sites F, I, J and N), summer speeds average 8 to 10 cm/s (16 cm/s at the nearshore location N), with maximum speeds of 40 to 50 cm/s (56 cm/s at location N). Currents exceed 20 cm/s approximately 10% of the time (40% of the time at location N).

Over the middle portion of the shelf, current speeds are reduced (sites B, G, H, K, L, M, O, P and Q); means speeds are generally near 5 cm/s, with maximum values limited to 16-29 cm/s. The occurrence of speeds exceeding 20 cm/s are rare, ranging from 0% (sites H, K, O and Q) to 2% (site G). Within this middle portion of the shelf, there may be a reduction in energy levels from west to east. A comparison of summer speed data from sites D and L/M located in the western and central sections of the shelf, reveal higher summer speeds at the western location (mean values of 8 versus 6 cm/s; maximum values of 25-27 versus 20-21 cm/s).

Over the outer portion of the Tuktoyaktuk shelf, speeds increase from the adjoining middle portion. At stations C and E located near the western edge of the shelf, mean speeds of 10.8 and 7.4 cm/s were attained with maximum values of 40.9 and 22.6 cm/s, respectively. Further to the east, the offshore shelf stations S, T, O, U, Q and R exhibit more variability, with typical mean speeds of 9 cm/s (range of 5 to 13 among locations). The maximum speeds also vary considerably, from 14 to 32 cm/s, about a median value of 22 cm/s. The high degree of variability observed over the eastern portion of the outer shelf may reflect interannual changes or may be related to the proximity of the measurement site to the presence of an east to northeastward bottom current, widely observed over the outer shelf.

Outer Shelf Bottom Current

The eastward flowing bottom current on the outer portion of the shelf is the only significant mean current resolved in the existing data (Figure 32). The vector averaged magnitude of this current ranges from 5 to 8 cm/s among data sets obtained at stations C, E and R. At other sites located over the inner and middle portions of the shelf, the vector averaged magnitudes generally range from 1 to 3 cm/s (with the exception of site D data in the summer and autumn of 1981 at 4.4 and 3.6 cm/s). The vector averaged flow direction tends to fall in the north to eastward quadrant over most of the inner and middle shelf, but this may simply reflect a dominance of westerly over easterly winds in the period of measurements. Given the very small magnitude of the vector averaged velocity in relation to mean speeds, typically less than 30% (Table 7), there appears to be no significant net bottom current over the inner and middle portion of the shelf.

The spatial scale of the eastward bottom current is unknown. Empirical data suggests that the flow may be stronger at locations near the upper continental slope; for example, compare speeds at stations C and E; the latter site, having lower speeds, is located approximately twice the distance from the shelf break (3.0 km) as the former site (1.5 km). Furthermore, the continental slope in the vicinity of site C is considerably steeper due to large-scale slides than is the case near site E. However, at the eastern end of the shelf, the bottom currents are stronger at site R located in shallower water at a greater distance from the shelf break than sites O and Q.

The eastward current flowing over the outer shelf could be driven by two alternative mechanisms: sea-level differences between Bering Sea and Baffin Bay, as proposed by Aagaard (1982), and haline circulation forced locally by freezing processes (Melling, 1983). For the latter mechanism, dense shelf water resulting from brine extrusion during ice formation would descend and flow seaward. In the process of geostrophic adjustment, a net eastward flow would result over the outer continental shelf; calculations by Melling and Lewis (1982) derived from a stream-tube model for the flow yield speeds of 3 to 5 cm/s. The time scale of the seasonally-induced flow (autumn and winter) would amount to more than 6 months to transit the width of the Tuktoyaktuk shelf.

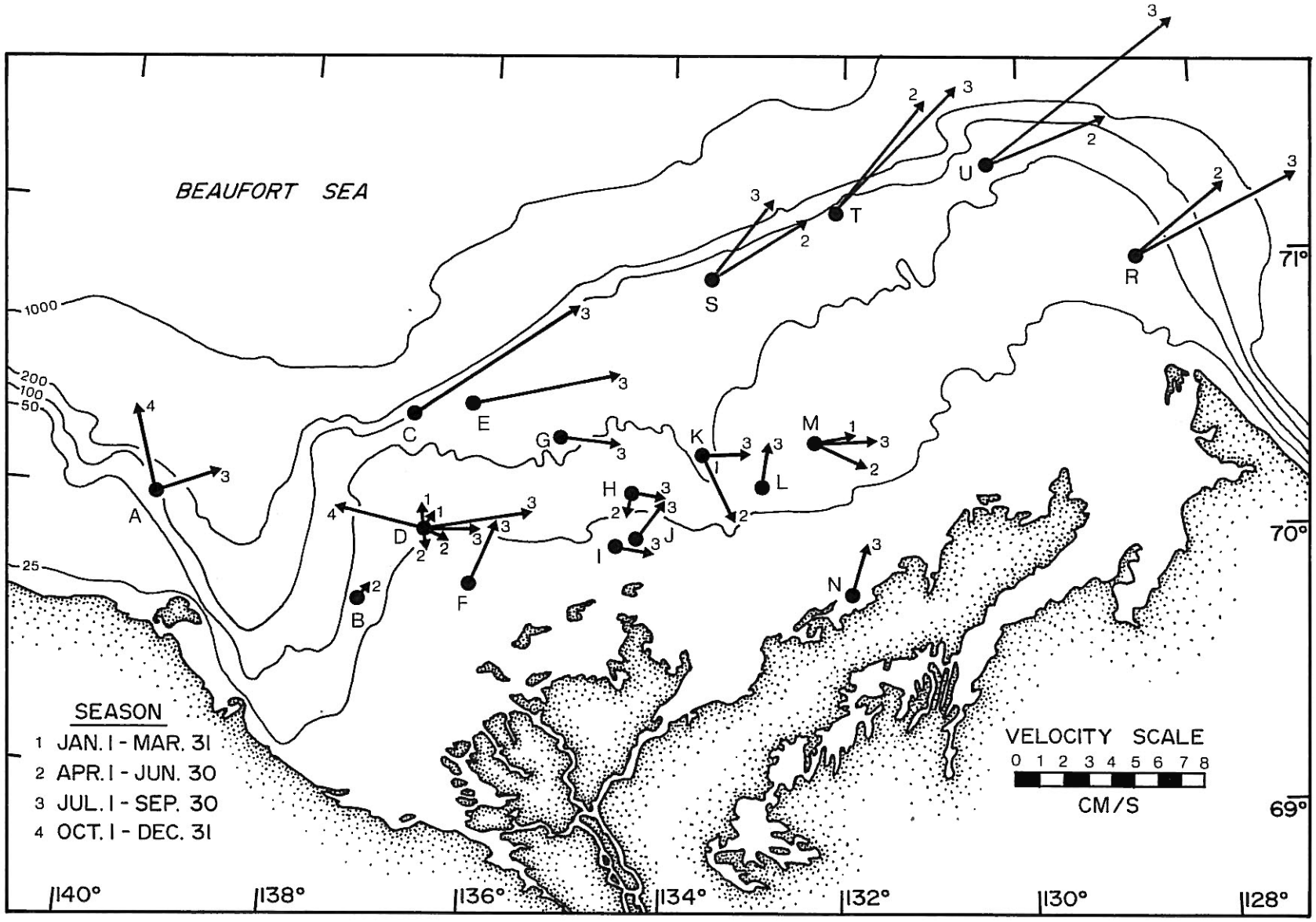

Figure 32: The vector averaged velocities computed for all available near-bottom current meter data sets, exceeding 30 days in duration. The results are presented by season.

Seasonal Variability

A comparison of the speed distributions suggest that important seasonal variations occur in the bottom currents. Based on the 11 data sets of current meter measurements obtained in the spring and summer of the same year at locations C, D(2), H, K, M, O, P, Q and R(2) the speeds in summer increased from those of the spring by an average of 43%, with the increases ranging from 140% (site C) to -4% (site Q). Based on the very limited available data for the autumn and winter seasons at sites D and M the speeds exhibit an increase throughout the summer months which continues into autumn (Figure 33). The speeds then decrease markedly in late autumn to minimum levels in winter. This decrease is likely related to the onset of complete ice formation, reducing the surface forcing by wind, with the increase commencing in late spring and continuing through summer, resulting from clearing of the ice cover. Speeds may reach their seasonal maximum in early autumn, although the evidence for this is based on data from a single year at only one location (site D).

Auto-Spectra

Auto-spectra were computed from a record of near-bottom currents obtained at the Tarsiut site from August 1981 - September 1982. The results (Figure 34) reveal that current variability is concentrated in two frequency bands: low frequency (2 to 20 days) and semi-diurnal (0.5 days).

The frequencies of low frequency activity (Figure 29) are similar to those of the wind, extending over periods ranging from 2 to approximately 20 - 30 days. Like the wind auto-spectra, individual peaks are present, but their frequencies differ among the various auto-spectra.

A pronounced seasonal variation is evident in the low frequency auto-spectral levels, with the maximum values occurring in late summer and autumn and minimum levels occurring during winter and spring. The very marked reduction in the winter and spring is associated with the landfast ice cover extending over the Tarsiut site (Birch et al., 1982a), which virtually eliminates the generation by wind of low frequency current fluctuations. The very large auto-spectral values of August 11 - October 22 are due, in large part, to strong currents (20-38 cm/s) occurring from September 26 - October 26. This suggests an increase in the level of low frequency current fluctuation in autumn, prior to freeze-up. Unfortunately, as this is the only current meter record obtained in autumn over the Tuktoyaktuk

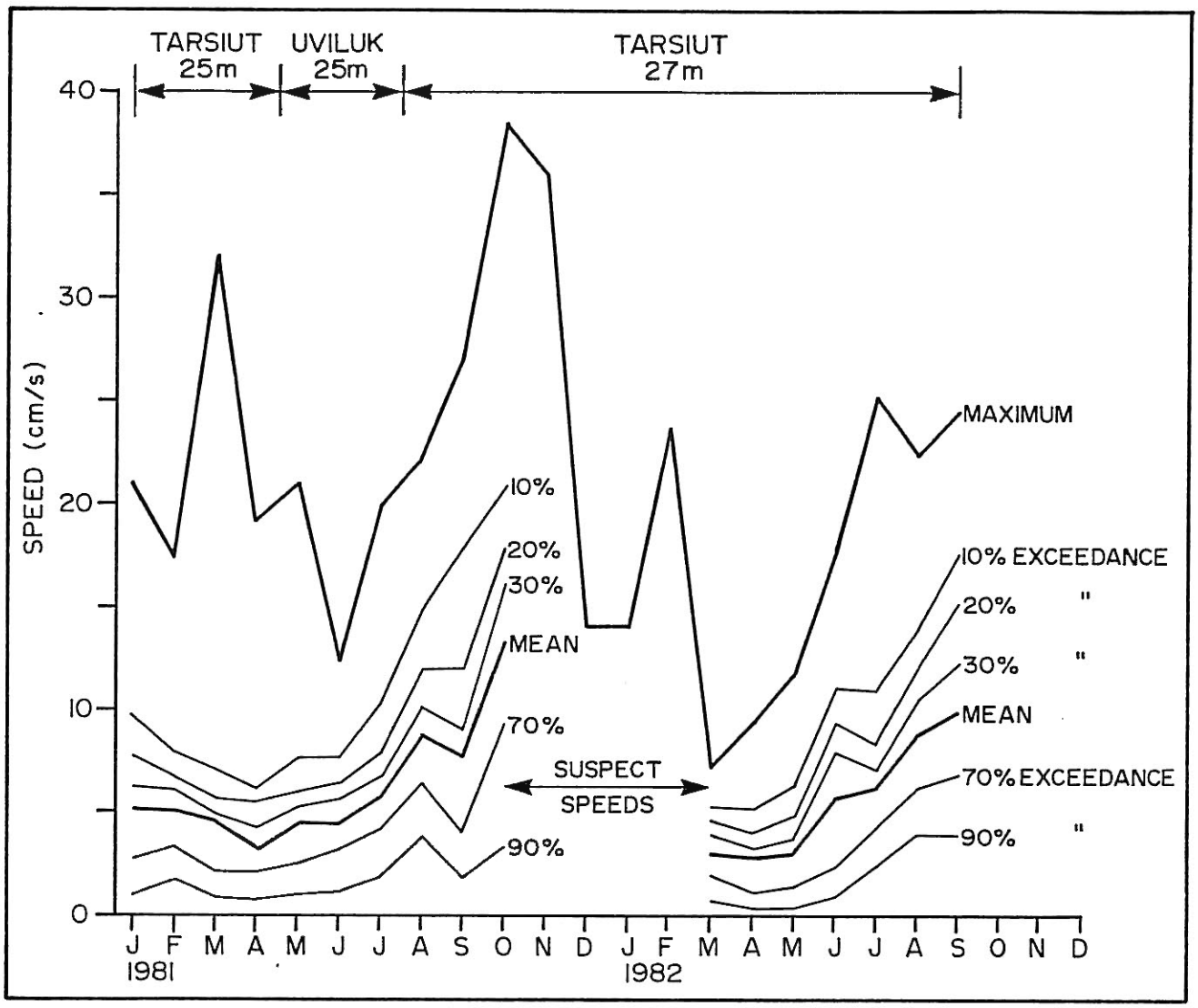

Figure 33: Computed monthly mean and percent exceedance values of near-bottom current speeds obtained near the Tarsiut and Uviluk (D and M) from January 1981 to September 1982.

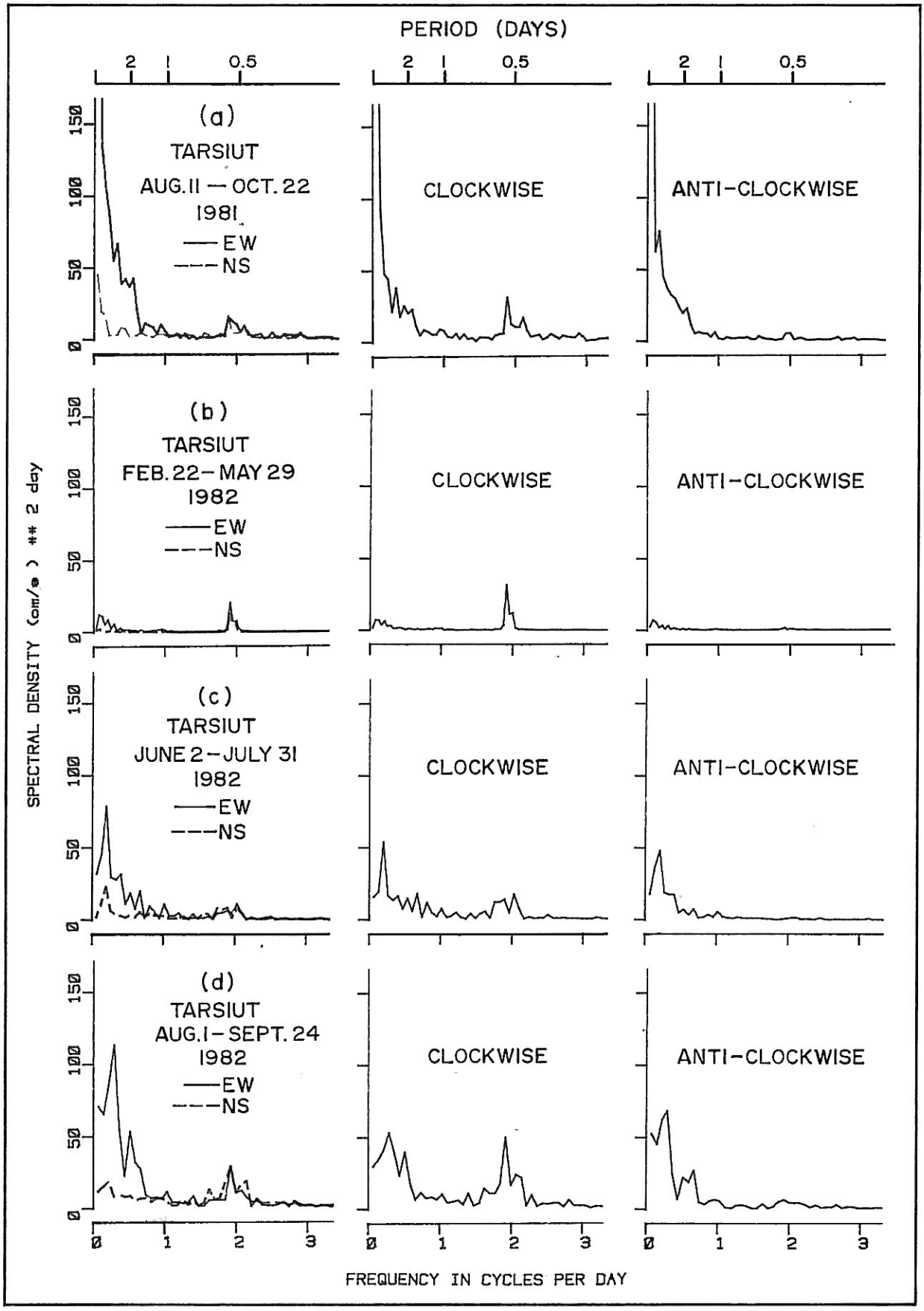

Figure 34: The auto-spectral densities for near-bottom current meter data obtained near the Tarsiut site: a) August 11-October 22, 1981 - 4 blocks of 432 hourly records; b) February 22-May 29, 1982 - 4 blocks of 576 hourly records; c) June 2-July 31, 1982 - 4 blocks of 354 hourly records; d) August 1-September 24, 1982 - 4 blocks of 324 hourly records.

shelf, it is not clear as to how representative this result is of other years. However, the increased low frequency activity appears to result primarily from an increase in current wind coupling, likely associated with reduced stratification of the water column (see Section 3.1) rather than a proportionate increase in wind speeds from the summer levels.

Semi-Diurnal Currents

Seasonal changes in semi-diurnal activity are small (Figure 34). In all of the seasonal auto-spectra, the currents of semi-diurnal frequency exhibit a high degree of circular polarization, with rotations occurring in a clockwise manner. These semi-diurnal currents result from tidal flows and wind-driven inertial oscillations. Because the latter occur within the range of semi-diurnal tidal constituents, these two possible sources cannot be differentiated on the basis of frequency. The semi-diurnal tidal flows associated with the surface tide (barotropic) are small, ranging from 1 to 3 cm/s over the Tuktoyaktuk shelf (Huggett et al., 1975; Henry and Foreman, 1977); however, the amplitude and spatial patterns of internal semi-diurnal tidal currents are poorly understood in this region.

Inertial oscillations have typical amplitudes of about 5 cm/s in the near-bottom currents over periods of a few to several days (Huggett et al., 1975; Fissel, 1981; Birch et al., 1982a; Fissel and Birch, 1983). Semi-diurnal current speeds exceeding 10 to 15 cm/s occur intermittently (Fissel, 1981; Fissel and Birch, 1983); these are usually associated with an abrupt change in the wind field. The response to changes in the wind in the form of inertial oscillations of near-bottom currents is complex, depending on the frequency of the shift in the wind field and the stratification in the water column (Pollard, 1980). At the surface, the optimum response is realized when the change in the wind occurs near the inertial period (approx. 12 hours); thus small variations in the wind field due to a weather system moving across an oceanic area can generate quite different responses. Furthermore, differences in the stratification will change the way in which the inertial oscillations propagate through the water column. As a result, inertial oscillations in near-bottom currents have relatively small horizontal scales, generally less than 10 km, and are not predictable in the absence of local measurements of wind and water column density profiles.

Unlike the low frequency variations, the semi-diurnal activity at the Tarsiut site remained comparatively high through the ice covered period (February 22 - May 29 in Figure 33). This finding suggests that inertial oscillations (or tidal flows) are

present under the ice cover; indeed, Birch et al. (1982a) report the intermittent occurrence of inertial activity throughout this period, with typical amplitudes of 5 cm/s. These inertial oscillations are likely generated in the region of open water or thin ice of the transition zone (Section 2.3) which was located within a few kilometres of the Tarsiut site in the spring of 1982 (Marko, pers. comm.). The absence of wind-driven currents at low frequencies for this same period indicates that the horizontal scale of the low frequency response may have been smaller than that of the inertial response to winds.

2.5.3 SUSPENDED SEDIMENT CONCENTRATIONS WITHIN THE WATER COLUMN

Data Sources

Suspended sediment concentration (SSC) data available for the Canadian Beaufort Sea fall into three categories:

1) Most recently, satellite imagery have been analyzed to map surface distributions of SSC (Harper and Penland, 1982; Marko and Oberski, 1982; Marko et al., 1983).

2) In a number of oceanographic surveys, SSC data have been collected using the more traditional methods of measurements from water samples. Such data are available for nearshore areas (generally landward of the 10 m isobath) in 1974 and 1975 (McDonald and Martin, 1976) and 1977 (Fraker at al., 1979). In offshore areas, large-scale surveys were carried out in 1975 (Bornhold, 1975; Matsumoto and Wong, 1977), while more recent data have been collected at particular sites (e.g. sampling near Issungnak in 1981-1982; Erickson et al., 1983).

3) Beginning in 1974, vertical profile data have been collected using transmissiometers; such data lack absolute calibration standards (permitting comparison with other data) but do offer a measure of relative changes.

The satellite imagery results (see, for example, Figure 35), while very useful in determining the large-scale horizontal distributions at the surface, have also some distinct limitations. The available measurements are almost always obtained under easterly or weak wind conditions because westerly winds are associated with cyclonic weather disturbances accompanied by a high degree of cloud cover. In addition, while

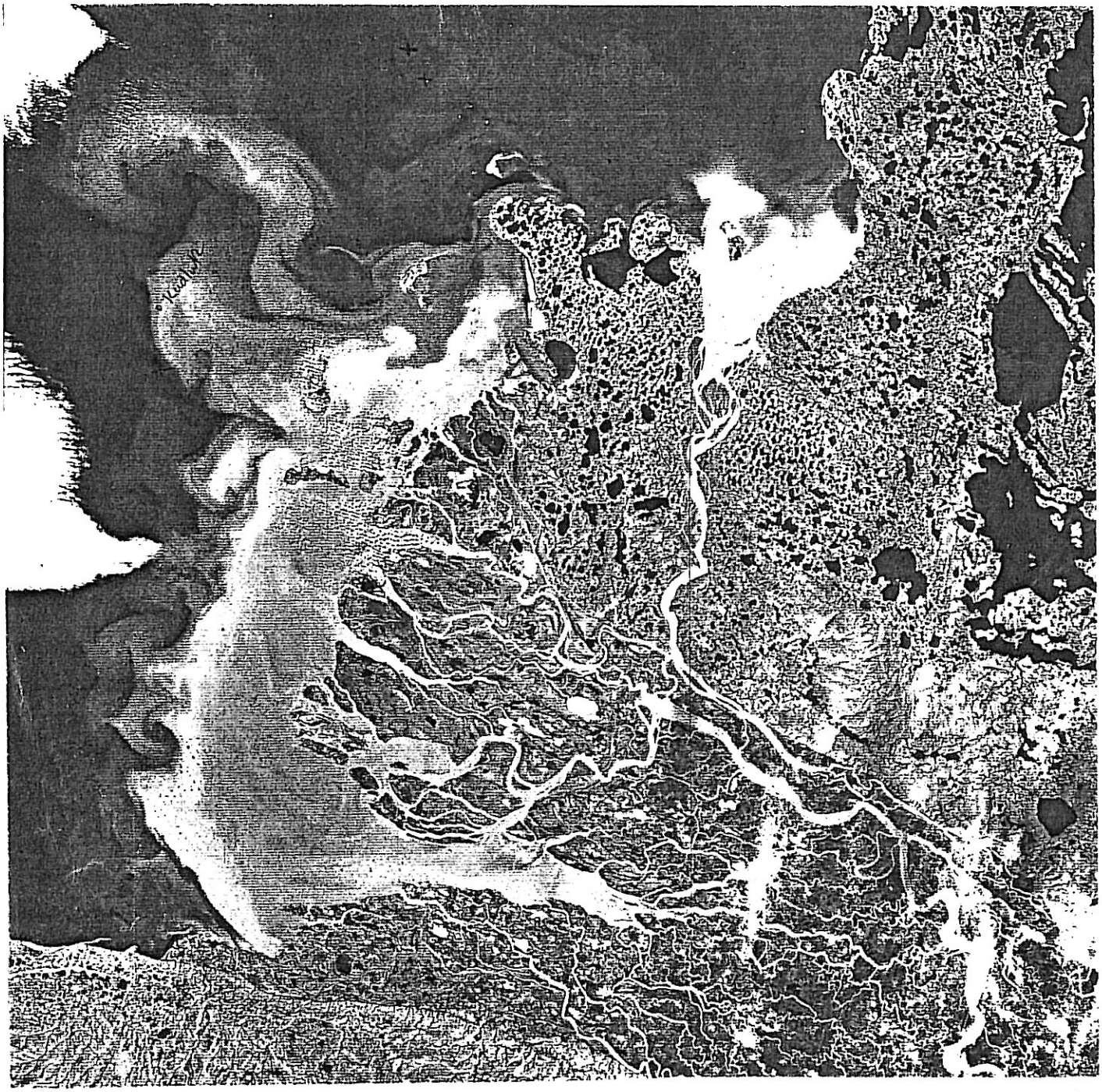

Figure 35: September 1973 ERTS satellite image (visual band) of the Mackenzie River plume in Mackenzie and Kugmallit Bays (Herlinveaux and de Lange Boom, 1975).

quantitative values for SSC can be obtained from measured radiance values (Amos and Alfoldi, 1979), no calibration data were available from the Beaufort Sea, leading to uncertainties in the resulting values.

Nearshore Areas

The SSC values in nearshore locations are considerably larger than further offshore. This very pronounced difference is most apparent in the satellite imagery studies of Harper and Penland (1982) and Marko et al. (1983). In both studies, for all images examined, a very strong gradient in SSC levels was evident, separating the very turbid water located offshore of Mackenzie River discharge channels from the much reduced SSC values occurring further offshore. Through this gradient or front, a reduction of nearly two orders of magnitude occurred over distances of a few kilometres (see, for example, Figure 36 from Harper and Penland, 1982). The areas having the highest SSC levels are Shallow Bay to East Mackenzie Bay and Kugmallit Bay; the strong gradients marking the offshore side were determined to occur "inside the 10 m isobath and often inside the 5 m isobath" by Harper and Penland (1982) while Marko et al. (1983) situated this boundary between the 1 m and 5m isobath. In both studies, these two turbid areas were separated by a zone of comparatively low turbidity adjacent to the Mackenzie delta, roughly bounded by Pullen and Hopper Islands and North Point on Richards Island.

A large degree of variability is evident from both the satellite and oceanographic survey data in the SSC levels of the highly turbid nearshore areas. The surface measurements reflect the observation (Fraker et al., 1979) that "there is greater year-to-year variation in turbidity in the Mackenzie estuary than in either salinity or temperature". The highest levels of turbidity tended to occur at times close to the June or July peaking of the Mackenzie flow, with maximum values reaching approximately 200 ppm in the relatively typical early summer periods of 1975 and 1977. In 1974, when the extreme inshore position of the ice pack confined the River Water to a relatively narrow coastal zone of open water, the maximum measured turbidity levels were two to three times higher than the corresponding 1975 and 1977 values. These maximums were attained during the month of August and were attributed (Fraker et al., 1979) to abnormally high precipitation in the Mackenzie River watershed as reflected in the extremely high turbidity values recorded in the river during the same period (Section 2.1).

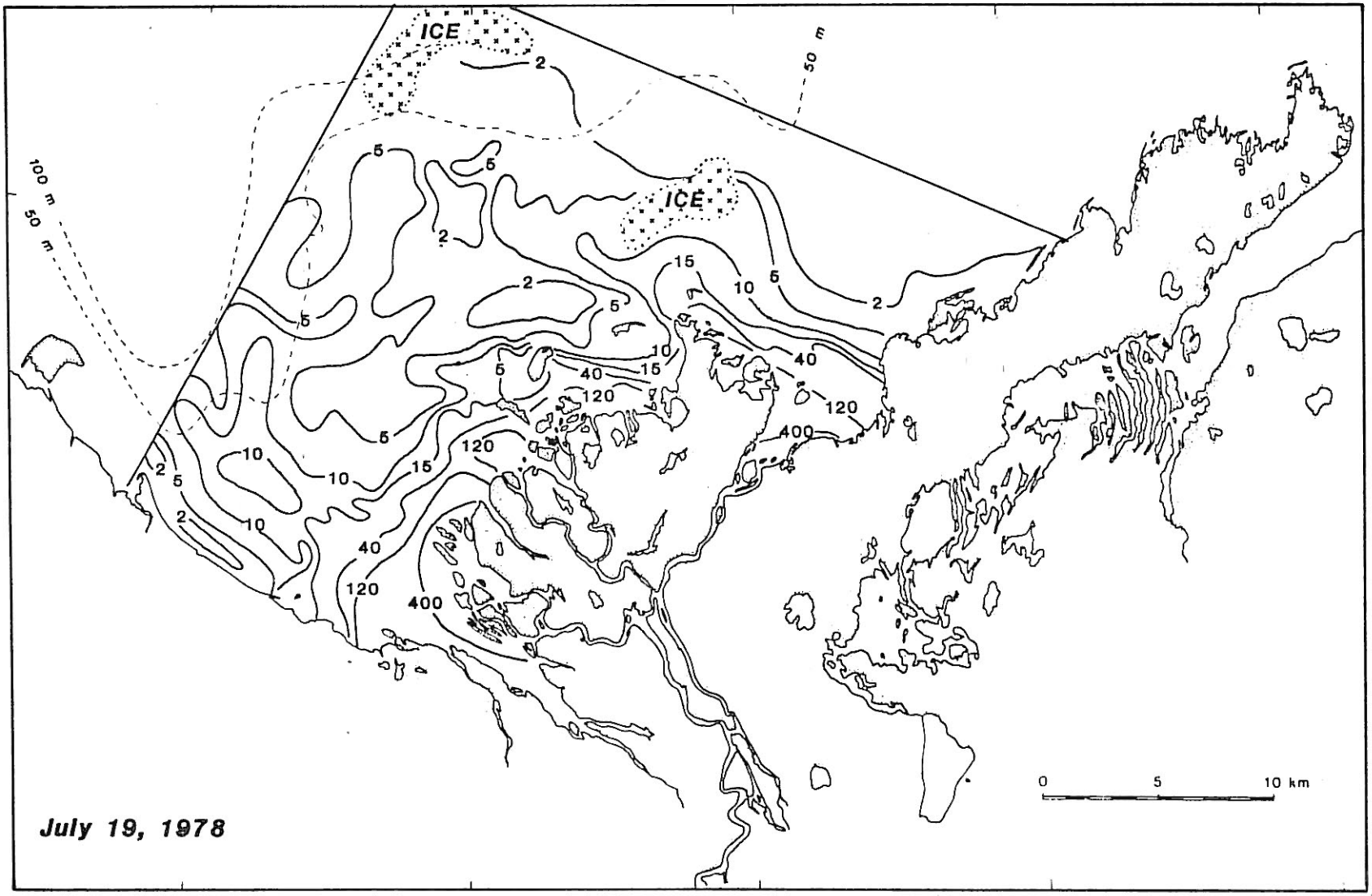

Figure 36: Suspended sediment concentrations (mg/ℓ) computed from July 19, 1978 Landsat data (from Harper and Penland, 1982).

Other influences can also account for some of the variability in turbidity levels of the nearshore zone. Resuspension of bottom sediments due to wave action have been associated with increases in turbidity observed on specific occasion in both 1975 (July 26-30 following moderate northwesterly winds; McDonald and Martin, 1976) and 1977 (August 4 following east-northeasterly winds and wave heights of up to 1.2 m; Fraker et al., 1975 as shown in Figure 37). An indication of such resuspension is seen in the higher values of near-bottom turbidity over those at the surface (McDonald and Martin, 1976). Coastal upwelling driven by prolonged easterly winds (Section 2.5.1) can alter nearshore turbidity levels by displacing the usually turbid water along the coastline, with clear, higher salinity water at locations away from discharge points. An example of this can be seen in the low SSC levels off the Tuktoyaktuk Peninsula on July 19, 1978 (Figure 36).

Offshore Areas - Surface

Beyond the shallow water areas adjoining the Mackenzie delta, surface SSC values are much reduced, generally less than 2 ppm (Figure 38), although occasionally reaching levels of 5-10 ppm. Two reasonably distinct patterns of surface SSC distributions occur, determined by the overall wind field. Under westerly or calm conditions, the diffuse, outer plume is confined to a relatively narrow coastal band, confined to perhaps 20 km of the coastline extending along the Tuktoyaktuk Peninsula. (Few data are available to delineate this pattern, due to the rarity of satellite imagery for westerly wind conditions.)

Under easterly winds, the outer plume is deflected to the west along the Yukon coastline and to the north and east offshore of the delta. The outer perimeter of the sediment plume is often obscured by the offshore pack. To the east of Kugmallit Bay the surface sediments are often distributed in two distinct eastward-tending bands. One of these is offshore and rather broad in character with its core located, typically, 75 km from the coastline. The second band is narrower, often less than 20 km in width, and adjoins the coastline (Marko and Oberski, 1982; Marko et al., 1983). The two bands are separated by a stretch of water 20 to 60 km in width having apparently little sediment content. In most cases, the offshore band is faint and difficult to detect in the offshore region between Cape Dalhousie and Cape Bathurst and the coastal band seldom has been observed to extend beyond Cape Dalhousie.

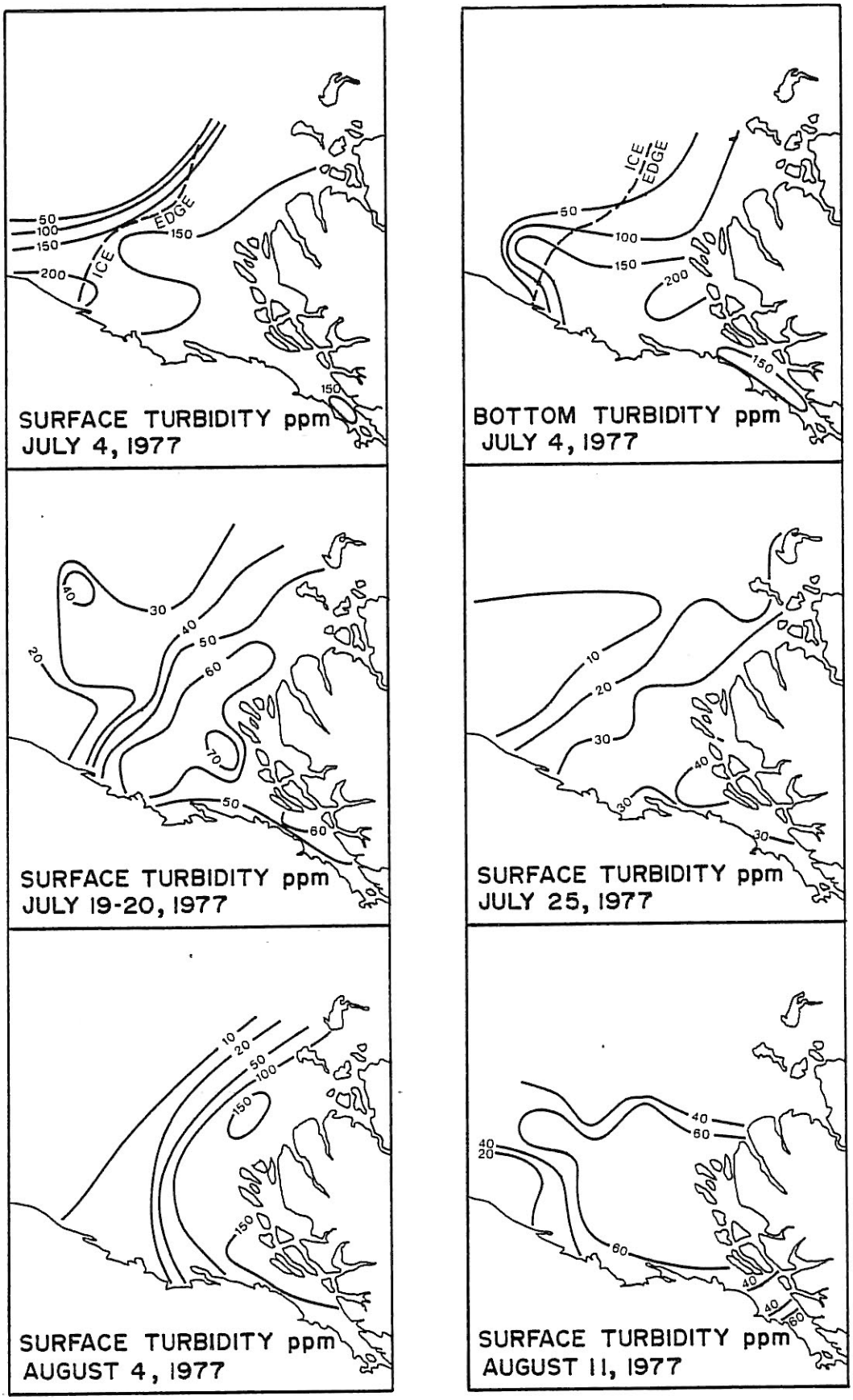

Figure 37: Turbidity distributions measured in Mackenzie Bay in the summer of 1977 (from Fraker et al., 1977).

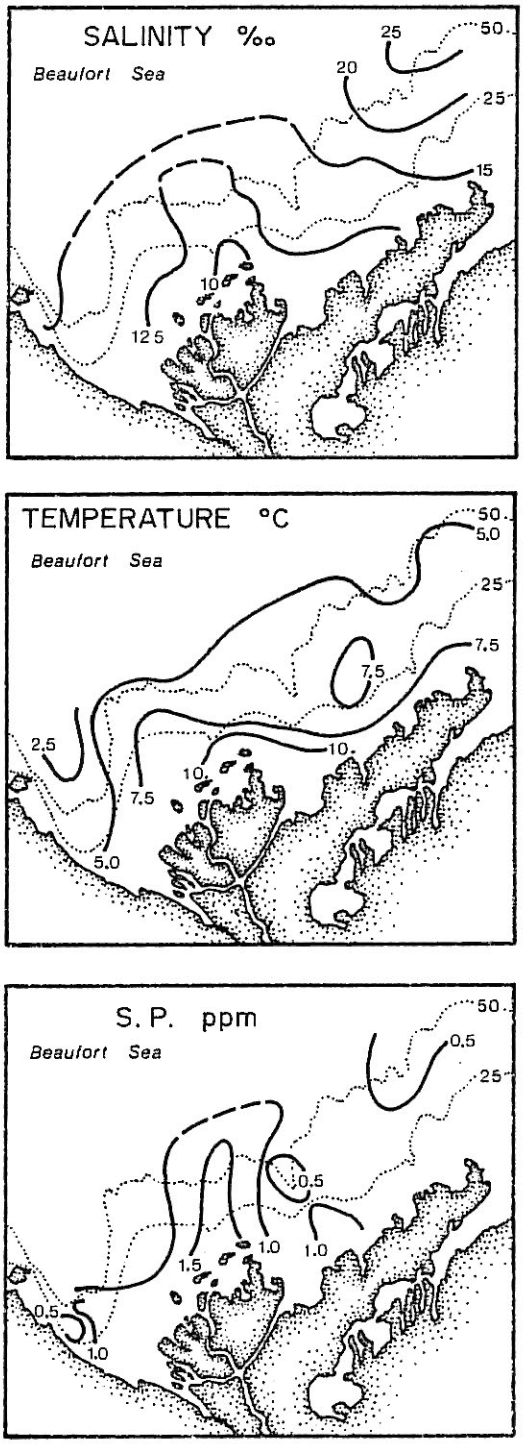

Figure 38: Surface distributions of temperature salinity and suspended sediment concentrations, August 5-23 (from Matsumoto and Wong, 1977).

For all wind conditions many prominent smaller-scale features resembling eddies and gyres occur along the boundaries of the sediment plume (Figure 35). These are particularly evident in the vicinity of Herschel Island, northern Mackenzie Bay and along the Tuktoyaktuk Peninsula. The structures have spatial scales ranging from less than 1 km to 30 km or more and often appear to be related to surface current shears (Marko et al., 1983).

Matsumoto and Wong (1977) show that the offshore levels of surface SSC decrease more rapidly with increasing salinity than would be expected on the basis of ideal mixing (Figure 39). This finding suggests that settling is occurring in these offshore areas, causing the enhanced reduction with increased salinities. At many locations, a maxima of SSC in the subsurface layer (2 to 10 m depth) can be attributed to this settling (Matsumoto and Wong, 1977).

Offshore Areas - Subsurface

Seaward of approximately the 20 m isobath, available data consistently reveal the occurrence over the continental shelf of a maxima in turbidity at or near the surface and in the near-bottom boundary layer (Figure 40), with generally reduced sediment concentrations at mid-depth. The SSC levels of the near-surface and near-bottom maxima are similar, typically 0.5 to 2.0 ppm. Both maxima exhibit considerable variability with time, although these changes seem to occur independently between the surface and bottom. On the basis of size distribution of sediments, Matsumoto and Wong (1977) argue that the near-bottom maximum consisting primarily of very fine sediments, is composed of resuspended sediments to a greater degree than in the surface maximum (Figure 41).

Bornhold (1975) attributes the existence of the near-bottom SSC maximum to a number of possible mechanisms: 1) unidirectional bottom currents; 2) surface waves associated with storms; 3) tidal currents; and 4) breaking internal waves. The possibility of turbidity currents flowing seaward along the bottom were rejected, as the SSC levels are low by at least two orders of magnitude to replace the more dense offshore bottom waters with less dense nearshore bottom water under spring and summer conditions (Bornhold, 1975).

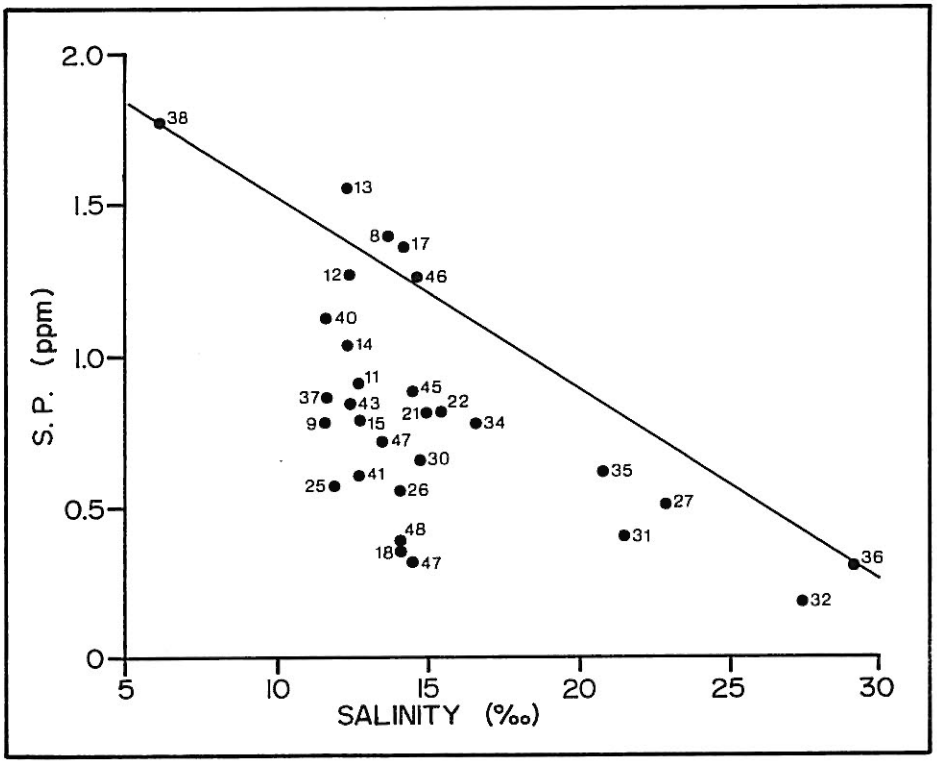

Figure 39: A plot of suspended particulate (S.P.) against salinity for the surface measurements obtained at the locations of Figure 38. The solid line represents an ideal mixng curve (Matsumoto and Wong, 1972).

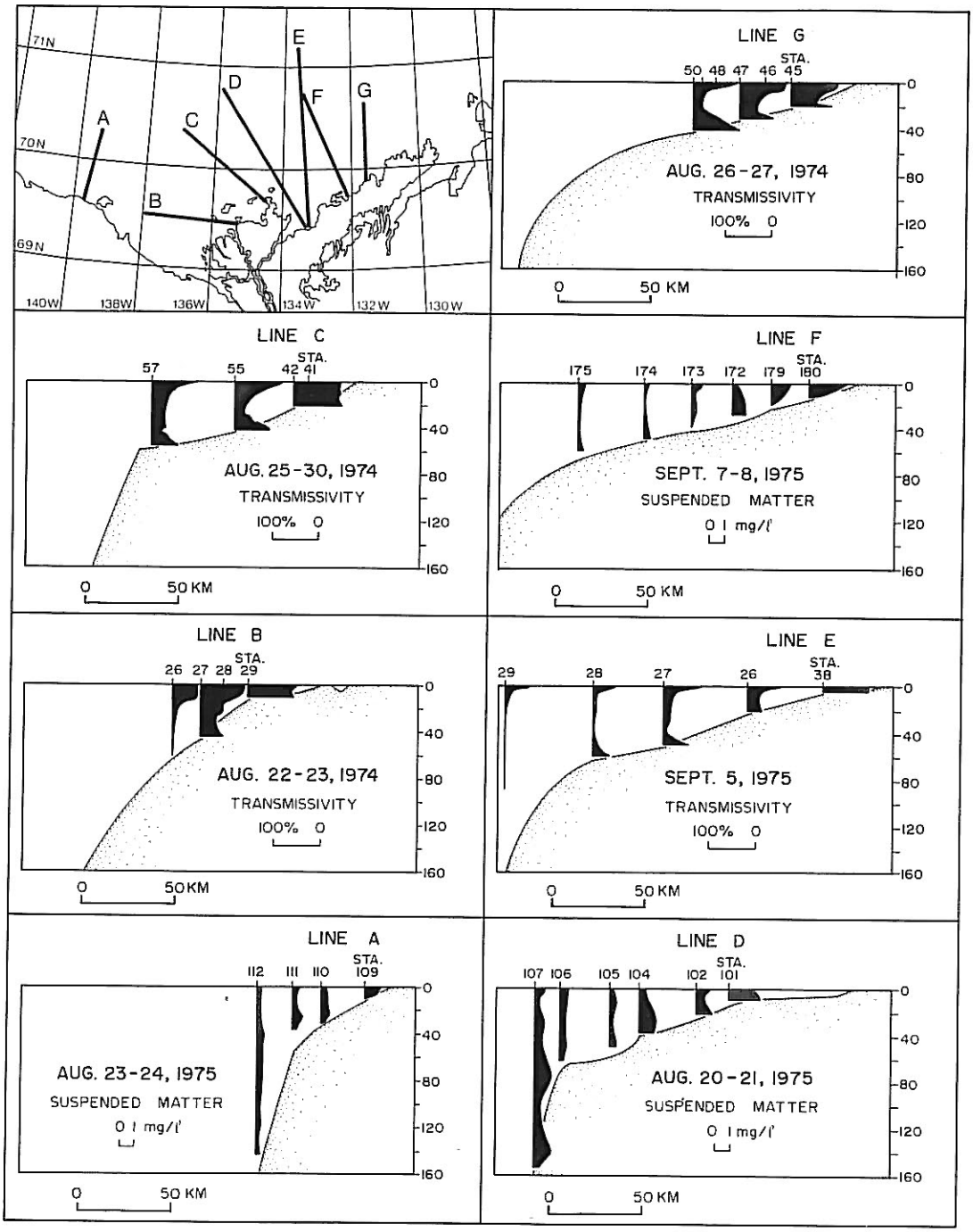

Figure 40: Vertical profiles of turbidity or transmissivity compiled for various on- to offshore transects in the Canadian Beaufort Sea.

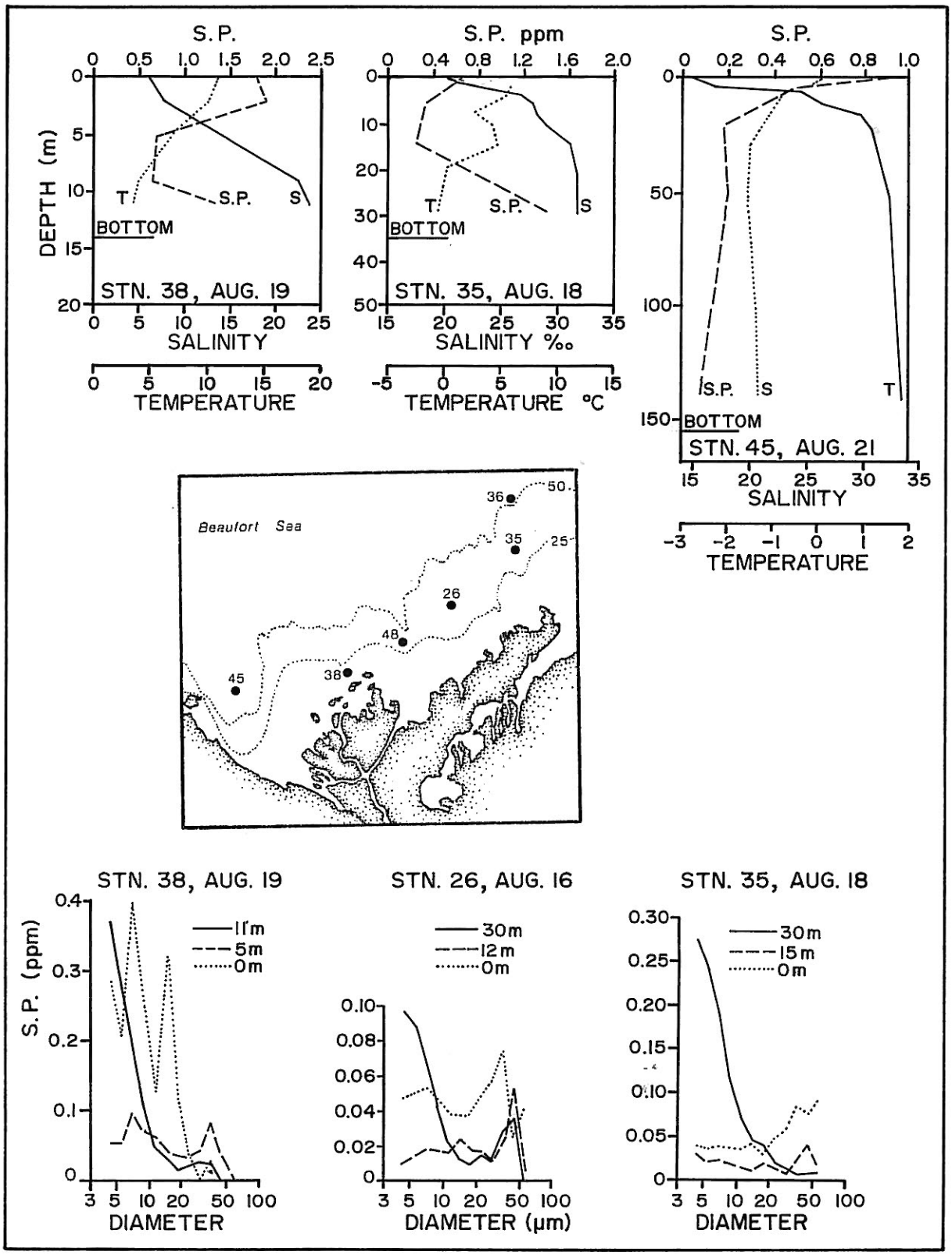

Figure 41: Vertical profiles of suspended sediment concentration, temperature and salinity at three stations occupied August 18-21, 1975. Also shown are analyses of sediment particle size distribution for near-surface, mid-depth and near-bottom samples.

3. OCEANOGRAPHIC ANALYSIS RESULTS

3.1 FORCING OF NEAR-BOTTOM CURRENTS

3.1.1 WIND-BOTTOM CURRENT COUPLING

Theoretical understanding of the response of currents to winds in shallow continental shelf regions such as the Beaufort Sea, is only now beginning to emerge. The oceanic response to large-scale wind systems takes the form of transient shelf waves which vary in a complex manner according to a variety of factors including local topography, degree of oceanic stratification and the spatial/temporal patterns of the wind forcing. In view of the limitations of existing ocean current data for the Beaufort Sea, a more empirical approach was applied to analyze the response of bottom currents to winds in the present study. Linear regression analyses were performed for selected time series of near-bottom currents with the best available local wind data. The lines of regression between the wind and current velocities were computed according to

$$V_C = A+B \cdot V_W$$

where V_C and V_W are the bottom current and wind speeds respectively; A and B the regression coefficients. The dominant wind and current patterns are oriented east-west; therefore in most cases regression coefficients were computed separately for the east-west velocity components and the speeds. If the velocity distribution was not primarily east-west, then major current components were used.

The correlation coefficient (R) relating the pair of time series was also computed. The proportion of the variance of current velocity that can be attributed to the wind velocity can be approximated as the square of the linear correlation coefficient (R^2). Significance levels for R were based on the standard formula (Panofsky and Brier, 1958)

$$R = [3.814/(N+1.814)]^{1/2}$$

where N is the number of independent samples used in computing the regression. The value of N was determined by arbitrarily assuming 4 independent samples occur each day.

The results for summer conditions are presented in Table 8 (east-west or major component) and Table 9 (speed). Note that B is presented as a percentage of the winds. The correlation results are given for the lag time (positive when the current

Table 8: Results of linear regression analyses between marine winds and bottom currents for east-west or major components

No.	Current Meter Data Sets	Wind Data Set	Period	Depth (m) CM	Depth (m) Water	Major Component Direction	Regression Coefficients R	Regression Coefficients A (cm/s)	Regression Coefficients B(Z)	Number of Data Points	Significance Level of R	Time Lag (hrs)
1	BSP.13	TUK.	Aug. 6-Sept. 8 1975	30	33	70	.63	-.5	.62	130 (6 hrly)	0.17	6
2	BSP.5	TUK.	Aug. 4-Sept.11 1975	64	67	50	.58	7.1	1.09	151 (6 hrly)	0.16	24
3	KPN'77	KPN.	Aug. 4-Sept.30 1977	50	57	90	.52	3.8	.56	1331 (hrly)	0.13	5
4	NKT'77	NKT.	July 31-Oct.13 1977	60	62	90	.40	6.7	.34	1559 (hrly)	0.12	17
5	UVILUK	TUK.	July 1-Aug. 5 1981	19	25	60	.72	2.0	.74	140 (6 hrly)	0.16	12
6	TARSIUT	TUK.	Aug.11-Sept.30 1981	25	28	90	.53	4.2	.69	198 (6 hrly)	0.14	12
7	TARSIUT	TUK.	Aug. 1-Sept.24 1982	27	30	90	.59	2.8	.90	218 (6 hrly)	0.13	12
8	W.ATK.	ISSUNGNAK	Aug. 8-Sept.26 1981	7	8	50	.80	2.2	2.41	1189 (hrly)	0.13	7
9	KADLUK	TARSIUT	Aug. 6-Sept.25 1982	11	13	90	.32	2.1	.47	1221 (hrly)	0.13	1
10	ISSERK	TARSIUT	Aug. 6-Sept.14 1982	6	7	90	.69	3.7	1.17	936 (hrly)	0.16	3

Table 9: Results of linear regression analyses between marine winds and bottom currents for speeds

No.	Current Meter Data Sets	Wind Data Set	Period	Depth (m) CM	Depth (m) Water	Regression Coefficients R	A (cm/s)	B(°)	Number of Data Points	Significance Level of R	Time Lag (hrs)
1	BSP.13	TUK.	Aug. 6-Sept. 8 1975	30	33	.50	2.5	.44	130 (6 hrly)	0.17	6
2	BSP.5	TUK.	Aug. 4-Sept.11 1975	64	67	.55	4.6	1.14	151 (6 hrly)	0.16	30
3	KPN'77	KPN.	Aug. 4-Sept.30 1977	50	57	.24	5.8	.35	1329 (hrly)	0.13	7
4	NKT'77	NKT.	July 31-Oct.13 1977	60	62	-.14	no significant correlations			0.12	N/A
5	UVILUK	TUK.	July 1-Aug. 5 1981	19	25	.66	1.1	.75	140 (6 hrly)	0.16	12
6	TARSIUT	TUK.	Aug.11-Sept.30 1981	25	28	.61	2.9	.78	198 (6 hrly)	0.14	12
7	TARSIUT	TUK.	Aug. 1-Sept.24 1982	27	30	.37	6.4	.47	218 (6 hrly)	0.13	12
8	W.ATKINSON	ISSUNGNAK	Aug. 8-Sept.26 1981	7	8	.55	5.9	1.72	1192 (hrly)	0.13	4
9	KADLUK	TARSIUT	Aug. 6-Sept.25 1982	11	13	.39	4.3	.74	1210 (hrly)	0.13	12
10	ISSERK SHOAL	TARSIUT	Aug. 6-Sept.14 1982	6	7	.44	1.2	.95	936 (hrly)	0.16	0

lags the wind) which provides the maximum correlation coefficient. The wind time series are from offshore locations (10 m), whenever possible; when marine winds were not available, the Tuktoyaktuk winds, increased by factors of 1.20 for east-west and 1.25 for speed, were used to approximate marine conditions. These latter scaling factors are based on the comparison of Tuktoyaktuk and marine winds (Section 2.2).

The regression analysis results for summer conditions (July to September) are presented in Tables 8 and 9. For all but one location, statistically significant correlation levels were computed between the near-bottom currents and the winds. The correlation results suggest that the coupling between currents and winds differs according to distance from shore (Figure 42). At the only available near-shore location, the West Atkinson site (station 8) situated within 3 km of the coastline, the coupling is large, with the currents responding, on average, as approximately 2% of the wind speed. Over the portion of the continental shelf with depths from 25 m to near the shelf break, the response coefficients (B) are markedly reduced, ranging from 0.4 to 0.9%, with weak evidence suggesting a general reduction in response with increasing depth. (Note that the results from the Isserk Shoal location, site 10, are not representative of the surrounding area, since the shoal protrudes to within 7 m of the surface, from the 12-15 m water depths of the adjoining sea-floor.) Near the edge of the continental shelf, the near-bottom response to winds was larger at site 2 in 67 m of water, situated very near the shelf break. However, at site 4 located 20 km to the northeast in 62 m of water, the response to winds was much smaller, being more representative of the other stations located on mid-shelf. The difference in response to winds between sites 2 and 4 may be associated with the greater distance from site 4 to the shelf break (3 km as compared to 1.5 km from the 100 m isobath).

The response of bottom currents to surface winds are highly variable for individual wind events. Fissel and Birch (1983) carried out regression computations for eight individal wind events, occurring between August 12 and September 22, 1982 (including sites 9 and 10 of this study). The results (Figure 43) reveal that the maximum response to individual wind events can be 2-3 times greater than the mean response, as computed from the entire record length of 33 days or greater in duration (Tables 8 and 9). The variability of the regression results among individual wind events underscore inherent problems in applying a time independent linear regression model of current to wind response over many wind events. As discussed above, wind-driven currents in shallow shelf seas are much more complex,

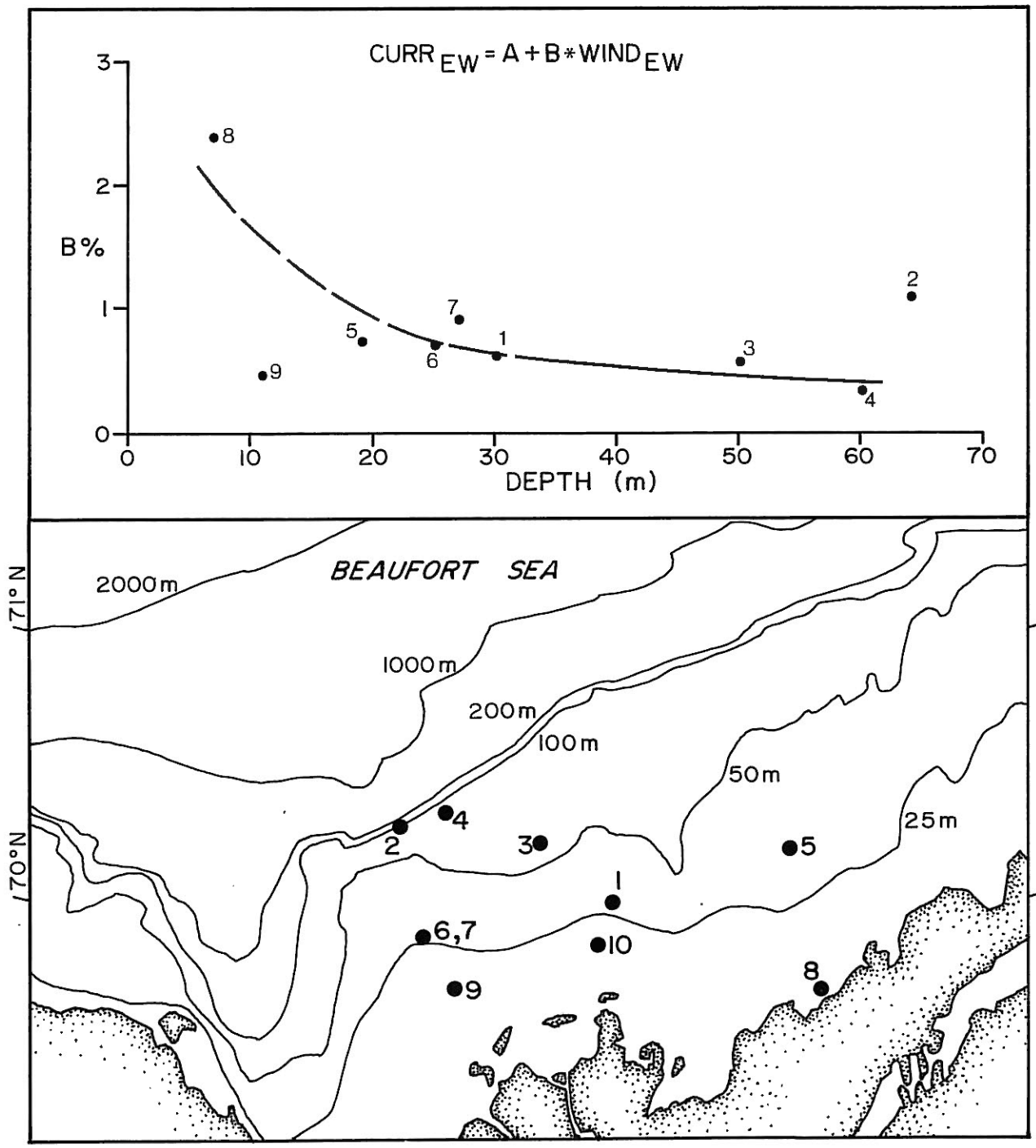

Figure 42: The response factor of bottom currents to marine winds as a function of measurement depth, as computed from the linear regression results.

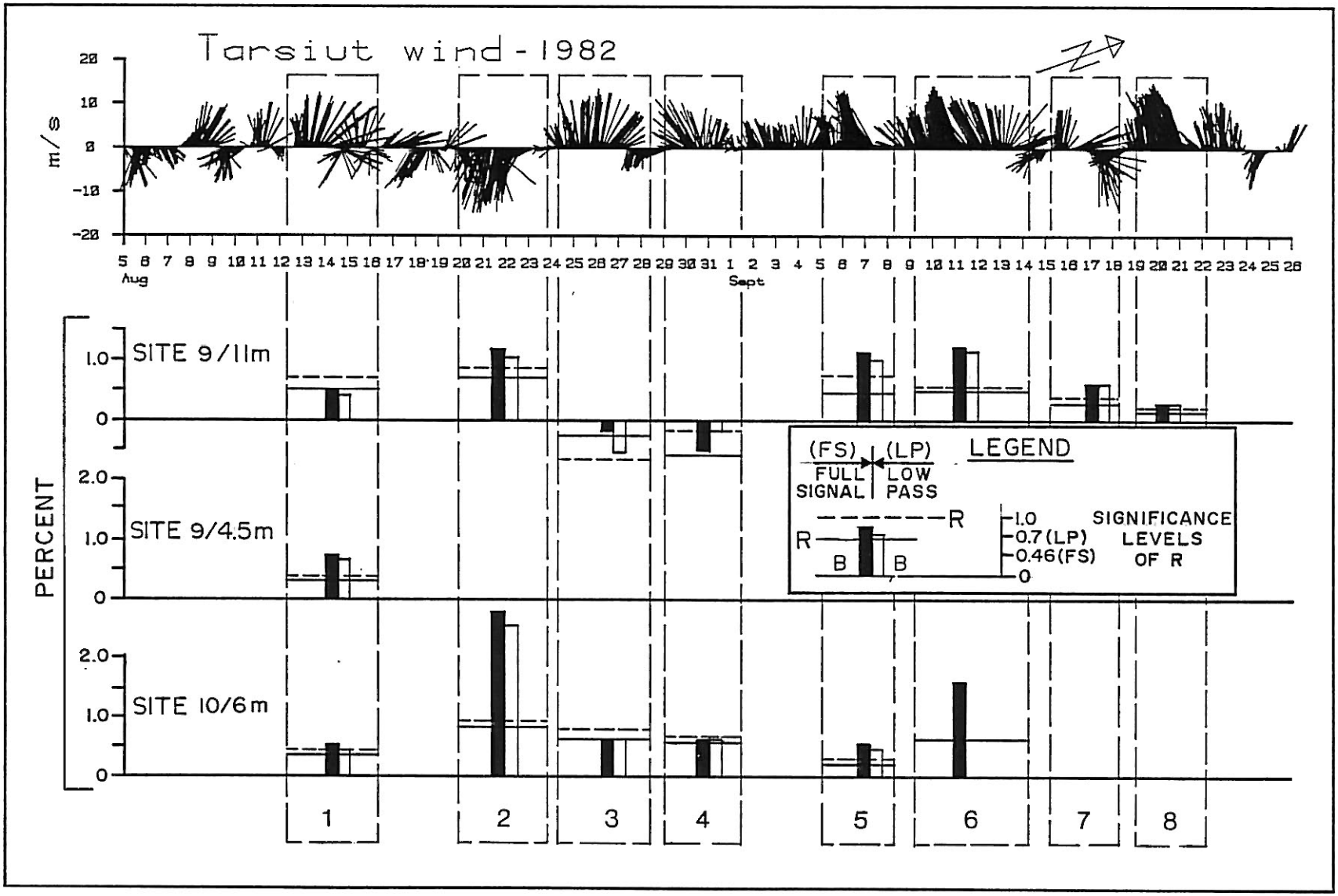

Figure 43: The linear regression coefficients (R and B) computed for the full signal and the low passed wind and easterly current components derived from individual wind events in 1982 (from Fissel and Birch, 1983).

both spatially and with time, than the linear regression model. Moreover, the variation in individual factors among wind events contributes to response differences among wind events; these include variations in wind fetch, the degree of changes in stratification within the water column and steadiness in the wind speed and direction.

As summer progresses, wind fetches generally increase as the pack ice retreats offshore, particularly during September in the westernmost portion of the Canadian Beaufort Sea (Section 2.3). During this same time, stratification in the water column is decreasing (Section 2.5.1). Both changes will result in enhanced responses of bottom currents to winds. Based on the single set of current meter data available over the Tuktoyaktuk shelf (near Tarsiut (site 6 and 7) in 1981 (Birch et al., 1982a), the response coefficient of bottom currents to winds exhibits a marked increase in autumn from that of the summer (Figure 44 and Table 10). In 1981, the pack ice edge retreated offshore from August to September; by late September the ice edge was near the median position derived from ice climatology. Thus, the strong coupling of bottom currents to surface winds observed in the autumn of 1981 may be representative of most years. More autumnal near-bottom current meter data are needed to verify this hypothesis.

3.1.2 MACKENZIE RIVER DISCHARGE AND NEAR-BOTTOM CURRENTS IN THE BEAUFORT SEA

A visual examination for correlation between the Mackenzie River volume discharge values at Arctic Red River and near-bottom currents at shelf locations was carried out for three current meter records. The current meter records were examined for the months of May and June, over the freshet period of river discharges, when the influence of river discharges would be expected to be maximal:

Site	Depth	Year	Reference
BSP Site 13	30 m	1975	Huggett et al. (1977)
BSP Site 15	51 m	1975	Huggett et al. (1977)
Uviluk	25 m	1981	Fissel et al. (1981)

These current data sets are all from the central portions of the continental shelf (sites H, K and M on Figure 32). The current meter records were first low-pass filtered using a cutoff frequency of about 1.3 cpd. The data were then plotted against

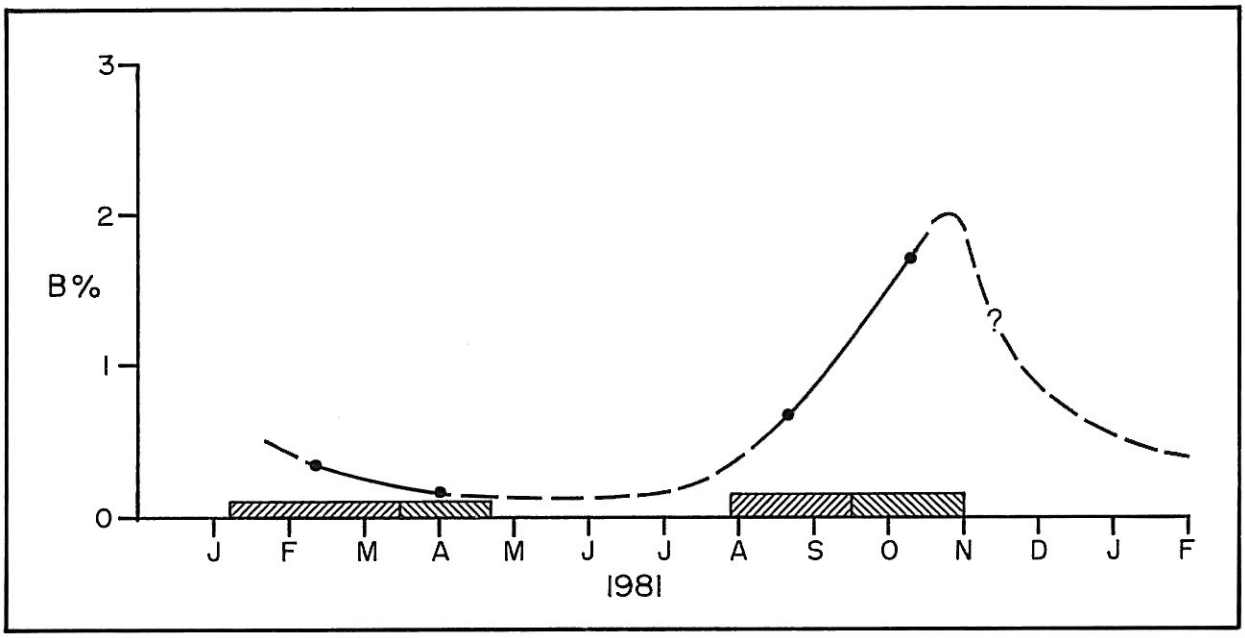

Figure 44: The response factor of the near-bottom easterly current component to marine winds at Tarsiut (site 6, Fig. 42) for various periods of the year, January-November, 1981.

Table 10: Results of linear regression analyses between marine wind and bottom currents at Tarsiut location (site 6, Fig.42)

Period 1981	Regression Coefficients			No. of 6 Hourly Data Points	Significance Level of R	Time Lag (hrs)
	R	A (cm/s)	B (%)			
East-West Components						
Winter	.42	0.5	.36	287	0.12	6
Spring	.23	1.1	.18	138	0.17	12
Summer	.53	4.2	.69	198	0.14	12
Fall	.71	0.7	1.71	118	0.18	12
Speed						
Winter	.38	2.4	.40	287	0.12	6
Spring	.31	2.8	.22	137	0.17	18
Summer	.61	2.9	.78	198	0.14	12
Fall	.66	5.3	1.19	118	0.18	12

Winter Jan.19-Mar.31, 1981
Spring Apr. 1-May 5, 1981
Summer Aug.11-Sep.30, 1981
Fall Oct. 1-Nov.15, 1981

river discharge and winds in order to visually search for any correlation requiring further cross-correlation analyses.

Uviluk, May-June, 1981, 25 m Depth

The main freshet began during May 16-17 and, even allowing several days lag for the effects to reach Uviluk, there was no obvious response in either the T-S characteristics or the velocity of the bottom waters at the Uviluk site (Figure 45). The dominant event in this section of the current meter record occurred on May 11-12 and almost certainly represents a response to strong west-northwesterly winds. Other increases in bottom current speeds (May 21, May 28-29) also appear to be related to wind events, rather than river discharge.

Beaufort Sea Project - Stations 13 and 15

Both stations 13 and 15 (sites H and K on Figure 32) were located in the central region of the shelf; however station 15 was located in a trough which intersects the shelf. In 1975, river freshet began in mid-May and peaked by the end of May. There is no apparent change in the character of the currents at either stations 13 (Figure 46) or 15 (Figure 47) as the river discharge increased. Many of the periods of strong currents can be related to wind events, but in no case is any correlation apparent with increased river discharge. At station 13 the current direction, as well as speed, correlated well with changes in the wind. The current speeds at station 15 correlate with wind speed, but the flow direction is primarily to the south which is likely related to the local bathymetric slope.

The lack of correlation between currents and river discharge apparently results from current measurement locations being too far offshore at depths too deep to be significantly affected by increased river discharge. Unfortunately, there are no current meter records nearer shore which span the spring freshet period. At locations directly off the river tributaries, the bottom currents most certainly respond to the magnitude of river discharge. It remains to be determined how far offshore the effect is felt.

In estuarine systems, the fresh River Water flows out over the denser marine waters and entrainment of saline water into this surface flow results in a compensating landward return flow at depth. Immediately offshore of Mackenzie and Kugmallit Bays, concentrated thin freshwater beneath the landfast ice could produce typical estuarine characteristics. As such, some landward flow should occur at depth. The magnitude of this flow

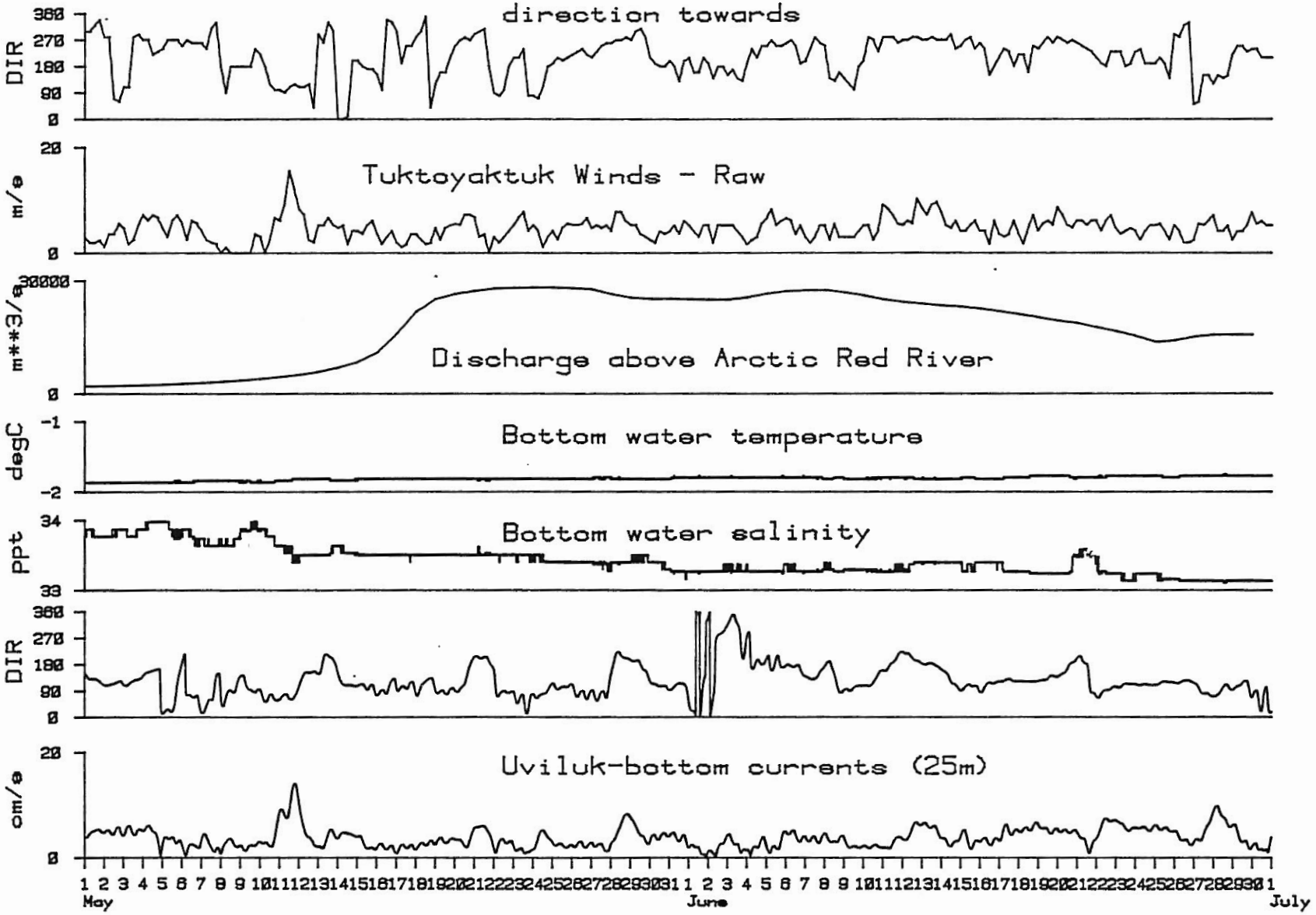

Figure 45: Comparative time series plots of the winds at Tuktoyaktuk, measured Mackenzie River discharge at Arctic Red River, and near-bottom measurements of temperature, salinity and current speed (low-passed) at the Uviluk site, May-June 1981.

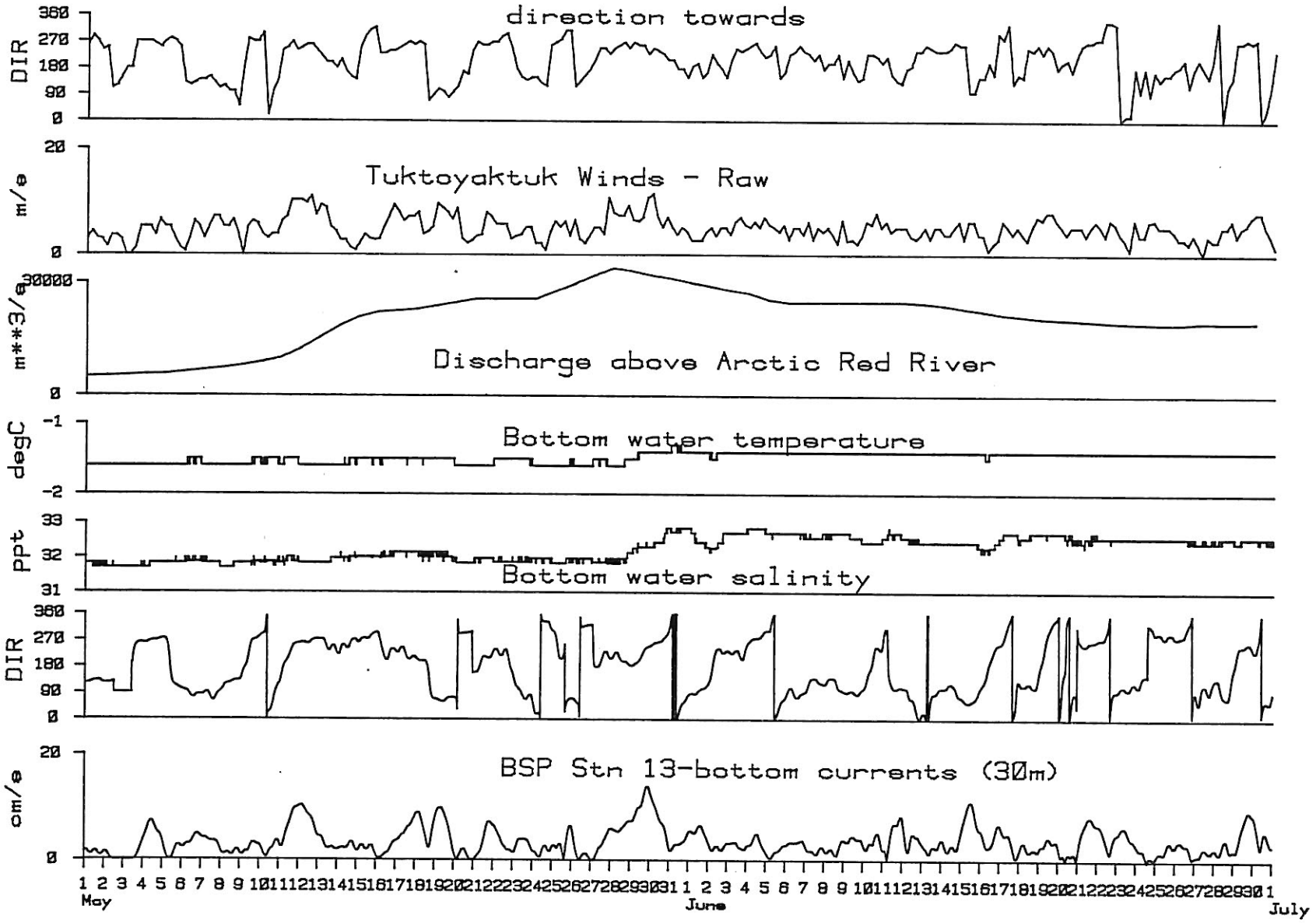

Figure 46: Comparative time series plots of the winds at Tuktoyaktuk, measured Mackenzie River discharge at Arctic Red River, and near-bottom measurements of temperature, salinity and current speed (low-passed) at the Beaufort Sea Project Station 13, May-June 1975.

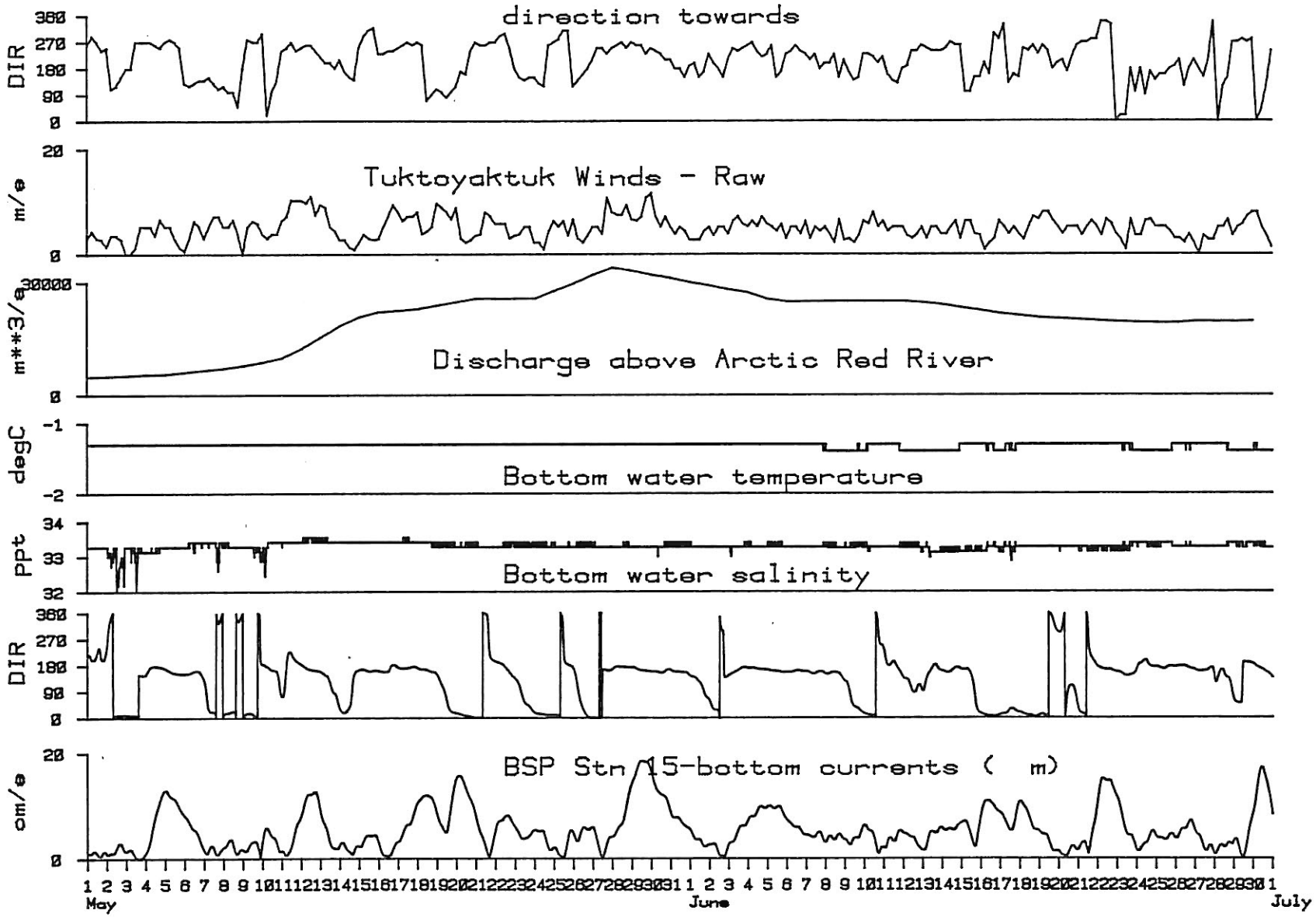

Figure 47: Comparative time series plots of the winds at Tuktoyaktuk, measured Mackenzie River discharge at Arctic Red River, and near-bottom measurements of temperature, salinity and current speed (low-passed) at the Beaufort Sea Project Station 5, May-June 1975.

would be small and may be obscured by other processes. Furthermore, these effects may be confined to the shallows closer to the coastline; unfortunately no time series current measurements are available during freshet in water depths of less than 25 m. Current meter records obtained at locations closer to shore may be required in order to quantify the effect of river discharge on bottom currents. Over the mid-continental shelf, bottom currents, in the 25 to 50 m depth range, do not respond directly to river discharge.

3.1.3 RELATIONSHIP OF BOTTOM CURRENTS TO WIND AND WATER LEVEL

In a simplified coastal marine system, both the currents and the water level respond to wind forcing. Winds blowing with the land on the right-hand side (looking in the direction that the wind is blowing toward) transports water downwind. Because of the Coriolis force, a net onshore flow (Ekman transport) develops (in the northern hemisphere) and the coastal water level rises. Conversely, when the wind blows in the opposite direction, with the land to the left, there is a net offshore movement of water, and coastal water levels drop.

In the Beaufort Sea, the dominant winds during open water season are northwesterly and southeasterly to northeasterly. Winds having a northwesterly component should be accompanied by an increase in water levels, and winds having a southeasterly component by decreased water levels. Figure 48 shows that the coastal water level does respond in this way.

It has been suggested that changes in coastal water level may be used as an indication of the coastal currents. There is a definite correlation, evident for most individual events as shown in Figure 48. Regression analyses were applied to determine, in particular, if water level is a better indicator than Tuktoyaktuk winds to determine coastal currents. In order to remove tidal variations, the water level data were low pass filtered prior to use in the regression analysis.

Figure 49 shows the regression results for current speed at sites 13 and 5 (locations H and C, Figure 32), versus water level (modulus) and wind speed (see Table 11). For site 13, the correlation coefficient for the regression of current to modulus water level was 0.67, better than the correlation of 0.47 for current with winds at Tuktoyaktuk. Given either wind speed or relative water level, the current speed can generally be predicted to $\pm$4-5 cm/s. Best fits occur with currents lagging winds by 6-12 hours and currents lagging water level by 1 hour.

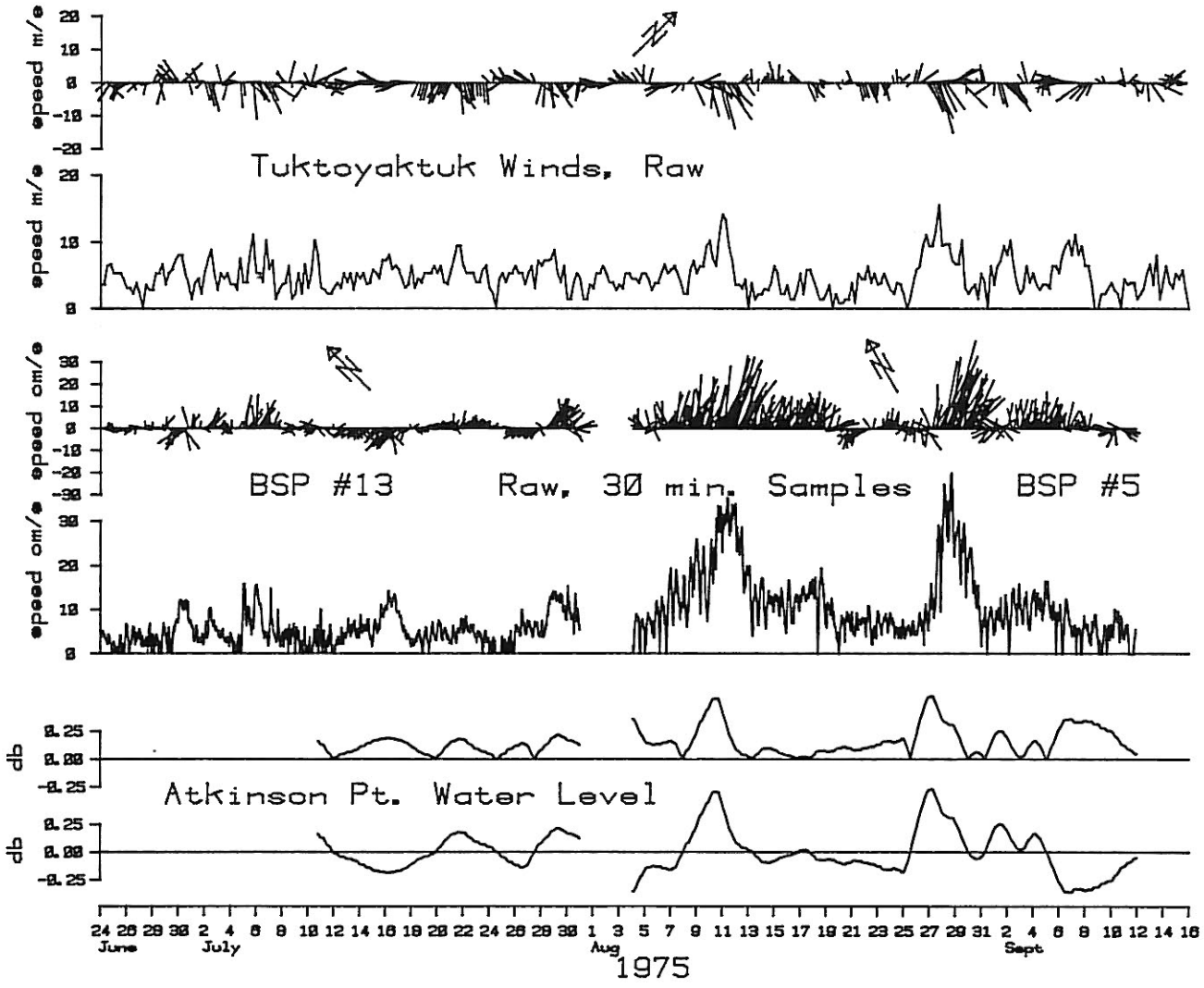

Figure 48: Comparative time series plots of the uncorrected Tuktoyaktuk winds, near-bottom currents measured at Beaufort Sea Project Stations 13 and 15 and low-passed filtered water level data (and modulus thereof), at Atkinson Point.

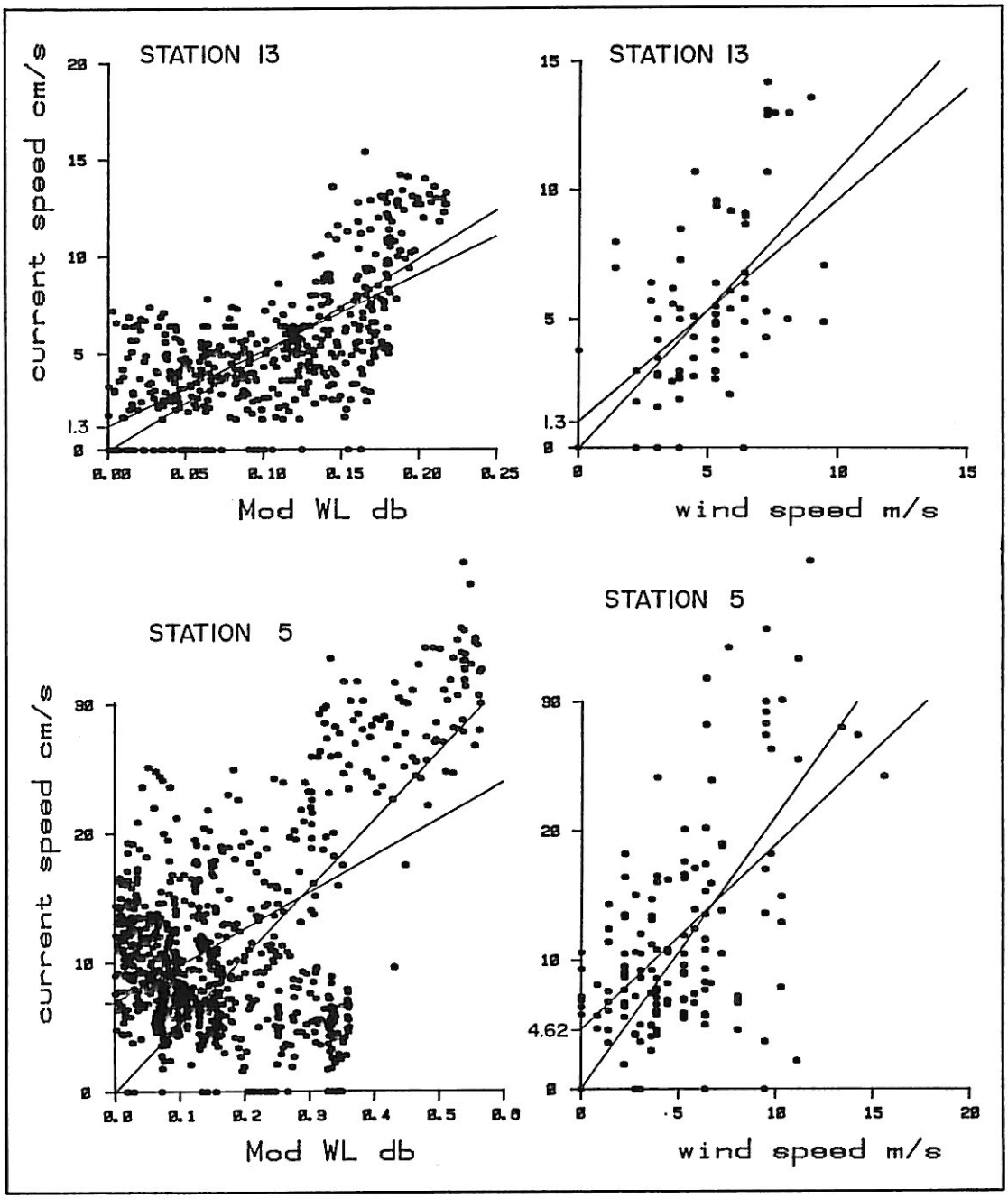

Figure 49: Scatter plots of current speed data of Beaufort Sea Project stations 5 and 13 as a function of Tuktoyaktuk wind speed and low-passed water levels.

Table 11: Results of regression analyses for near-bottom currents with winds and water levels for y = a + bx, where y is the current, x is the wind or water level and a and b are the linear coefficients, using a least squares fit with correlation coefficient R. The regression was also computed for the equation y = bx.

Current Measmn't Site	Record Length (days)	Current Lag (hr)	Corr. Coeff. R	Correlation Coefficients a	b	b (a = 0)
(a) Current speeds in cm/s and water levels in dbar (low passed)						
13	20.1	1	0.670	1.3	39.29	48.76
5	37.4	33	0.490	6.9	27.87	52.05
(b) Current speed in cm/s and wind in m/s						
13	19.5	12	0.473	1.3	0.84	1.07
5	37.3	24	0.548	4.6	1.42	2.09
(c) Major components of current in cm/s (low passed) and water level in dbar (low passed)						
13	19.2	4	0.863	0.3	37.52	37.35
5	35.0	33	0.806	8.6	35.42	38.53
(d) Major components of current in cm/s (low passed) and of wind in m/s						
13	18.5	12	0.884	-0.1	1.18	1.18
5	35.5	24	0.603	7.57	1.30	1.74

At site 5, the two correlation coefficients are similar; 0.49 for current to water level and 0.55 for current to wind. The scatter is greater than at site 13; using water level or wind to predict current speeds would produce results of typically $\pm$10 cm/s. Currents again lag winds, but by 24 hours. In contrast to the site 13 results, currents lag water level by 33 hours, as is evident in the two major events of August 10-12 and

August 27-30 (Figure 48). Site 5 is near the shelf break, whereas site 13 near mid-shelf. The fact that the peak current speeds occurred during falling sea levels suggests a different current regime from that on the shelf. In view of the northeasterly current flowing along the slope region (Section 2.5.2), the response of bottom currents at site 5 may represent a delayed response of the current system to wind forcing.

At both sites the current direction is preferentially aligned parallel to the bottom contours. Wind forcing was not identical for the two sites, as greater wind speeds occurred during the period of site 5 measurements.

A similar analysis was carried out using major current components, rather than speeds (E-W at station 13; NE-SW at station 5) and the major wind component (E-W was chosen to best represent the dominant northwesterly and southeasterly to northeasterly winds). The current components were low-pass filtered in order to remove motion at frequencies $\geq$ 2 cpd (tidal, inertial, and higher frequencies). The water level record used was the relative water level measured at Atkinson Point, also low-pass filtered. Figure 50 shows the low-pass filtered major components, and Figure 51 the regression analysis results.

The correlation coefficients for the low-passed major current components at station 13, with relative water level and low-pass filtered major wind speed component, are similar, 0.862 and 0.884 respectively. As might be expected due to reduced number of degrees of freedom in the current and wind data, these regression coefficients are greater than those for the unfiltered current and wind speed. The results show that either coastal water level or Tuktoyaktuk winds may be used to predict the low frequency current offshore. Predicted current speed (major component) would generally be to within $\pm$5 cm/s.

At site 5 the correlation coefficients are reduced, being 0.806 for current/water level and 0.603 for current/wind. The results suggest water level to be a better indicator of offshore flow, although neither would be very accurate; using water level the offshore low frequency current component could be reasonably predicted to about $\pm$13 cm/s, and to only $\pm$17 cm/s using Tuktoyaktuk winds.

Based on the regression results of this rather limited comparison, coastal winds (at Tuktoyaktuk) and water level records appear to serve equally well as indicators of near-bottom currents in summer at mid-shelf locations. However, as computation of near-bottom currents by either method results in

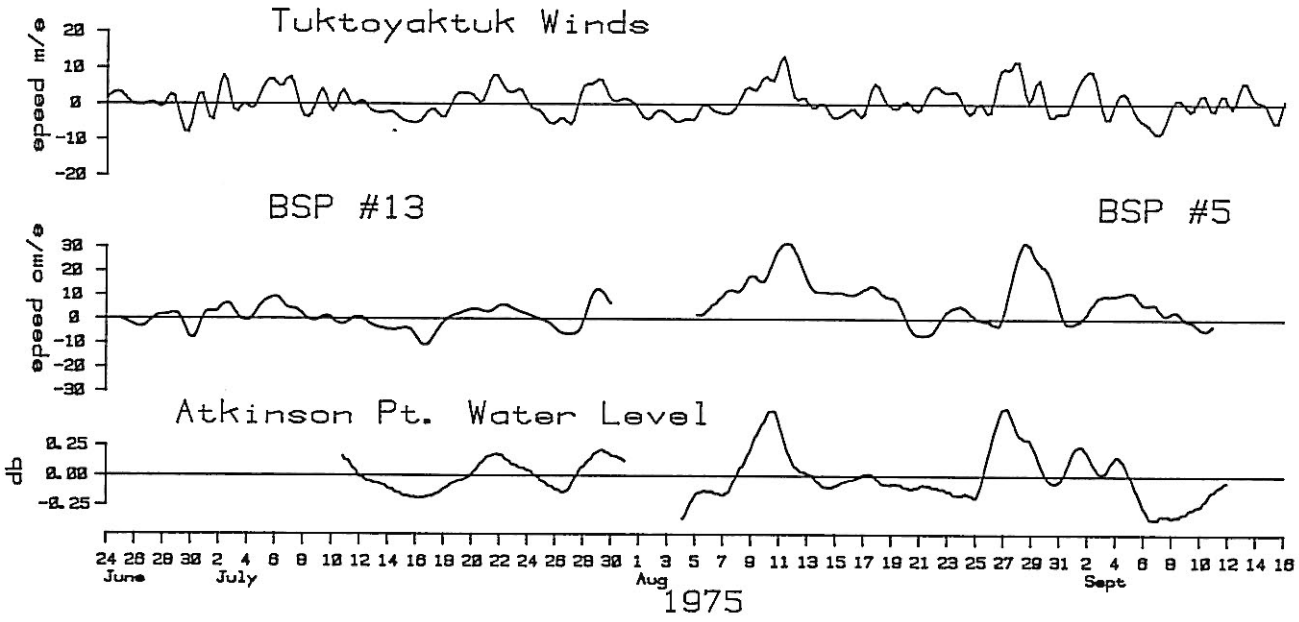

Figure 50: Comparative time series plots of the uncorrected, low-passed Tuktoyaktuk wind speed (E-W component), low-passed current speeds (major component) at Beaufort Sea Project stations 13 and 5 and the low-passed Atkinson Point water level data.

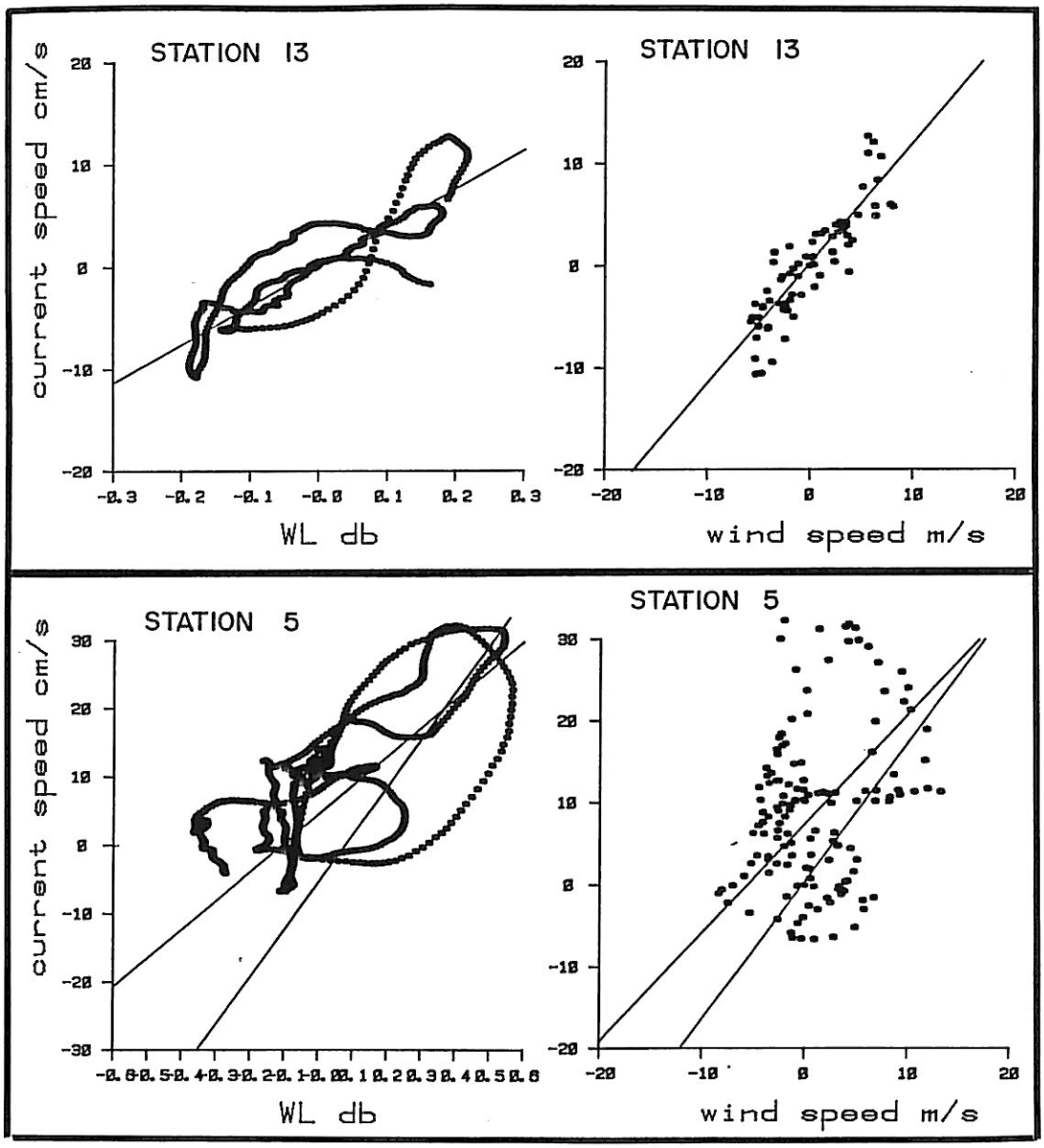

Figure 51: Scatter plots of low-passed values of current speeds (major component) measured at Beaufort Sea Project stations 5 and 13 with Atkinson Point water levels and Tuktoyaktuk wind speeds (E-W component).

considerable deviations from the actual bottom currents, this technique has limited utility for most applications.

3.2 SUSPENDED SEDIMENT CONCENTRATION: RELATIONSHIP TO WINDS AND WAVES

3.2.1 NEARSHORE AND DELTA ZONES

The most extensive sets of available nearshore SSC data were used to examine the reduction of the concentrations with increasing station depth and salinity. Working from small vessels in 1975, McDonald and Martin (1976) collected turbidity data as derived from surface and near-bottom water samples along with temperature-salinity data. The measurements were obtained in the shallow waters from east Mackenzie Bay to Kugmallit Bay (Figure 52). The sampling times and the prevailing wind conditions are summarized in Table 12. The 1977 data were obtained by Fraker et al. (1979) in for the following periods (and prevailing winds):

July 4, 1977	N, 4 m/s
July 19-20, 1977	NE, 5-8 m/s
July 25, 1977	W, 3-4 m/s
August 4, 1977	Variable, weak (preceded by E winds up to 8 m/s on August 3)
August 11, 1977	E, 6 m/s

Maps of surface turbidity based on the 1977 data are presented in Figure 37. The ice conditions for both 1975 and 1977 were reasonably typical; in 1975, the ice edge was further offshore in early July than in 1977, but the persistent northeasterly winds of July 12-27 for the latter year, resulted in an offshore movement of the pack ice.

In Figures 53 and 54, surface and bottom SSC values are plotted as a function of station depth. Note that the 1977 study includes measurement locations in the deeper water of the Mackenzie trough, along with the shallower, nearshore stations. The expected reduction of SSC with increasing depth is most pronounced in the 1977 near-bottom values (Figure 53). At stations with depths exceeding 5 m, near-bottom SSC levels are much reduced (typically, less than 5 ppm) in comparison with a) stations having depths of 5 m or less (5-200 ppm) or b) the surface levels measured at the same sites. (Note that the near-

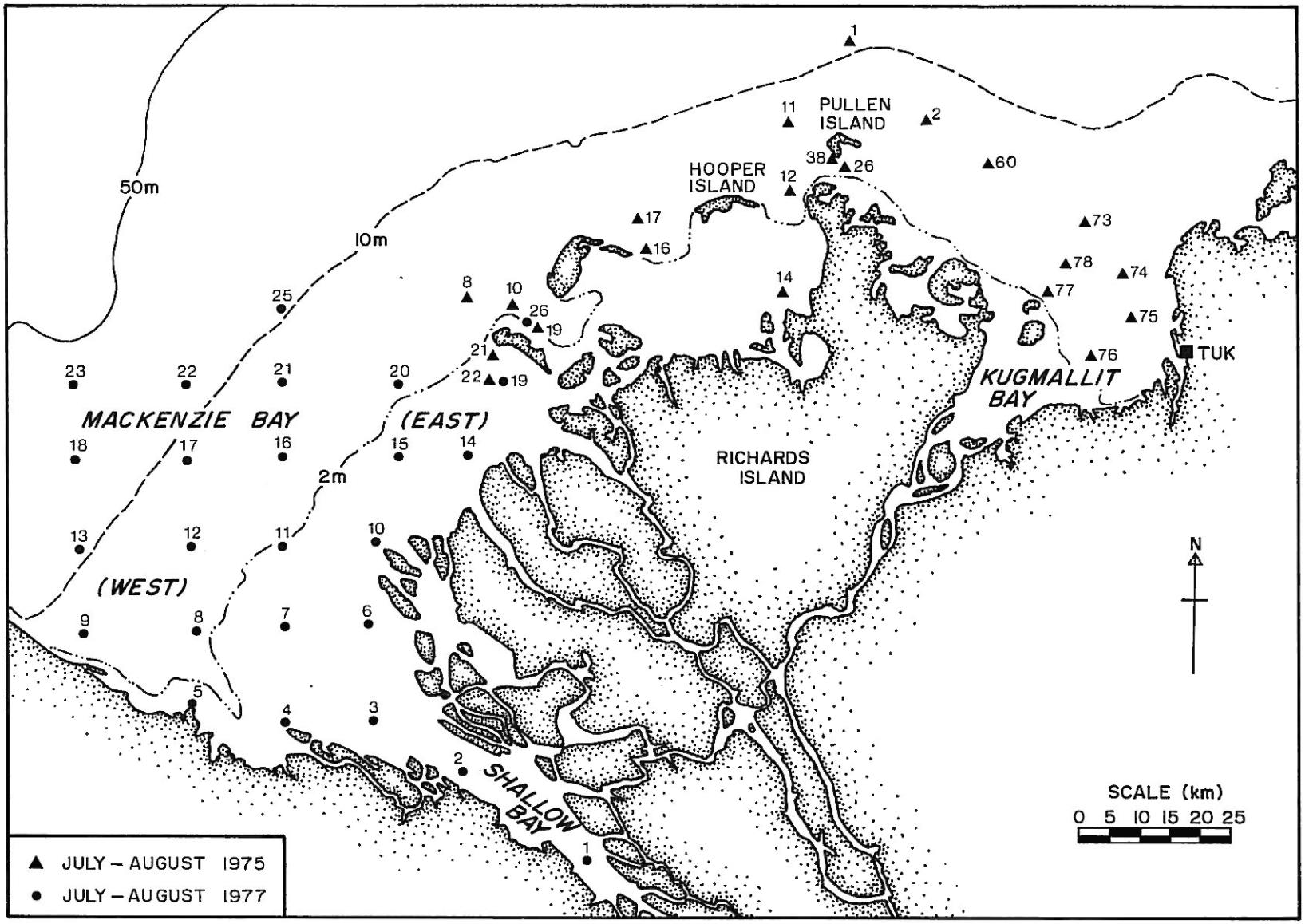

Figure 52: Locations of nearshore SSC data obtained in 1975 (McDonald and Martin, 1976) and 1977 (Fraker et al., 1979).

Table 12: Summary of sampling times for nearshore turbidity data obtained by McDonald and Martin (1976), July 11-August 20, 1975 along with prevailing winds at Tuktoyaktuk. Data are subdivided according to areas: East Mackenzie Bay (EMB), vicinity of Pullen and Hooper Islands (PH) and Kugmallit Bay (KB) as shown in Figure 45. Numbers in parentheses indicate station numbers.

Time	EMB	PH	KB	Wind
July 11-13		(11,12,38)		NE-N, 4-5 m/s
July 14-15			(73,74,75,77,78)	NE-N, 5 m/s
July 17			(2)	N, 5-7 m/s
July 28-30	(8,16)	(12)		W-NW, 4-8 m/s
Aug. 1-2		(26)	(2,60,73,74,78)	NE-N, 5 m/s
Aug. 3-4	(8,10,16,17,19,21,22)	(1,11,12,14,26)		E, 5 m/s
Aug. 19-20			(2,60,73,74,75,76,77)	Variable, weak (< 3 m/s)

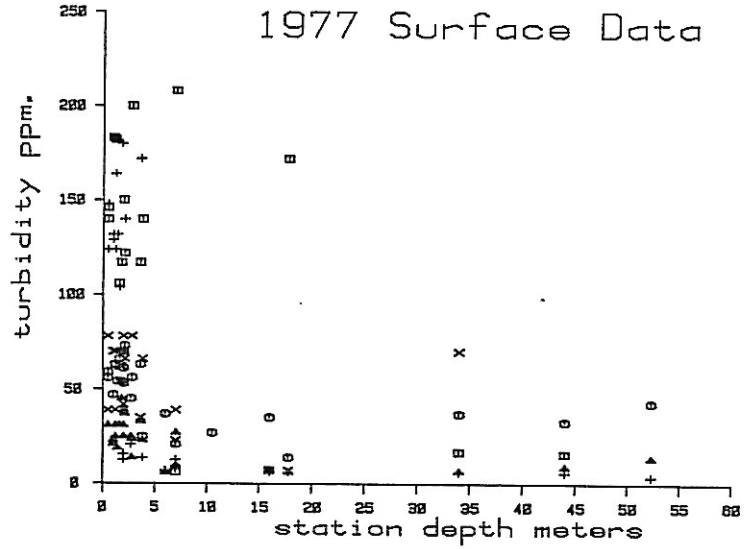

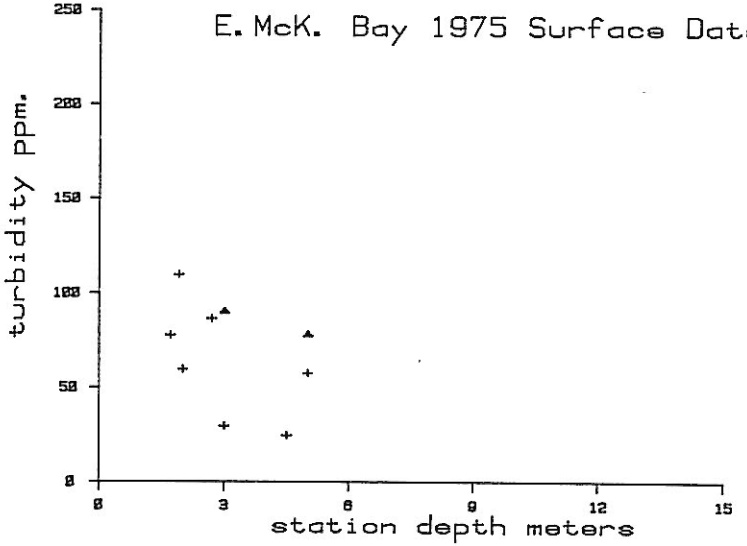

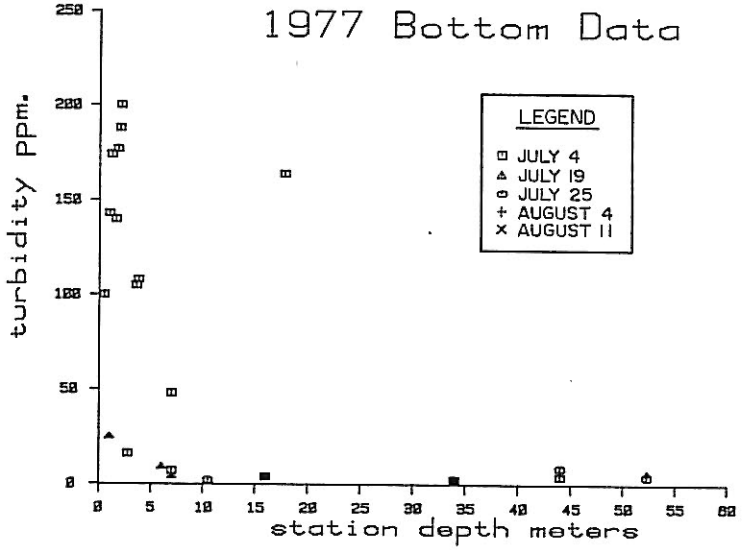

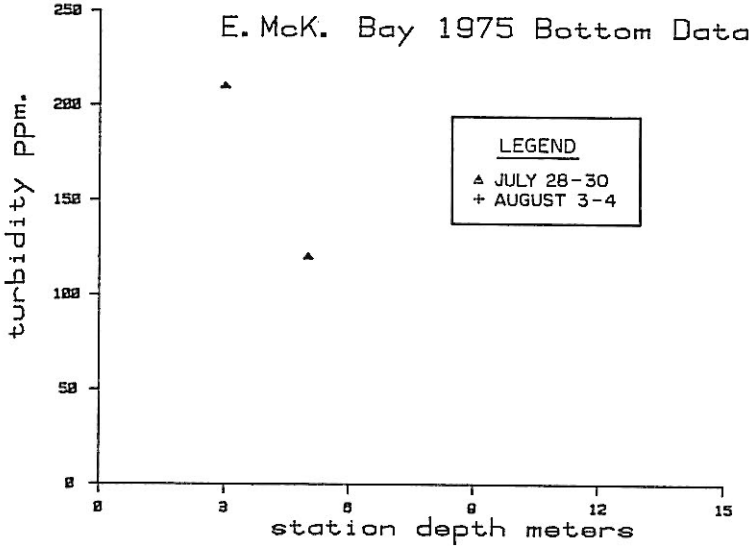

Figure 53: SSC data obtained in West Mackenzie Bay (1977) and in East Mackenzie Bay (1975) plotted as a function of station depth for near-surface and near-bottom levels.

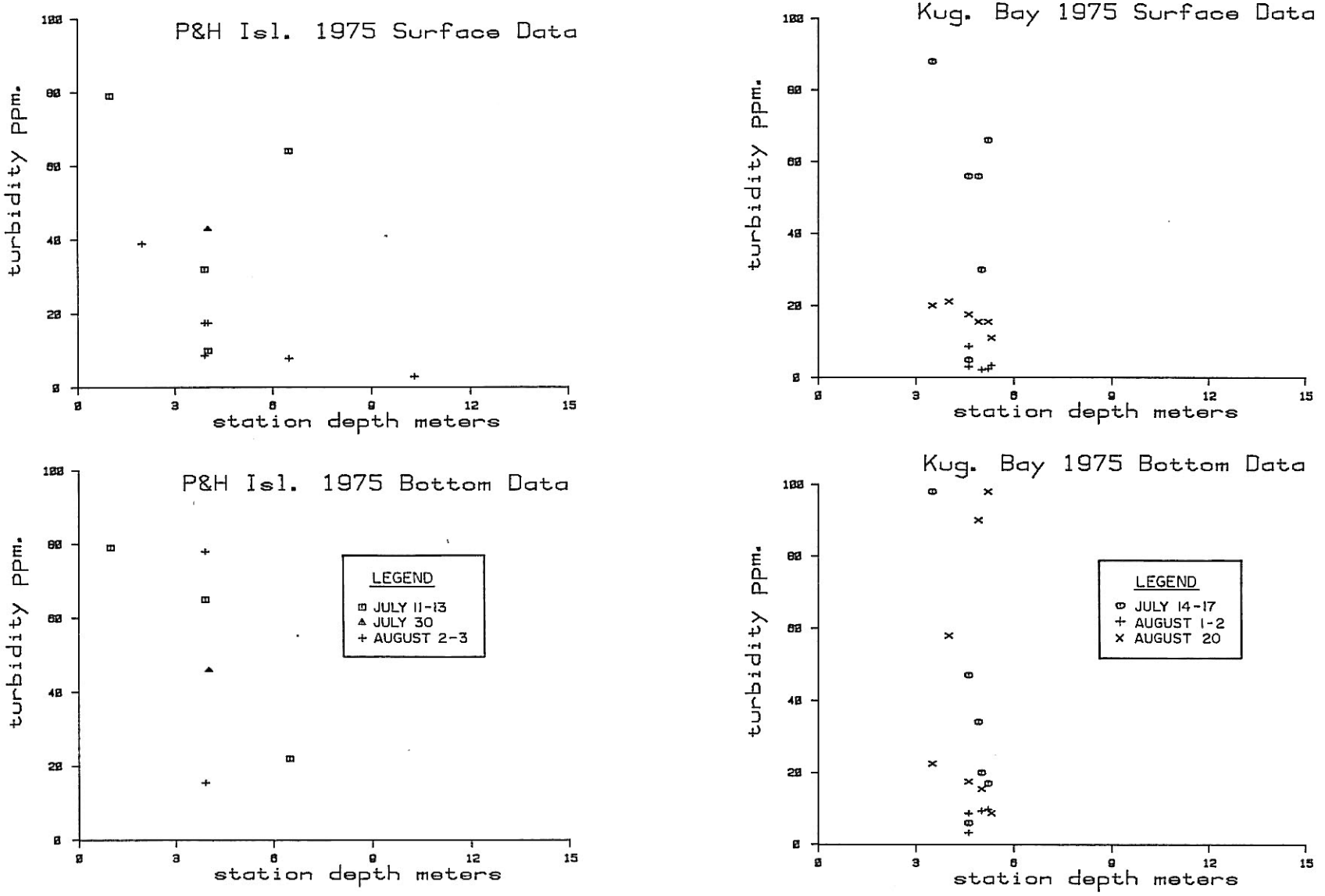

Figure 54: 1975 SSC data obtained between Pullen and Hooper Islands and in Kugmallit Bay plotted as a function of station depth for near-surface and near-bottom levels.

bottom value for station 13 on July 14 is excluded from these results due to the extremely low salinity (4.9) obtained for a depth of 17.8 m; because the T-S characteristics appear reasonable, an error in station depth is suspected.)

The surface turbidity results also exhibit a general reduction at stations having depths in excess of 5 m, but the reduction is not nearly as marked or consistent. At the 1977 locations, to the north of Western Mackenzie Bay (sites 9, 13, 18, 22, 23 and 25), a very wide range in turbidity levels occurred throughout the sampling period, with values ranging from less than 5 ppm (August 4) to over 30 ppm (July 19). In the latter case, prolonged easterly winds had driven the River Water northwestwards over the deeper water of the Mackenzie trough (see Figure 37). This suggests that under suitable easterly winds relatively high surface SSC levels could input sediments through settling into deep water of the Mackenzie trough than would occur in the other, shallower areas adjoining the Mackenzie delta.

At locations with water depths of 5 m or less, the levels of observed values are generally higher in West and East Mackenzie Bay, than in the Pullen-Hooper Island and Kugmallit Bay regions. The lower levels for the Pullen-Hooper area reflect the absence of any major river discharge channel into the area and, possibly, the reduced wind fetches because of the nearby islands. Evidence for the importance of the latter process can be seen at stations 8 and 16 in East Mackenzie Bay (July 28-30, 1975) where bottom SSC values are considerably greater than the surface levels. At this time, moderate winds were blowing from the west-northwest, a direction with large fetch lengths for this area.

In Kugmallit Bay, turbidities are highly variable (Figure 54). Under easterly winds, the high SSC values of the East Channel plume are found on the western side of the Bay, turning offshore toward the northwest off Pullen Island (July 14-17). Under weak or westerly winds this same turbidity plume is found on the eastern side of the Bay extending northward along the Tuktoyaktuk Peninsula (August 20). For the latter set of observations, SSC values at most stations were higher near the bottom. In this case wind-induced resuspension seems unlikely, given the low wind speed measured at Tuktoyaktuk. More likely, the large bottom turbidities result from either current-induced resuspension or settling from the surface.

The nearshore SSC data of 1975 and 1977 were also plotted as a function of salinity (Figures 55 and 56). The results show a general trend of reduced SSC levels with increased salinities. For most of the data, SSC levels were limited to values of 5 ppm

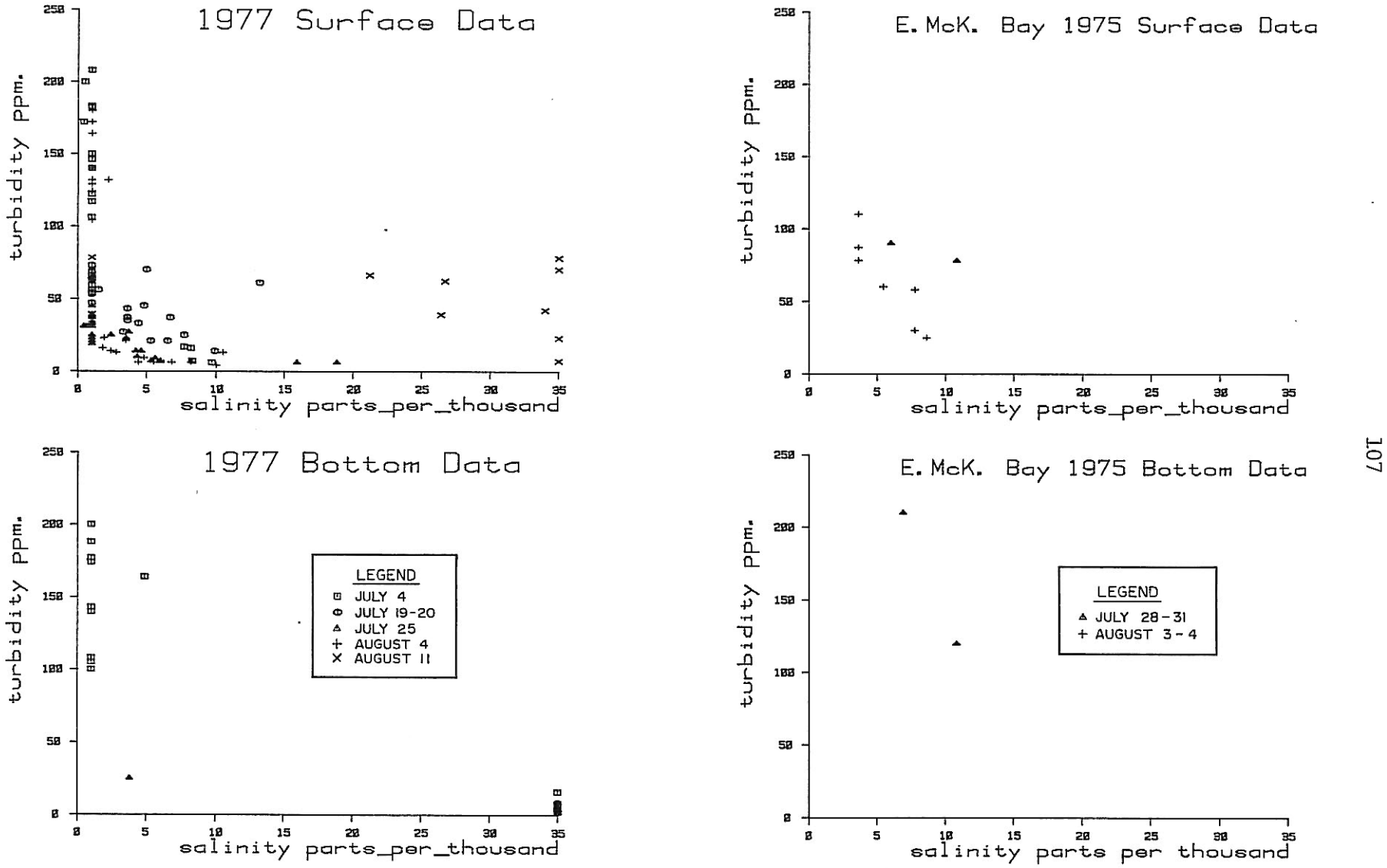

Figure 55: SSC data obtained in West Mackenzie Bay (1977) and East Mackenzie Bay (1975) plotted as a function of salinity for near-surface and near-bottom levels.

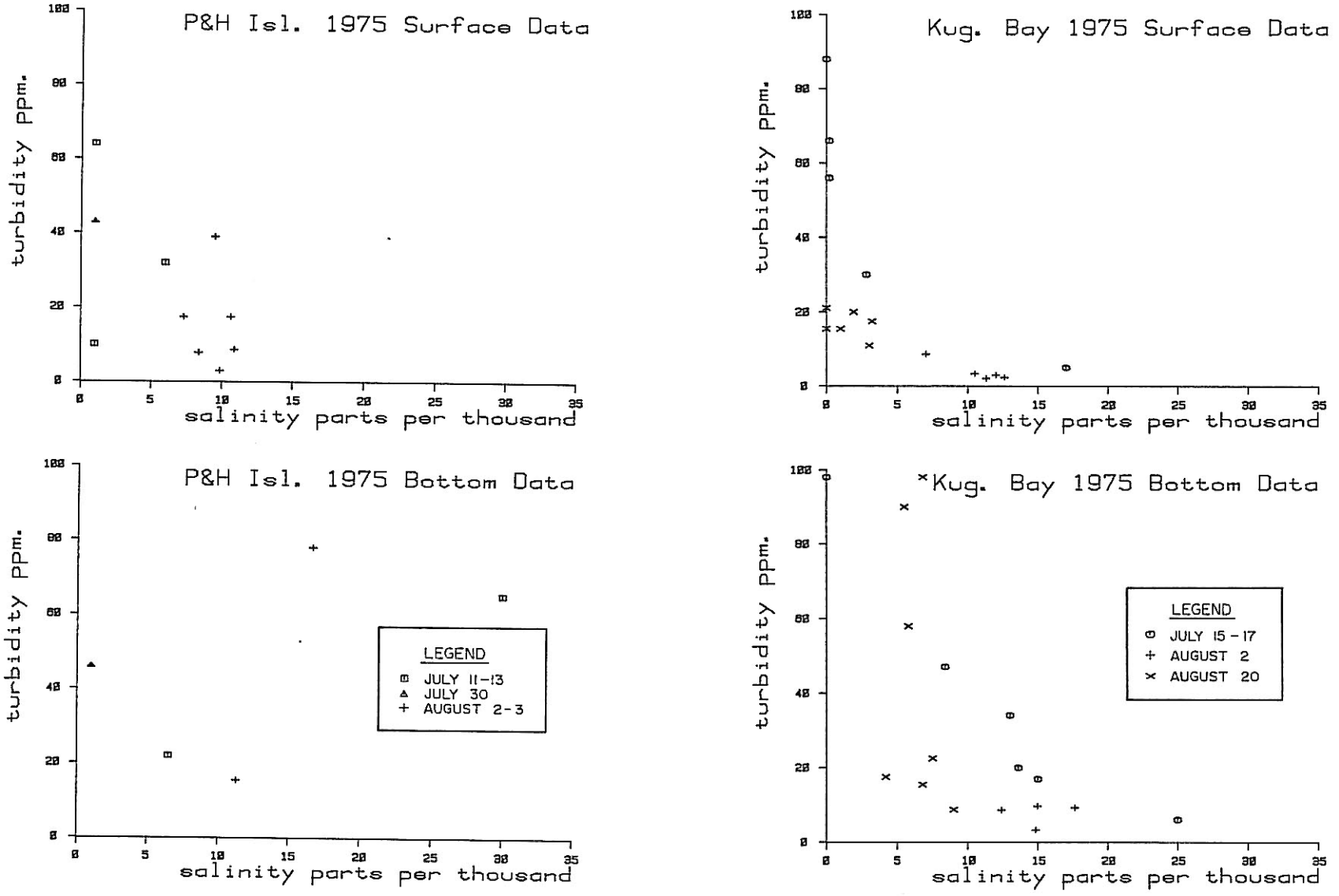

Figure 56: 1975 SSC data obtained between Pullen and Hooper Islands and in Kugmallit Bay plotted as a function of salinity for near-surface and near-bottom levels.

or less at salinities in excess of 10-15°/oo. However, relatively saline water was observed to contain higher levels of SSC in some of the measurements. This is most apparent in the 1977 data of August 11, when surface waters of the offshore portions of Mackenzie Bay (salinities >20°/oo) contained SSC levels of up to 78 ppm. In the near-bottom data obtained in the Pullen-Hooper Islands (Figure 55) and Kugmallit Bay (Figure 56) areas, water of relatively high salinity (>15°/oo) and high SSC (>10 ppm) were also measured. The simultaneous occurrence of high salinity and SSC values, particularly in the surface layer, suggests that enhanced flocculation of sediment particles associated with increased salinity, may not be of major significance in inducing higher settling and depositional rates, in the areas adjoining the Mackenzie delta. In fact, the results of studies in other estuarine areas (Krank, 1979) suggest that flocculation is most important at relatively low salinities (2-3°/oo), which would extend up the river channels within the Mackenzie delta.

3.2.2 VARIABILITY IN THE NEAR-BOTTOM BOUNDARY LAYER OVER THE CENTRAL AND OUTER CONTINENTAL SHELF

Over the central and outer portions of the Tuktoyaktuk continental shelf, a maximum in SSC levels just above the bottom has been widely observed (Section 2.5.3; Figure 40). Repeated transmissivity profiles have been obtained from drillships (Lemon and Kowalski, 1982) over extended periods of time. While the data collection procedures are not well documented, these data are generally consistent with the much more limited set of directly measured SSC levels (Figure 40). The transmissivity data (Figure 57) suggest that the SSC's of the near-bottom layer exhibit considerable variability with time, both in terms of magnitude and thickness (for example, see Figure 58). An examination of transmissivity with concurrent salinity data indicated no evidence of any correlation.

Transmissivity data were plotted as a function of near-bottom current speed (Fissel, 1981), averaged over the preceding 24 hours, for 1976 data obtained at the Tingmiark site and Kopanoar site in 1977 (Figure 59). The data of the shallower Tingmiark site (28 m water depth), revealed a high degree of scatter, indicating no correlation between SSC and bottom current speed. However, a large amount of experimental uncertainty is suggested for the transmissivity data due to variations in the recorded measurement depths; on some occasions, the depth of the transmissivity was given as 40 m, 12 m in excess of the water depth. Furthermore, the very low transmissivity readings are also unlikely to have actually occurred.

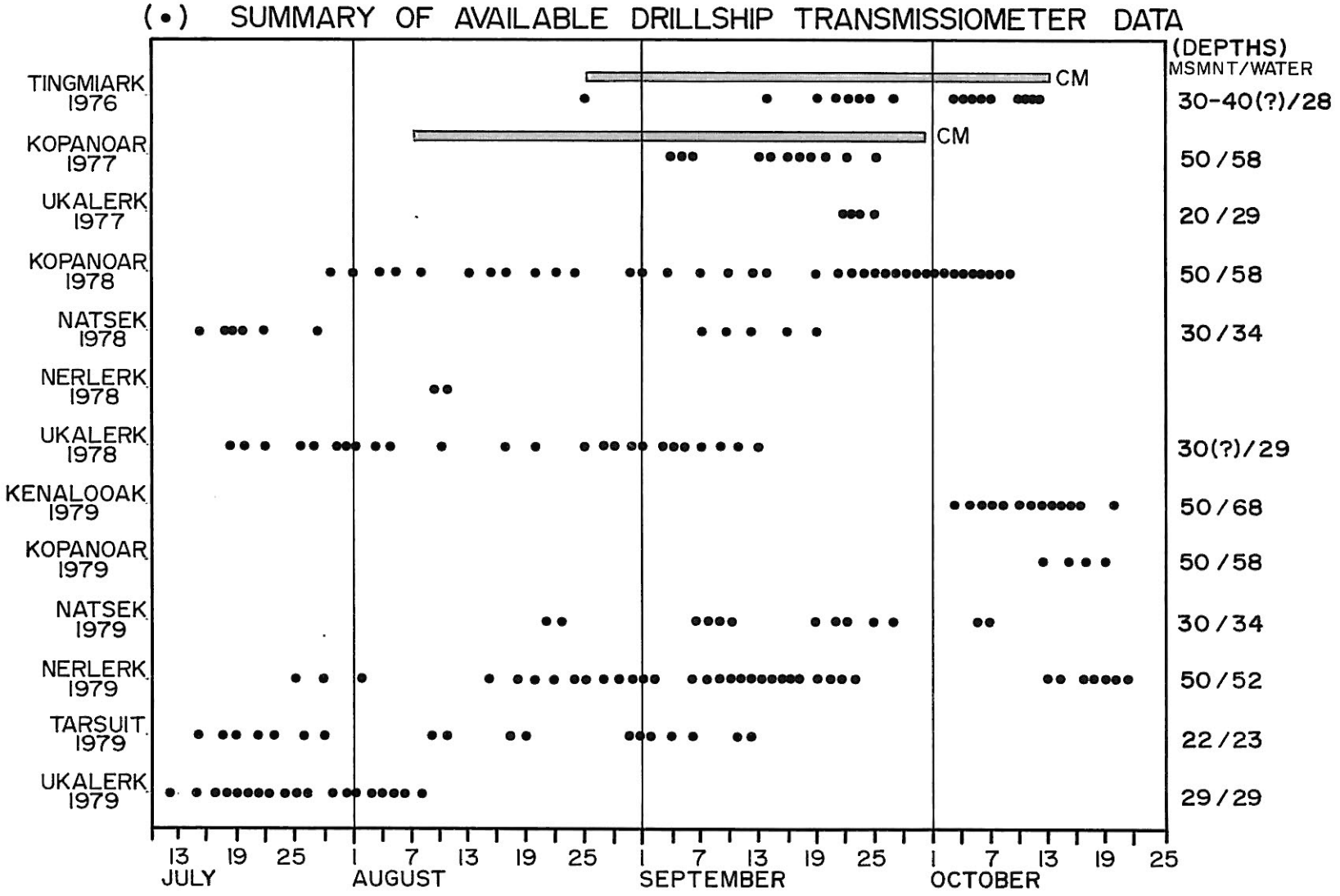

Figure 57: A diagram illustrating the times and locations of available transmissivity profile data obtained from the Canmar drillships, 1976-1979 (Lemon and Kowalski).

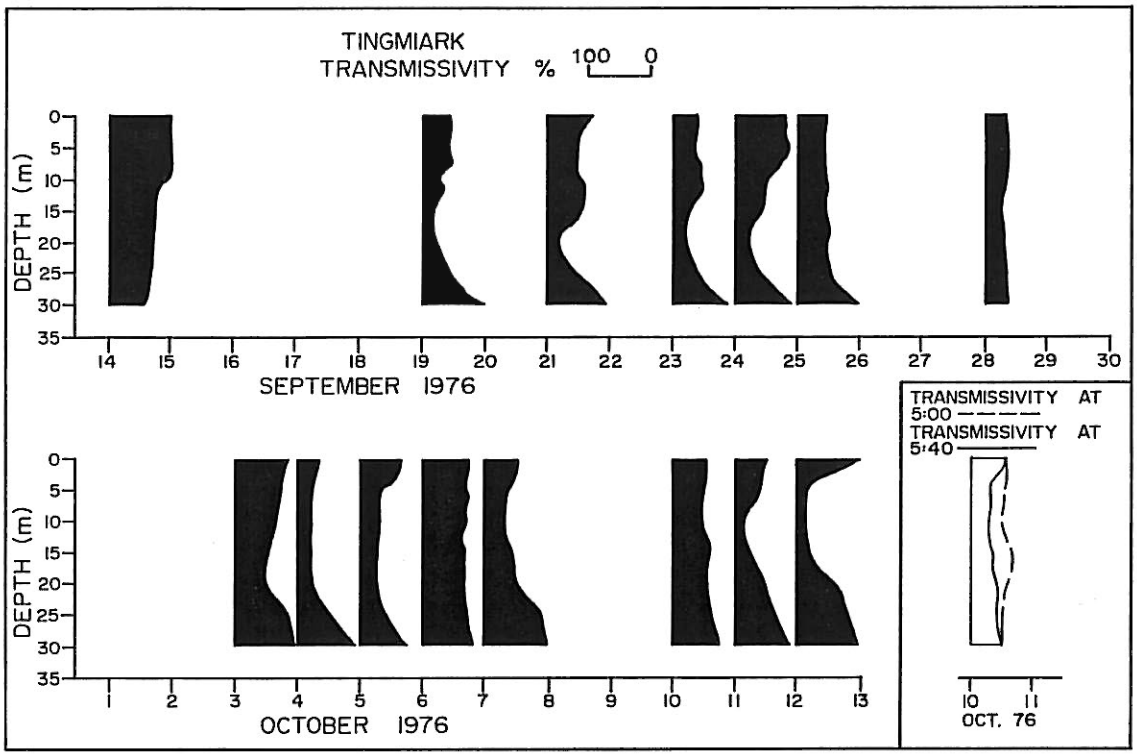

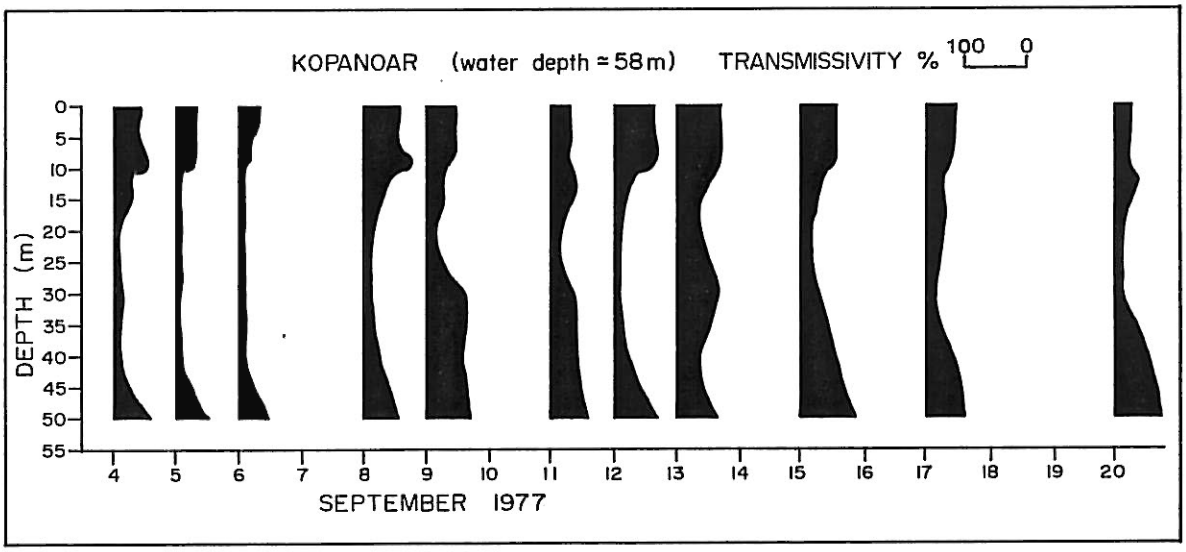

Figure 58: Vertical profiles of transmissivity at the Tingmiark site, September 14-October 12, 1976 and the Kapanoar site, September 4-25, 1977.

For the 1977, Kopanoar transmissivity data obtained at 50 m depth in 58 m of water (Figure 59), a negative correlation is evident between transmissivity and near-bottom current speeds, implying a positive correlation of SSC with near-bottom currents. Although a considerable degree of scatter occurs, the correlation coefficient is -0.45. Taking each measurement to be an independent sample, the statistical significance level for N=11 samples would be 0.55 at the 95% significance level (Section 3.1.1).

Despite the low degree of correlation, the results were considered sufficiently encouraging, in view of measurement uncertainties and the 8 m distance separating the measurement depth and the bottom, that further comparisons were made. Because simultaneous near-bottom current measurements were only made in 1977, the transmissivity data available for 1978 and 1979 were compared with the nearest available offshore wind measurements. The use of surface winds is based on the correlations found between bottom currents and the winds (Section 3.1), although additional scatter will be introduced as a result of this substitution. The transmissivity and wind data used consisted of:

Site	Year	**Depth**		**Location of**
		Water	**Transmissivity**	**Wind data**
		(m)		
Natsek	1978	34	30	Ukalerk
Kopanoar	1978	58	50	Ukalerk
Nerlerk	1979	52	50	Nerlerk
Ukalerk	1978	29	29	Ukalerk

The results (Figures 59 and 60) suggest that a correlation between near-bottom SSC levels and currents may have occurred at the Ukalerk and Kopanoar sites in 1978. The computed correlation coefficients were -0.40 and -0.42, compared to significance levels of -0.38 (N=25) and -0.43 (N=19), indicating the correlation to be marginally significant at the 95% level. For the Nerlerk transmissivity data, a negative linear correlation was indicated for wind speeds exceeding 8 m/s; at lesser winds, no correlation was evident. For the Natsek site, located on the continental shelf to the west of the Mackenzie trough, there was no indication of any significant correlation. This may be due to

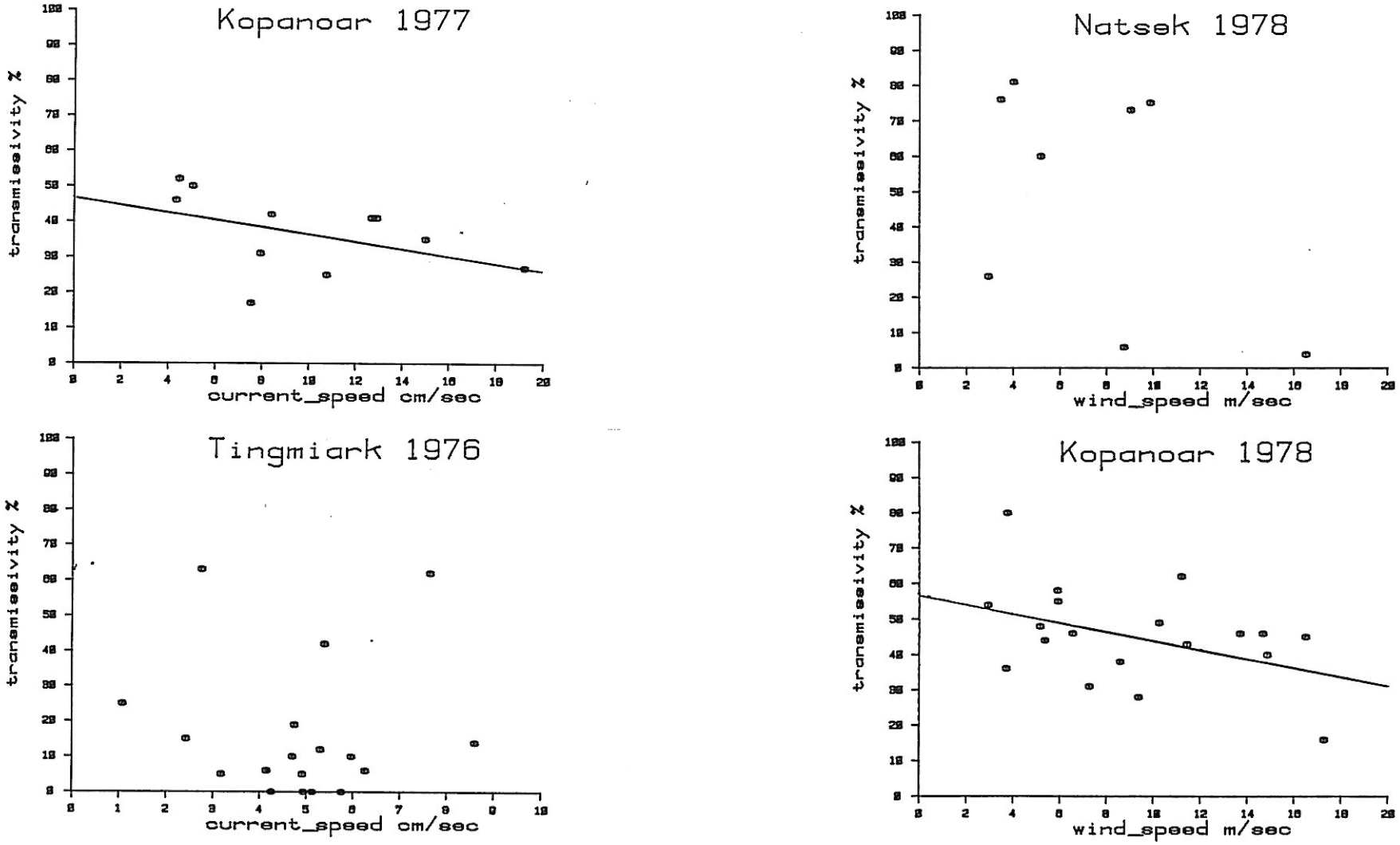

Figure 59: Near-bottom transmissivity plotted as a function of current speed (or wind speed in 1978) averaged over the 24 hour period preceding the time of the transmissivity data for the Tingmiark site in 1976, the Kopanoar site in 1977 and the Natsek and Kopanoar sites in 1978. The plotted line indicates the computed least squares fit of transmissivity on current speed.

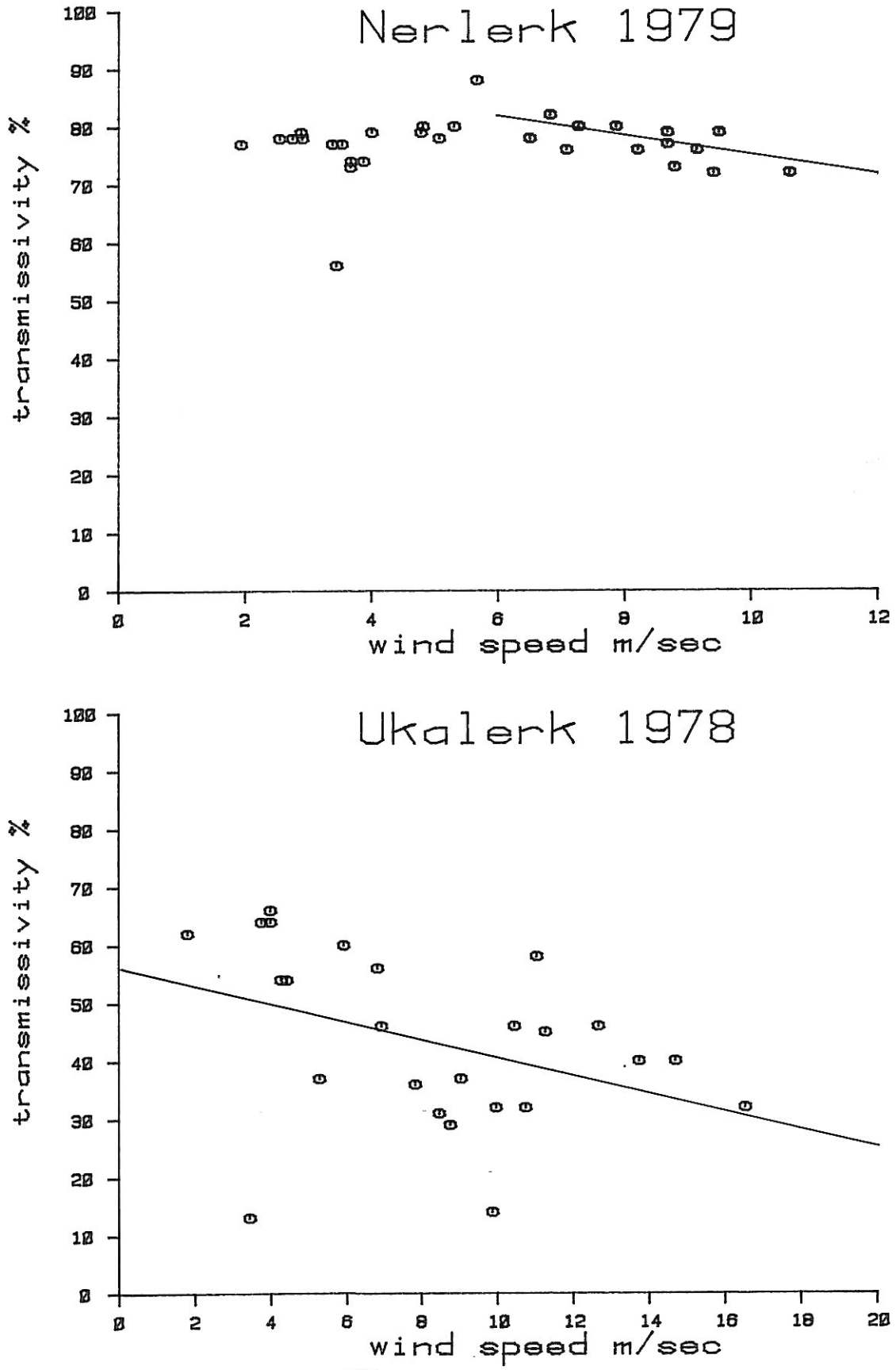

Figure 60: Near-bottom transmissivity plotted as a function of wind speed averaged over the 24 hour period preceding the time of the transmissivity data for the Nerlerk site in 1979 and the Ukalerk site in 1978. The plotted line indicates the computed least squares fit of transmissivity on current speed.

the dominance of strong currents independent of the wind commonly encountered here (Section 2.5.2).

The results, while far from conclusive, do support the hypothesis that wind-induced, near-bottom currents are correlated with increases in the near-bottom SSC levels. Further evidence for such a mechanism is suggested in the SSC data collected near the Issungnak artificial island (water depth of about 20 m) by Erickson et al. (1983) as shown in Figure 61. A very large maximum in SSC at all depths was measured on October 10, 1981, with the largest levels occurring near the bottom. Prior to the time of measurements strong (up to 18 m/s) westerly winds had occurred to October 7; from October 8-10, moderate to strong northeasterly winds (6-10 m/s) were present. These winds resulted in strong near-bottom currents at 27 m depth at the Tarsiut site (located 50 km to the west) of up to 30-38 cm/s on October 4-6 and 10-20 cm/s on October 8-10. While no bottom current meter data are available at Issungnak, the very high SSC levels are likely the result of wind-driven currents or surface waves. During this period, very large surface waves of up to 5 m in height were reported on October 4-5, but the waves were reduced to 1 m or less by October 8-10 (Beaufort Weather Office, 1982).

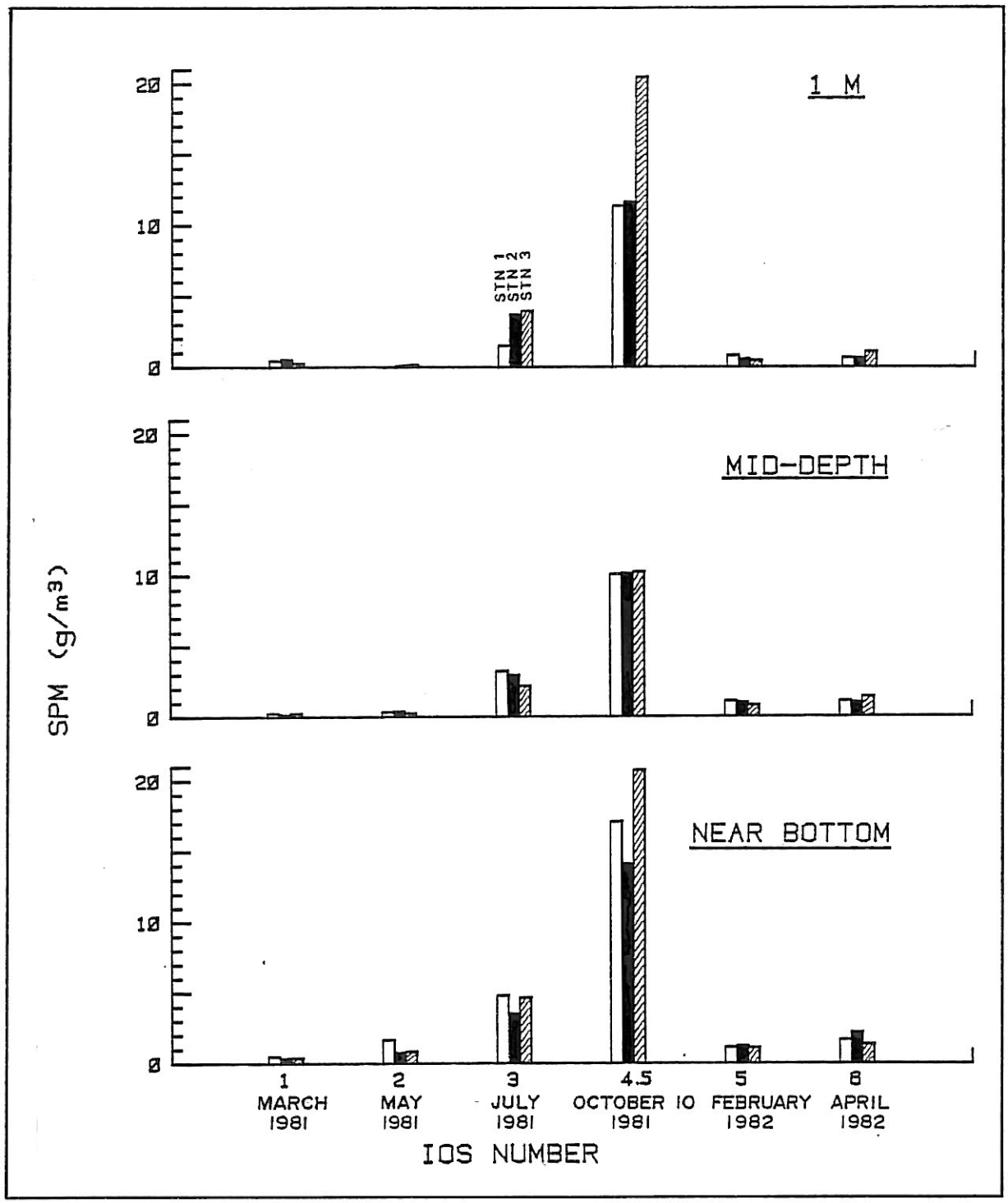

Figure 61: Measurements of turbidity obtained at three stations in the vicinity of the Issungnak artificial island at 1 m below the surface, mid-depth and near-bottom (Erickson et al., 1983).

4. CONCEPTUAL MODEL OF SEDIMENT TRANSPORT

In this section, a conceptual model of sediment transport in the Canadian Beaufort Sea is developed. The conceptual model of the present study is based, in large part, on an earlier model (Harper and Penland, 1982; Harper et al., 1984), as described in Section 1.2. However, the model includes a number of significant modifications based on: 1) a thorough and updated review of relevant elements of the physical environment (Mackenzie River input, surface winds and waves, sea-ice, regional physical oceanography and sediment distributions) derived from the existing literature (see Section 2); and 2) analyses of existing data to provide improved understanding into important aspects of physical processes related to sediment transport (Section 3). Moreover, the model of this study places more emphasis on the physical mechanisms which produce sediment transport and dispersal, and the interrelationships between these various mechanisms.

Model Organization

The conceptual model (Figure 62) connects a set of sediment sources to a set of sediment sinks through transport pathways. These pathways are highly simplified, consisting of links between varying forms of suspended (or deposited) sediments. The boundary of the modelling area consists (see Figure 63) of the Tuktoyaktuk continental shelf, bounded by Mackenzie trough on the west, the continental shelf break to the north, the Amundsen Gulf trough to the east and the coastlines of the Mackenzie delta, Tuktoyaktuk Peninsula and Liverpool Bay to the south. The pathways are divided among three spatial units: the nearshore shelf, the mid-depth shelf and the outer shelf. The choice of the offshore boundaries of the modelling area is approximate, being based on the paucity of available information concerning sediment accumulation rates and (to a lesser degree) SSC values in these generally deeper regions adjoining the Tuktoyaktuk shelf.

Within the modelling area, the defining characteristics of each zone can be summarized, as follows:

1) The nearshore zone, having an outer boundary in the depth range of 10 to 20 m, is characterized by high levels of: sediment accumulation (Figure 3); suspended sediment concentrations (Section 2.5.3); and mechanical energy in the form of both currents (Section 2.5.2) and wave orbital velocities (Section 2.4).

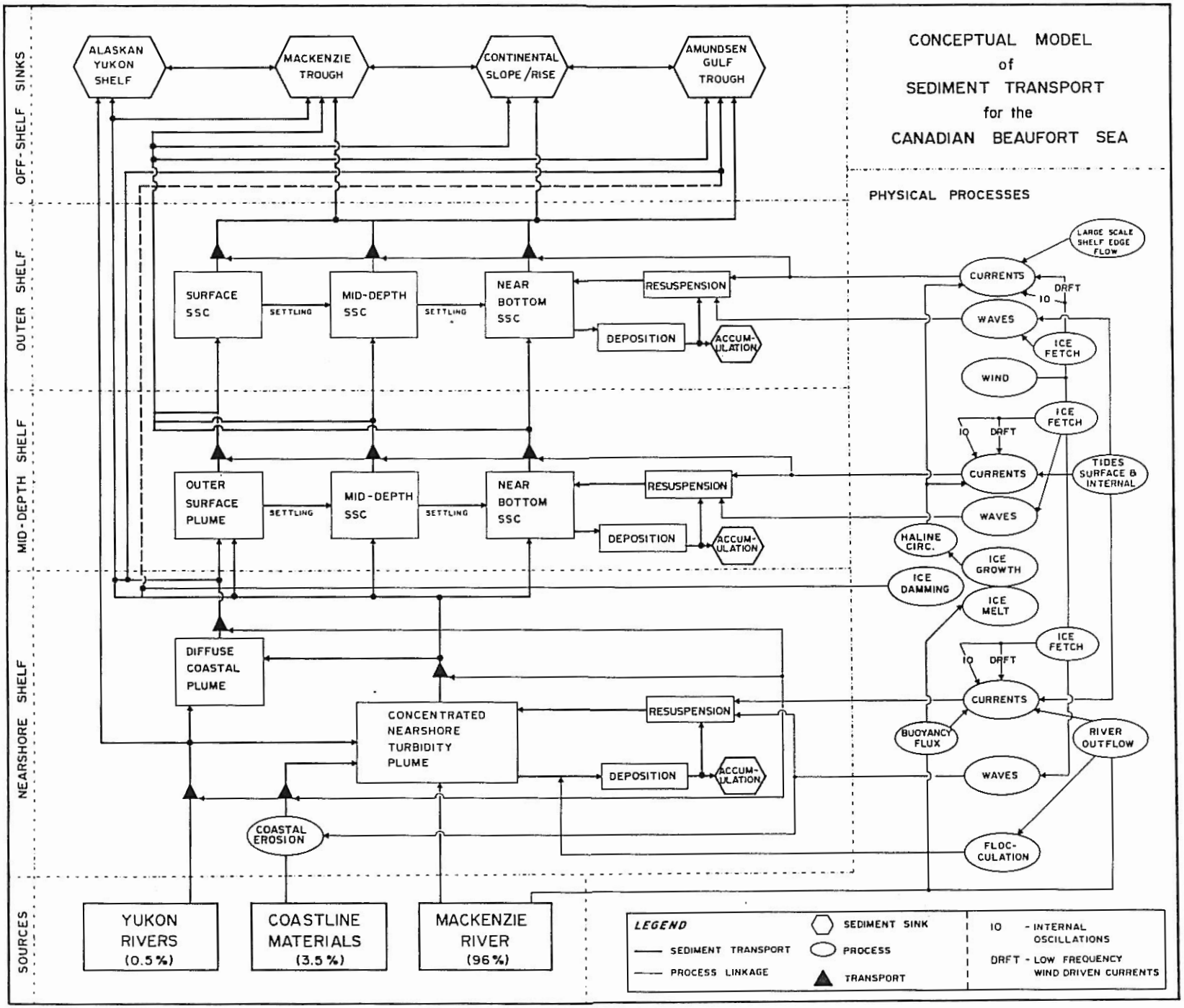

Figure 62: Schematic diagram illustrating a conceptual model of sediment transport in the Canadian Beaufort Sea.

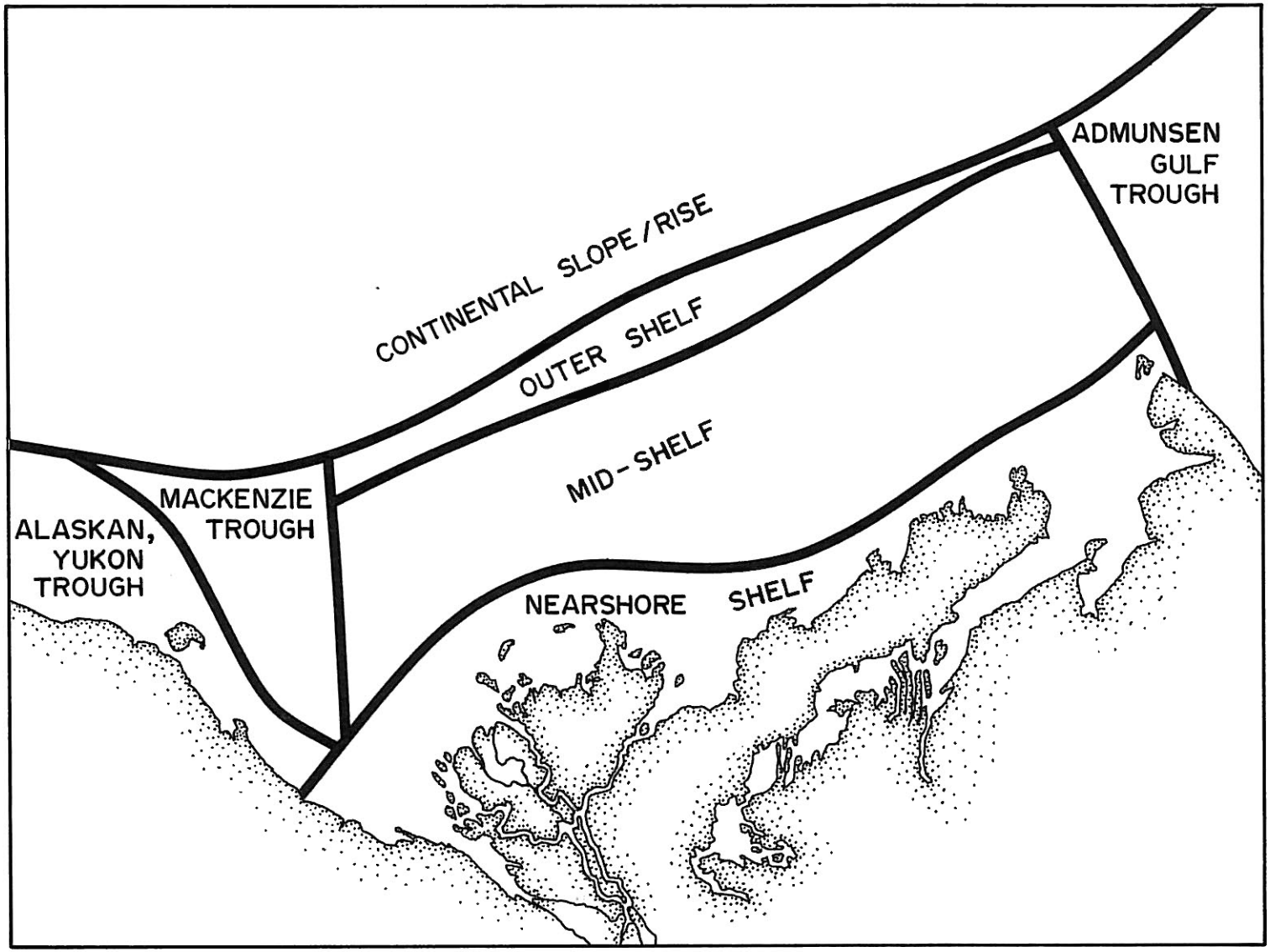

Figure 63: Boundaries of the conceptual model for sediment transport.

2) The mid-depth shelf zone extends offshore of the nearshore zone to water depths of approximately 50 to 75 m. In this zone, sediment accumulations and SSC's are much reduced from the levels of the nearshore zone; however, a feature commonly observed throughout the zone is a SSC maximum just above the bottom. Currents are also reduced, but by a lesser amount than sediment accumulation rates and wave disturbance of the bottom is occasional but occurs at least once each summer.

3) The outer shelf zone differs from the mid-shelf zone, primarily in terms of mechanical energy levels: near-bottom currents appear to be somewhat greater while the frequency of occurrence of bottom disturbance due to surface waves is reduced.

Note that the zones chosen for the conceptual model of the present study differ from those of Harper's model. The outer boundaries of both the nearshore zone, and the mid-depth zone of the present study extend further offshore than in the previous study. The nearshore zone extends to 10-20 m depth rather than 10 m and the mid-depth zone extends to 50-75 m while this zone was limited to depths of 20 m or less in Harper's model. This difference reflects the belief that active reworking of bottom sediments can extend to much greater depths than described by Harper and Penland (1982) due to: the likely underestimation of the strength of wave orbital velocities using the results of Baird and Hall (1980) (see Section 2.4), the possibility that the effective threshold velocity for sediment resuspension could be considerably less than the 40 cm/s value used by Harper and Penland (1982), and the fact that strong near-bottom currents are expected to often coincide with large orbital wave velocities due to the common dependence on pronounced wind events (see Sections 2.4 and 3.1). This contention, supported by the common occurrence of a near-bottom SSC maximum to considerable depths (up to at least 60 m), is described in Sections 2.5.3 and 3.2.2.

The model also delineates the most important physical processes in terms of producing the pathway links between the sediments in each of the internal zones, sources and sinks. These physical processes are presented as a parallel set of links, which induce exchanges between spatial units and the various forms of the area sediments.

The conceptual model is applicable only to the July to October period of open-water conditions in the Canadian Beaufort Sea. At other times of the year, energy levels within the ocean are markedly reduced due to extensive sea-ice cover and the

resulting reduction in wind-driven currents and waves. In addition, the input levels of sediment sources are decreased due to lower river discharges (with the exception of the mid-May to mid-June Mackenzie River freshet) and lesser amounts of coastal erosion. Different processes, including ice scouring and current scouring associated with intensified flows around grounded ice would occur during the winter months, but these were not considered significant on a regional basis (Harper and Penland, 1982). The transport of sediments during freshet could be of some significance, since there may be relatively high levels of sediment input (although little in the way of direct measurements are available for this period; Section 2.1). However, energy levels would be expected to be low by comparison to the summer on the basis of the still extensive landfast ice cover during freshet. Again, there is no direct measurements of currents under the landfast ice during this period to verify this hypothesis.

The conceptual model contains two implicit time scales. The synoptic period (elevated wind speeds associated with the passage of storms) is the first time scale of importance: this period ranges from approximately 2 to 20 days. The importance of the synoptic period is due to the fact that the level of mechanical energy within the water column is highly dependent on the wind blowing over the water surface, producing wind-driven currents and wave orbital velocities. The second important time scale is longer, approximately an annual event, but is not as clearly defined. This time scale reflects the increased levels of mechanical energy within the water column later in the open water season; by means of a number of different factors: greater amount of open water resulting in longer wind fetches, reduced degree of density stratification within the water column and (possible) increases in wind speeds from summer to autumn. While the relative importance of the above-factors are not clear, there is empirical evidence for higher levels of subsurface currents and surface wave amplitudes occurring later in the open water season (September and October).

Sediment Sources

Following Harper and Penland (1982), three sources of input sediment fluxes are considered: the sediment discharges of the Mackenzie River (85.6×10^6 m^3/yr), sediment discharges of the rivers draining the Yukon (0.45×10^6 m^3/yr) and the erosion of coastal sediments (2.9×10^6 m^3/yr) based on estimated coastal retreat rates (Harper and Penland, 1982), including the Yukon coastline (52%), the Mackenzie delta including outer islands (32%) and the Tuktoyaktuk Peninsula (16%). The input of sediment

originating in the Mackenzie accounts for over 96% of the total sediment sources. The river sediments enter the Beaufort Sea from the three major distributary channels with the relative proportion of sediment input expected to correspond approximately to that of volume discharges: 38% entering Shallow Bay, 28% into East Mackenzie Bay and 34% into Kugmallit Bay (Davies, 1975). The absence of major distributary channels in the vicinity of Richards Island results in significantly lower levels of sediment concentrations in the nearshore waters, between East Mackenzie and Kugmallit Bays.

Sediment Sinks

Of several possible sediment sinks for the Canadian Beaufort Sea, Harper and Penland (1982) identified the largest as accumulation of sediments on the continental shelf. Based on post-glacial mud thickness maps in conjunction with a derived sea-level curve, sedimentation rates were computed for the Mackenzie trough and Tuktoyaktuk shelf by Harper and Penland (1982) as discussed in Section 1.2. Integration of the sediment rate estimates (Figure 3) indicates that approximately 4.2 x 10^7 m^3/yr accumulates on the Tuktoyaktuk shelf and Mackenzie trough. It should be noted that within the 10 m depth contour, only "qualitative estimates" of mud volumes were available (Harper and Penland, 1982); however, nearly half of the total sediment accumulation occurred in shallow waters due to the high (average of 2.2 mm/yr) accumulation rate attributed to this zone. In addition to the data deficiencies, the calculations of Harper and Penland (1982) represent an average over the past 8,000 years; present yearly rates may differ from this long-term mean value. Clearly, the uncertainties in the current sediment accumulation rates within the 10 m isobath of the Tuktoyaktuk shelf and over the inner portion of the Mackenzie trough represent a major uncertainty in understanding of regional sediment dispersal.

Other possible sediment sinks considered by Harper and Penland (1982) included:

1) Accumulation in estuaries. No volumetric estimates were available but this sink is thought to be small on the Mackenzie River estuary, as the Mackenzie delta is considered to be presently stable to eroding in most areas.

2) Accretion on coastal landforms (e.g. barrier islands and spits). Data are available only for the Yukon coastline (excluding the barrier islands to the west of Herschel

Island) where McDonald and Lewis (1973) calculated depositional rates of 3.0 x 10^4 m^3/yr. Harper and Penland (1982) estimated that similar volumes could be expected for the Mackenzie delta and Tuktoyaktuk Peninsula coastlines. If so, total deposition would amount to approximately 3 x 10^4 m^3/yr, only 3% of the estimated coastal erosion rate.

3) Sediment accumulation over the deeper waters adjoining the Tuktoyaktuk shelf can only be estimated for the Mackenzie trough (approximately 0.84 x 107 m^3/yr or about 20% of the total of 4.2 x 107 m^3/yr computed by Harper and Penland (1982) on the basis of mud thickness data). For the continental slope and rise, there is contradictory information as to the amount of sediment accumulation (Harper and Penland, 1982). Meagher (1978) mapped thick mud deposits on the continental slope but the work of O'Connor (1982) suggests that the volume of sediments originating in the Halocene period are low. However, from the more recent seismic and core data of Hill et al. (1984), higher (approximately 1 mm/yr) sedimentation rates were estimated. In the absence of data, sediment accumulation in the Amundsen Gulf trough can be assumed to be very low, given the marked regional decrease in measured mud thickness from west to east along the Tuktoyaktuk shelf.

The Nearshore Shelf Zone

Suspended sediments within the nearshore zone (depth <10-20 m) occur as: 1) a highly concentrated nearshore turbidity plume adjacent to the main source of sediments (the Mackenzie River delta); and 2) an outer, much less concentrated (diffuse) coastal plume found in most of the remainder of the zone. The spatial distribution of these plumes vary primarily according to prevailing winds. Under westerly winds, the concentrated plume extends eastward from the delta along the Tuktoyaktuk Peninsula. For easterly winds, the concentrated plume extends west and across West Mackenzie Bay, occasionally reaching the Yukon coastline; under these conditions, the diffuse outer plume moves offshore, and is replaced by clear, cold Arctic Water along the Tuktoyaktuk Peninsula. While the wind-driven surface currents play the dominant role in determining the advection of suspended sediments, the buoyancy flux driven by the fresher water input of the Mackenzie River (and to a lesser extent by melt of the landfast ice in early summer), results in a net eastward flow along the coastline. However, the resulting currents are likely limited to 3-10 cm/s (McNeill and Garrett, 1975) as compared to

wind-driven currents of approximately 3% of the local wind speed (15-30 cm/s for winds of 5-10 m/s).

Based on the relatively sparse SSC data available for the nearshore zone (Section 2.5.3), the highly concentrated nearshore plume adjoining the Mackenzie delta typically has values of 100-200 ppm in early summer, declining later in the summer. This plume always occurs within the 10 m isobath, and often within the 5 m isobath. The SSC levels appear to be relatively uniform through the water column. A very pronounced horizontal gradient or turbidity front separates the concentrated nearshore plume from the diffuse outer plume, which has surface SSC levels reduced typically by two orders of magnitude. Unfortunately, there is only one set of data available on the subsurface SSC values in the diffuse outer plume obtained off Mackenzie Bay (Fraker et al., 1979) which suggests that near-bottom turbidity are reduced to levels of less than 5 ppm, while the surface values are highly variable, ranging from less than 5 to 30 ppm.

An order of magnitude calculation of residence time in the concentrated nearshore plume in July can be deduced from a planimeter estimate of area adjoining the Mackenzie delta from West Mackenzie Bay to Kugmallit Bay within the 5 m isobath (5.5×10^9 m^3), mean depth of 2 m and typical SSC of 100 ppm, yielding a total sediment volume of approximately 1.1×106 m^3. Representative river inputs for this time of year amount to about 0.5×106 m^3/d as seen in Appendix A (although larger peaks of several times this value can occur for short periods) suggesting a typical residence time of only 2 days.

In view of the small residence time of 2 days computed for water depths of 5 m or less, large sediment losses occur within this region over time scales smaller than the synoptic period. The great bulk of this loss must occur through sediment accumulation or advection. For the former process, virtually no information is available on sediment accumulations within the 5 m isobath. In the adjoining deeper areas (up to 20 m depth) Harper computed values of 3 mm/yr or less (Figure 3). If <u>all</u> of the sediment input went to the zone of depths of 5 m or less, the accumulation over the 120 day period of open water would amount to 11 mm/yr. Such a high rate seems unlikely given the preponderance of silt and sand in the surficial bottom sediments observed within the 10 m isobath (Figure 2) and the much lower measured sedimentation accumulation rates determined for the adjoining deeper waters. This suggests that most of the river sediment is advected to the adjoining offshore waters. Undoubtedly, sediment deposition will occur at times of low energy (i.e. low wind speeds) but most if not all of the

sediments will be subsequently resuspended with the passage of the next weather system.

Beyond the 5 m isobath, comparatively high rates of deposition occur in the concentrated nearshore plume, as suggested by the large sediment accumulation rates (Figure 3), as well as the commonly observed pronounced surface SSC gradient. This results from settling associated with the general decrease in velocity associated with dispersal of the Mackenzie River fresh water as it leaves the delta. Flocculation due to increased salinity may also account for some of the deposition, with the salinity increasing from 0-5 ppt at the delta to 10-15 ppt as a result of mixing with the oceanic waters. Comparisons of available nearshore SSC and salinity values do not reveal any pronounced decrease in SSC as a function of salinity (Section 3.2.1), suggesting that flocculation associated with salinity increases may not be important.

Within the nearshore zone, resuspension of bottom sediments occurs frequently. Unfortunately the frequency of bottom sediment resuspension cannot be accurately estimated due to lack of adequate information concerning: the critical shear stress required for resuspension, the near-bottom wave orbital velocities and the near-bottom currents. Uncertainties in the first of these three quantities, critical shear stress levels, are the most important for this conceptual model. A review of information obtained in laboratories and other continental shelf zones (Appendix B) suggests that the critical shear stress for resuspension would likely be associated with threshold velocities velocities having a range of 10 to 40 cm/s, with a most probable value of approximately 20 cm/s. Using the 20 cm/s value, wave orbital velocities (Section 2.4) are expected to exceed this value one half the time at a depth of 7 m. Because near-bottom current velocities average approximately 10-16 cm/s (Section 2.5.2) and both the waves and currents are strongly coupled to the wind, total near-bottom current exceeding 20 cm/s occur more than 50% of the time. A depth of 10 m, where the 50% exceedance levels of both wave orbital velocities and near-bottom currents would each amount to approximately 10 cm/s, would be expected to be a reasonable approximation of the outer boundary of the region; at this depth (10 m) total current exceeds the assumed critical shear stress of resuspension (taken as 20 cm/s near-bottom velocity) over 50% of the time. The corresponding depth for a critical shear stress equivalent to a 10 cm/s bottom current is estimated as 17 m (50% exceedance levels of wave orbital velocities and near-bottom currents taken as 2 cm/s and 8 cm/s respectively, at this depth), while for a shear stress equivalent to a 40 cm/s bottom current, the appropriate depth is

estimated as approximately 6 m (50% exceedance levels of wave orbital velocities and near-bottom currents taken as 24 cm/s and 16 cm/s, respectively, at this depth). Thus, the nominal offshore boundary of the area of frequent bottom resuspension (taken as occurrences of 50% or more) could vary in water depth from 6 to 17 m, about an expected value of 10 m.

Wind-driven resuspension events will be accompanied by a generally unidirectional flow parallel to the coastline in the nearshore zone. During such events, considerable dispersal of sediments is likely to occur with a net transport from the area adjacent to the Mackenzie delta along the coastline, either eastwards or westwards depending on the wind direction. For example, during an 8 m/s wind event of 2 days duration, net alongshore displacement would amount to 35 km, assuming the mean currents respond as 2.5% of the wind speed. A sequence of four events directed eastwards would result in a net displacement equal to the length of the Tuktoyaktuk Peninsula, while two westward events would transport sediment from Mackenzie Bay over the inshore axis of the Mackenzie trough. Over many individual wind events, the eastward displacements are expected to be larger, due to the greater fetch associated with westerly to northwesterly winds than is the case for easterly winds, resulting from the orientation of the coastline and patterns of open water (Section 2.3).

While wind-driven sediment transport will be directed primarily parallel to the coastline, the currents are sufficiently variable in direction, even during strong winds, that an offshore dispersal occurs. The occurrences of current components perpendicular to the coastline, and local isobaths, are associated with wind-driven inertial oscillations, along with tidal currents and baroclinic instabilities believed to occur along the strong horizontal density gradients on the outer side of the concentrated Mackenzie River plume. Based on the limited number of nearshore current measurements, a distinct tendency for increasing directional variability and reduced wind-driven coupling is suggested with increasing distance from the coastline (Section 2.5-2). Offshore dispersal is also enhanced under easterly winds due to the net offshore displacement of the surface. Prominent offshore filaments in the surface temperature and turbidity distributions have been observed from satellite imagery under easterly wind conditions (Marko and Oberski, 1982).

At present, quantitative estimates of sediment transport in the nearshore zone are not possible, with the dearth of information on the distribution of SSC's and currents. Direct measurements of SSC's are limited to two studies (McDonald and

Martin, 1976; Fraker et al., 1979), each of which covered only a portion of the Mackenzie delta area. There is virtually no direct measurements available for the nearshore zone off the Tuktoyaktuk Peninsula, Liverpool Bay and the Yukon coastline. Studies based on satellite imagery, while providing much useful information, are limited to surface measurements, are uncertain as to absolute SSC levels due to possible calibration errors and do not include data for strong wind conditions associated with the passage of cyclonic disturbances, when sediment transport and dispersal is largest. The very limited extent of available current information in the nearshore zone further compounds the difficulty in estimating transport values. While the absence of SSC and current data are a problem throughout the nearshore zone, perhaps the most acute difficulties arise in trying to estimate dispersal through the offshore boundary of the concentrated plume into the poorly defined diffuse outer plume. At present, only qualitative data (including satellite-based measurements calibrated according to Bay of Fundy ground truth data, Section 2.5.3) are available for the surface under easterly winds. Data on subsurface conditions, in terms of SSC levels and currents, are virtually non-existent.

Mid-Depth Zone

Within the mid-depth zone, the water column can be divided into three segments in terms of SSC values: 1) the uppermost portion, typically 5-10 m deep with relatively high levels; the largest SSC values usually occur at the surface or immediately beneath it; 2) the middle portion of the water column with markedly reduced SSC levels; and (3) the bottom portion of the water column (lower 10-15 m) with relatively high levels, almost always increasing to a maximum at the greatest measurement depth. Surface values of SSC appear to range from 0.5 to 2.5 ppm, and it is likely that the range of near-bottom SSC's would be similar on average, although distinctly greater at some times. Mid-depth SSC levels are typically reduced by a factor of 2 to 3.

Input into this zone results from offshore advection from the nearshore zone, although it is unknown as to what proportion enters directly from the concentrated nearshore turbidity plume, as distinct from a diffuse coastal plume formed within the nearshore zone. In the case of the former source, one major uncertainty involves the possible existence of a continuous turbid bottom layer originating from nearshore turbidity plumes. Alternatively, the high turbidity bottom layer could be explained as resulting solely from local resuspension of bottom sediments during the passage of storms.

Resuspension of sediments from the bottom clearly plays an important role in maintaining the near-bottom SSC maximum. Evidence for resuspension exists in the correlation between SSC levels and wind speed (Section 3.2.2). In addition, the dominance of smaller diameter particles in the near-bottom waters (Figure 41) as opposed to surface and mid-depth levels also indicates that the larger particles are preferentially settling from the surface, while smaller particles are being introduced into the near-bottom layer, either through resuspension, advection or both of these processes.

The energy levels for near-bottom resuspension are provided by waves and currents: the amplitude of both processes decrease rapidly with increasing depth. The depth-dependent reduction in near-bottom wave disturbance is the most pronounced, decreasing approximately exponentially with increasing depth. The frequency occurrence of wave disturbances exceeding 20 cm/s decreases from 30 to 50% at the inner boundary to only one event per open water season at the outer boundary (Section 2.4). The corresponding reduction in near-bottom currents is smaller, decreasing from typical mean (maximum) speeds of 10 cm/s (35 cm/s) to 4 cm/s (20 cm/s).

The near-surface and near-bottom currents are primarily wind-driven: at the surface, the mean response amounts to approximately 2% of the wind speed, while the near-bottom current response is less, on average, amounting to 0.5-1.0% of the wind speed. In addition to the sub-tidal wind-driven current response, inertial oscillations also result from wind forcing, having amplitudes of up to 5-10 cm/s near the bottom and up to 20-30 cm/s near the surface. Tidal flow also contributes to the currents at all levels through the water column, while haline-driven circulation resulting from ice formation of the previous winter could produce flows near the bottom. The near-bottom currents tend to follow a broad bimodal distribution, with easterly-northeasterly directed flows being more common than the westerly flows resulting in a net east-northeast directed flow of 1 to 3 cm/s.

Over the mid-shelf, there is evidence of increasing energy levels in late summer-early autumn due to generally longer open-water fetches combined with reduced stratification within the water column. Both of these factors would increase wind-driven near-bottom currents, while the former would also increase the level of wave disturbance. While very little data of any kind are available for this time of year, the existing current data (Figures 34, 44) and SSC data (Figures 58, 61) does suggest stronger flows and increased near-bottom SSC values.

Sediment transport fluxes can be approximated to perhaps an order of magnitude accuracy for two different scenarios. In the first, during the passage of a typical synoptic wind event over say a 2-day period, the flux (Q) directed parallel to the wind can be estimated as the product of the mean concentration (C), layer thickness (D), width of the zone (W) and the net current velocity (U). For a wind speed of 8 m/s, the surface layer flux would amount to 0.9 x $10^4 m^3/d$ (C=1 ppm, D=5 m, W=100 km, U=0.025 x 8 =0.2 m/s). Under the same conditions, the transport in the bottom boundary layer would be 0.4 x $10^4 m^3/d$ (C= 1 ppm, D=8 m, W=100 km, U=0.008 x 8= 0.064 m/s). In addition, this level of sediment transport will tend to be directed east-northeastwards over the eastern portions of the shelf and into the Amundsen Gulf trough, or alternatively westward into the Mackenzie trough.

On a very limited number of occasions, most likely in late summer and early autumn, transport levels in the bottom boundary layer could increase by about an order of magnitude. Due to the high levels of wave and current disturbance, and resulting resuspension, SSC levels of perhaps 5-10 ppm and 10 m in thickness could be realized. Stronger net currents, of say 2% of 15 m/s wind or 0.030 m/s would result in a bottom sediment transport of 21 x $10^4 m^3/d$ (C=8 ppm, D=10 m, W=100 km, U=0.3 m/s), an increase by a factor of 50 from the transport of 'typical' summer wind events. These calculations suggest that the transport due to intense disturbance and advection in the bottom boundary layer could play a major role in the overall level of sediment transport on the middle portion of the shelf. However, better data coverage is required to substantiate the values used, being derived from a very limited data sampling.

A net offshore dispersal will also occur through the mid-shelf zone, because of the non-zero cross-shelf component of the currents. In the bottom boundary layer, the offshore movement will move sediments into areas of reduced energy levels; because of the reduced likelihood of resuspension, a net accumulation of bottom sediments will result. This source of bottom accumulation will augment the accumulation of sediments settling from the surface and mid-depth portions of the water column.

Outer Shelf Zone

In many respects the outer shelf zone represents a continuation of conditions described previously in the Mid-Depth Zone: maximum SSC's are usually found near the surface and near

the bottom, although absolute levels are reduced; and sediment accumulation rates are generally proportional to, but reduced from, those of the adjoining mid-depth zone.

The distinguishing feature between the outer and mid-depth zones is the energy regime of the near-bottom boundary layer. In the outer shelf zone, the near-bottom currents are generally larger than those of the mid-depth zone, with a persistent net flow setting to the northeast (Section 2.5.2). Mean current speeds amount to 7-10 cm/s, with maximum levels of 20-40 cm/s, varying according to location. In addition, the coupling between bottom currents and winds may be stronger (Section 3.1.1). On the other hand, the wave orbital velocity levels are reduced due to the greater water depth. Wave events generating near-bottom velocities in excess of 20 cm/s are unlikely to occur more than once each year and may occur even less frequently (Section 2.4).

Based on very limited and uncertain data, resuspension of sediments does appear to occur over synoptic time scales (see Figure 58). Given the low wave orbital velocities expected for all but the extreme storms of the season, the apparent resuspension would appear to result largely from the wind-driven near-bottom currents. For a 8 m/s wind speed, the bottom currents would respond as 0.6 to 1.1% of the wind (i.e. as a 5 to 9 cm/s current). In addition, a net flow of about 5-6 cm/s results in a total current of 10-15 cm/s directed northeasterly. (In itself, this calculation suggests that critical shear stress for resuspension on the outer shelf may lie at the low end of the possible range (i.e. 10-20 cm/s) described in Appendix B.) Over a period of a few days at these speeds, a net displacement of 2 to 3 km would be expected. Given the unidirectional nature of the currents, a cumulative displacement over, say, 10 such events per open water season would amount to 20-30 km. In comparison with the mid-shelf zone, the net eastward transport associated with synoptic wind events is expected to be larger due to the greater degree of unidirectional currents.

The reduced degree of wave disturbance levels on the outer shelf imply that extreme events (about once per year) may play a less important role than is the case for the mid-depth shelf. Furthermore, such events almost certainly would be associated with the longest open-water fetches available; thus, the winds would be blowing from the west, which would tend to increase the eastward advection near the ocean bottom. The effect, then, is to enhance the sediment transport potential occurring over synoptic time scales, by means of increased levels of resuspended sediments as well as a greater rate of advection to the east. Given the rarity of occurrence of such events (which is itself

uncertain due to deficiencies in the description of the return periods of extreme waves; Section 2.4), it is not possible to quantitatively estimate the degree of enhancement for these rare situations of extreme waves.

In addition to the eastward transport near the bottom, a net offshore dispersal is likely to occur, resulting in depositions onto the much deeper waters of the continental slope. Such dispersal would result from directional perturbations from the dominant northeasterly transport, largely associated with inertial oscillations and tidal currents. Once the sediments reach the deeper offshore water, they would enter a markedly different hydrodynamic regime. Due to settling into markedly greater depths, energy levels would likely decrease as a result of the now negligible wave disturbance levels. However, information on the vertical profile of the currents over the continental slope is very limited, as no direct current measurements are available. At some unknown point on an offshore transect, the effects of the northeastward transport would likely give way to the westerly flow associated with the large-scale Beaufort Gyre. However, at depths in excess of 200 m, the amplitude of these currents (as deduced from indirect density profile data, Melling, 1983) are limited to speeds of a few cm/s or less. It should be noted that off Alaska, direct current measurements over the inner portion of the continental slope have shown that a highly energetic current regime exists with flows of 20 cm/s occurring over periods of a few to several days. In the absence of direct current measurements, it is not known whether this oceanographic feature exists in the Canadian Beaufort Sea.

On the basis of the description of the hydrodynamic regime given above, it is anticipated that net sediment transport would be portioned between: 1) net eastward transport along the shelf edge resulting in sediment accumulation over the outer shelf or ultimately into the eastern end of the shelf and Amundsen Gulf trough and 2) a net offshore dispersal onto the continental slope. Because information on modern rates of sediment accumulation is very limited for the outer shelf, Amundsen Gulf trough and the continental slope regions, it is not possible to determine the proportions accumulated in these areas.

Recent studies by the Atlantic Geoscience Centre suggest that comparatively high deposition rates (1 mm/yr) could occur over the inner portion of the continental slope (Hill, pers. comm.). Bottom sediment grain-size data collected during the Beaufort Sea Project (Pelletier, 1975) have been interpreted as indicating generally higher energy levels on the eastern portion of the continental shelf to the inner slope region and Amundsen

Gulf trough. This hypothesis is not supported by the existing information on the hydrodynamic environment which indicate that energy levels decrease from west to east in both the mid-depth and outer shelf zones. Pelletier (1975) suggested that the Beaufort Gyre, acting in combination with upwelling events driven by easterly winds, explains higher energy levels and a net westward sediment transport on the eastern end of the shelf. However, again the oceanographic data do not support this hypothesis but rather suggest a pronounced net eastward transport over the outer shelf. Furthermore, there is no indication that the Beaufort Gyre extends over the continental shelf. These results lend support to the alternative hypothesis of Harper and Penland (1982) that the observed grain-sized distributions results from relict Pleistocene sediments deposited at a time of a more energetic hydrodynamic regime.

5. SUMMARY AND CONCLUSIONS

In this study, existing data on sediment transport and dispersal in the Canadian Beaufort Sea were assembled and analyzed. In addition to examining the data on the major sediment source, the Mackenzie River discharge and the regional distribution of suspended sediments, emphasis was placed on describing the important aspects of the physical processes: surface winds, sea-ice cover, waves and currents. Based on this collection of information (Section 2) and specific analyses of selected data sets (Section 3), a conceptual model of sediment transport was presented (Section 4). The model, derived in large part from an earlier study (Harper and Penland, 1982; Harper et al., 1984), describes the most important transport pathways and relates these to the relevant physical processes.

The surface wind provides the dominant environmental forcing of sediment transport in the Beaufort Sea, acting in two distinct ways: 1) as wind-generated currents throughout the water column in the form of low-frequency drift flows and inertial oscillations; and 2) generation of surface waves producing orbital velocities which resuspend bottom sediments and maintain these in the water column. Beaufort Sea winds are bimodal, with the strongest and most frequent winds blowing from the west-northwest and easterly sectors. The dominant time scale of wind variability occurs at synoptic periods (2 to 20 day periods). At longer periods, variations at intra-annual and annual time scales are low in the Beaufort Sea. The longest time series wind data are available for coastal locations. Regression analyses of offshore winds onto winds measured at Tuktoyaktuk demonstrate that offshore winds are highly correlated, with the offshore winds approximately 20% greater in terms of major components, and 25% greater for speeds, as compared to the coastal winds.

An examination of regional sea-ice concentrations reveals a large amount of interannual variability in the position of the Arctic Ocean pack ice and the resulting amount of open water to the coastline. A general trend of offshore movement of the pack ice edge occurs in most summer seasons, leading to maximum open-water fetch in September and October. However, reversals of such trends have been observed in individual years at virtually all points in this seasonal progression.

The wave climate in the Beaufort Sea also exhibits a high degree of interannual variability due in large part to the differences associated with highly variable polar pack ice edge location. The results of two recent wave climate studies (Baird and Hall, 1980; Hodgins et al., 1981) were compared and found to

differ significantly. Given the results of the former model, bottom disturbances due to waves are confined to depths of 30 m or less (one-year return period orbital speeds of 40 cm/s or more). Using the results of the latter study, the same conditions would extend to depths of 70 m. Based on an assessment of the limitations of each model, the actual wave conditions likely fall between the results of these models. Further wave climate studies and extension of the rather limited (8 years) set of direct wave measurement is required to resolve this uncertainty.

Analysis Results

The response of bottom currents to wind forcing during summer was examined through linear regression analysis on existing data, for ten different sites ranging in depth from nearshore to shelf-edge locations. The results show that a statistically significant level of coupling occurred at all sites. The largest responses were determined for a single nearshore station (depth of 8 m) with the bottom currents responding as 2.2% of the wind. Over most of the shelf, the response of bottom currents to winds averaged 0.5 to 1.0%. There appeared to be a general tendency of decreasing response with increased depths. However, at one site location near the shelf edge, the response coefficient increased to 1.2%. The computed response coefficients represent average levels, typically over a 2-month period. Responses to individual wind events often differ significantly from these averages; on some occasions, the bottom currents response was larger by a factor of 2-3 over the responses computed from the entire season-long data record.

Based on an analysis of a single set of extended measurements of near-bottom current measurements (record length of over one year) obtained near the Tarsiut site in 25 m water depth, marked seasonal differences were evident in the wind-generated bottom currents. As expected, the response coefficient is low (0.2-0.4%) in late winter and spring beneath the sea-ice cover. With the open-water conditions of summer the response increases to 0.7%, and further increases in early autumn to 1.7% prior to freeze-up. This marked increase in autumn may reflect the seasonal increase in both wind fetch and the reduced degree of vertical stratification.

The results of linear regression analyses of bottom currents on winds and bottom currents on water levels were compared. Neither wind nor water levels account for more than 65% of the

standard deviation of the bottom currents. However, the water levels appear to provide a somewhat better indicator of the subtidal variations in bottom currents than do the winds.

Existing SSC data (obtained in 1975 and 1977) for nearshore zones were examined. A sharp reduction in SSC levels throughout the water column was noted for depths in excess of 5 m. Comparisons of SSC levels with salinity reveal a high degree of scatter, suggesting that enhanced flocculation of sediment particles due to increasing salinity may not be of major significance in the nearshore zones.

For greater water depths (25 to 58 m), time series of transmissiometer profile data were compared to simultaneous measurements of offshore wind. For four of the six available data sets, a statistically significant correlation was determined through linear regression analyses, with transmissivity inversely correlated to wind speed. The results, while far from conclusive in view of the considerable experimental uncertainties in the transmissivity data, suggest that changes in the amplitude of the near-bottom SSC maximum result from wind-generated bottom currents causing enhanced resuspension or advection over waters of considerable depth on the Tuktoyaktuk shelf.

Conceptual Model

The conceptual model relates the known sources of sediments in the Canadian Beaufort Sea (96.5% due to the Mackenzie River) to a set of sediment sinks (deposition onto the continental shelf and advection beyond the shelf into the Mackenzie trough, Yukon shelf, continental slope and the Amundsen Gulf trough). The transport pathways are resolved into three spatial units: the nearshore shelf (out to 10-20 m depth), the mid-depth shelf (50-75 m depth) and offshore shelf (to the shelf edge). While the model follows the framework of the earlier work of Harper and Penland (1982) it differs in a number of ways:

1) Greater emphasis is placed on relating sediment transport to the physical processes in the ocean: particularly waves and currents, both of which are primarily driven by the surface wind.

2) Two time scales are represented in the driving transport of suspended sediments: a) the synoptic time scale associated with the passage of individual weather systems (2-20 days) and b) a longer period representing extreme events occurring once or twice each season, usually in late September or October when open-water

fetches tend to be at their maximum. The synoptic time scale is likely dominant for transport in the nearshore zone, but the longer period time step may be of considerable importance at the greater depths of the mid-depth and outer shelf zones.

3) Suspended sediment transport within the bottom boundary layer extends well beyond and offshore of depths of 20-35 m or greater, in contradiction to the model of Harper and Penland (1982). In fact, transport likely occurs intermittently within each summer out to the edge of the continental shelf. This contention is based on observations of fluctuating near-bottom SSC values and the likelihood that the combined effects of wave orbital velocities and currents in the bottom boundary layer exceed the expected critical shear stress for sediment resuspension (threshold velocity estimated as 10-40 cm/s, with a most probable value of 20 cm/s). While the available data suffers from many gaps and shortcomings, sediment transport on the Canadian Beaufort shelf has the appearance of being active throughout the summer. Within the same season, transport from the Mackenzie River delta to the Mackenzie and Amundsen Gulf troughs would appear to be very likely within the nearshore zone. The rate of offshore dispersal over the continental shelf to the continental slope is more difficult to estimate, but could conceivably extend over a few successive summers. However, sediments reaching the eastern flank of the Mackenzie trough may move comparatively rapidly northeastward along the continental slope under the influence of the near-bottom current setting in this direction parallel to the shelf edge.

6. RECOMMENDATIONS

In this section, recommendations are presented which offer the potential of leading to significant advances in the present understanding of sediment transport in the Canadian Beaufort Sea. These recommendations are ordered by component within the conceptual model (Section 4), rather than by overall priority in terms of improvements of knowledge of regional sediment transport.

Sediment Sources

1) Better estimates are required of the time dependent Mackenzie River sediment output. At present, data are limited to a few years at a site (Arctic Red River) upstream of the delta. The very high degree of variability in the observations at this location demonstrates a need for obtaining a better measure of the sediment discharge levels into the Beaufort Sea and improved understanding of the physical causes of the variability of sediment discharges.

Sediment Sinks and Nearshore Zone

2) Data on sediment accumulations are required for the nearshore zone (at water depths of less than 10 m), and the offshore areas bordering the Tuktoyaktuk shelf (Mackenzie trough, continental slope and Amundsen Gulf trough). These data should have at least the same accuracy and spatial resolution as the estimates based on mud thickness measurements currently available for most of the shelf. Direct determination of accumulation rates reqires a measure of sediment age. Such a measure could be provided by vertical sampling of isotope concentrations (e.g. Pb 210/Cs137) at selected stations.

3) More data are required on the distribution of SSC levels throughout the water column of the nearshore zone. The early summer period, subsurface levels throughout the most pressing data deficiencies are associated with the open- water season and the spatial distributions under strong westerly wind conditions. An ongoing program consisting of a number of elements would provide the optimum solution.

- direct profile measurements from surface vessel (or helicopters), repeated over the summer season. These would also serve to provide ground truth data for satellite studies;

- 'in-situ' internally recording transmissiometers providing extended time series at a small number of locations. Calibrations with turbidity samples are required to convert the results to SSC levels.

4) Satellite-imagery data for additional measurements of the spatial distribution of the surface plume. The use of NOAA/Tiros satellite imagery rather than Landsat would provide much more frequent samplings (i.e. a greater range of images to select from) and would provide synoptic data collection over the entire Canadian Beaufort Sea. Successive mappings of surface SSC distributions over large areas would be most useful in delineating the response of the surface plume to wind events.

5) Additional time series measurements of currents. At present, only one set of current data is available for depths of less than 10 m. Emphasis should be placed on extending the measurements into the autumn. In addition, simultaneous collection of transmissivity and current meter data at the same location would have considerably more value than measurements of only one of these quantities; this type of data in combination with simultaneous wind information would permit time series computation of sediment transport values for the site and could be used to provide insight into the degree and frequency of resuspension events.

Mid-Depth and Offshore Zones

6) More direct measurements of SSC profiles are required in these areas. The distribution of existing data are very limited in both time and space. Profiles obtained over a short period, preferably repeated 2 or more times within one season, are needed. On a more limited basis, sampling of particulate size distributions at a few levels within the water column (see, for example, Matsumoto and Wong, 1977) would be valuable.

7) A program for obtaining simultaneous time series data from a self-recording transmissivity and current meter sensor in the near-bottom boundary layer, over periods

of at least 2 months at a number of locations. If at all possible, these data should be collected into autumn until just prior to freeze-up. A prerequisite for this program would involve a pilot experiment with frequent collection of turbidity samples to assess the usefulness of transmissivity in providing a reliable means of determining absolute SSC values.

General Recommendations

8) Direct measurements of critical shear stress for resuspension of sediments in the bottom boundary layer are required. An instrumentation package which meets this requirement (e.g. Atlantic Geoscience Centre's RALPH) involves an array of rapidly sampling current sensors placed in the bottom boundary layer combined with SSC measurements to determine when sediments are resuspended. For the latter requirement, acoustic profiling techniques offer considerable promise. In analyzing the resulting data, efforts should be made to examine the utility of using the bulk drag formula in determining shear stress from a single current meter 1-2 m above the bottom (see Appendix B discussion).

9) Further studies of the regional wave climate are required, with emphasis on delineating extreme wave events. An important requirement for the verification of such studies, is the continuation of the Wave Climate Study for the region, sponsored by the Marine Environmental Data Services Branch, Dept. of Fisheries and Oceans, Ottawa.

10) Further analysis of existing near-bottom current meter data in order to better define and understand the response of near-bottom currents to surface winds. Emphasis should be placed on the time dependent response associated with individual wind events through newly emerging analytical techniques (e.g. modal structures of continental shelf waves).

11) Additional documentation of summer and autumn sea-ice cover and open-water fetch lengths. With 11 years of satellite imagery now available, in addition to earlier aircraft and ship-based data sources, a representative ice climatology for the area is feasible.

12) Further research is required into the time and spatial scales and physical causes of the intense but small-scale cyclonic disturbances known to occur over the Canadian Beaufort Sea. These disturbances, which are not fully resolved on the standard atmospheric charts, cause potential difficulties in wave climate studies and the use of coastal winds to determine offshore winds.

13) A continuation and increase in the efforts to collect offshore wind data. Such data are routinely collected throughout the year from fixed drilling platforms as well as drilling vessels in the summer months. Through quality control and routine archival, these measurements would provide an invaluable data base for climatic studies.

Priorities

While each of the recommendations given above would individually provide valuable new information and insight, considerably greater value could be achieved through the coordinated and simultaneous execution of combinations of these recommendations. Therefore, the planning of multidisciplinary studies involving geological, physical and chemical components is highly recommended.

While all of the recommendations are important, certain items in the above list can be singled out as addressing the most fundamental deficiencies in our present understanding of sediment transport in the Beaufort Sea. These most important studies are: improved measurements of bottom boundary layer shear stress (Recommendation 8) and investigation of correlations between bottom currents and suspended concentrations (Recommendations 5 and 7). For the latter studies, emphasis should be place on extending observations, beyond the conventional open water measurements period (mid-July to mid-September), to include the time of river freshet and in autumn immediately prior to freeze-up.

7. REFERENCES

Aagaard, K., 1982. Circulation of the Arctic Ocean: recent developments. Joint Oceanographic Assembly, 2-13 August 1982, Halifax (abstract only).

Amos, C.L. and T.T. Alfoldi, 1979. The determination of suspended sediment concentration in a macrotidal system using Landsat data. Jour. Sed. Petrology, 49, pp. 159-174.

Amos, C.L. and D.A. Greenberg, 1980. The simulation of suspended particulate matter in the Minas Basin, Bay of Fundy. Proceedings of the Canadian Coastal Conf., Burlington, Ontario. National Research Council, Ottawa, pp. 2-20.

Baird, W.F. and K.R. Hall, 1980. Wavehindcast study, Beaufort Sea. Report to Gulf Canada Resources Inc., Calgary, Alberta by Hydrotechnology Ltd., Ottawa, Ontario. (Available from Pallister Resource Management Ltd., Calgary, Alberta, T2C 2B3 as Beaufort EIS Report RWE 28).

Berry, M.O., P.M. Dutchak, M.E. Lalonde, J.A.W. McCulloch and I. Savdie, 1975. Weather, waves and icing in the Beaufort Sea. Beaufort Sea Technical Report No. 21, Institute of Ocean Sciences, Sidney, B.C.

Birch, J.R., D.B. Fissel and G.R. Wilton, 1982a. Subsurface current measurements near Tarsiut artificial island, August 1981-September 1982. Unpublished manuscript. Arctic Sciences Ltd., Sidney, B.C. for Dome Petroleum Ltd., Calgary, Alberta. 31 p.

Birch, J.R., G.R. Wilton and D.B. Fissel, 1982b. Shallow water current measurements in the southeast Beaufort Sea - summer 1982 (including August 8-16, 1981 record from W. Atkinson site). Unpublished data report prepared by Arctic Sciences Ltd., Sidney, B.C. for Esso Resources Canada Ltd., Calgary, Alberta. 66 p.

Birch, J.R. and D.B. Fissel, 1982. Shallow water, near-bottom current measurements in the southeast Beaufort Sea - summer 1981. Unpublished data report prepared by Arctic Sciences Ltd., Sidney, B.C. for Esso Resources Canada Ltd., Calgary, Alberta. 41 p.

Bornhold, B.D., 1975. Suspended matter in the southern Beaufort Sea: Beaufort Sea Project Technical Report No. 25b. Institute of Ocean Sciences, Sidney, B.C. 23 p. plus 7 p. appendix.

Bretschneider, C.L., 1977. Deep-water wave forecasting as a function of wind speed, fetch and duration. Shore Protection Manual, Vol. 1, Chapter 3, 3rd Edition. U.S. Army Coastal Engineering Research Center.

Brower, W.A. Jr., H.W. Searby, and J.L. Wise, 1977. Climatic Atlas of the Outer Continental Shelf Waters and Coastal Regions of Alaska, Vol. III, Chukchi and Beaufort Sea. U.S. Dept. of Commerce, NOAA/OCSEAP, 3, 409 p.

Bussinger, J.A., 1973. Turbulent transfer in the atmospheric surface layer. In: Workshop on Micrometeorlogy. D.A. Haugen, Ed. American Meteorological Society, Boston. pp. 67-100.

Chriss, T.M. and D.R. Caldwell, 1982. Evidence for the influence of form drag on bottom boundary layer flow. J. Geophys. Res. 87, pp. 4148-4154.

Danard, M. and M. Gray, 1984. Extreme wind stresses over the Beaufort Sea as determined from Tuktoyaktuk winds. Unpubished manuscript. Atmospheric Dynamics Corp., Victoria, B.C. for Institute of Ocean Sciences, Sidney, B.C.

Davies, K.F., 1975. Mackenzie River input to the Beaufort Sea. Beaufort Sea Project Technical Report 15. Institute of Ocean Sciences, Sidney, B.C. 72 p.

Dome Petroleum Ltd., 1983. Artificial islands and their effect on regional landfast ice conditions in the Beaufort Sea. Unpublished discussion paper, Calgary, Alberta.

Dome Petroleum Limited, Esso Resources Canada Limited and Gulf Canada Resources Inc., 1982. Environmental impact statement for hydrocarbon development in the Beaufort Sea - Mackenzie Delta region. Vol. 3A Beaufort-Delta setting, Calgary, Alberta

Erickson, P., D. Thomas, R. Pett and B. de Lange Boom, 1983. Issungnak oceanographic survey, Part A: oceanographic properties. A report for Esso Resources Canada Limited, Gulf Canada Resources Inc. and Dome Petroleum Ltd. by Arctic Laboratories Limited, Inuvik, N.W.T. 194 p.

Fissel, D.B., 1981. An analysis of current meter data obtained at CANMAR drillships, 1976 - 1979. Report to Dome Petroleum Ltd., Calgary, Alberta by Arctic Sciences Ltd., Sidney, B.C. 126 p. (Available from Pallister Resource Management Ltd., Calgary, Alberta, T2G 2B3 as Beaufort EIS Report BEISSD 29).

Fissel, D.B. and J.R. Birch, 1983. Inshore currents in the Canadian Beaufort Sea. Unpublished manuscript. Arctic Sciences Ltd., Sidney, B.C. for Esso Resources Canada Ltd., Calgary, Alberta. 84 p.

Fissel, D.B., G.R. Wilton and D.N. Knight, 1981. Subsurface measurements at Tarsiut and Uviluk drill sites, January-August, 1981. Unpublished manuscript. Arctic Sciences Ltd., Sidney, B.C. for Dome Petroleum Ltd., Calgary, Alberta. 50 p.

Forbes, D.L., 1980. Late quartenary sea levels in the southern Beaufort Sea. In Current Research, Part B, Geol. Surv. Canada, Paper 80-1B, pp. 75-87.

Fraker, M.A., C.D. Gordon, J.W. McDonald, J.K.B. Ford and E. Chambers, 1979. White whale (Delphinapterus leucas) distribution and abundance and the relationship to physical and chemical characteristics of the Mackenzie Estuary. Canada Dept. of Environment, Fisheries and Mar. Serv. Res. and Dev. Directorate, Tech. Rept. 863.

Giovando, L.F. and R.H. Herlinveaux, 1981. A discussion of factors influencing dispersal of pollutants in the Beaufort Sea. Pacific Marine Science Report 81-4. Institute of Ocean Sciences, Sidney, B.C. 198 p.

Grant, W.D. and O.S. Madsen, 1979. Combined wave and current interaction with a rough bottom. J. Geophys. Res. 84, pp. 1797-1808.

Harper, J.R. and S. Penland, 1982. Beaufort Sea sediment dynamics. Unpublished report to Geol. Surv. Canada, Dartmouth, Nova Scotia by Woodward-Clyde Consultants, Victoria, B.C. 125 p. with appendices.

Harper, J.R., S.M. Blasco and P.R. Hill, 1984. Sediment transport on the Canadian Beaufort Sea shelf. Submitted to Can. J. Earth Sci.

Henry, R.F. and M.G.G. Foreman, 1977. Numerical model studies of semi-diurnal tides in the southern Beaufort Sea. Pacific Marine Science Report 77-11, Institute of Ocean Sciences, Sidney, B.C. 71 p.

Herlinveaux, R.H. and B.R. de Lange Boom, 1975. Physical oceanography of the southeastern Beaufort Sea: Beaufort Sea Project Technical Report 18. Institute of Ocean Sciences, Sidney, B.C. 97 p.

Herlinveaux, R.H., B.R. de Lange Boom and G.R. Wilton, 1976. Salinity, temperature, turbidity and meteorological observations in the Beaufort Sea: summer 1974, spring and summer 1975. Pacific Marine Science Report 76-26, Institute of Ocean Sciences, Sidney, B.C. 244 p.

Hill, P.R., K.M. Moran and S.M. Blasco, 1984. Creep deformation of slope sediments in the Canadian Beaufort Sea. Geomarine Letters (in press).

Hodgins, D., P.H. LeBlond and O. Brink-Kjaer, 1981. A hindcast study of extreme water levels in the Beaufort Sea. Report for Esso Resources Canada Limited by Seaconsult Marine Research Ltd., Vancouver, B.C., 231 p. (Available from Pallister Resources Management Ltd., Calgary, Alberta, T2C 2B3 as Beaufort EIS Report RWE 36.)

Huggett, W.S., M.J. Woodward and A.N. Douglas, 1977. Data record of current observations, Vol. XVI, Beaufort Sea, 1974 to 1976. Data Report Series. Institute of Ocean Sciences, Sidney, B.C. 139 p.

Komar, P.D., 1976. Beach Processes and Sedimentation. Prentice-Hall, Englewood, N.J. 429 p.

Krank, K., 1979. Dynamics and distribution of suspended particulate matter in the St. Lawrence Estuary. Nat. Can. 106, pp. 163-179.

Lemon, D.D. and D.M. Kowalski, 1982. Water column measurements at CANMAR drillsites in the Beaufort Sea, 1976-1908. Report prepared fo the Institute of Ocean Sciences, Sidney, B.C. by Arctic Sciences Ltd., Sidney, B.C. (unpublished manuscript).

Marko, J.R., 1975. Satellite observations of the Beaufort Sea ice cover: Beaufort Sea Project Technical Report 34. Institute of Ocean Sciences, Sidney, B.C. 137 p.

Marko, J.R. and S. Oberski, 1982. An examination of the utility of digitally-enhanced NOAA and TIROS satellite imagery in the southeastern Beaufort Sea. Report prepared for the Institute of Ocean Sciences, Sidney, B.C. by Arctic Sciences Ltd., Sidney, B.C. (unpublished manuscript).

Marko, J.R., D.B. Fissel, M.A. Wilson and D. Huston, 1983. Background and evaluation of impacts of Liard River hydroelectrical development in the southeastern Beaufort Sea. Prepared for B.C. Hydro and Power Authority, Vancouver, B.C. by Arctic Sciences Ltd., Sidney, B.C. 81 p. plus appendices.

Matsumoto, E. and C.S. Wong, 1977. The distribution of suspended particles in the southern Beaufort Sea. J. Oceanographical Soc. Japan, 33, pp. 227-232.

McDonald, B.C. and C.P. Lewis, 1973. Geomorphic and sedimentologic processes of rivers and coasts, Yukon Coastal Plain. Env.-Social Comm., Northern Pipeline, Task Force on Northern Oil Dev. Report 73-79, 245 p.

McDonald, J.W. and L.C. Martin, 1976. A summer survey of the physical oceanography and water chemistry of the Mackenzie River estuary, N.W.T., 1975. Part 3. pp. 18-82. In: Summer environmental program Mackenzie River estuary, Vol. 1. Aquatic Studies. Prepared for Imperial Oil Ltd., Calgary by F.F. Slaney and Company Limited, Vancouver, B.C. 149 p.

McKay, G.A, 1966. Design winds for reservoirs in southern Manitoba. Can. Dept. of Agriculture, PFRA Eng. Br. Met. Rep. No. 20.

MacNeill, M.R. and J.F. Garrett, 1976. Open water surface currents. Beaufort Sea Project Technical Report 17. Institute of Ocean Sciences, Sidney, B.C.

Meagher, L., 1978. Compilation of the thickness of recent soft sediment and ice-related features in the Beaufort Sea, Northwest Territories. Unpublished report to Geol. Surv. Canada, Ottawa, by Geomarine Associates Ltd., Halifax, Nova Scotia. 74 p. with maps.

Melling, H., 1983. Oceanographic features of the Beaufort Sea in early winter. Can. Technical Rep. Hydrogr. Ocean Sci. No. 20, 131 p.

Melling, H. and E.L. Lewis, 1982. Shelf drainage flows in the Beaufort Sea and their effect on the Arctic Ocean pycnocline. Deep-Sea Res., 29, pp. 967-985.

Milliman, J.D. and R.H. Meade, 1983. World-wide delivery of river sediments to the oceans. J. Geol., 91, pp. 1-21.

Newton, J.L., 1973. The Canada Basin: mean circulation and intermediate scale flow features. Doctoral Dissertation, University of Washington (unpublished).

O'Connor, M.J., 1982 (in prep.). Depth to transgressive unconformity, southern Beaufort Sea shelf. Unpublished report to Geol. Surv. Canada, Dartmouth, Nova Scotia by M.J. O'Conner Associates, Calgary, Alberta.

Panofsky, H.A. and G.W. Brier, 1958. Some applications of statistics to meteorology. Pennslyvania State University, University Park, PA. 224 p.

Pelletier, B.R., 1975. Sediment dispersal in the southern Beaufort Sea. Beaufort Sea Project Technical Report 25a. Institute of Ocean Sciences, Sidney, B.C. 80 p.

Phillips, O.M., 1966. The Dynamics of the Upper Ocean. Cambridge University Press, Cambridge, 261 p.

Pollard, R.T., 1980. Properties of near-surface inertial oscillations. J. Phys. Oceanogr. 10, pp. 385-393.

Reimnitz, E., C.A. Roderick and S.C. Wolf, 1974. Strudel scour: a unique arctic marine geological phenomenon. Journal of Sedimentary Petrology, 44(2), pp. 409-420.

Richards, T.L., H. Dragert and D.R. McIntyre, 1966. Influence of atmospheric stability and over-water fetch on winds over the lower Great Lakes. Mon. Weather Rev., 94, pp. 448-453.

Tummers, E.L., 1980. Heat budgets of the southeast Beaufort Sea for the years 1974 and 1975. M. Sc. Thesis, U.S. Naval Postgraduate School. 205 p.

APPENDIX A

SUMMARY OF MACKENZIE RIVER VOLUME AND SEDIMENT DISCHARGES, 1973-1982

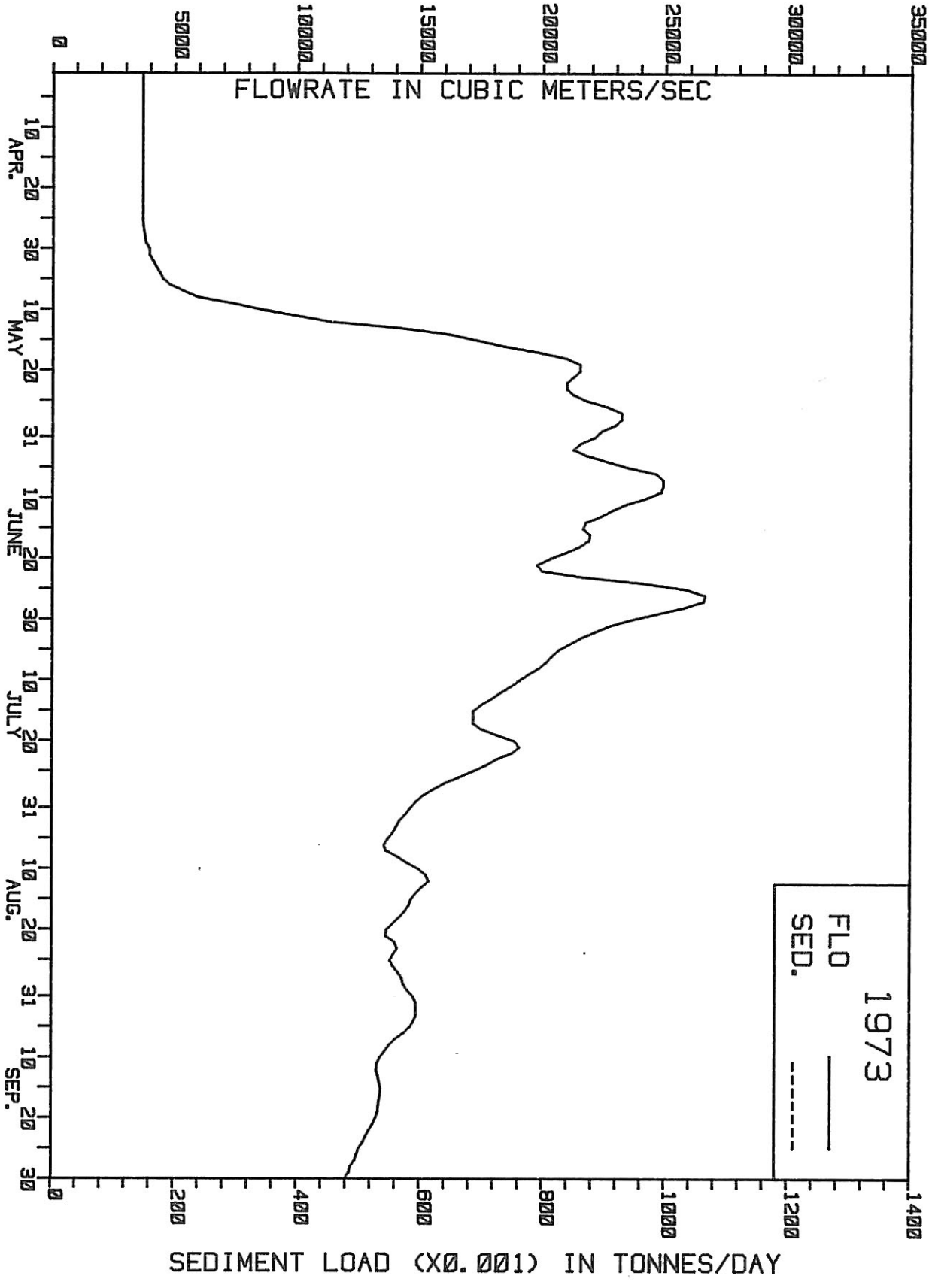
FLOWRATE IN CUBIC METERS/SEC
0
5000
10000
15000
20000
25000
30000
35000
APR.
MAY
JUNE
JULY
AUG.
SEP.
10
20
30
31
FLO
SED.
1973
0
200
400
600
800
1000
1200
1400
SEDIMENT LOAD (X0.001) IN TONNES/DAY

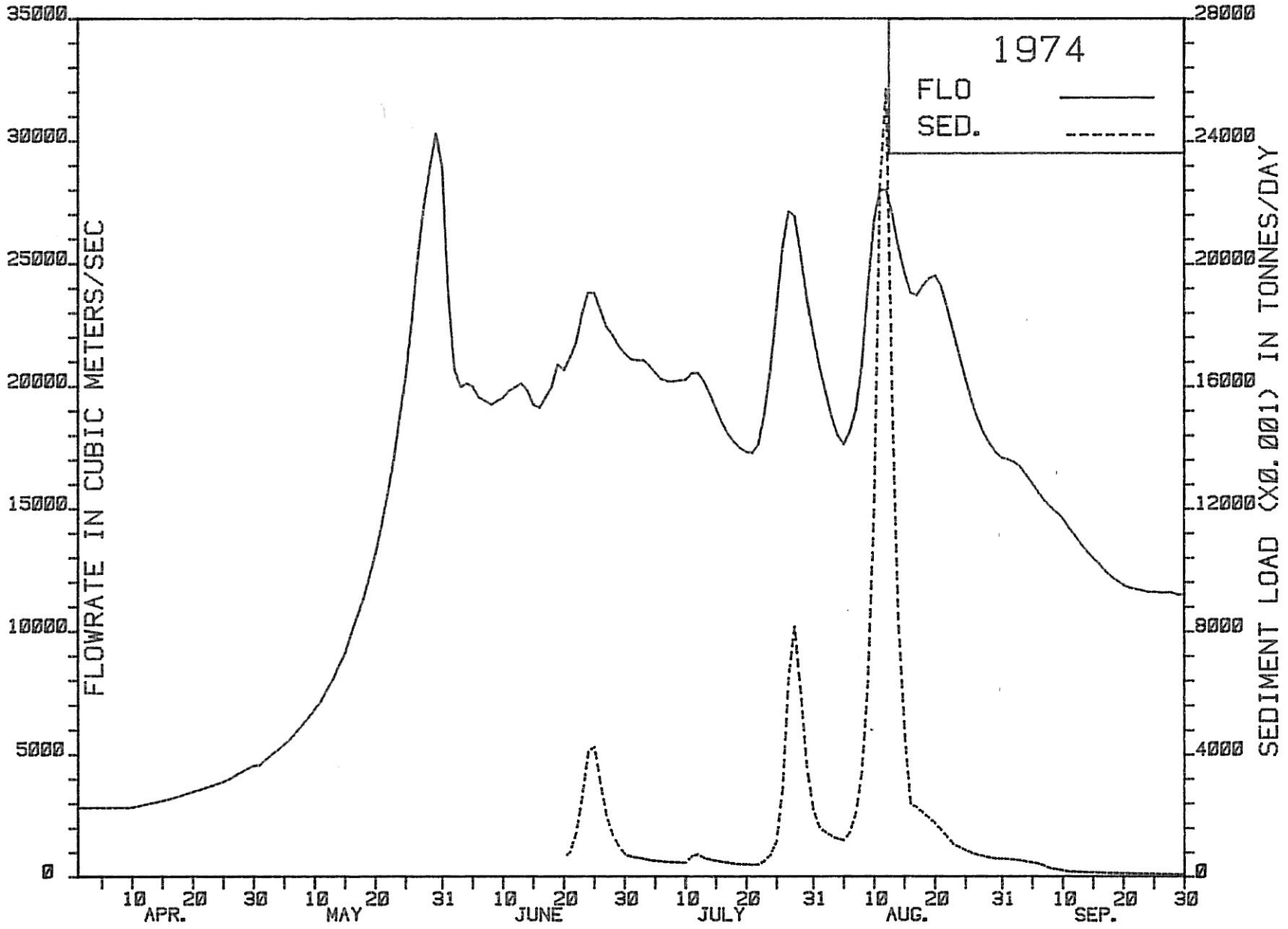
1974
FLO
SED.
FLOWRATE IN CUBIC METERS/SEC
SEDIMENT LOAD (X0.001) IN TONNES/DAY
35000
30000
25000
20000
15000
10000
5000
0
28000
24000
20000
16000
12000
8000
4000
0
10 20 30
APR.
10 20 31
MAY
10 20 30
JUNE
10 20 31
JULY
10 20 31
AUG.
10 20 30
SEP.

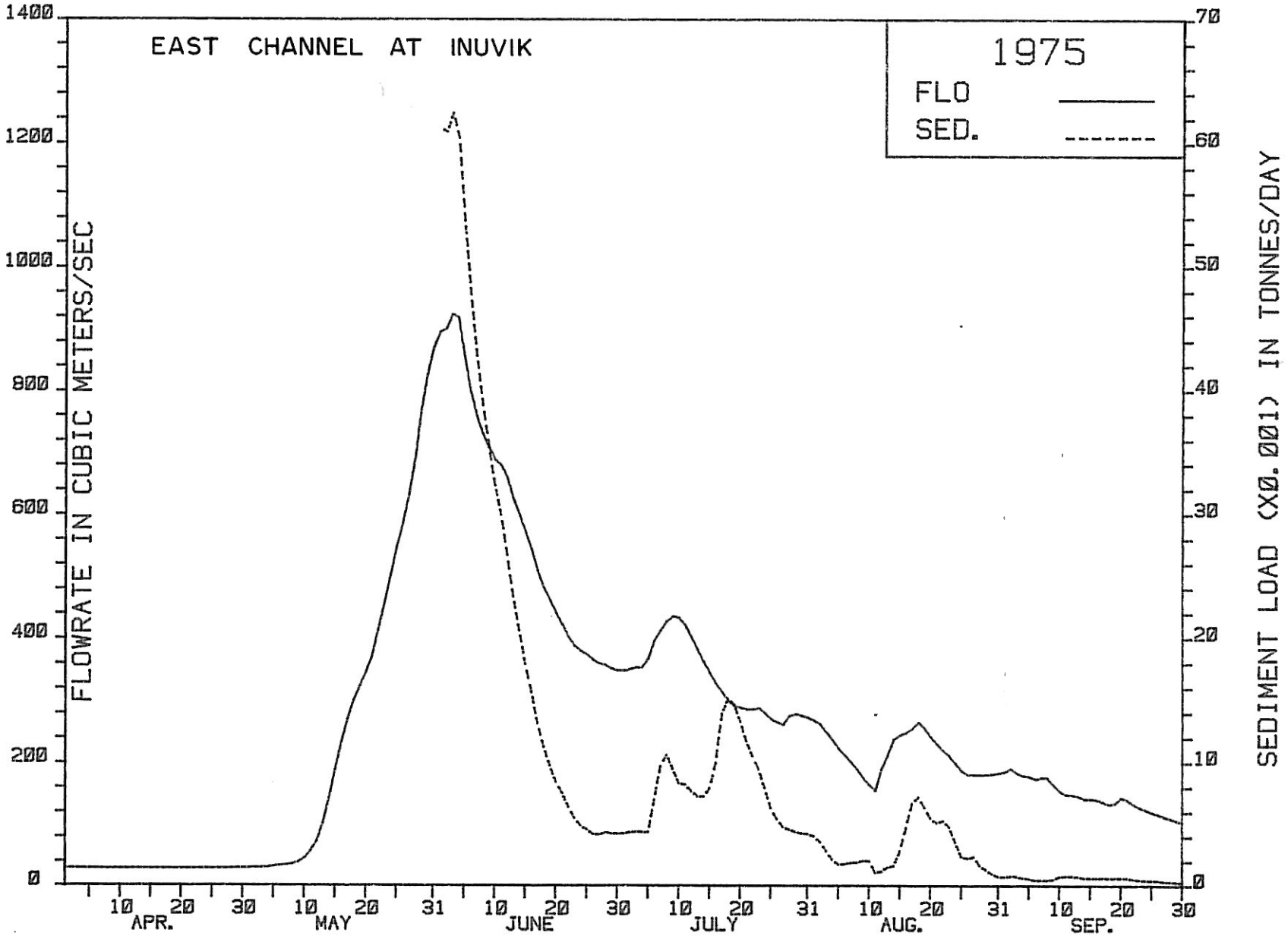
EAST CHANNEL AT INUVIK
1975
FLO
SED.
FLOWRATE IN CUBIC METERS/SEC
SEDIMENT LOAD (X0.001) IN TONNES/DAY
1400
1200
1000
800
600
400
200
0
70
60
50
40
30
20
10
0
10 20 30 10 20 31 10 20 30 10 20 31 10 20 31 10 20 30
APR.
MAY
JUNE
JULY
AUG.
SEP.

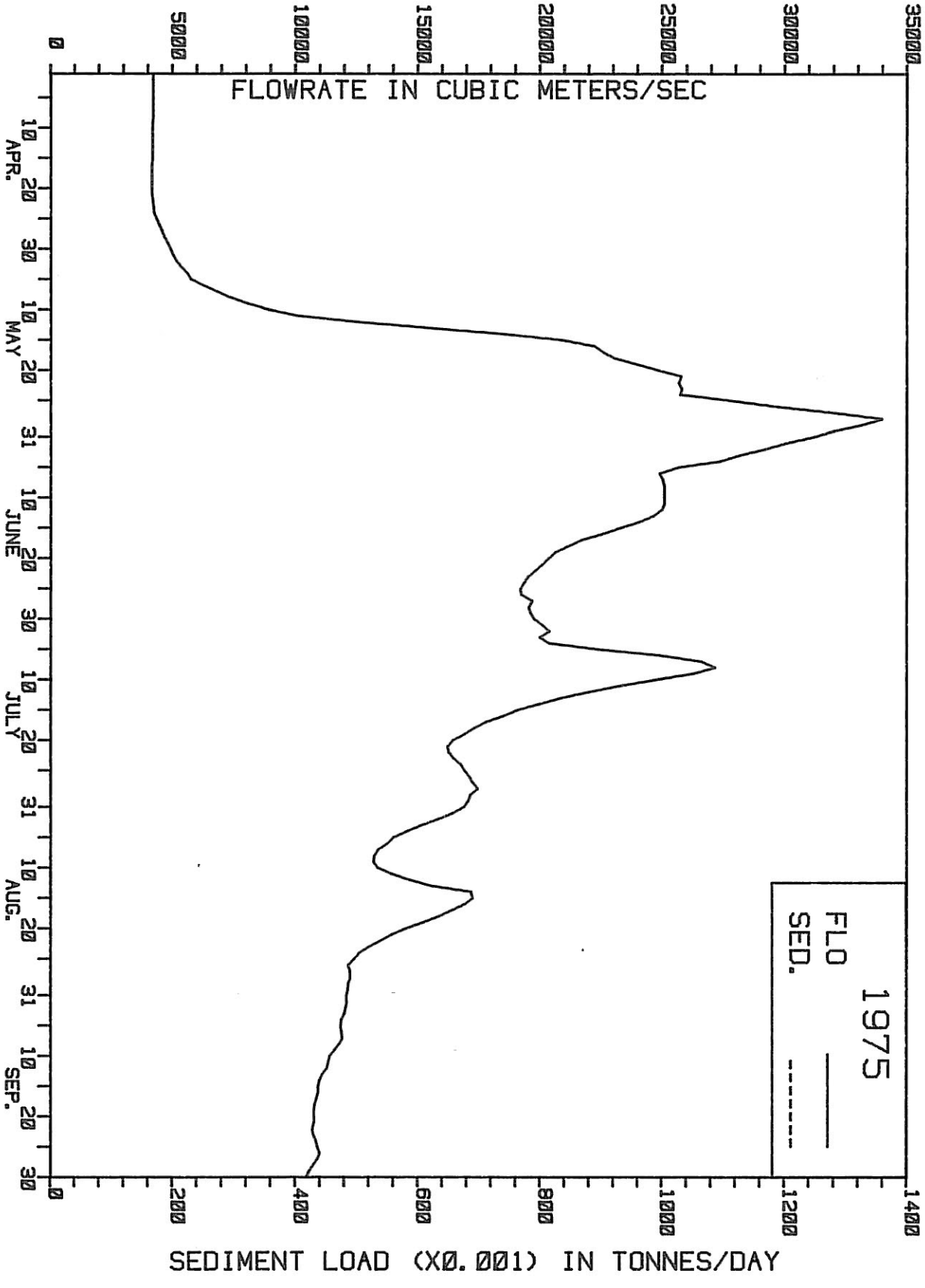
FLOWRATE IN CUBIC METERS/SEC
0
5000
10000
15000
20000
25000
30000
35000
10 APR.
20
30
10 MAY
20
31
10 JUNE
20
30
10 JULY
20
31
10 AUG.
20
31
10 SEP.
20
30
0
200
400
600
800
1000
1200
1400
SEDIMENT LOAD (X0.001) IN TONNES/DAY
1975
FLO
SED.

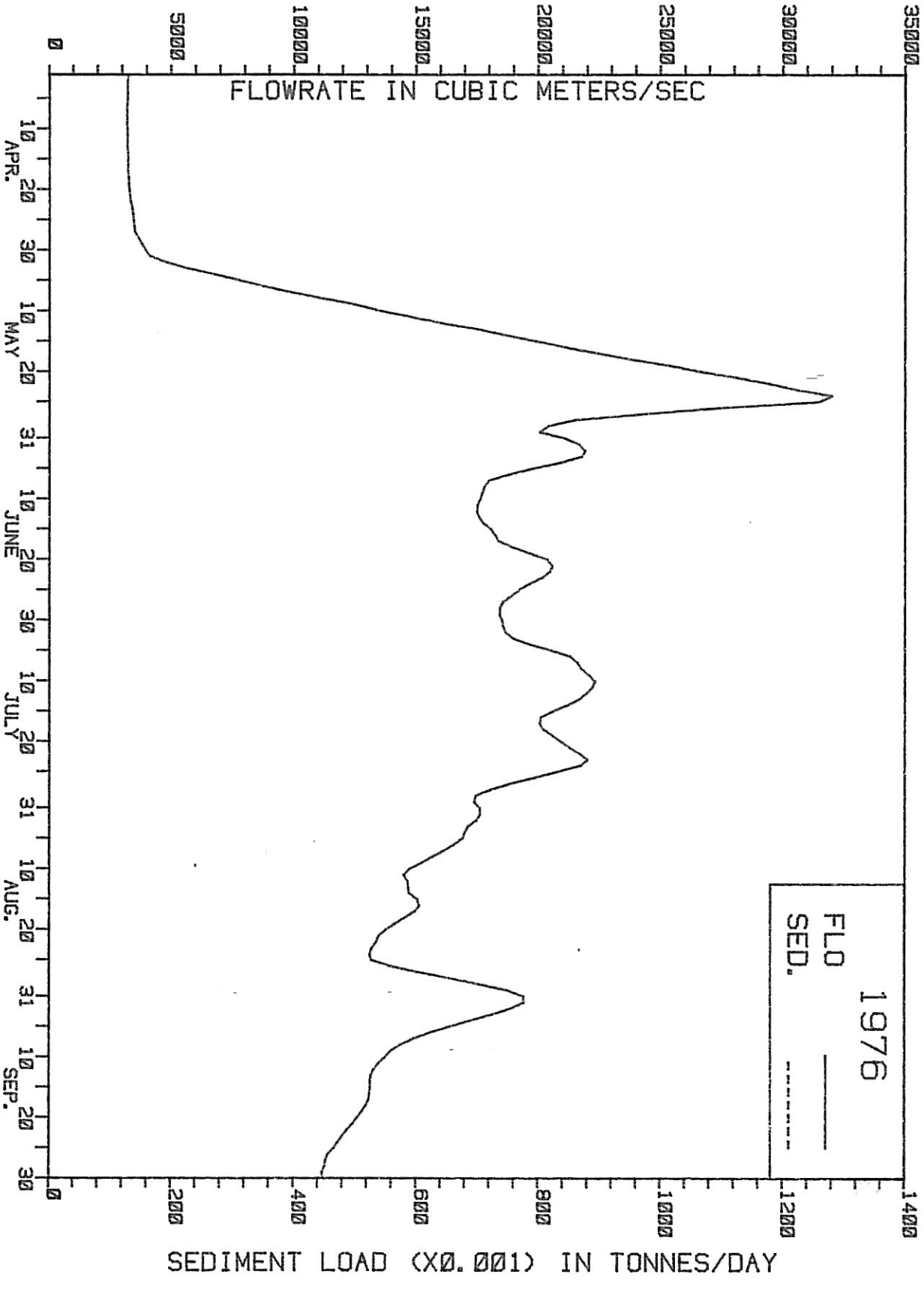
FLOWRATE IN CUBIC METERS/SEC
0
5000
10000
15000
20000
25000
30000
35000
APR.
10
20
30
MAY
10
20
31
JUNE
10
20
30
JULY
10
20
31
AUG.
10
20
31
SEP.
10
20
30
0
200
400
600
800
1000
1200
1400
1976
FLO
SED.
SEDIMENT LOAD (X0.001) IN TONNES/DAY

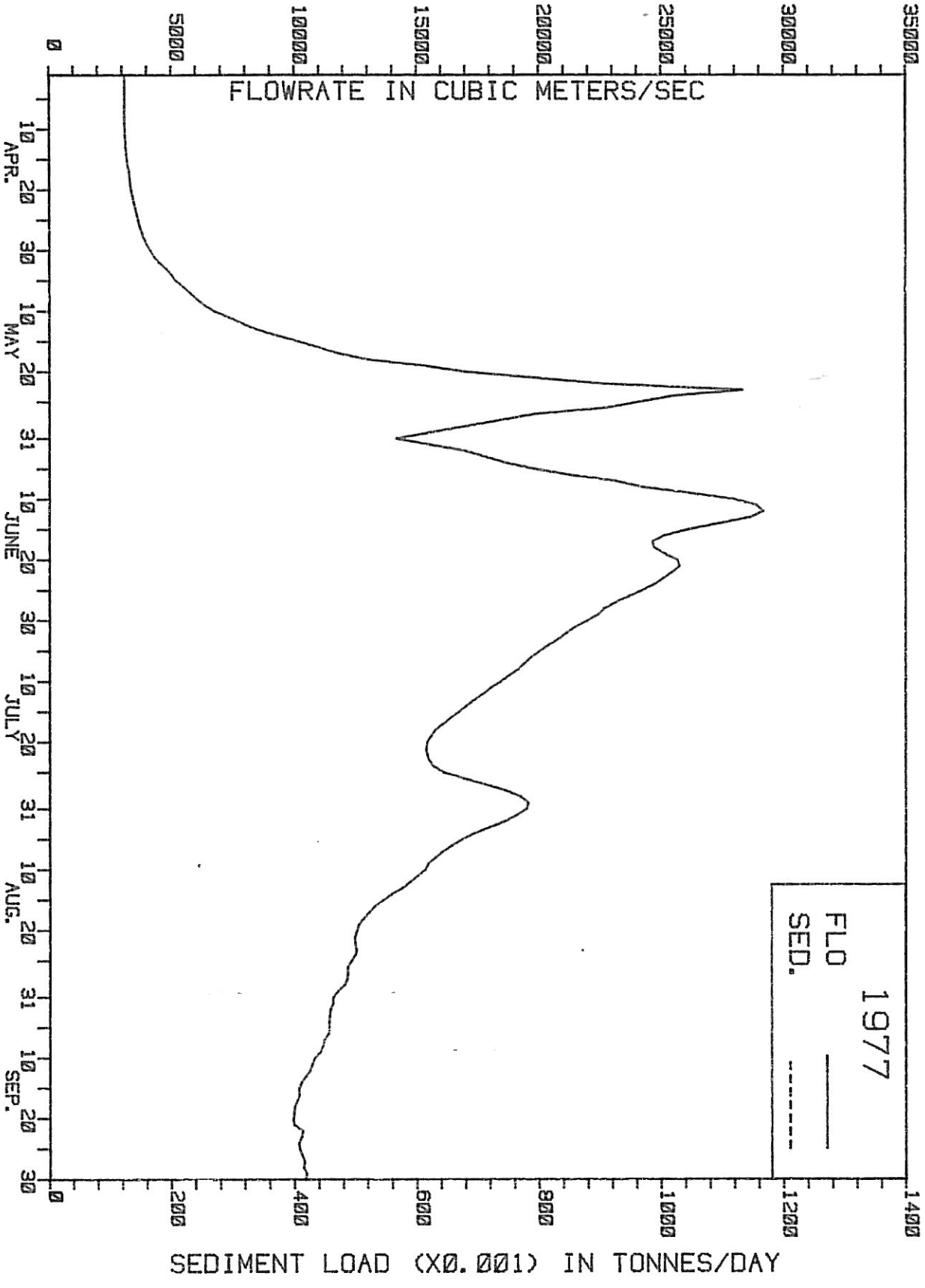
FLOWRATE IN CUBIC METERS/SEC
0
5000
10000
15000
20000
25000
30000
35000
APR.
MAY
JUNE
JULY
AUG.
SEP.
10
20
30
31
FLO
SED.
1977
0
200
400
600
800
1000
1200
1400
SEDIMENT LOAD (X0.001) IN TONNES/DAY

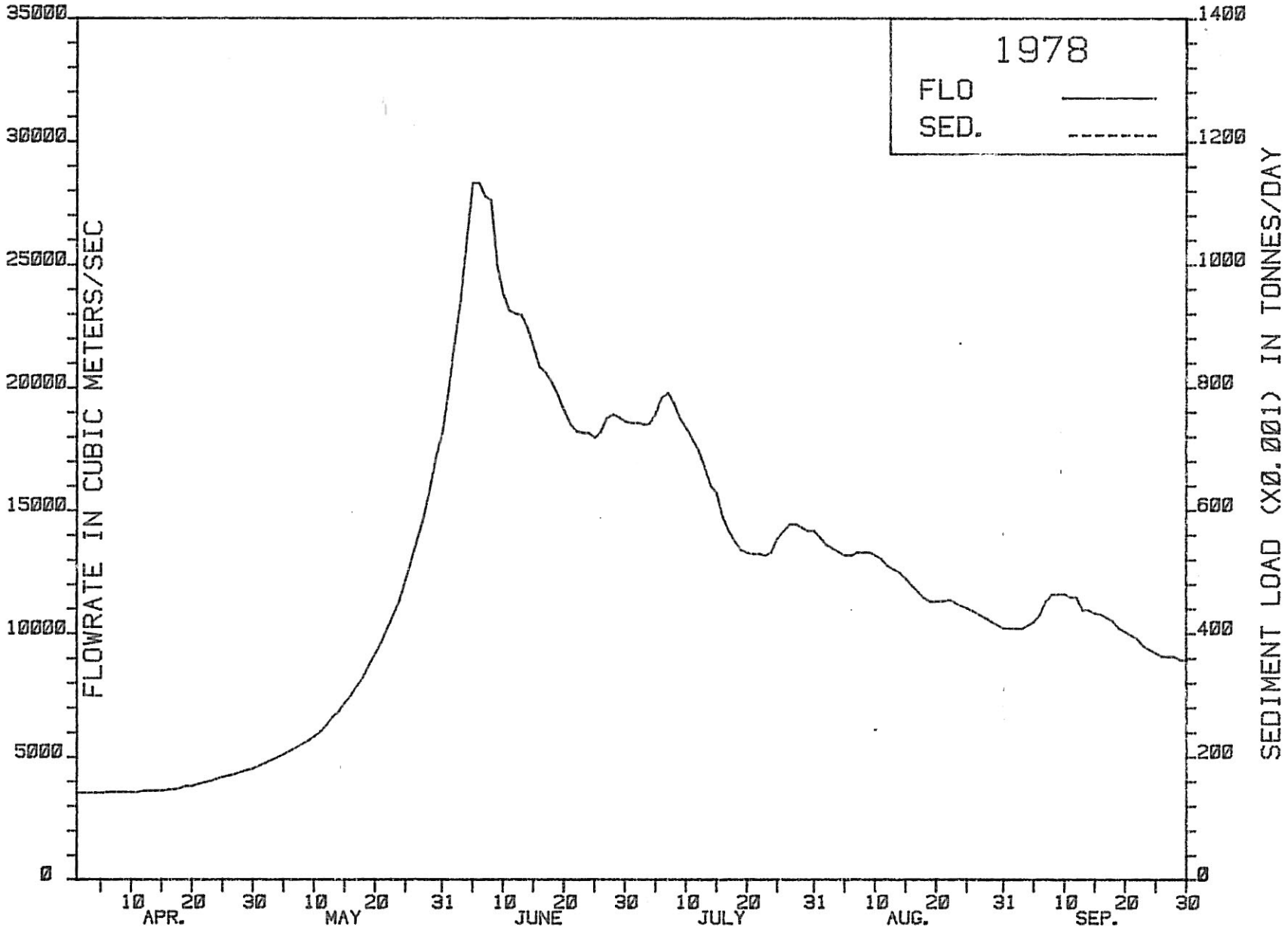
1978
FLO
SED.
FLOWRATE IN CUBIC METERS/SEC
SEDIMENT LOAD (X0.001) IN TONNES/DAY
35000
30000
25000
20000
15000
10000
5000
0
1400
1200
1000
800
600
400
200
0
10 20 30 10 20 31 10 20 30 10 20 31 10 20 31 10 20 30
APR. MAY JUNE JULY AUG. SEP.

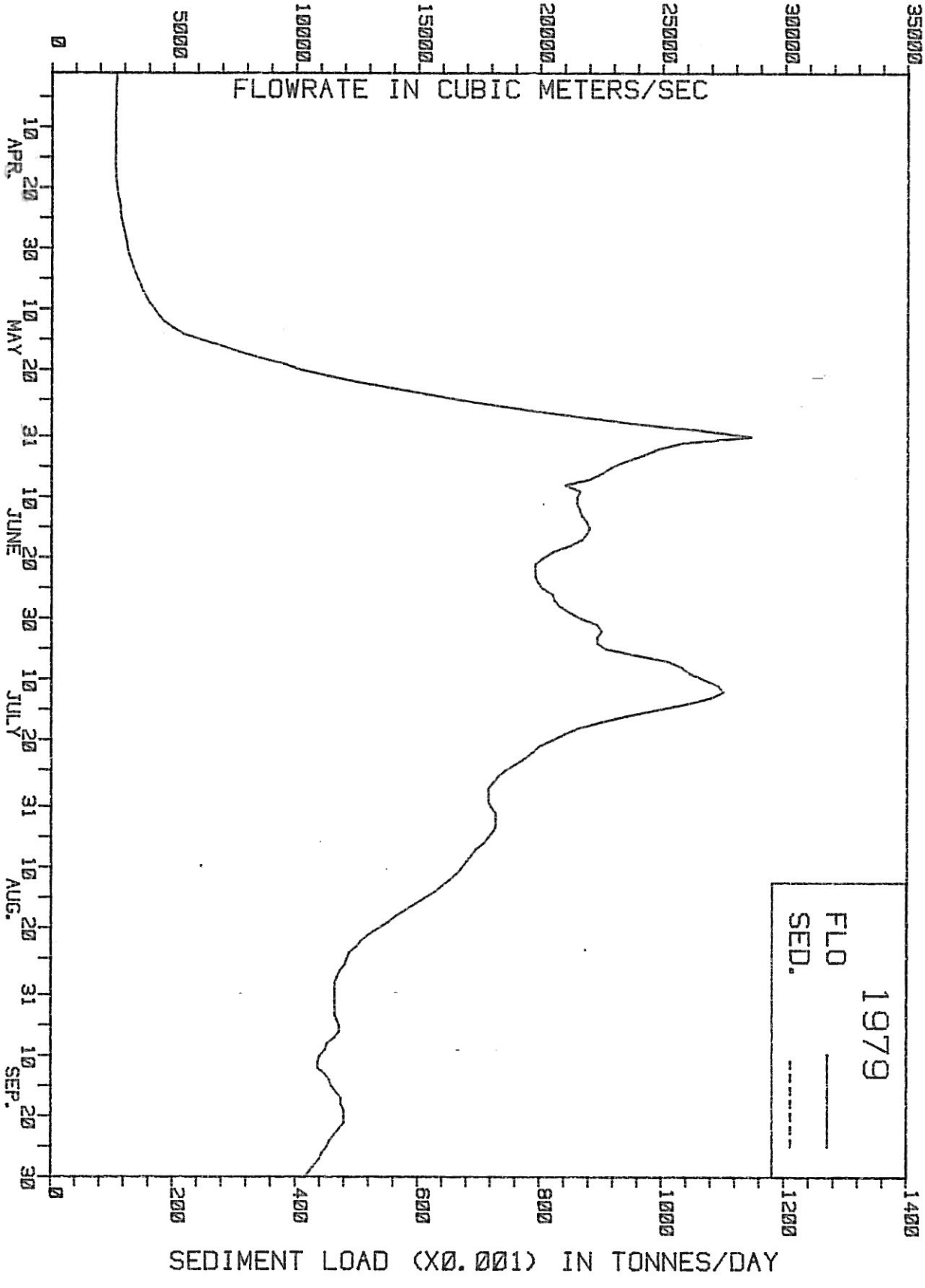
FLOWRATE IN CUBIC METERS/SEC
0
5000
10000
15000
20000
25000
30000
35000
APR.
MAY
JUNE
JULY
AUG.
SEP.
10
20
30
31
FLO
SED.
1979
0
200
400
600
800
1000
1200
1400
SEDIMENT LOAD (X0.001) IN TONNES/DAY

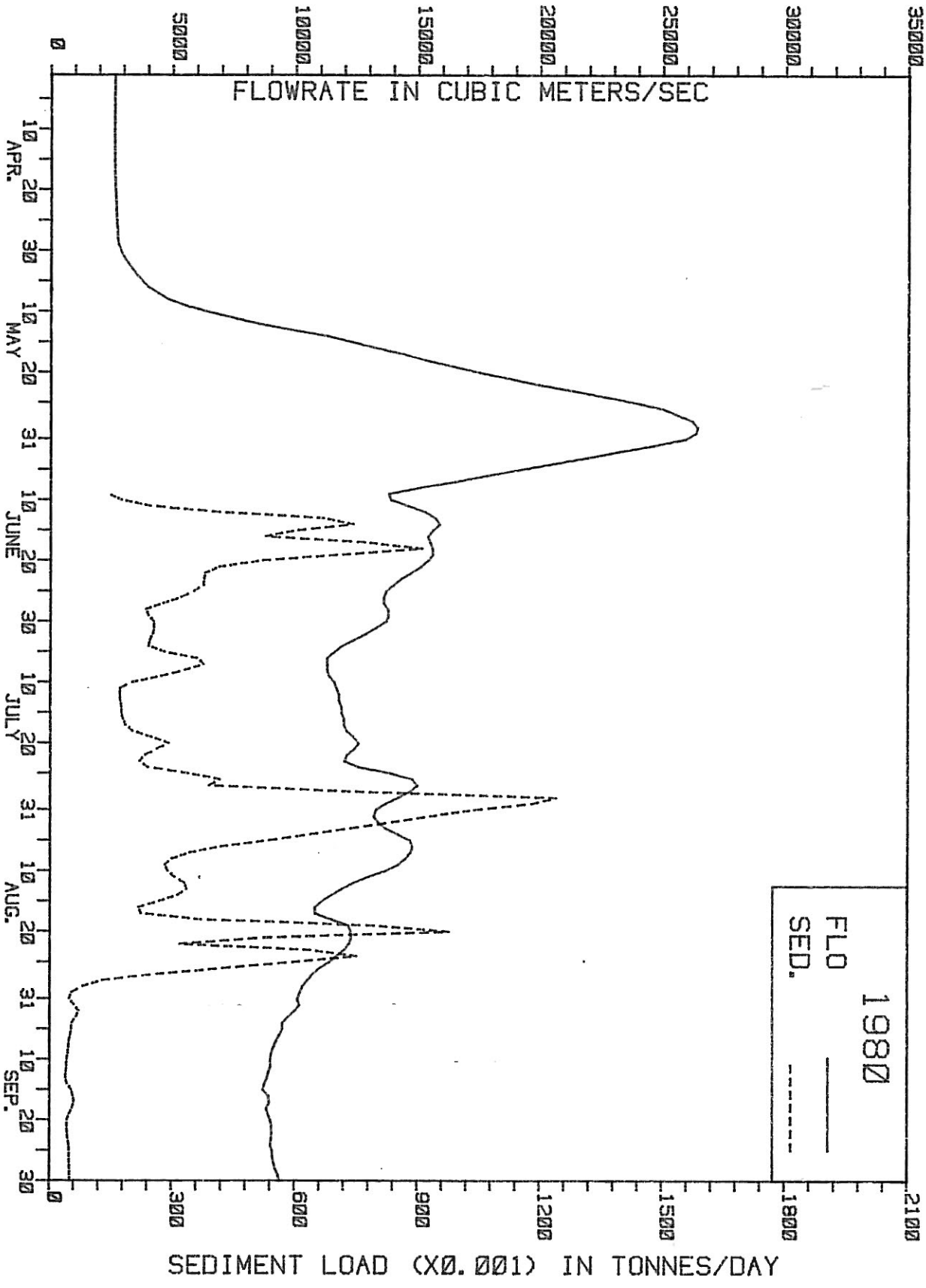
FLOWRATE IN CUBIC METERS/SEC
0
5000
10000
15000
20000
25000
30000
35000
10 APR.
20
30
10 MAY
20
31
10 JUNE
20
30
10 JULY
20
31
10 AUG.
20
31
10 SEP.
20
30
1980
FLO
SED.
0
300
600
900
1200
1500
1800
2100
SEDIMENT LOAD (X0.001) IN TONNES/DAY

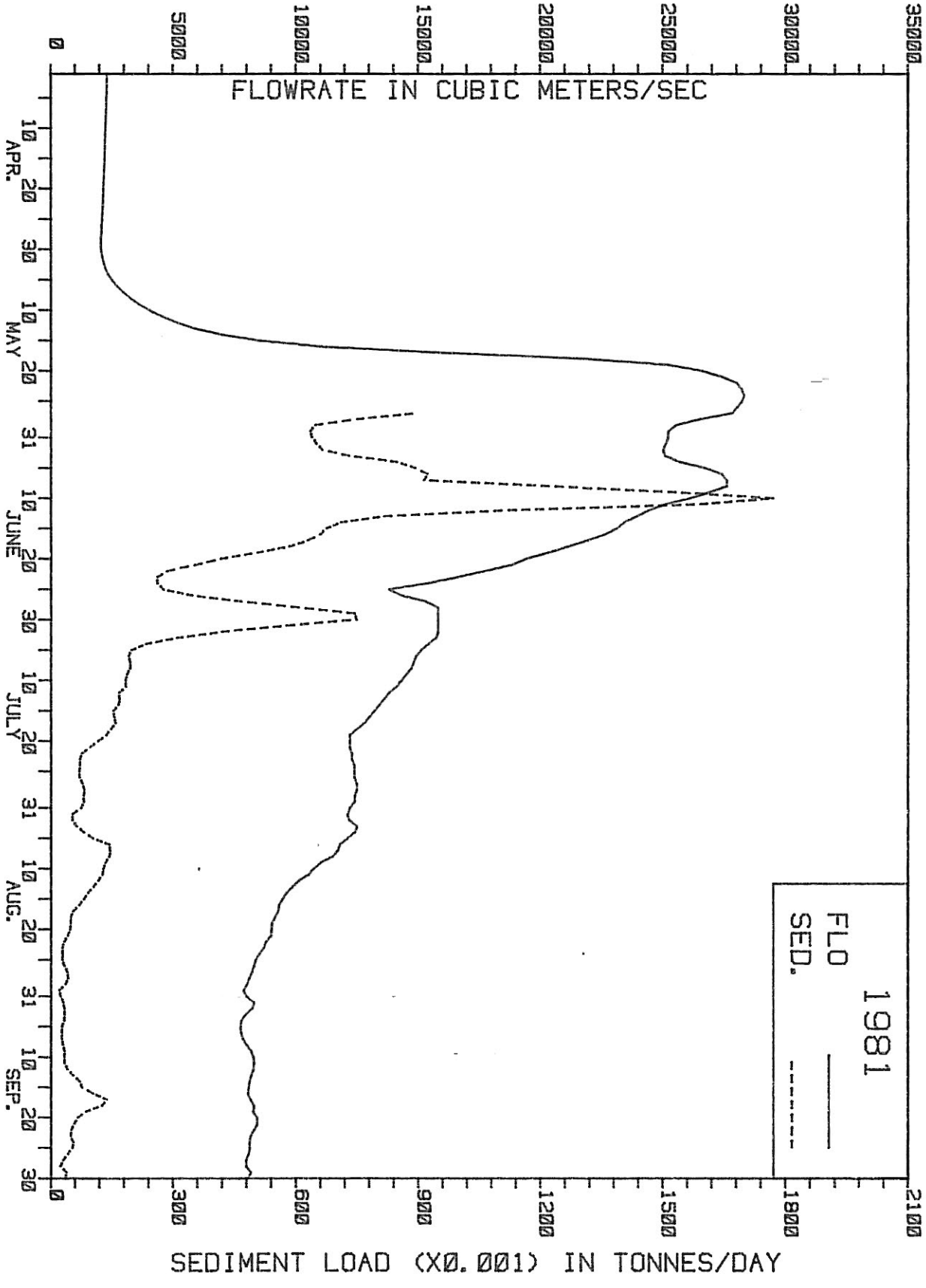
FLOWRATE IN CUBIC METERS/SEC
0
5000
10000
15000
20000
25000
30000
35000
APR.
MAY
JUNE
JULY
AUG.
SEP.
10
20
30
31
FLO
SED.
1981
0
300
600
900
1200
1500
1800
2100
SEDIMENT LOAD (X0.001) IN TONNES/DAY

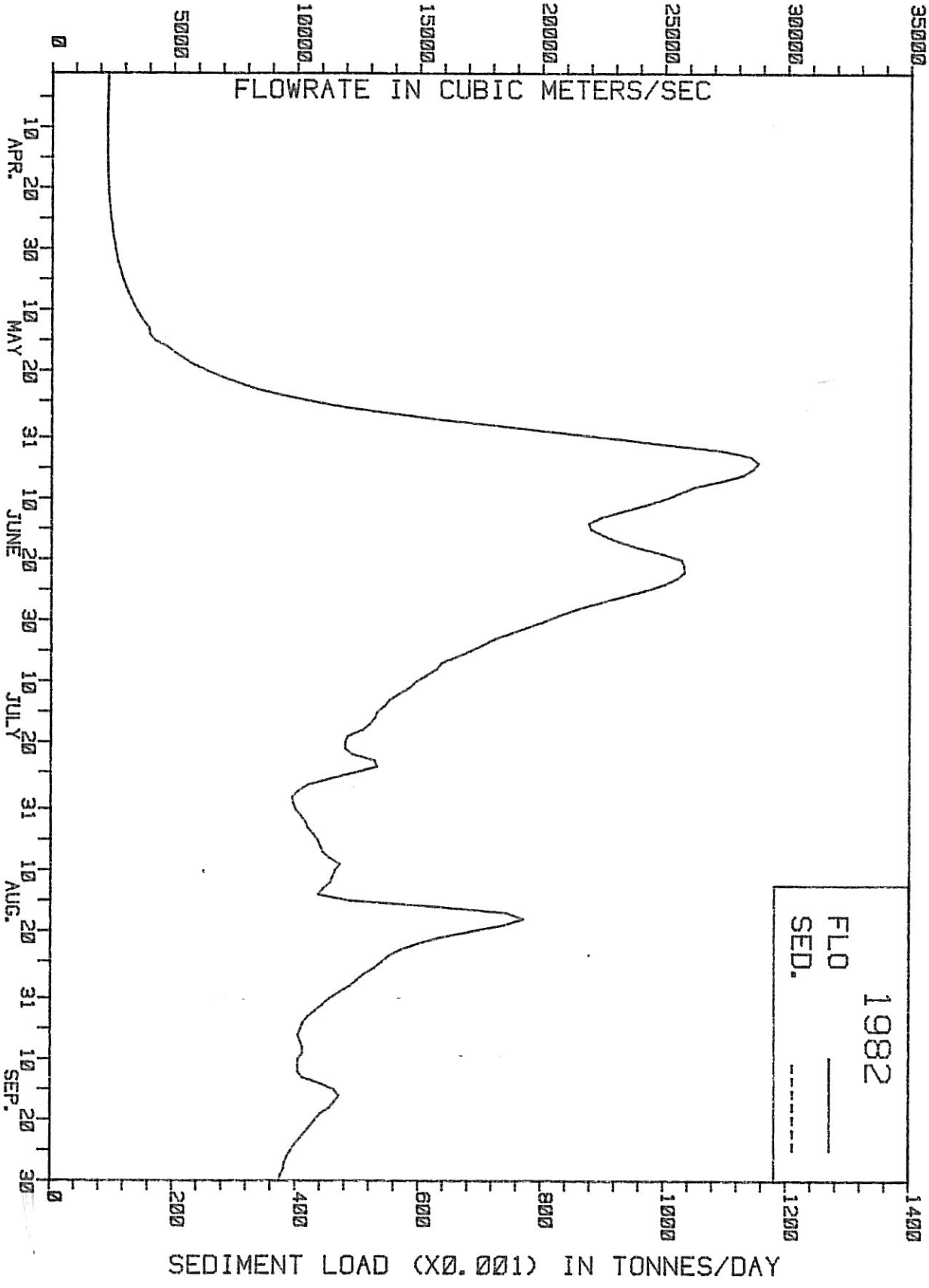
FLOWRATE IN CUBIC METERS/SEC
0
5000
10000
15000
20000
25000
30000
35000
APR.
MAY
JUNE
JULY
AUG.
SEP.
10
20
30
31
FLO
SED.
1982
0
200
400
600
800
1000
1200
1400
SEDIMENT LOAD (X0.001) IN TONNES/DAY

APPENDIX B

CRITICAL BOTTOM SHEAR STRESSES FOR RESUSPENSION OF SEDIMENTS

Following deposition onto the sea floor, sediments will be resuspended into the water column when the shear stress of the overlying water acting on the seabed exceeds a minimum value. The appropriate value for this critical shear stress for resuspension in the Canadian Beaufort Sea (or erosion) is not known, as there are, at present, no direct measurements available from which such a quantity could be computed. A recent survey of measured critical shear stresses for the erosion of cohesive substrates was tabulated by Amos and Greenberg (1980; Table 2, pp. 11-12) for a study of suspended particulate matter in the Bay of Fundy. Derived from both laboratory and in situ measurements, 14 tabulated values ranged from 0.11 to 4.52 dynes/cm^2, about a median value of 0.83. Excluding the two values of 3.7 and 4.52 dynes/cm^2 derived from a laboratory substrate consisting of 39% sand, the largest remaining value was 1.43 dynes/cm^2. Thus the most likely critical shear stress values for the silty and clayey bottoms of the Beaufort Sea would appear to occur in the range of 0.20 to 1.5 dynes/cm^2.

A considerable degree of uncertainty occurs in prescribing reasonable shear stress values due to the difficulty of correctly relating the shear stress to the measured water velocity. Common practice is to use a bulk dynamical coefficient of the form

$$\tau_b = \rho C_D \bar{U}^2 \qquad (1)$$

where τ_b is the bottom stress, ρ is the water density, U is the mean speed at a height 1 m above the bottom and C_D is a dimensionless drag coefficient (Komar, 1976). Values of C_D within the literature, as summarized by Chriss and Caldwell (1982), are highly variable, ranging from 1 x 10^{-3} to 1 x 10^{-2}, with a mean of 3 x 10^{-3} to 5 x 10^{-3}. This variability reflects the inherent complexity of turbulent boundary layer flows and its sensitivity to widely various roughness scales, static stability and mechanical energy levels. Furthermore, Chriss and Caldwell (1982) argue that the bulk dimensional formula often significantly overestimates the actual stress applied on the seabed. This is due to the apparently not uncommon existence of very small-scale (approx. 15 cm) viscous sublayer immediately above the seabed. In this situation, the use of the values of C_D and $\bar{U}$ at 1 m height can lead to an overestimation of shear stress applied to the seabed by a factor of 3 to 5. In view of the above considerations, the most likely values of C_D would appear to lie in the range of 1.0 to 4.0 x 10^{-3}.

To relate the assumed ranges of critical seabed shear stress and bottom layer drag coefficient to the wave orbital velocity and current information available for the Beaufort Sea, the

threshold velocity at 1 m ($\bar{U}$) at which resuspension would commence was computed using formula (1) and the ranges of τ_b and C_D discussed above. The results, as presented graphically in Figure B-1, suggest that while the range in possible threshold velocities could conceivably range by an order of magnitude from 6 to 60 cm/s, a more likely range would be 10 to 40 cm/s, about a median level of 20 cm/s (τ_b = 0.8, $C_D = 2 \times 10^{-3}$).

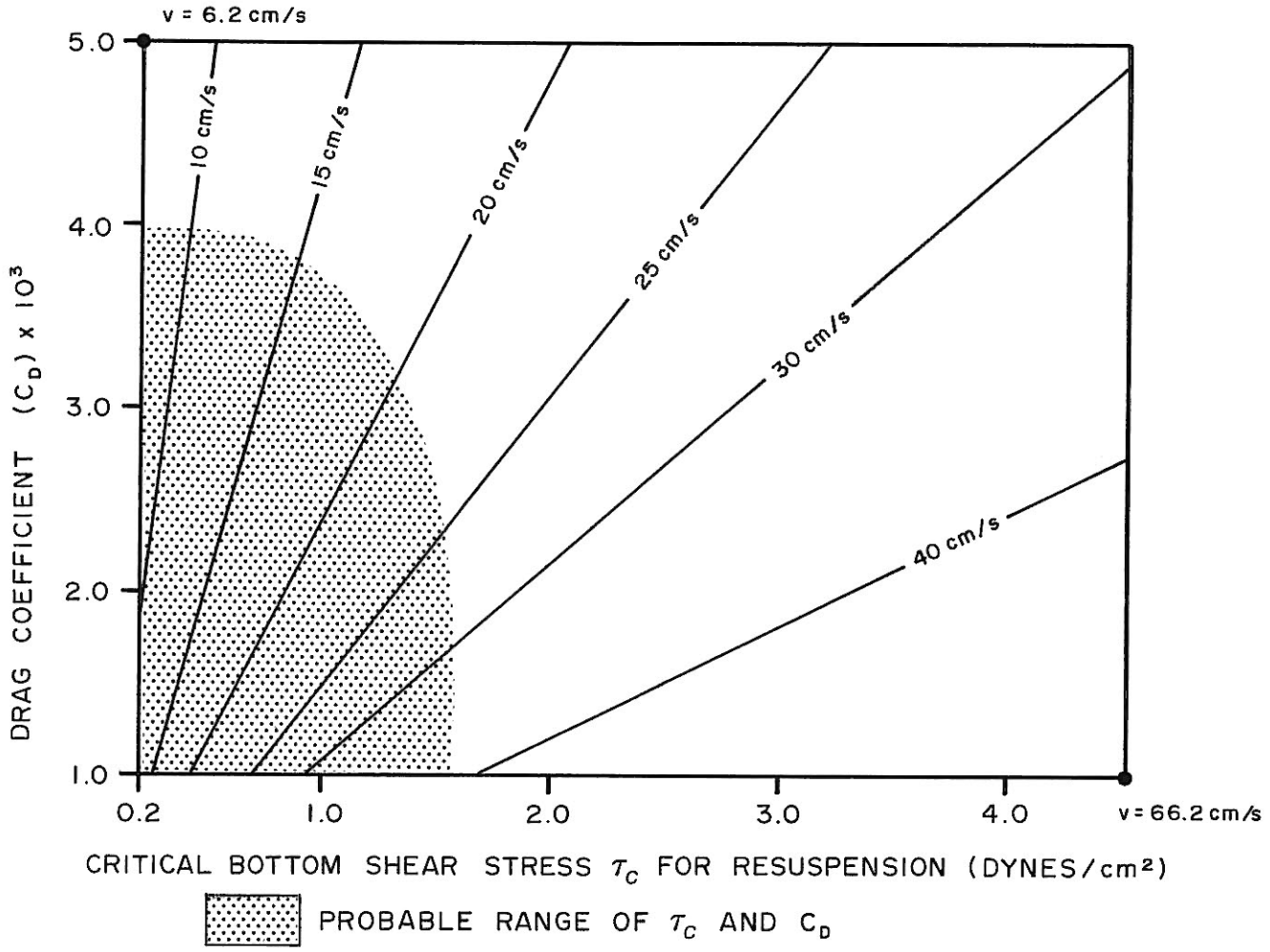

Figure B-1: Computed threshold velocities for bottom sediment resuspension as a function of critical bottom shear stress and drag coefficient. The shaded area highlights the more probable range of values.